UNIVERSITY OF LONDON THESIS

Degree PhD Year 2006 Name of Author ANDRE, Cecile M

Thesis submitted for the degree of Doctor of Philosophy (PhD)

Adsorption Treatment for the Removal of Humic Substances from Drinking Water Supply, using Granular Activated Carbon and Iron-Containing Adsorbents

Cécile M. André

August 2006

University College London
Civil & Environmental Engineering Department
Chadwick Building - Gower Street - London - WC1E 6BT – UK

ProQuest LLC
789 East Eisenhower Parkway
P.O. Box 1346
Ann Arbor, MI 48106-1346

I, Cécile M. André, confirm that the work presented in this thesis is my own. Where information has been derived from other sources, I confirm that this has been indicated in the thesis.

ACKNOWLEDGMENTS

I am very grateful to my supervisor, Dr. Majeda Khraisheh, who kindly reviewed this thesis. Not only did she advise me well but was also a great source of motivation to complete the thesis.

Grateful acknowledgement is extended to Pr. John Gregory, Pr. Andrew Wheatley and Dr. Graham Glasgow, who provided fruitful advice and guidance during the first year of this project. I also want to thank Dr. Caroline Fitzpatrick for her support over these years.

This project would not have been completed without the support of the Engineering and Physical Sciences Research Council, Swindon. EPSRC awarded the research grant number 31239.

Thank you to Tim (whose advice was "just don't do another one!"), Yann and Marius, for being so patient. In their own way, they constantly supported me through the difficult times.

SUMMARY

This thesis investigates the removal by adsorption of potentially harmful natural organic matter, humic substances (HS), from the water supply using three different media; granular activated carbon (GAC), iron-coated alumina (AAFS) and ferric oxihydroxide (akaganeite β-FeOOH).

The adsorbents were characterised using Fourier transform infrared, scanning electron microscopy, pH of zero point of charge and surface area analysis. While GAC is microporous, the two iron-containing adsorbents are mesoporous with low microporosity. Further work is required to investigate media attrition. The HS solutions were fractionated into three ranges of molecular weights (from 0 to 50 kDa) and were characterised by UV absorbance at 254 nm, DOC and the SUVA (ratio UV_{254}/DOC).

Results from the kinetics study indicated that different mechanisms control the adsorption rate at defined stages throughout the process. Five kinetic adsorption models were assessed to describe the adsorbent-adsorbate systems behaviour; pseudo-first and second order models, the Elovich equation, intraparticle diffusion and external diffusion models.

Adsorption in batch systems showed that low molecular weight HS preferentially adsorbed onto GAC whereas heavy molecular weight HS would adsorb better onto AAFS and β-FeOOH. Adsorption capacities were estimated using the Freundlich isotherm. Large residual DOCs were required before adsorption would commence, caused by a non-adsorbable fraction with very low molecular weights. This also led to a minimum residual DOC concentration in the column effluent during continuous flow experiments. Furthermore, significant HS removal was only observed in the columns once a concentration gradient had built up. The Thomas equation accurately predicted the adsorption and the bed depth service time model indicated that contact time is a more important criterion than bed depth.

Finally, simulations of adsorption in the columns were carried out using the computer model GACMan. These were only successful over a narrow range of molecular weights.

ABBREVIATIONS

AA	Activated alumina
AAFS	Iron coated activated alumina
BDST	Bed depth service time
BET	Brunauer, Emmett and Teller
BJH	Barret, Joyner and Halenda
DOC	Dissolved organic carbon
EBCT	Empty bed contact time
FTIR	Fourier transform infrared
GAC	Granular activated carbon
HK	Horvath-Kawazoe
HP-SEC	High pressure size exclusion chromatography
HS	Humic substances
HSDM	Homogeneous surface diffusion model
IAST	Ideal Adsorption Solute Theory
LDF	Linear driving force
MTZ	Mass transfer zone
MW	Molecular weight
MWCO	Molecular weight cut-off
NOM	Natural organic matter
PAC	Powder activated carbon
PES	Polyethersulfone
PSD	Pore size distribution
ROS	Refractory organic matter
SEM	Scanning electron microscopy
SRFA	Suwanee river fulvic acid
SUVA	Specific UV absorbance
TDS	Total dissolved solids
THM	Trihalomethane
TOC	Total organic carbon
UF	Ultrafiltration
UV_{254}	Ultra-Violet absorbance at 254 nm
ZPC	Point of zero charge

TABLE OF CONTENTS

LIST OF TABLES

LIST OF FIGURES

CHAPTER 1

AIMS AND SCOPE OF THE PROJECT

1.1 Introduction

Along with the better knowledge and understanding of water treatment, the demand for water and water quality standards keep increasing. Humic substances (HS) are natural organic constituents of aquatic resources which are always present in natural waters. Some characteristics of HS may give rise to detrimental "health effects" and adverse "aesthetic effects" in the water supply, as well as reducing the efficiency of the water treatment itself. Consequently, humic substances need to be removed during the drinking water treatment, in order to improve the water quality.

Health effects are a major concern for the day to day consumption of water. An intake of a large amount of humic acids might be one of the etiological factors for the Blackfoot disease (Lorenc-Grabowska and Gryglewicz, 2005). In addition, humic substances, depending on their molecular weight and aromaticity, are generally known as precursors for the formation of organic halogen compounds, namely the trihalomethane (THM) formed during chlorine-based disinfection of water. It is suspected that THM may be carcinogenic to humans. Short term and long term chronic toxicity showed a low level adverse effect but chloroform has been found positive on a mutagenicity test (AWWA, 1990). Humic substances react with THM as follows (Montgomery, 1985):

$$\text{Humics} + Br^- + NH_3 + Cl_2 \longrightarrow CO_2 + \textit{New Organics} + \text{smaller humics} + N_2 + Cl^- \quad (1.1)$$

New Organics include THM

According to Bolto et al. (1999), natural organic matter (NOM) concentration is more important than NOM type for THM formation potential, hence the necessity to reduce their concentration.

Humic substances also tend to keep metals in solution via the process of complexation (as explained in chapter 2). Consequently, HS induce an additional health risk in the case where complexation occurs with toxic metals such as heavy metals.

The presence of such natural organic matter in water has also aesthetic effects which are the colour and the taste. As expected from their origin and high energetic functional groups content, humic substances exhibit an earth colour. They give the water its brown colour, which makes it unattractive to drink. As for the taste generated by the same substances, it is indirectly due to the disinfection's sub-products like chloroform, bromoform (AWWA, 1990).

The third problem caused by humic substances in water concerns their interference with specific compounds. According to Ding and Wu (1997), humic substances associate and interact with synthetic organics such as organochlorine pesticides, which increase their transport. This is also applicable to heavy metals.

The wide range of molecular weight and size and both the hydrophilic and hydrophobic behaviour of humic substances interfere with the adsorption of specific compounds during water treatment. Particularly, the breakthrough of a GAC column, to remove geosmin by adsorption, is accelerated very significantly (Montgomery, 1985). The displacement of specific compounds has been observed, due to competition with humic substances (Gu, 1996a,b). Uptake of small organic pollutants, e.g. tricholethylene, was found to be reduced by up to 70% in the presence of natural organic matter (Quinlivan et al., 2005, Wigton and Kilduff, 2004). In addition, the adsorption bed life is decreased when the aim is to remove a specific contaminant (Othman, 2001). This emphasizes the need to understand their behaviour towards adsorption. Hesse et al. (1999) showed, using chromatography to characterise the refractory organic substances, that low molecular weight humic substances were adsorbed first on PAC. The heavier fraction was left in the water, absorbing high levels of UV at 254 nm; it is also the fraction the more likely to react with chlorine to produce THM.

1.2 Aims and objectives of the research

The general aim of this project is to investigate the removal of humic substances by adsorption on inorganic media. More specifically, research is focussed on using new iron based adsorbents and activated carbon, and on the impact of the molecular weight of the organic matter on the efficiency of adsorption. In order to achieve this goal, specific objectives were defined and are presented in chapters 2 to 10, covering the literature review, the characterisation of the humic substances and adsorbents, the kinetics, equilibrium and column studies, and the modelling trials. These objectives are explained in greater detail below:

Chapter 2

This chapter initiates the literature review essential to this project. It focuses on the particular binome "adsorbate-adsorbent" investigated in this work. The adsorbate represents the humic sustances whose origin, composition, characteristics and properties are reviewed. The assessment is useful to select the most relevant characterisation to be carried out on the humic substances used in this investigation. It also briefly reviews the current techniques to remove humic substances from drinking water. The adsorbents are various inorganic materials with specific characteristics and properties which are explained in this chapter.

Chapter 3

The adsorption process is thoroughly reviewed in this chapter. The basic concepts and tools are considered. These are the isotherms, the kinetics, the adsorption models, both in batch or continuous mode. This review of various aspects of adsorption is carried out keeping in mind that the adsorbate is the natural organic matter. Finally, models used in simulation and prediction of humic substances removal by adsorption are briefly reviewed.

Chapter 4

This chapter presents the analytical tools used throughout the project, in relation to the characterisation of the humic substances and of the adsorbents. It also describes the way the kinetics, equilibrium and column studies were set up.

Chapter 5

This chapter examines the characteristics of the adsorbents and the adsorbate (humic substances). Both the chemical and the physical aspects of the adsorbents are examined which will be useful in understanding, interpreting and explaining the adsorption results obtained from the experiments (kinetics, equilibrium and column studies). The four adsorbents considered here are GAC 207C (used as a reference), activated alumina (AA), iron coated activated alumina (AAFS) and ferric oxihydroxide in its beta form (akaganeite β-FeOOH). Their Fourier Transform Infra-Red spectra give information about the functional groups in the samples. The physico-chemical information is the pH of Zero Point of Charge (pH_{zpc}) which gives an indication of the surface charge of the adsorbent. Physical characteristics are the grain size distribution, density, surface area, pore size distribution and Scanning Electronic Microscopy (SEM). As for the humic substances, each fraction is analysed using methods described in chapter four and the most likely conformation of the humic substances in the working solutions is suggested. The investigation also considers the errors done on the measurements and discusses the limits of separation techniques so as to make better use of the analyses performed.

Chapter 6

Various mechanisms take place simultaneously during the process, widely referred to as "adsorption". These cover the several stages whereby an HS molecule travels from the bulk solution to the surface of the adsorbent where it effectively adsorbs, each of which has a specific resistance to adsorption. Since the overall kinetics of the process is limited by the slowest mechanism, it is essential to know which one is dominant. The scope of this chapter is to test several kinetics models (detailed in chapter three, literature review), based on different mechanism assumptions.

Five models are tested. On the one hand, three models consider the adsorption sites as chemical species reacting with the adsorbate. These models are; the pseudo-first and

pseudo-second order models which consider the adsorbent as a homogeneous surface and the Elovich equation model which considers the adsorbent to have a heterogeneous surface (Al-Ghouti, 2004). On the other hand, two models draw attention to microscopic mechanisms of mass transport. These models are the intraparticle diffusion and the external diffusion models. Finally, an error function enables the determination of which model fits the best.

Chapter 7

This chapter is concerned with the adsorption in equilibrium conditions. The classification of the isotherms is first introduced, followed by the experimental results, in terms of DOC and UV_{254} absorbance. These are discussed in sections corresponding to each fraction F1, F2, F3 as well as to the multicomponent adsorbate via F123. The shape of the isotherm is first examined to qualitatively describe the adsorption behaviour, followed by the application of the selected adsorption models (Langmuir, Freundlich and Henry) to fit the experimental data and to calculate the theoretical adsorption capacities.

Chapter 8

Adsorption is widely used as a continuous flow process, where equilibrium cannot be reached for cost and time reasons. In such a situation, breakthrough curves are obtained from the column studies and these are presented in this chapter, in turn for the influents solutions F1 (HS<5 kDa), F12 (HS<10 kDa) and F123 (HS<50 kDa).

The first section of this chapter investigates the influence of the column depth on the extent of adsorption. The second section examines the quality of the effluent treated through a column of GAC, AAFS or β-FeOOH. Finally two analytical models, the Thomas equation and the bed depth service time, are applied and the results are discussed. They simulate the breakthrough, serving two purposes; *(i)* to predict the results and *(ii)* to enable the design of the columns. However there are also thoroughly discussed in view of the particular behaviour of humic matter.

Chapter 9

The computer model GACMan model allows the prediction of the removal of various contaminants (single or multicomponent system) by various adsorbents, in the field of water treatment. The first part of this chapter presents the parametric and concludes on the importance of the parameters to be input in the model. The second part of the chapter relates to the simulation of adsorption. Simulation results are compared to experimental results obtained from the column runs and conclusions are drawn as to the effectiveness of the simulation obtained when using GACMan for this particular study.

Chapter 10

This chapter closes the project by concluding on the results obtained throughout the experimental work and comparing these with relevant external studies. It also opens onto aspects of the research that would require more attention for future work.

CHAPTER 2

HUMIC SUBSTANCES AND THEIR ADSORBENTS

2.1 Introduction

Humic substances are part of the natural organic matter (NOM) found in soil and water. Since they are always present in water resources, it is essential to understand its behaviour so as to target the best methods of removing it from the water supply. The scope of this chapter is to review the origin and composition of humic substances (HS) together with their characteristics and properties. Relevant information to characterise the HS are their molecular weight, size, surface properties and possible reactions.

Current methods to remove such NOM are also briefly reviewed. Finally, since this work will focus on HS removal by adsorption, the essential characteristics of the adsorbents are presented and explained.

2.2 Origin and composition of humic substances

Humic substances, which consist of both dissolved and suspended organic matter, are yellow to dark brown. They are mainly constituted of Carbon, Hydrogen and Oxygen (see table 2.1), and are present in soil, marine waters and estuaries, fresh and groundwaters. Although inorganic compounds dominate quantitatively in soil matter, it is organic matter which has more importance with respect to qualitative aspects and composition evolution (Mustin, 1987). In rivers, lakes and ground waters, which are of interest to this work, humics come from the leaching of soils, sediments, aquatic animal and vegetal life, as well as from the effluents of sewage plants.

Humus degradation (stabilised organic matter) leads to humic substances, which include humins, humic acids and fulvic acids. The latter are the more easily used by microorganisms and as they mature, they form bigger and more complex aggregates, the

Table 2.1 Elemental distribution in humic and fulvic acids

%	Humic In soil[a]	Fulvic In soil[a]	Fulvic in river [b]
C	53.8-58.7	40.7-50.6	53.8
H	3.2-6.2	3.8-7.0	4.3
O	32.8-38.3	39.7-49	40.9
N	0.8-4.3	0.9-3.3	0.7
S	0.1-1.5	0.1-3.6	0.6
P			0.1

[a] Montgomery (1985) [b] Suwannee river, Drever (1994)

humic acids. It is agreed by the literature (e.g. Thurman, 1985) that solubility is the criterion used to classify humic substances into 3 categories:

- Humin: insoluble at any pH
- Humic acids: soluble at pH above 2
- Fulvic acids: soluble at any pH

Humin will not be investigated because of their insolubility in water, hence being less of a problem as regards its elimination.

To understand the presence of humics in water, a simplification of the elements interactions is shown in figure 2.1. In addition to leachate and aquatic fauna and flora decomposition, anthropogenic origin should also be included. This is particularly important when examining sewage treatment plants effluents. Humic substances are also classified according to their origin: peat, soil or aquatic humics are the main categories met.

Since they do not degrade further to a measurable extent over time, humic substances (HS) are also called refractory organic matter (ROS). In some cases, the term "natural organic matter" (NOM) is used, although this also includes petroleum residues and micro-organisms.

Humic substances are the result of microbiological and chemical oxidation, which decompose carbohydrates of the vegetal and animal cells into small units. Vegetal cell walls (lignin and tannins family) are used as substrates for polymerisation and polycondensation. Hence, humic substances are expected to be a mixture of aliphatic and aromatic units with functional groups including carboxyle, ester, alcohol, ether, ketone, phenol, amine, amide, pyridine, pyrrole (Leenheer, 1994). Many models have been suggested for the structure of humic substances. Two of them are presented in figure 2.2. The aromatic structure (figure 2.2a) encloses peptides, carbohydrates, metals, and phenolic acids. The distribution of these functional groups and their environment determine the behaviour of aquatic humic substances. From earlier studies (see table 2.2), fulvic acids are found to have an important aliphatic structure (characteristic groups linked to a straight or branched carbon chain) with many carboxylic groups, and humics have a high aromaticity with many carbonates and phenolic groups.

Cook and Langford (1998) suggested the following models:

- Fulvic:
  - ✓ large relatively immobile structural units (aliphatic and unfunctionalised)
  - ✓ mobile unfunctionalised units (aromatic)
  - ✓ highly substituted functionalised (carbohydrates)
- Humic:
  - ✓ immobile highly substituted units, associated with small aromatics which act for metal binding

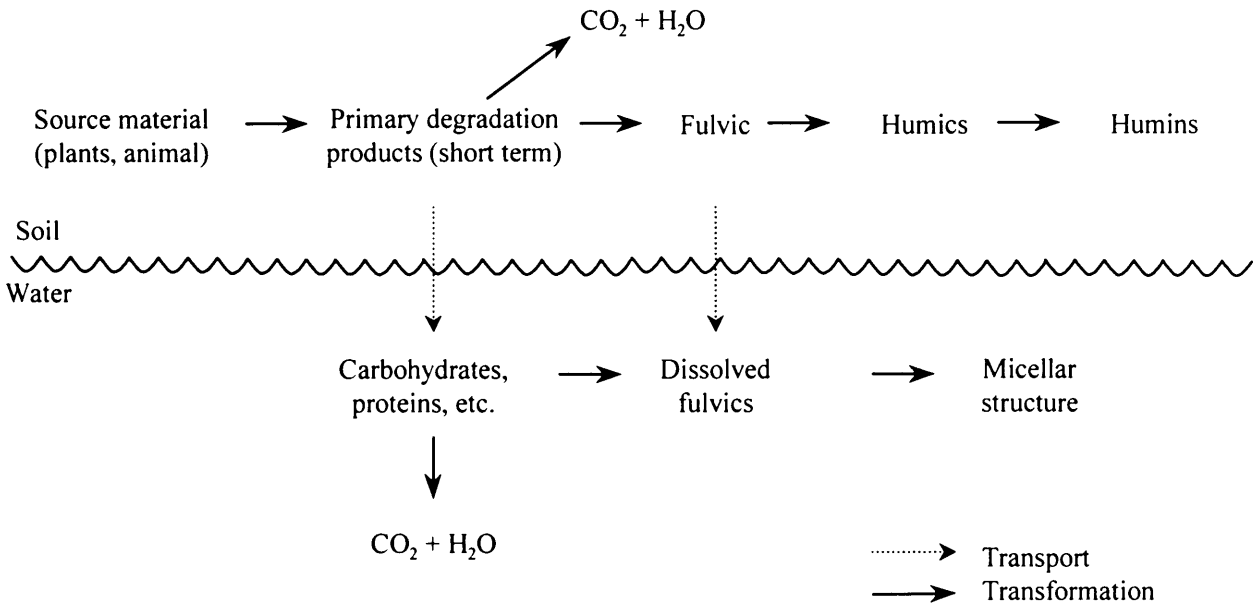

Figure 2.1 Hypothetical interactions between soil and water (Montgomery, 1985)

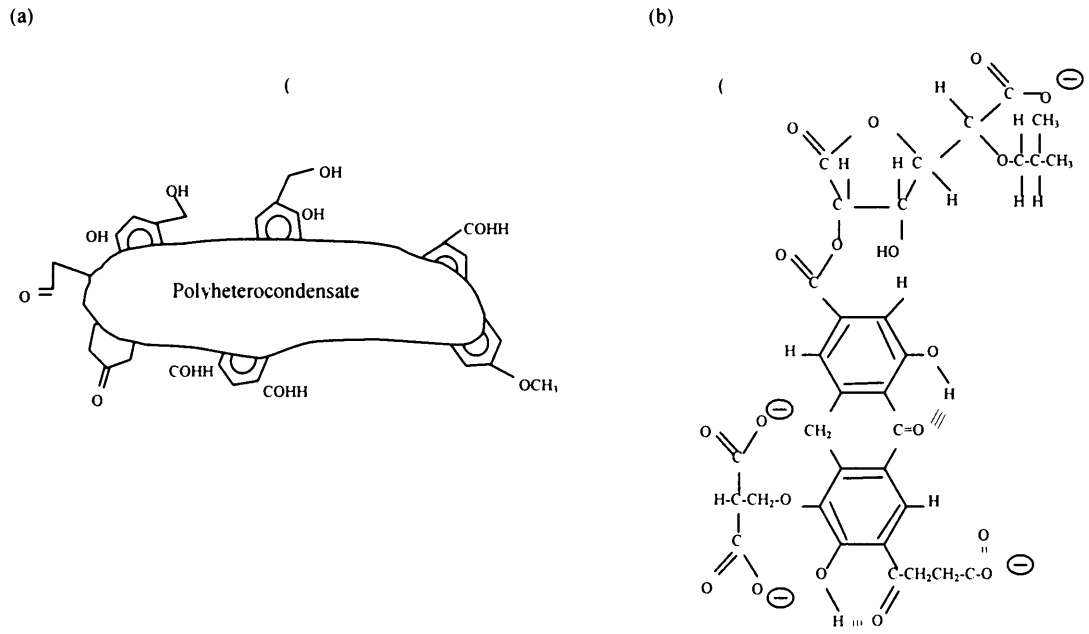

Figure 2.2 Model of humic substances (a) Montgomery (1985) (b) Suwannee river, from Drever (1994)

Table 2.2 Functional groups and structure of humic and fulvic acids

Author (year)	Analysis method [a]	H.S.origin	Results, conclusion [b]
Chin et al. (1994)	HP-SEC	River Commercial	FA: Aromatic increase with MW
Cook and Langford (1998)	NMR	Soil	FA: aliphatic, carbohydrates, carboxylic, very functionalised HA: aliphatic, aromatic
Mc Knight (2000)	Fluorescence	Lake water	Low aromaticity High N content
Myneni et al.(2002)	Soft X-rays, NMR	Aquatic Soil Peat	3 origins: similar groups, different concentrations $\left[\frac{Carboxylic}{Aromatic}\right]_{FA} > \left[\frac{Carboxylic}{Aromatic}\right]_{HA}$ FA: carboxylic, aliphatic HA: carboxylic, aromatic, carbonates, phenolic, ketonics

[a] HP-SEC: High Pressure Size Exclusion Chromatography, NMR: Nuclear Magnetic Resonance

[b] FA Fulvic Acid, HA Humic Acid, MW: Molecular Weight

2.3 Characteristics and properties of humic substances

Understanding the composition of humic substances is a step towards identifying their characteristics and properties. Hayes (1989) states that "humic substances in solution carry a large negative charge and exhibit pronounced charge effects expected of a polyelectrolytic macromolecule". The tendency is nowadays to consider humic substances as superstructures rather than as macropolymers. Such structure only appears to have a large size. It is in fact self-assembled by relatively small molecules held together mainly by hydrophobic dispersive forces (Piccolo, 2001).

2.3.1. Molecular weight and size

The molecular weight of humic substances has been discussed for many years and remains a current research and discussion topic. More than thirty years ago, Cameron et al. (1972) suggested a molecular weight ranging from 20000 to 50000 Da for humic substances. Later Thurman's definition (1985) became the most commonly adopted whereby fulvic and humic acids have a molecular weight ranging from respectively 500 to 2000 Da, and 2000 to 5000 Da. Methods used for such evaluation are gel permeation chromatography, ultrafiltration and the scattering of X-rays or light. Bolto et al. (1999) explained that size exclusion chromatography uses steric exclusion, ionic exclusion and hydrophobic attraction and so it allows to fractionate the HS. Low pressure size exclusion chromatography has been used but showed many inconveniences, e.g. a long separation time. Currently, high pressure size exclusion chromatography (HP-SEC) is used and requires preparative columns. Hesse et al. (1999) used a chromatogram to illustrate the main difference between natural waters (brown water, lake and rivers) and wastewaters: the former contain low retention time organic compounds (i.e. high molecular weight) and the latter are mostly composed of long retention time substances (i.e. low molecular weight). Teermann and Jekel (1999) have shown that reservoir water exhibited a peak for high molecular weight but that, when using artificial fulvic acid solution, no peak appeared at the same retention time. Montgomery (1985) described the size of humic substances as being between 500 pm and 1 nm. However a size of 11 nm for 10^5 dalton humic molecule was suggested when using membrane filtration (Ratnaweera, 1999). Later, Bian et al. (1999) have shown that membrane fouling was due to humic substances larger than 100 nm. In both cases, it situates the larger HS molecules in the low colloidal range, as regards the molecular weight. However, the majority of HS will have a MW within the range which is soluble in water, and it has been shown that observation of these larger sizes were due to the aggregation of humic substances (Lead et al., 2000).

It is necessary to take into account the ionic surrounding of humic substances since charge effects, as described by Hayes (1989) make the molecules expand due to intramolecular charge repulsion. On the other hand, intermolecular repulsion, together with dragging action of the counter ions, also alters the molecules'movement. This is also supported by Sutton and Sposito (2005), who reviewed the molecular structure of humic substances derived from soil; they mention an average molecular mass beyond 66000 Da in a concentrated solution, decreasing to 2500 – 6100 Da in similar but more

diluted solution. Aquatic humic substances were found to have 22.9% of the molecular weight distribution above 10000 Da and 46.3 % below 1000 Da (Kim and Yu. 2005). An aerated groundwater was also found to have a large proportion of its DOC (61%) falling within the range of molecular weight between 4000 and 10000 Da, although this was justified since groundwater contains more soil-like humic substances than superficial waters (Allpike et al., 2005).

Further separation into various ranges of molecular weight is called fractionation. This is carried out in order to investigate the behaviour of each MW range towards adsorption. Each fraction may be regarded as a component during adsorption enabling a multicomponent adsorption model to be applied. Several fractionation methods were investigated:

- High pressure size exclusion chromatography (HP-SEC) provides very accurate separation but it is very slow and does not allow large amounts of solution to be treated. The cost of the specific column is also a limitation to using this method, since very precise separation is not the main objective of this work.

- Centrifugation: humic substances require a long time to settle. In practice, considering the sedimentation coefficient and a centrifuge running at 10000 RPM, 325 hours would be necessary to deposit the molecules of 5000 Da (André, 2003). This makes the procedure unrealistic.

- Ultrafiltration: membranes modules are available as compact units providing a method compatible with a bench scale investigation, which requires less humic substances than a larger scale operation. The membranes are quickly fouled and plugged and can be successfully backwashed and regenerated (following Sartorius technical information sheet's method) which requires less humic substances than a larger scale. This method is also used in water treatment to remove HS from water supply (see section 2.5.3).

2.3.2 Organic carbon content

Of the utmost interest in the field of organic matter and water analysis and treatment technology, is the measure of organic carbon content. Since humic substances do not correspond to a well defined and unique molecule, selecting a good representative and measurable characteristic is not a straightforward task. Total organic carbon (TOC) is

considered as a good "lump index" as it involves the total of the oxidisable organic matter, independently of its composition, biodegradability and oxidation state (Lambert, 1992). The oxidation product is carbon dioxide, quantified by the infra-red absorbance. By filtering the initial solution through a 0.45 μm membrane, the dissolved organic carbon (DOC) is measured instead of the TOC (Standard Methods for the Examination of Water and Wastewater, 1998).

2.3.3. Colour and light absorbance

Chin et al. (1994) found a very good correlation between molecular weight and molar absorptivity and also between aromaticity and molar absorptivity. Absorbance of UV-visible light is due to electronic excitation. The absorption of energy between the ground and excited state is ΔE (h is the Planck constant, c is the light velocity and λ the wavelength):

$$\Delta E = \frac{hc}{\lambda} \tag{2.1}$$

Humic substances exhibit numerous double bonds and aromatic rings, all highly energetic. This corresponds to many possibilities for ΔE, and as a consequence, absorbance at a specific wavelength is not expected. Water absorbs at wavelengths below 190 nm, so that the interest for aquatic humics is in wavelengths which exceed this value. The following aspects are of interest in relation to the structure of complex humic substances (Workman and Springsteen, 1997, Hayes, 1989):

- Carboxylic acids (and also esters) absorb at 205 nm
- Typical UV-Visible-Near Infrared methods are: aromatic, phenols and ketones are characterised by the absorbance at 254 nm; international blue colour is at 440 nm
- pH is very important since by increasing the pH, ionisation increases and so does absorption; this also shifts the absorbance towards higher wavelengths
- Fulvic acids absorb at 280 nm
- Humic substances absorb between 280 and 285 nm, at low pH between 3.4 and 7, due to ionisable COOH and OH

- As regards absorbance in the visible range, the ratio E_4/E_6 (absorbance at 465 nm divided by absorbance at 665 nm) is estimated, using 0.05 M $NaHCO_3$ for a pH~8 and a constant salt concentration. However, absorbance is related to the degree of unsaturation and can be affected by scattering according to the conformation of the molecule (coiled or extended).

In the visible range, humic substances absorb mostly the energetic short wavelengths of light (blue-green between 550 and 600 nm) and appear to us as yellow to dark brown. Absorbance in the visible violet is also used at 420 nm as an indicator HS molecular weight.

UV light absorbance (high energy) is also used as a measure of non-specific organic matter in water. Maximal germicidal effect is observed at 260 nm and the closest monochromatic source is 253.7 nm (254 nm) from the low-pressure lamp (Kulovaara, 1996). Particularly nucleic acids and proteins (specific organic matter) are destroyed in this UV region (Weber, 1972). Consequently, the remaining organic matter is humic substance. The higher the molecular weight, the carbon content and the aromatic to aliphatic structure ratio, the higher the absorbance; this means that humic acids will absorb more UV than fulvic acids. It is important to mention that, as underlined by Montgomery (1985), the wide range of both structure and size of organic matter (including low range for colloidal matter) involve light absorption and also light scattering. This explains the smooth increase of absorbance with the wavelength decrease instead of a peak absorption.

Low molecular weight humics have a high DOC content but absorb little UV. As a consequence, one might notice no decrease in UV absorbance after treatment, although low molecular weights may have been adsorbed. On the other hand, a DOC decrease cannot indicate which type of humic substance has been adsorbed (high or low MW). Therefore, the third parameter of interest is the SUVA index, expressed as the ratio between the UV absorbance (in m^{-1}) and the DOC (in mg/L). It is a good indicator of organic matter composition and reactivity changes, particularly for the kind of humic substances removed (Weishaar, 2001). To measure the extent of the distribution of HS as fulvic / humic acids, the SUVA (Specific UV Absorbance) ratio is extensively used and interpreted (see table 2.3):

Table 2.3 Interpretation of SUVA according to Edzwald and Tobiason (1999)

SUVA	Composition
> or = 4	Mostly aquatic humics High hydrophobicity High MW
2-4	Mixture of aquatic humics and other NOM Mixture of hydrophobic and hydrophilic NOM Mixture of MW
<2	Mostly non-humics Low hydrophobicity Low MW

$$SUVA = \frac{UV_{254}}{DOC} \tag{2.2}$$

This SUVA index will also be intensively used throughout this work.

According to Imai (2001), SUVA is larger for humic acids than for dissolved organic matter, which itself is larger than SUVA of hydrophilic acids (smaller molecules). Allpike et al. (2005) obtained a SUVA close to 5 when they analysed a groundwater which agrees with the high hydrophobicity of tannin-derived substances present in such water. Also, Van Benschoten and Edzwald (1990) mention that a fraction of the DOC does not absorb much light at 254 nm. Therefore, after a water treatment, an increase of SUVA (as an example) can reflect a lower DOC without much decrease in UV absorbance, i.e. the fulvic acids have mainly been removed, whereas humic acids are still present.

Infrared spectroscopy is used more frequently to compare humic substances and understand the structure of these molecules. In particular, OH groups (from phenols or carboxyls) absorb at wavelengths of around 3400 cm^{-1} and characterise the hydrogen

bonds OH···OH. Peaks at around 1600 cm^{-1} are characteristic of Humus. They show the interatomic vibrations in the double bonds: C=C, C=O (acid, ketones or quinone), C=N.

2.3.4. Charge density

Carboxyl is the main organic functional group to dissociate, leaving on the molecule the anionic charge COO^-. Kam and Gregory (2001) have estimated the charge densities on humic substances. Four different methods showed a good agreement, leading to the result of 2-6 meq/g DOC for a commercial humic acid and an extract from water. For fulvic acids only, Edzwald and Tobiason (1999) give a higher figure of 15 μeq/mg C (i.e. 15 meq/g C), however this is very dependent on the pH. In the same range, Fettig (1999a) measured charge densities from 5.2 to 7.6 meq/g DOC, using a cationic polyelectrolyte and a Stream Current Detector for the end point detection.

2.3.5. Reactions of humic substances

Although in general, organic matter on this planet is unstable thermodynamically, humic material is exceptionally stable to oxidant attack, which illustrates that kinetics, and not thermodynamics, is the determining factor in stability (AWWA, 1990). In that context, the wide variety in the structure of humic substances and their origin gives scope for numerous potential reactions as discussed below.

2.3.5.1 Acid-base characteristics

On the one hand, carboxyl groups have a low pK_a, between 3.5 and 5 (pK_a being equal to $-\log K_a$, K_a itself being the ionisation constant for weak acids) which shows the humics' hydrophilicity; on the other hand, phenolic groups have a high pK_a (about 10), which puts forward their hydrophobic side. This makes their dissolution, as presented in equations (2.3) and (2.4) hard to predict:

Dissociation of carboxylic group: $RCOOH = RCOO^- + H^+$ (2.3)

Dissociation of phenolic group: 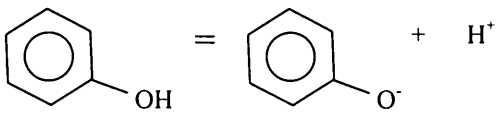 (2.4)

Cook and Langford (1998) described the carboxylic and phenolic groups as being weak in humic substances. The result of this is that humic substances will only be partially ionised in water, according to the ionic environment and the concentration. The acid/base behaviour is also due to the NH_2/NH_3^+ groups.

These acid/base properties, together with the molecular weight consideration, explain why fulvic acids dissolve over a wider range of pH than humic acids, which contain more of a hydrophobic structure like benzene rings. The anionic polyelectrolyte behaviour of HS is consequently expected (see figure 2.2b). In that aspect, the viscosity will be affected according to the pH and the configuration of HS in the water (coiled or extended). Bolto et al. (1999) divided the NOM in 4 fractions: (1) Very Hydrophobic Acids, (2) Slightly Hydrophobic Acids, (3) Hydrophilic Charged of Anionic Material and (4) Hydrophilic Charged of Neutral Material.

2.3.5.2 Oxidation

Oxidative agents attack humic substances by scavenging their electrons. Electronegativity and reactivity of aromatic rings are the main criteria for degradation (Hayes, 1989). In general NOM lose their original structure and are broken into more biodegradable substances such as aldehydes, carboxylic acids and aminoacids (Huck, 1999).

2.3.5.3 Complexation and chelation

In presence of humic substances, iron concentration in water has been found much larger than its solubility would allow (Snoeyink and Jenkins, 1980) which is explained by the complexation of metallic ions by humics. The central ion (metal, cation M^{2+} here) is kept in solution by a ligand. In figure 2.3, an illustration is proposed for the case of humic substances.

Myneni (2002) mentions the importance of humics aggregation, in addition to a coiled (low pH) or elongated structure (high pH). River humic substances formed globular and ring aggregates at high concentration and low pH. The aggregates could be formed at high pH only if multivalent cations were present. In alkaline conditions, the aggregates were dispersed and small. As a consequence, alkalinity and hardness (calcium and magnesium bivalent cations) will play an important role. Under 1mg/L of

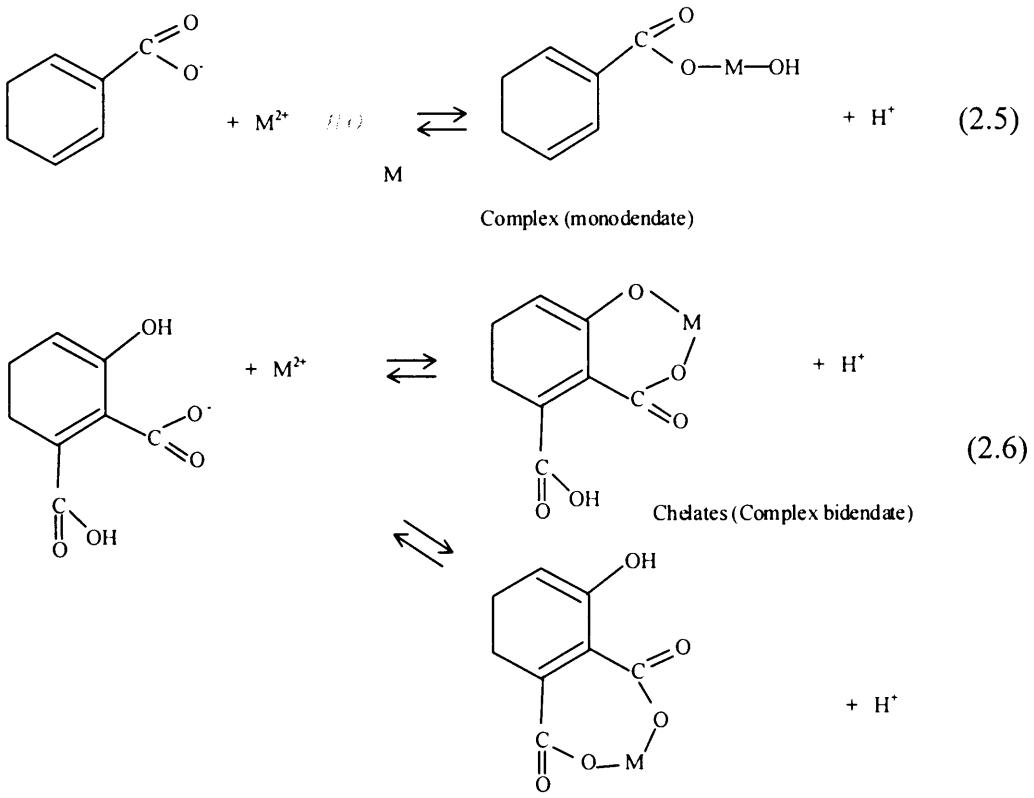

Figure 2.3. Chelation of humic substances

carbon, no measurable structure could be identified. The fractal dimension measures the density of the floc using light scattering. On a log scale graph, the scattering wave vector is plotted against the scattered light intensity (Lee et al., 2005). The linear regression provides a slope which corresponds to the fractal dimension dF. dF was measured by Diallo et al. (2000) and was equal to 2.3 at a pH of 5, showing a reaction limited cluster cluster aggregation (RLCCA), i.e. a slow aggregation leading to a dense aggregate. A higher pH led to a lower fractal dimension (1.8-2) meaning a diffusion limited cluster cluster aggregation (DLCCA), with an open aggregate (fast).

To summarise humic substances behaviour in water: they dissociate and ionise; they undergo oxidation and form complexes with metallic ions. In addition, Vermeer et al. (1998) specify that, as macromolecules, humic substances will also have the behaviour of polyelectrolytes, i.e. lateral repulsions and conformation are to be considered. These aspects, in the context of water treatment, explain the operations used to remove such organic matter and are particularly relevant to the adsorption process. This will be extensively reviewed in the next chapter.

2.4. Concentration of humic substances in water

According to Bolto et al. (1999), groundwater contains more high molecular weight humic substances than surface water, possibly due to the fact that the less hydrophobic compounds has also adsorbed soil. This is unexpected since high molecular weights are more hydrophobic and therefore adsorb better. Nissiken et al. (2001) found that groundwater mainly contained intermediate and small fractions of molecular weights, while lake and river water contained large and intermediate fractions. Such controversial observations lead to extra careful considerations as regards the experimental conditions. On the other hand, river water and even more so, reservoir water (older water), is exposed to UV light, which provides energy to polymerise fulvic acids into heavier and more mature humic substances. It is generally agreed that in water, fulvic acids account for the largest fraction of natural organic matter. According to Thurman (1985), 50% of the DOC in natural water is due humic substances, most of which (half to three quarters) have molecular weights between 1000 and 2000 Da. The other 50% are due to hydrophilic acids and identifiable simple compounds (Imai, 2001).

According to Graham (1999), two main categories of surface water can be used to qualitatively describe humic substances:

- Lowland water (high hardness, alkalinity>200 mg/L (as $CaCO_3$), pH>7, moderate colour and turbidity): low to moderate contribution of humic substances to NOM
- Upland water (low total dissolved solids, alkalinity<50 mg/L, low pH and turbidity): very high contribution of humic substances to NOM

Typical DOC concentrations are given by Drever (1994):

- Rivers and lakes: 2-10 mg/L
- Rivers draining swamps and wetlands: 60 mg/L
- Groundwater and ocean: 0.5 mg/L
- Soil water: up to 260 mg/L

It is wise to mention here that it is not always possible to use natural water in experimental investigations. Suwannee River fulvic acids are often used for research purposes. Lambert and Graham (1995a) used extracts of natural English water.

Dissolved matter from surface water was extracted using reverse osmosis and lyophilisation (freeze dry). As seen in table 2.4, they compared this reconstituted water with the fresh raw upland water, and with a commercial humic acid (soil-derived humics). The reconstitued water was obtained by the freeze-drying method described by Lambert (1992) and then redissolved in deionised water.

Table 2.4 Comparison of characteristics for various samples (from Lambert and Graham, 1995a)

	Raw upland water	**Reconstituted water**	**Commercial humic acid**
Mass reconstituted (mg/L)	n.a.	110	24
DOC (mg/L)	7.98	8.78	7.78
UV_{254} abs. (m^{-1})	37.25	36.10	68.00
SUVA	4.67	4.11	8.76

These figures show a good reconstitution of the water. The commercial humic substances contained more UV absorbing compounds than natural water and its extract, meaning (as confirmed by SUVA) that it contained mostly high molecular weight humic acid. This is due to the soil origin of the commercial substances. Lambert and Graham (1995a) confirmed this by measuring the proportion Humic / Fulvic. This ratio was 1 / 9 for both raw and reconstituted waters, and 7 / 3 for commercial humic substances.

However, working with the same humic substances extracts, Kam and Gregory (2001) confirmed a poor reconstitution of the water: 200 mg/L of extract provided 16.2 mg DOC /L, most of the humic substances remaining insoluble. This observation raises the question of the best way to mimic humic substances and the effect their background has on their properties. The origin, the age and the handling of the substances, bring differences in their behaviour. This is also mentioned by Teermann and Jekel's results

(1999) when working on a pilot plant (i.e. raw water): a rapid breakthrough of the adsorbent bed occured due to fulvic acids. This was unexpected from laboratory results. Guo's results (2001) agree by observing the breakthrough in a soil packed column to be slower for high MW than for low MW.

2.5 Brief review of humic substances removal using physicochemical processes

2.5.1 Coagulation

Colloids are particles from 1 nm to 1 μm with surface charge which is usually negative (Reynolds, 1982). Their brownian motion together with the Van der Waals forces explains the stability (and turbidity) of a colloidal suspension. By breaking such stability (coagulation), the colloids can be separated from the solvent water. Humic substances are in some respects similar to colloids since they also present negative charges. The largest molecules may reach the low size range for colloids and can therefore be seen as colloidal solutions. They also have long chains, can form aggregates and bridging can be considered to occur, although this was shown not to be the main mechanism (Kam and Gregory, 2001).

When coagulant (metallic salt like alum, ferric chloride) is added to water, it breaks the stability of the colloidal solution by screening the surface charges of the suspended matter. Similar idea can be applied to humic substances. Hence the interest of using cations to remove the NOM.

It has been shown that pH and temperature play a fundamental role in the removal of HS (O'Melia et al., 1999,Van Benschotten and Edzwald, 1990). Cations such as Ca^{2+} and Mg^{2+} can cancel the charge of humic substances and therefore, hardness is the third decisive parameter as regards the efficiency of HS coagulation (O'Melia et al., 1999). It has also been observed that the higher the molecular weight of NOM, the better its coagulation (Krasmer and Amy, 1995; Eikebrokk, 1999; Ratnaweera, 1999; Chow et al., 1999; Edzwald and Tobiason, 1999) as seen from table 2.5.

Table 2.5 Coagulation efficiency for DOC removal

MW	Coagulation	DOC removals
High	NOM controls	>50% for alum
	Good DOC removals	Little greater for Ferric
Medium	NOM influences	25-50% for alum
	DOC removals should be fair to good	Little greater for Ferric
Low	NOM has little influence	<25% for alum
	Poor DOC removals	Little greater for Ferric

2.5.2 Filtration (biofiltration)

If DOC is mainly due to humic substances, between 9 and 15% may be removed by slow sand filtration (the corresponding mean Colour and UV_{254} removal levels are respectively 42% and 18%) according to Graham (1999). Hozalski et al. (1999) obtained up to 60% of DOC removal for MW less than 1000 Daltons. However, there is little history in studying a clear relationship between biofiltration and humic substances removal. With more and more stringent water quality standards, biofiltration requires improvement for correct removal of humic substances. Currently, attention is focussed on oxidation, particularly ozonation, and also adsorption as possible means to improve biofiltration. Adsorbed natural organic matter (NOM) increases the colloids stability; ozone oxidises NOM and modifies its conformation on the adsorbing particles used as the adsorbent; the new conformation brings colloidal particles to destabilisation (Becker et al., 2001), and hence a significantly reduced particle count in the filtered water.

2.5.3 Membrane filtration

Filtration using membranes is a technique increasingly being used because of its high efficiency and its ease of use. It is also rather insensitive to influent water quality change. The choice of membranes for humic substances removal is difficult, since the molecules of interest cover a broad range of sizes, and the Molecular Weight Cut Off (MWCO) is a major element that defines the membrane (Thorsen, 1999). Mainly ultrafiltration and nanofiltration (better removal) are used.

Membrane filtration can be used to fractionate humic substances, which will be of interest in this project as it enabled work to take place on various ranges of MW. Mainly ultrafiltration and nanofiltration are used. In Norway and Great Britain, cellulose acetate membranes are mostly used, due to their low cost and high hydrophilicity which reduces the fouling (Thorsen, 1999). A correspondence between ultrafiltration membrane MWCO and pore diameter is shown in table 2.6:

Table 2.6 MWCO – pore diameter relationship

MWCO (Kdalton)	**Pore diameter (nm) By Ratnaweera et al. (1999)**	**Pore diameter (nm) By Thorsen (1999)**
5	2.5 (extrapolated)	1.6
10	3.5	2.7
50	8	6.9
100	11	10.2

The main problems met during filtration by membrane are fouling and the operation of the process. The treatment shows a quick reduction in the product flow and a pressure drop along the membrane. Marteens et al. (1999) used capillary polysulphone membranes and observed a colour removal dropping quickly from 85% to 75% (approximately) with the flux dropping to 60% of its original value. Amy and Cho (1999) studied the interactions between NOM and several types of membrane. As

expected, nanofiltration removed NOM better than ultrafiltration. The rejection mechanism is interpreted to be electrostatic exclusion (the more negative ζ potential, the more negative charges on the humic substances) and steric exclusion, particularly for nanofiltration. NOM characteristics affected the fouling more than the flux. Their results show that hydrophilic NOM are the main foulants; in particular, polysaccharides and fragments of bacteria. Ca^{2+} and low pH slightly improved the rejection. According to Thorsen (1999), inorganic ions can also be retained in the smallest pores, and coagulate the HS which in turn block the pores.

2.5.4 Ion exchange

Anionic exchange resins allow the ionised humic molecules (L^-) to swap as follows:

Strong base resin: $R_4N^+OH^- + L^- = R_4N^+(L^-) + OH^-$ (2.7)

Weak base resin: $R_3N + H^+Cl^- = R_3NH^+Cl^-$ (2.8)

$R_3NH^+Cl^- + L^- = R3NH^+(L^-) + OH^-$ (2.9)

Similar reactions take place during adsorption when ligand exchange and complex formation occur with surface components of the adsorbent.

From a review written by Fettig (1999b), strong anionic resins are of particular interest, involving the ions chloride and sulphate, together with the organics. A non-removable fraction of NOM remains after regeneration (up to 40%). Sorption on anionic exchange resins has been studied more in comparison to GAC use. In that context, they show a more homogeneous removal of NOM.

In general, improvement and studies involving resin exchange process are linked to adsorption processes, since both treatments use sorption based principles.

2.5.5 Summary

Zhou and Smith (2001) foresee membrane and oxidation techniques using UV, Hydrogen peroxide or Ozone, to be the next generation of methods to remove organic

matter. In 1999, Ødegaard published a review of several processes used in Norway to remove humic substances. The comparison shows:

- Coagulation / filtration is cheap to operate, but difficult to control; only when using a 3 media filter (anthracite, sand and $CaCO_3$), are results in general satisfying in most aspects
- Membrane filtration has the highest cost of operation, but gives more satisfying results, with regards to efficiency and ease of use. It is also rather insensitive to influent water quality change
- Ion exchange was not as efficient as expected and would need more pre-treatment

Adsorption has not been mentioned yet. As a traditional treatment, it needs innovative aspects like using inorganic adsorbents in order to be able to apply it to non-specific organic matter. This is the main interest of this work and the characteristics of potential adsorbents are presented in the next section.

2.6 Adsorbents for humic substances

Adsorption is a surface phenomenon. Consequently, the adsorbents are selected according to their surface characteristics. The relevant criteria to choose an adsorbent include *(i)* physical characteristics such as surface area, porosity and pore size distribution which will be described below, *(ii)* chemical characteristics such as surface functional groups analysed from Infrared Fourier Transform spectra (FTIR), and *(iii)* physicochemical characteristics including the Zero Point of Charge (ZPC). FTIR and ZPC are not reviewed in this section, the methodology for their application is described in chapter 4. Additional practical characteristics when studying the installation of a full adsorption process system are the capacity to withstand regeneration and dissolution in solvent and friability.

2.6.1 Adsorbent types

Traditionally, activated carbon is the most commonly used adsorbent. It is economical and efficient. Although its surface is slightly negative (between –0.4 and 0 mmol/g according to Newcombe, 1999) it is considered as non-polar and not very selective, which is why it is widely used (e.g.: hydrophobic pesticides removal). Activated carbon

presents a very high surface area, up to 1500 m^2/g, either for GAC (granules) or PAC (powder), and the pore size usually covers the range of; macropores (>25 nm), mesopores (1-25 nm) and to a lesser extent, micropores (< 1 nm, hardly accessible for most sorbates) (Montgomery, 1985). GAC is easier to regenerate and to handle and its grain size ranges from 0.25 to 3 mm (Degrémont, 1989). Dissolution of activated carbon does not occur, but a high friability can bring some loss of adsorbent. Activated carbon can also host microorganisms and partly acts as a biological filter. Biologically activated carbon was found more efficient than GAC or PAC to remove the low molecular weight fraction of humic substances (Nissinen, 2001). This can be explained by the microbial activity which involves small, rather than large molecules. To be efficient and eliminate all adsorbates (microorganisms and others), regeneration is done thermally, using temperatures of up to 1000°C. This represents the main disadvantage since it means the filters must be emptied and the carbon transported, treated and brought back on site. However, Heijman (1999) has regenerated carbon chemically and observed good results.

Modifications to GAC can also significantly increase the natural organic matter adsorption. Cheng et al. (2005) applied two parallel treatments to the activated carbon *(i)* the carbon surface was impregnated with iron and *(ii)* the carbon was treated with nitric acid and ammonia (leading to etching of the surface). Both treatments resulted in a higher uptake of humic substances, showing that the surface chemistry and the pore size are two aspects that can be improved.

Compared to activated carbon, inorganic adsorbents are fairly new. These are activated aluminas (mainly hydroxyl groups on the surface) and other metallic oxides (like iron). Their surface area is only 300-400 m^2/g (Degrémont, 1989) or less (~ 180 m^2/g according to Lambert and Graham, 1995a) but they are more specific and remove more polar compounds. As a consequence, one can expect them to adsorb humic substances well. They can be regenerated on site, chemically and therefore are of greater interest for water treatment.

In 1994, Gu et al. used hematite (α-Fe_2O_3) to adsorb NOM from a swamp water and Suwannee River fulvic acid and obtained from 0.176 to 0.329 mg TOC/m^2. Vermeer et al. (1998) found that the hematite particle diameter did have much influence on the adsorption with regards to the conformation of the adsorbed macromolecules. Lambert and Graham (1995b) compared activated carbon to activated bauxite, χ-alumina and γ-

alumina. On a raw water, activated carbon adsorbed up to 27.5 mg DOC/g, compared to 3.2 to 4.4 for the three inorganic adsorbents, under the same conditions. However, after ozonation, the carbon capacity decreased significantly and was not better than inorganics, whose capacity reached 6.03 mg DOC/g (bauxite). Heijman et al. (1999) used iron oxide (Darco); its capacity was around 1 mg TOC/g only and required 20 minutes contact time for the same removal compared with 1.7 minutes for activated carbon. The regeneration of the oxide (both adsorbents at 60°C, for 20 hours, with NaOH) proved to be inefficient, which resulted in a very short life for this adsorbent.

In 1999 too, Teermann and Jekel (1999) used highly activated granulated β-FeOOH (0.32-2 mm), ground and sieved to an average size of 11 μm. The Zero Point of Charge corresponded to a pH of 8. Initially, the specific area was 280 m^2/g with 97% of the pore size below 6 nm. The removal of DOC reached 90 % and the capacity of the β-FeOOH was 30-60 mg DOC/g. The performance of this adsorbent will be of particular interest for further studies, although only fulvic acids were tested. Very recently, Seida and Nakano (2000) used hydrotalcite and hydrotalcite-like compounds, where an anion is inserted between two hydroxide layers. A very slight dissolution of the adsorbents acted as a pH buffer. 98% of humic substances was removed due to strong binding forces and as a consequence, regeneration was poor (using Na_2CO_3 or NaOH).

Sander et al. (2004) showed the efficiency of metal oxides to adsorb the humic substances. They measured the force between two oxide surfaces (Fe and Al) with atomic force microscope (AFM) and found that in the presence of HS, the same forces were measured for aluminium or iron oxide proving that the true surface properties were masked. The mask could only be adsorbed HS. Silica adsorbents also had their surface modified by the addition of iron, resulting in good adsorption of humic and fulvic acids (Moriguchi et al., 2005).

Another type of adsorbent is obtained through the coating of hard supports (sand, alumina). For example, iron coated olivine has been found efficient in removing NOM by Chang et al. (1997).

In some cases, the adsorbent is readily used without any preparation (e.g. iron oxide used by Gu et al. in 1994). In other cases, a thorough preparation was carried out using NaOH, followed by HCl wash and $CaCO_3$ conditioning for two weeks (Lambert and Graham, 1995a). Sometimes a strict procedure was followed to synthesize the adsorbent

(see Atkinson et al. (1967) for goethite, Avena and Koopal (1999) for iron and aluminium oxides, Fettig and Sontheimer (1987a) for activated carbon purification). This way, the adsorptive characteristics of the adsorbent are optimised for the experiments. However, such treatment might be problematical as regards a continuous process and regeneration in-situ.

Table 2.7 shows the efficiency of removal of humic substances by adsorption when using activated carbon or activated alumina. The variability of the results is evidence of the importance of experimental conditions. Most of the results are from batch tests and it might not be possible to reach such an equilibrium in a continuous process. However, it is noticed that activated alumina is a promising inorganic adsorbent. These results show that inorganic adsorbents can be effective for humic substances removal, but still need investigation to be used, and controlled on a full scale.

2.6.2 Surface area

The surface area of the adsorbent is given by the number of gas molecules saturating a monolayer. Brunauer Emmett Teller (BET) isotherm BET is the standard equation for determining the surface area from inert gas adsorption data. However it is known not to be theoretically correct, as it assumes there is no limit to the number of adsorbed layers. It considers the rate of adsorption to be proportional to the pressure and to the number of free adsorption sites. It is also equal to the desorption rate. Both rate constants k_a and k_d involve a frequency factor and a Boltzmann factor (k_B is the Boltzmann constant) which refers to the interaction energy between adsorbent and adsorbate (E_i) and to the vaporisation energy (E_v), the temperature T (in Kelvin) and ν the frequency factor:

$$k_a = \nu e^{-E_i/k_B T} \quad \text{for the adsorption} \tag{2.10}$$

$$k_d = \nu e^{-E_v/k_B T} \quad \text{for the desorption} \tag{2.11}$$

Finally the BET equation is obtained:

$$\frac{P/P_0}{V(1-P/P_0)} = \frac{1}{V_m C} + \left(\frac{C-1}{V_m C}\right)\left(P/P_0\right) \tag{2.12}$$

Table 2.7 NOM removal efficiency by adsorption

Authors	Adsorbent	Initial DOC	% removal	Loading
Lambert and Graham (1995a)	PAC (1 gL^{-1})	~ 8 mgL^{-1} (batch exp.)	69% DOC 75% UV_{254}	~5.52 mg DOC g^{-1}
	AA (1 gL^{-1})		46% DOC 47-63% UV_{254}	~3.68 mg DOC/g
Heijman et al. (1999)	GAC (154 mg/l)	2.4 mgL^{-1} (batch exp.)	72% UV_{254} and 30% after 4th regeneration	10-30 mg DOC g^{-1}
	Iron oxide (2.04 gL^{-1})		72% UV_{254} and 10% after 4th regeneration	1-3 mg DOC g^{-1}
Fettig (1999a)	AC AA	5 mgL^{-1} (batch exp.)	20-80% DOC	65 mg DOC g^{-1} 20-30 mg DOC g^{-1}
Teermann and Jekel (1999)	β-FeOOH	25-37 mgL^{-1} (batch exp.)	Up to 90% DOC	30-60 mgDOC g^{-1}

$$C = e^{(Ei-Ev)/k_B T} \qquad (2.13)$$

with P/P_0 = Relative pressure

V = Volume adsorbed as [cm^3/g]

V_m = Volume monolayer [cm^3]

Considering equation 2.12 as $y=ax+b$, a straight line (over a limited range of P/P_0) is obtained when plotting y vs x. The value of C affects the shape of the isotherm. As C increases, (i.e. the heat of adsorption is larger), the adsorbed first layer is adsorbed more strongly (as type I isotherm in figure 3.3 in chapter 3, section 3.4.1.1). A weaker adsorption corresponds to lower C value, with an isotherm more like type III. Then, the adsorbent surface area SA is calculated taking into account the area occupied by one molecule of nitrogen N_2:

$$SA(m^2/g) = \frac{V_m(cm^3/g)}{22414(cm^3/mol)} \times N_a \times 16.2 \times 10^{-20}(m^2/molecule) \qquad (2.14)$$

with (Sawyer et al., 1994):

V_m: massic volume of the gas [$cm^3\ g^{-1}$]

22414 $cm^3\ mol^{-1}$: molar gas volume in standard conditions

N_a: Avogadro constant = 6.023×10^{23} molecules mol^{-1}

16.2×10^{-20} m^2 $molecule^{-1}$: surface covered by a Nitrogen gas molecule (N_2)

The result provides essential information as regards the efficiency of an adsorbent. Progressive filling of the pores by the inert gas corresponds to the filling of different pore diameters. Information supplied during such analysis enables the estimation of the pore size distribution.

At this stage, it is worth mentioning the t-plot to estimate the external surface area as well as the micropore area. Such plot uses the relative pressure varying with the adsorbed volume, as described above for BET isotherm. The statistical thickness of the adsorbed layer is calculated using Harkins and Jura equation expressed below (Marczewski, 2002):

$$t = \left(\frac{13.99}{0.034 - \log\left(\frac{P}{P_s}\right)} \right)^{0.5} \qquad (2.15)$$

with t: Statistical thickness [nm]

P/P_s: Relative pressure (P_s is the saturation pressure)

As the pressure is increased, the calculated t value increases too, and so does the adsorbed volume. The graph of t vs the adsorbed volume is called the t-plot. For values of t between 0.354 and 0.5 nm (which corresponds to a monolayer and a relative pressure between 0.1 and 0.2 according to Marczweski, 2002), points can be connected by a straight line on the plot. This line corresponds to the total adsorbed volume. Since micropores are assumed to be filled in that pressure range, the slope of the line corresponds to the external surface area and the intercept represents the volume adsorbed in the micropores. This reasoning is expressed by the De Boer equation (Marczewski, 2002), for each relative pressure:

$$V_{ads} = V_{micro} + kS_{ext}t \tag{2.16}$$

with t: Statistical thickness calculated by equation 3.6 [nm]

V_{ads}: total adsorbed volume [$cm^3\ g^{-1}$]

V_{micro}: volume adsorbed in the micropores (intercept) [$m^3\ g^{-1}$]

k: adjusting coefficient according to the units used

S_{ext}: external surface area (pores larger than micropores) [$m^2\ g^{-1}$]

Once the external surface area is calculated from the slope, its value is subtracted from the total surface area estimated by the BET method (described above by equation 3.5). The result is the micropore area.

2.6.3 Pore size distribution

Pore size distribution in the adsorbent is an essential characteristic to select the most relevant material. Mainly two methods are used, namely the Barrett, Joyner and Halenda method (BJH) which focuses on the mesoporous range and the Horvath and Kawazoe method (HK), more relevant to the micropore range.

The BJH method is based on the Kelvin equation (equation 2.17) and relates the relative pressure of the nitrogen gas in equilibrium with the adsorbent to the size of the pore where the capillary condensation takes place (Sing, 2001):

$$\ln\left(\frac{P}{P_s}\right) = \frac{-2\gamma V_m}{r_K RT} \qquad (2.17)$$

with P/P_s: relative pressure (as in equation 2.12)

r_K: pore radius [m]

γ: surface tension of the condensed phase [J/m^2]

V_m: molar volume of the condensed phase [m^3/J]

R: gas constant [8.3145 J/mol.K]

T: temperature [K]

The essence of BJH method is to replace the radius of the capillary in the Kelvin equation by the radius of the pore, minus the adsorbed layer thickness (Ravikovitch et al., 1998). Differences in pores size distribution are observed according to the data used, adsorption or desorption figures. These are attributed to the fact that BJH method was developed for open-ended cylindrical capillaries when the real pores might have a different shape (Marczewski, 2002).

The HK method is applicable to micropores and also relates the amount of gas adsorbed (via the partial pressure) to the pore width, by means of suitable theoretical calculations involving the free energy changes during adsorption (Ravikovitch et al., 1998). As a logical extension of BJH method, it assumes that the gas condenses to fill the slit-like micropores, although the mechanism is in fact more complex and the pores might have a different shape (Jarionec et al., 2003).

2.7 Conclusions

Humic substances represent a wide range of non-biodegradable organic matter that needs to be removed from drinking water supply. They are constituted of numerous organic functions, particularly carboxylic and phenolic groups that confer on them properties, such as the ability to ionise and to form complexes with metallic salts. Consequently, they can coagulate and be filtered through biofilters or membranes.

However, they cover such a large molecular weight range (from one to several thousands daltons) that a unique and excellent removal mechanism is hard to find and investigation in this area is required. As described in this chapter, their numerous physico-chemical properties favour a surface mechanism such as adsorption. The adsorbents need to present a favourable surface area with a wide pore size distribution such as the wide range of MW is able to penetrate the porous structure. A good adsorbent should also present a favourable zero point of charge and a variety of functional groups able to ionise.

CHAPTER 3

ADSORPTION MECHANISMS, THEORIES AND MODELLING

3.1 Introduction

Water treatment to remove humic substances can be a chemical, physical or most frequently, a physicochemical process. Adsorption involves several concepts which will be reviewed in this chapter. "Adsorption is the process of collecting soluble substances that are in solution on a suitable interface" (Metcalf & Eddy, 1991). The particular interest of this study is related to the interface between a liquid (water, the solvent) and a solid (the adsorbent). Important aspects related to the adsorbent and to the adsorbate (here the "contaminant" humic substances) have been described in the previous chapter.

But how does adsorption actually take place, under which conditions and mechanisms and how fast is it? Answers to these questions require an understanding of the kinetics and equilibrium adsorption models which are described in this chapter. Continuous processes in columns, together with the prediction of the results, are also of upmost interest to water companies and industries, and are reviewed in the last sections of the chapter.

3.2 Mechanisms of adsorption

The mechanisms involved in adsorption are: anion exchange, ligand exchange and surface complexation, hydrophobic interactions, entropic effect, hydrogen bonding and cation bridging (Gu et al., 1994). It is difficult to know which mechanism is dominant over another.

As stated earlier, humic substances characteristics make them prone to adsorb onto polar and non-polar compounds as well as to exchange anions. Newcombe (1999) summarised the aspects of NOM which play a major role in adsorption: molecular weight distribution, distribution of the hydrodynamic diameter of the molecules, hydrophobicity/hydrophilicity, charge distribution and groups capable of hydrogen bonding with the carbon surface. Most difficult to deal with is the "multi-solute aspect of humic substances" (Newcombe, 1999). Single solute adsorption is not relevant here due to the wide variety of natural organic matter. Hence, simple isotherms (Langmuir, Freundlich or Henry's, as detailed in section 3.4.1 of this chapter) might need transformation, to be applicable to this particular adsorbate. Evanko and Dzombak (1998) encountered difficulties simulating humic substances: although the trends for adsorption were similar when using series of simple organic acids, the adsorption parameter values were very different.

Since water is a polar solvent, hydrophobic compounds will tend to escape and adsorb easily. pH and ionic strength are the main parameters. A lower pH results in more protons surrounding the HS molecules, which in turn ionise less. Consequently, HS become less hydrophilic and have an increased tendency to escape from the water by adsorbing more. Similarly, Lead et al. (2000) measured the hydrodynamic radius by Fluorescence Correlation Spectroscopy to be, respectively for Suwannee River fulvic and humic acids, 1.5 and 1.7 nm. The radius of both acids increased to 2.1 nm when decreasing the pH. A higher pH, on the contrary, made the humic substances more soluble and did not favour adsorption. This has been observed experimentally by most of the references cited here. However, Teermann and Jekel (1999) found that the pH had little influence when fulvic acids adsorbed onto iron oxide.

Ionic strength is the second parameter with a strong influence on adsorption. The aspects linked to this are cationic bridging, the double-layer compression around the molecules and the conformation of the HS as a polyelectrolyte in solution. In most of the research works, the ionic strength was adjusted with NaCl, $NaNO_3$, Na_2SO_4, Na_2PO_4, $Ca(NO_3)_2$ or $CaCl_2$. The adsorption was increased when the ionic strength increased, according to Fettig (1999b). Salts screen the mutual repulsion between the adsorbed humic acid molecules. The alkalinity and hardness can also be adjusted so as to change the calcium concentration or to mimic a real water. Teermann and Jekel (1999) observed that Ca^{2+} allowed a better removal of smaller humic substances. It is

worth mentioning at this point that cationic bridging could explain the aggregation of humic substances. This can explain the existence of some "oversized" humic acid molecules, measuring several hundreds of nanometers (cf MWCO for membranes). Weber et al. (1980) also insisted on the necessity of using natural water (or mimicing its ionic background) for humic substances adsorption trials, since they found that tap water enhanced adsorption compared to distilled water.

If the adsorbent is a metal oxide (iron or aluminium in general), a chemical approach gives particular weight to surface complexation. Gu et al. (1994) defined the adsorption to be chemisorption when the heat generated was more that 20 kJ/mol, and physisorption otherwise (around 25 kJ/mol for H bond and less than 9 kJ/mol for dipole-dipole interaction). They also suggested that the principal mechanism for HS chemisorption is ligand exchange, most probably with the carboxylic and phenolic functional groups. In1998, Evanko and Dzombak agreed with this suggestion. Seida and Nakano (2000) propose a 2 step process for humic substances adsorption onto hydrotalcite: *(i)* humic molecules adsorb and *(ii)* humic molecules coagulate with aluminium or iron hydroxides (due to hydrotalcite slight dissolution) together with an anionic exchange between the humic substance and the intercalated anion (typical hydrotalcite).

Newcombe (1999) found the adsorption (pH~3, activated carbon) to increase directly with the pore volume. In agreement with Morris and Newcombe (1993), it was found that the degree of ionisation on the adsorbed NOM decreased as the surface concentration increased. It shows that as the surface becomes saturated, the adsorption mechanism changes, shifting from a strong electrostatic attraction initially to a physical adsorption, with the carboxyl groups remaining away from the surface. The Zero Point of Charge (PZC) of γ-Al_2O_3 equal to 9-9.1, which explains why no NOM adsorption occurs if the pH is above 9.1 (negative surface above the ZPC).

When using clay, Specht et al. (2000) found that the pH would not influence the quantity of NOM, but it would influence its type (high MW better adsorbed). Calcium concentration and zeta potential did not influence the adsorption on alumina either, providing evidence of physical rather than chemical adsorption. In 1985, Thurman described the adsorption of NOM to alumina as based on hydrogen bond and weak ion exchange, while with adsorption onto iron hydroxide, the ligand exchange mechanism is more important. Fe^{3+} can replace Al^{3+} in the alumina lattice, enabling some adsorption.

In reality, all of the cited mechanisms are likely to occur, either simultaneously or sequentially. Kinetics associated with the mechanisms are fundamental in the understanding of the adsorption phenomenon. Information on the mechanisms of adsorption can also be obtained from the best fitting adsorption models. These aspects are detailed in the section below.

3.3. Kinetics of adsorption and kinetics models

3.3.1 Rate of adsorption and rate limiting step

If the adsorption of humic substances is thermodynamically favoured, kinetics can be described as a four step process listed as below (AWWA, 1990, Montgomery, 1985). A resistance is associated with each step, which is also represented in figure 3.1. The largest resistance corresponds to the slowest step and will consequently determine the overall rate-limiting step to adsorption:

1. **Advection** (due to the bulk transport or water flow): transport of the humic substance very close to the adsorbent surface, to the diffusive layer (concentration of humic substances becomes large).

2. **Film, or external diffusion** (due to gradient of concentration in turbulences): transport of the humic molecule across the diffusion film (or hydrodynamic boundary layer). Equation 3.1 below rules the transport rate:

$$N_s = k_f (C_i - C) \qquad (3.1)$$

where N_s is the rate of mass transfer per unit of interfacial area (mg m^{-2} s^{-1}) equivalent to the rate of mass transfer in the film diffusion, k_f is the liquid phase mass transfer coefficient (ms^{-1}), and C_i and C are the concentrations of adsorbate (mg m^{-3}), respectively at the interface solid-liquid and in the bulk solution (see figure 3.1). Equation (3.1) is derived from Fick's first law whereby the concentration gradient is the linear driving force and the distance for diffusion is constant and equal to the film thickness (the flux has become a rate of transfer).

3. **Intraparticle diffusion**: including pore diffusion and surface diffusion to the final adsorption site. Transport from the surface towards the centre of the grain obeys the Fick's first law:

$$J_i = -D\frac{\partial C_i}{\partial z} \qquad (3.2)$$

where J_i is the flux in non-steady conditions (mg m^{-2} min^{-1}), D is the diffusion coefficient (m^2s^{-1}) and $\partial C_i/\partial z$ is the linear driving force along the z axis considered for diffusion, as appears in figure 3.1; C_i is as before. Further distinction between surface (often the slowest) and pore diffusion can be made and taken into account when modelling the process (Fettig, 1987a,b,c).

4. **Adsorption**: humic molecule binds to the surface, be it chemically or physically

In general, the last step is the quickest and therefore not limiting the rate of adsorption. In a batch experiment, the solution is under a state of permanent mixing; in a continuous process, the flow results in local turbulence. Hence, the first step is not rate-limiting either. It is then concluded that adsorption is limited by a diffusion process, either external or internal.

Figure 3.1 shows a porous adsorbent, where the sorbate travels into the pores. In the case of a low porosity or an adsorbent with mainly mesopore/macropore pores size, the internal diffusion is not considered. This could be applied to γ-aluminate (see pore size distribution by Lambert and Graham, 1995a). Big molecules (highest MW of HS) can cover the micropores and block their access to smaller molecules (fulvic acids).

3.3.2 Diffusion coefficients

The diffusion coefficient depends on the size of the molecules as shown in table 3.1. The figures show the diffusion coefficient D, the molecular weight MW and the radius of gyration R_G which represents the root mean square average of the distance of mass units from the centre of gravity (Cameron et al., 1972). Although these data are likely to represent an aggregation of molecules rather than a single one (see chapter 2, section 2.3.1), they still illustrate well the correspondence between the ability to diffuse and the size of the molecule. In general, small molecules diffuse quicker than bigger ones.

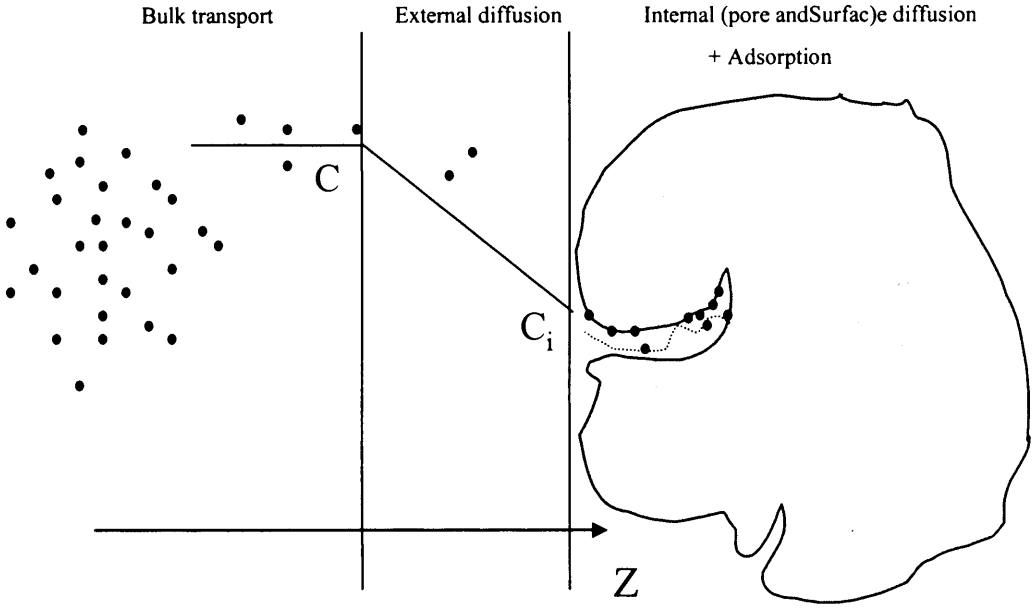

Figure 3.1 The four step process for adsorption from the solution to the diffusive layer and into the adsorbent grain pore (adapted from Montgomery, 1985)

After using Sontheimer et al.'s data (1988), Fettig (1999b) obtained a relationship between molecular weight and diffusivity. The equation is used in figure 3.2 (curve with $R^2=1$); correlation of Cameron's data (table 3.1, NaOH extractant) agrees well with this equation too.

The shift between the two curves could be explained by numerous different conditions under all aspects: HS origin and concentration, pH and ionic strength conditions, experimental methods.

Fettig's result (1999b) corresponds to the low MW range; he estimated a bulk diffusivity of 0.93×10^{-10} m^2s^{-1}. The calculated average surface diffusivities are 1.5×10^{-14} m^2s^{-1} (if 32.6 mg DOC L^{-1}) and 2×10^{-15} m^2/s (8.2 mg DOC L^{-1}); the 10 fold factor shows the importance of initial concentration. It is also coherent with the fact that surface diffusion is slower than external diffusion. Fettig (1987, 1999a,b,c 2005), in most of his cited works, has used a short bed technique to successfully determine the diffusion coefficients.

Chromatography also uses the adsorption process to fractionate humic substances: the heavier the molecule, the lower its retention time (see previously cited references).

Table 3.1. Diffusion coefficient data, from Cameron et al. (1972)

Extractant	D * 10^{-11} m^2s^{-1}	M.W. (Daltons)	R_G (nm)
Na pyrophosphate	21.4	2 400	1.5
	16.0	4 400	2
NaOH 20°C	10.2	12 800	3.2
	8.4	20 400	3.8
	7.7	23 800	4.2
	3.9	83 000	8.2
	3.1	127 000	10.5
	2.5	199 000	13.2
	2.1	412 000	15.3
NaOH 60°C	2.2	408 000	15
	1.3	1 360 000	25.5

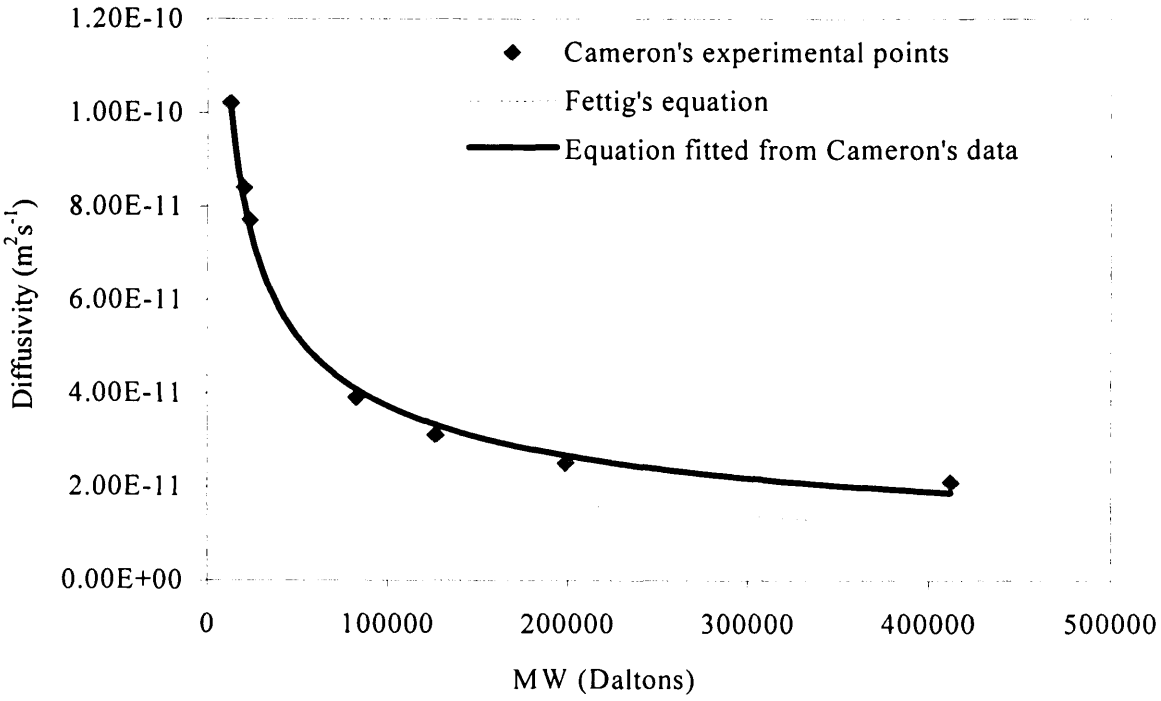

Figure 3.2 Diffusivity data vs MW: Cameron et al.'s data (1972) also fit Fettig's equation (Fettig 's equation $D=7.3\ 10^{-9}\ MW^{-0.5}$ with $R^2=1$, Cameron et al.'s fitted equation $D=10^{-8}\ MW^{-0.4865}$ with $R^2=0.9891$).

However, many other factors influence the measured value of the diffusion coefficient, viz pH, ionic strength (salt concentration), omitted steps (ignoring bulk transport), separation of external/internal diffusion and temperature. In 2000, Lead et al. measured the film diffusion coefficient over a wide range of pH and ionic strengths: the values were 2.0 x 10^{-10} and 2.8 x 10^{-10} m^2/s. They observed the intramolecular diffusion coefficient D to decrease as the pH increases; this is the consequence of more surrounding OH^- ions enhancing the intramolecular repulsion of anionic functional groups of humic substances. Diffusivity of Suwannee river humic substances has been measured during membrane separation by Clark et al. (2000). The values were in the range [2.3-4.5] 10^{-10} m^2/s for an 8 mg/L concentration in acidic conditions and with a calcium concentration from 11 to 33 mg/L. This corresponds to the global diffusion coefficient. Considering a global diffusion too (external and internal) and not taking into account the bulk transport, Avena and Koopal (1999) have studied the initial stage of adsorption of purified humic substances. The attachment was considered to occur on a bare surface site, without any desorption. However, a steady state equation was used for the transport meanwhile adsorption time lasted a maximum of 80 s. The adsorption was found to slow down after 20-80 s. The influence of salt concentration and pH were well represented.

The diffusion coefficient can also vary in the case of humic substances where a wide molecular range is involved, due to competition between low and heavy MW. As the lower molecular weights adsorb first, they are also displaced first. Gu et al. (1996b) noticed that heavier humic substances displaced lighter ones. This shows that not being kinetic preferences, either heavier molecules (humic acids) adsorb better for being more hydrophobic, or lighter molecules (fulvic acids) are weakly bound and easily desorb. Consequently, measurement of diffusivity varies until equilibrium between adsorption and desorption is reached.

Since Fick's law is based also on the concentration gradient, one expects the adsorption to slow down as the adsorbate surface becomes saturated and the concentration gradient decreases. In the particular case of humic substances, the adsorption rate does not always decrease following this rule. This was observed by Teermann and Jekel (1999) who attributed this phenomenon to the surface area increase. As the molecules adsorb on β-FeOOH, calcium fulvates precipitate and supply additional adsorbent surface.

3.3.3 Kinetics models for adsorption in a batch reactor

Kinetics models are selected according to the mechanism controlling adsorption. Several models must be tested when such mechanism is not well defined, particularly as adsorption is likely to be a multimechanisms process. If mass transfer is likely to be global, a lump analysis of kinetic data might be favoured (Wu et al., 2002). In this case, the pseudo-first order and pseudo-second order equations are considered. They include all steps of adsorption, which is why they are called "pseudo" models. The Elovich equation is the third model considered, particularly when chemisorption takes place as well as diffusion (Agbenin and van Raij, 1999). Two additional models consider diffusion as the rate-limiting step; these are the intraparticle diffusion and the external diffusion models. A fifth model called the Homogeneous Surface Diffusion Model (HSDM) is often considered and is presented in section 3.7.2 (GACMan model).

3.3.3.1 The pseudo-first order equation

The pseudo-first order equation uses a lumped analysis of kinetic data, based on the adsorbent capacity and called the Lagergen equation. Initially, adsorption is considered as a first order chemical reaction where adsorption sites on the adsorbent are considered as reactant species (-S) which react with the adsorbate (A) to give a product (i.e. occupied site -SA).

$$-S + A \Leftrightarrow -SA \tag{3.3}$$

The limiting reactant is –S (number of adsorption sites) hence the reaction rate of the first order shown in equation 3.3 (the exponent "1" is not necessary for clarity, but shows the "first order" aspect of this model):

$$\frac{d(-SA)}{dt} = k_1(-S)^1 \tag{3.4}$$

Some assumptions are necessary to derive the kinetic expression. These were applied to the pseudo-second order equation, according to Krishnan and Anirudhan (2002). They should also be applied to the pseudo-first order equation since both equations are developed following the same reasoning, i.e. the identification of adsorption with a chemical reaction. The assumptions are:

- adsorption onto the adsorbent occurs only on localised sites and involves no interaction between adsorbed humic molecules
- the energy of adsorption is independent of surface coverage
- maximum adsorption corresponds to a saturated monolayer of humic substances onto the adsorbent surface
- humic substances adsorption onto the adsorbent is governed by a first-order rate and is chemical in nature
- desorption rate is negligible

The Lagergen equation identifies the occupied adsorption sites as the products of the reaction and the free adsorption sites as the remaining reactants in the solution. Consequently, -SA is replaced by q_t (load at time t) and –S is replaced by (q_e-q_t) (additional load available before equilibrium). The kinetic model is then represented by the following mathematical expression, similar to a first order chemical reaction:

$$\frac{dq_t}{dt} = k_1(q_e - q_t) \tag{3.5}$$

with q_t: load of DOC on the adsorbent at time t [mg g^{-1}]

q_e: load of DOC on the adsorbent at equilibrium [mg g^{-1}]

k_1: rate constant f or the first order equation [min^{-1}]

After integration (the load is nul at time zero), equation 3.13 becomes:

$$\ln(q_e - q_t) = \ln q_e - k_1 t \tag{3.6}$$

In cases where the adsorption becomes unmeasurably slow, the value of q_e is obtained by extrapolation (Aksu and Dönmez, 2003). A plot of $\ln(q_e-q_t)$ vs t gives a straight line. The slope is the rate constant k_1.

The pseudo-first order model (and pseudo-second order described below) is usually applicable for adsorption for a liquid phase (Lorenc-Grabowska and Gryglewicz, 2005) and for homogeneous surfaces (Cheung et al., 2000).

3.3.3.2 The pseudo-second order equation

Reasoning in a similar manner as for the pseudo-first order equation, the reversible chemical reaction rate is of the second-order here. For the same reaction as in equation (3.3), the rate is expressed as in equation 3.7 (products concentration is proportional to the square of the limiting reactant concentration for the second-order reaction):

$$\frac{d(-SA)}{dt} = k_2(-S)^2 \tag{3.7}$$

Assumptions to develop the pseudo-second order equation are cited in the previous section for the pseudo-first order equation, and are not re-cited here. The chemical rate is assumed to be of the second order and k_2 is the rate constant [g $mg^{-1}min^{-1}$].

Using the same identification of the chemical species with the adsorption sites, the adsorption rate becomes as in equation 3.8 below:

$$\frac{dq_t}{dt} = k_2(q_e - q_t)^2 \tag{3.8}$$

q_e and q_t represent the load on the adsorbent, as for the pseudo-first order equation. Equation (3.8) is integrated (the load is nul at time zero) and becomes:

$$\frac{t}{q_t} = \frac{1}{h} + \frac{1}{q_e}t \tag{3.9}$$

$$h = k_2 q_e^{\,2} \tag{3.10}$$

h is the initial rate of adsorption (mg $g^{-1}min^{-1}$) and can be determined from the plot (t/q_t) vs t.

3.3.3.3 The Elovich equation

The Elovich equation is generally used for chemisorption of gases and rarely for a liquid state adsorption (Cheung et al., 2001). However, it is relevant when the surface is heterogeneous. It is formulated as in equation 3.11 (Cheung et al. 2000):

$$\frac{dq_t}{dt} = ae^{(-bq_t)} \tag{3.11}$$

Equation 3.11 is integrated to give equations 3.12 and 3.13 below. t_0 is a time constant and can be calculated from the initial conditions.

$$q_t = \frac{1}{b}\ln(ab) + \frac{1}{b}\ln(t + t_0) \tag{3.12}$$

$$t_0 = \frac{1}{ab} \tag{3.13}$$

with a: Elovich constant [mg^{-1} min^{-1}]

b: Elovich constant (indicates the number of sites available for adsorption) [g mg^{-1}]

t: time [min]

t_0: Elovich time constant [min]

q_t: load as DOC adsorbed on the adsorbent, at time t [mg g^{-1}]

The load q_t is plotted vs $\ln(t+t_0)$. At time t well beyond t_0, equation 3.12 is equivalent to equation 3.14 below:

$$q_t = \frac{1}{b}\ln(ab) + \frac{1}{b}\ln(t) \tag{3.14}$$

Constants a and b can then be calculated.

3.3.3.4 The intraparticle diffusion model

When the pseudo-first and -second models and the Elovich equation do not represent well the kinetics of adsorption, the diffusion rate is likely to be the limiting rate for the overall adsorption process. Porous adsorbents present a high internal surface area, favourable to adsorption of relevant size molecules. Intraparticle adsorption takes into account both surface adsorption, where the adsorbate migrate along the adsorbent surface, and pore diffusion where the adsorbate diffuses in the liquid phase filling the pore, towards the surface (see figure 3.1). Where the mean path length of the molecule travelling in the pore is larger than the pore diameter, internal diffusion is considered to be surface diffusion only, since the adsorbate is more likely to hit the surface rather than only diffuse in the liquid solvent.

Adsorption within the pore reaches equilibrium at a rate varying according to the radius of the pore. More precisely, the fractional approach to equilibrium is described by the function F(t), derived from Fick's law. It depends only on the dimensionless time parameter Dt/r^2 (Streat et al., 1995), where r is the radius of the adsorbent grain and D is the diffusivity in the grain. D includes pore and surface diffusivity. If the concentration in the bulk solution at time zero, at time t and at equilibrium are called C_0, C_t and C_e, then F(t) is defined as follows (Al-Ghouti et al., 2005):

$$F(t) = \frac{C_0 - C_t}{C_0 - C_e} = \frac{q_t}{q_e} = \left[1 - e^{\frac{-Dt\pi^2}{r^2}}\right]^{\frac{1}{2}} \qquad (3.15)$$

or

$$\ln\left[1 - F(t)^2\right] = \ln\left[1 - \left(\frac{q_t}{q_e}\right)^2\right] = -\frac{\pi^2 D}{r^2}t \qquad (3.16)$$

Therefore, the plot of $\ln[1-(q_t/q_e)^2]$ vs t is a straight line and the diffusivity D can be calculated from the slope.

It is further deduced that adsorption by intraparticle diffusion is a function of the square root of the time and the model is based on equations 3.16 and 3.17:

$$q_t = x_i + k_p t^{1/2} \tag{3.17}$$

with q_t: adsorption capacity at time t (load) [mg g^{-1}]

x_i: intercept, representing the boundary layer thickness and indicating the influence of the external film resistance (Al-Ghouti, 2004)

k_p: intraparticle (pore) diffusion constant [mg g^{-1} $min^{-1/2}$]

The plot of the load q_t vs $t^{1/2}$ can exhibit three different slopes corresponding to three stages of adsorption (Lorenc-Grabowska and Glyglewicz, 2005, Wu et al., 2002). The first slope is the steepest one, attributed to instantaneous adsorption on the external surface. Then during the second stage, adsorption is gradual and the rate is intraparticle diffusion limited. Finally in the third stage, adsorption slows down due to the low gradient of concentration between the surface and the solution, when reaching the equilibrium.

3.3.3.5 The external diffusion model

When considering a diffusion controlled adsorption, external diffusion dominates over intraparticle diffusion during the early stages of the process (under 5 minutes according to Al-Ghouti, 2004). This is assumed as the adsorbate has not yet reached the internal surface of the adsorbent grain and such concentration is equalled to zero. The external diffusion is also based on Fick's law and is ruled by the difference of concentration between the bulk solution and the film surrounding the adsorbent grain. The proportion of adsorbate left in solution (C_t/C_0) decreases as a function of the mass transfer coefficient k_f and the external area of adsorbent per volume of solution treated (A/V). It is expressed as follows:

$$\left[\frac{d\left(\frac{C_t}{C_0}\right)}{dt}\right]_{t<5\,\mathrm{min}} = -k_f \frac{A}{V} \tag{3.18}$$

By integrating equation 3.18 between time t and time zero, it becomes:

$$\ln\frac{C_t}{C_0} = -k_f \frac{A}{V} t \tag{3.19}$$

and

$$\frac{A}{V} = \frac{6m}{d_m \rho} \tag{3.20}$$

with C_t: adsorbate concentration in the bulk solution, at time t [mg L^{-1}]

C_0: initial adsorbent concentration in solution [mg L^{-1}]

k_f: external mass transfer coefficient [m min^{-1}]

t: time [min]

A: external surface area [m^2 g^{-1}]

V: volume of solution [L]

d_m: median adsorbent grain diameter [m]

ρ: density of the adsorbent [g L^{-1}]

$\ln(C_t/C_0)$ is plotted vs t as in equation 3.19 where k_f is calculated from the slope (A, V, d_m and ρ are known).

3.4 Isotherm models and equilibrium of adsorption

Adsorption equilibrium can be reached by carrying out batch trials so as to know the adsorbent capacity for a specific adsorbate. Initially, isotherms were developed for gas adsorption, respecting Henry's law (concentration on the surface proportional to gas partial pressure). These were then extended to be applicable to soluble adsorbates. Isotherms are used to describe the batch process and in turn, provide useful data for continuous process studies. Eventually, the interest is to predict the performance and breakthrough of a fixed or fluidised bed for adsorption.

3.4.1 Single solute isotherms

3.4.1.1 Isotherm and hysteresis shape

The simplest situation relates to the adsorption of only one species or component (eg: removal of a pesticide) and the isotherm can be of various shapes as described by Brunauer et al. (1940) and shown in figure 3.3. However the validity of the results in figure 3.3 should be considered cautiously when dealing with a liquid phase as it is the case for NOM in water, since these isotherm shapes were obtained for the adsorption of a gas. Type I corresponds to micropore solids (pores smaller than 1 nm according to IUPAC classification). Saturation occurs at very low pressure. Since the pore diameter is not much bigger than the gas molecules, it is quickly filled. A single layer can be adsorbed and it corresponds to the Langmuir adsorption pattern (Weber, 1972). It is typical of chemisorption rather than physisorption. The other types (II to V) represent Brunauer Emmett and Teller (BET) adsorption pattern, whereby several layers can be adsorbed and a given layer needs not complete formation prior to initiation of subsequent layers (Weber, 1972). Type II isotherm show a first inflexion point where a monolayer is completed and new layers start (in fact, a new layer can start before the first is completed). This corresponds to a wide range of pore sizes. It is typical of physisorption. Type III isotherm shows a steady increase of adsorption with increasing relative pressure. Both types II and III show a non-limited adsorption as the pressure increases. Types IV and V respectively correspond to types II and III, with the difference that saturation is reached (two layers adsorption for type IV). Convex shapes, as for type III and V occur when the heat of liquefaction is larger than the heat of adsorption (V represents water vapour adsorption). Shapes II, III, IV and V correspond to adsorbent with a wider range of pore size including mesopores (1-25 nm) and macropores (>25 nm).

Isotherms like type II to V are observed for NOM. Although non-specific characteristics like DOC and UV_{254} are used to describe humic substances adsorption, single component models do not achieve a good representation of the process. They need modifications which lead to complex models using a multicomponent system.

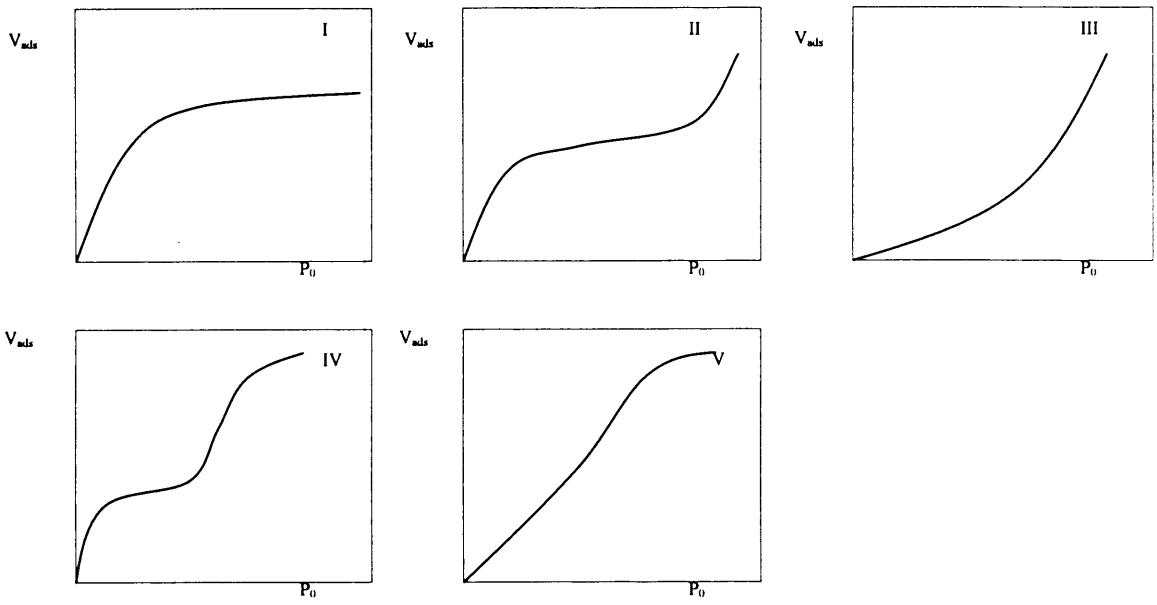

Figure 3.3 Isotherm types for gas adsorption (Brunauer et al., 1940) (volume adsorbed vs gas pressure)

Giles et al. (1960) have later extended the isotherms to liquid systems by using the concentration instead of the pressure. Four main categories (and subdivisions according to the solute type 1, 2, 3, 4...mx...) are suggested, according to the initial curvature of the isotherm, as seen in figure 3.4.

To fully study the adsorption phenomenon, desorption should also be carried out. This is where the importance of the pore shape appears since it explains the hysteresis loop on the isotherm.

At a given pressure, the adsorption branch displays less adsorbed material than the desorption branch. This is explained by the size and shape of the pores. Small pores are seen as capillaries in which the vapour condenses. The molecules adsorb onto the pore walls and a cylindrical meniscus forms on this surface liquid film. Filling of the pore continues with condensation of the molecules onto the cylindrical meniscus which then becomes a hemispherical liquid meniscus. However, evaporation from this hemispherical meniscus occurs at a lower partial pressure than condensation on the cylindrical meniscus. This means that desorption takes place at a lower partial pressure than adsorption, and the consequence of this is a hysteresis loop on the isotherm. The

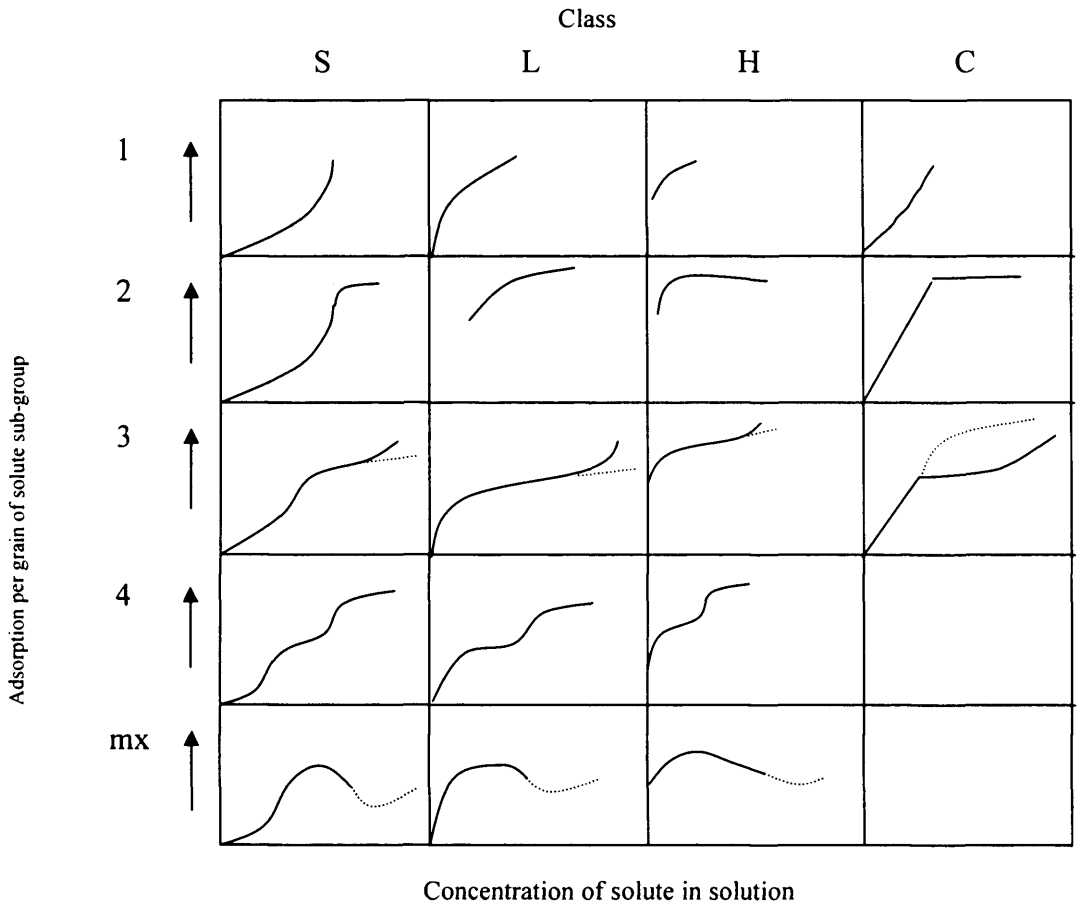

Figure 3.4 Isotherm types for liquid adsorption (Giles et al., 1960)

hysteresis shape is influenced by the shape of the pore as illustrated in figure 3.5. Shapes A, C and E show that desorption initially follows adsorption, A being a narrow but uniform pore size distribution. Conversely, shapes B and D indicate that the pressure is not low enough for desorption to take place. This is more obvious when the desorption branch is initially horizontal as in shape B. A large loop means that different sizes of pores are present, varying width or bottleneck pores (shapes B, D, E). These reasoning were applied to gas adsorption and are transferred to liquid adsorption, replacing the partial pressure by the fraction of the initial concentration in the solution.

The models generally used are Langmuir, Freundlich and Henry's, and these will be presented in the next section. Brunauer Emmett and Teller (BET) isotherm is a model used for adsorption of gases onto solids and enables an estimate to be made of the surface area of the same solid adsorbent. Therefore, it is also reviewed among the most used isotherm models.

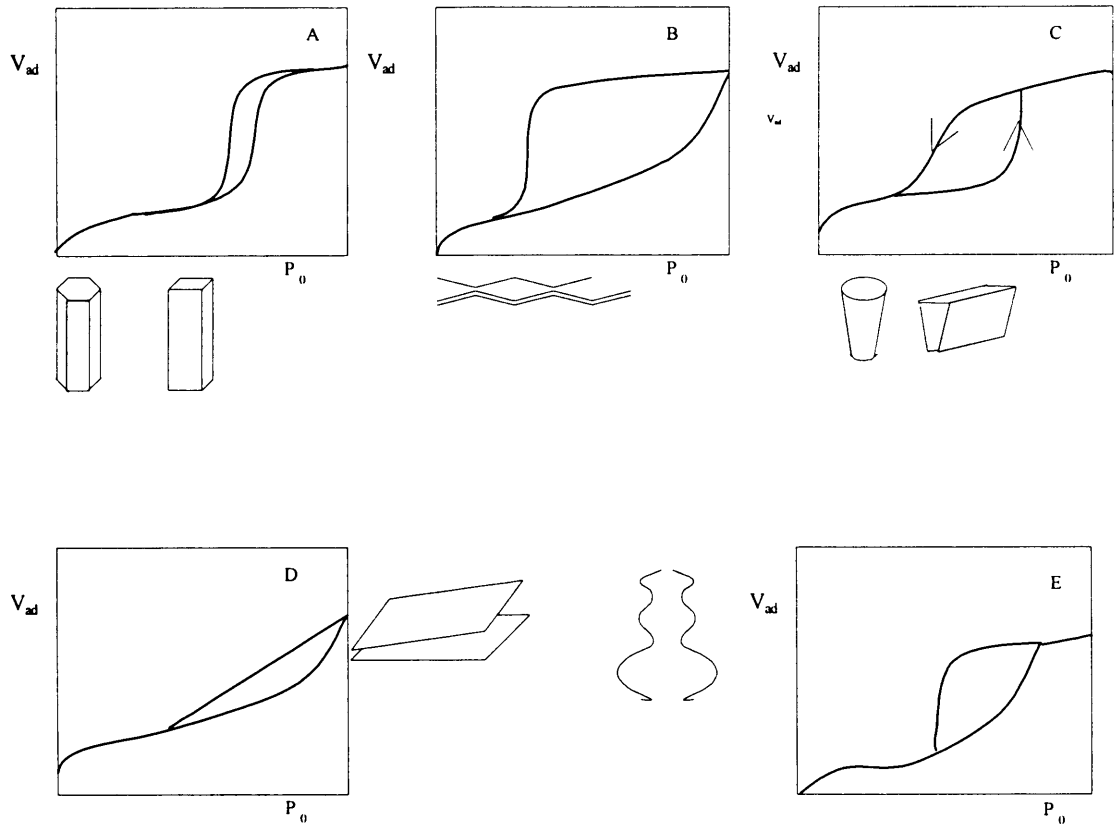

Figure 3.5 Relation between the 5 categories of hysteresis loops and the pore shapes (Thomas and Crittenden, 1998) (volume adsorbed vs gas pressure)

3.4.1.2 The Langmuir isotherm

The adsorption sites on the adsorbent are considered as reactants (-S) which react with the adsorbate (A) to give a product (i.e. occupied site -SA). Such reaction would have a free energy of ΔG:

$$-S + A \Leftrightarrow -SA \qquad \Delta G^0 \tag{3.21}$$

$$K_A = \frac{[-SA]}{[-S][A]} \qquad \Delta G^0 = -RT \ln K_A \tag{3.22}$$

where K_A is the equilibrium constant for reaction 3.21.

The assumptions made are: *(i)* there is a stoichiometry between the number of sites and the number of adsorbate molecule *(ii)* the number of sites is limited and all the sites have the same probability of being occupied (constant energy of adsorption) *(iii)* the adsorption is reversible and *(iv)* the adsorption is monolayer. In general, they are similar to the assumption made for the pseudo kinetics models (first and second order). On a

macroscopic scale, the relevant equation is (AWWA, 1990, Weber, 1972, Montgomery, 1985):

$$q_e = \frac{Q_{mon} b C_e}{b C_e + 1} \tag{3.23}$$

with q_e: adsorbed concentration on the adsorbent at equilibrium, i.e. load [mg or mol g^{-1}]

Q_{mon} : maximum adsorption capacity corresponding to the maximum value of q_e achievable as C_e is increased, i.e. monolayer capacity [mg or mol g^{-1}]

(Q_{mon} is also called q_{max}, according to the authors)

b: constant related to the energy of adsorption, increasing with the strength of adsorption bond [unit is the inverse of the concentration unit (Montgomery, 1985)]

C_e: adsorbate concentration in solution at equilibrium [mg L^{-1}]

Equation 3.23 can be linearised to become:

$$\frac{C_e}{q_e} = \frac{1}{Q_{mon} b} + \frac{1}{Q_{mon}} C_e \tag{3.24}$$

Constants Q_{mon} and b can be calculated from the plot of C_e/q_e vs C_e.

Langmuir model is rarely applicable for the whole range of data under study, probably due to the assumptions being valid only over a narrow range of concentration.

3.4.1.3 The Freundlich isotherm

This model is empirical and accounts for the heterogeneity of the adsorbent surface. It considers that each adsorption site has a specific energy. Applying Langmuir to each of them and using a probability density function of the site distribution leads to an expression for heterogeneous surfaces. The main equation is:

$$q_e = K_F C_e^{\frac{1}{n}} \tag{3.25}$$

Equation 3.25 can be linearised to give:

$$Log\ q_e = Log\ K_F + \frac{1}{n} Log\ C_e \tag{3.26}$$

where q_e and C_e are as before. K_F is the Freundlich constant in [mg g^{-1} (mg $L^{-1})^n$] and indicates the adsorption capacity since as the larger K_F, the larger q_e. The exponent 1/n indicates the strength of the adsorption. When the isotherm curve becomes almost flat, the exponent 1/n is small with strong adsorption tending towards irreversibility. However, this model fails for low concentration values (Tien, 1994). This isotherm does not apply for very high concentration values either since q_e cannot increase indefinitely and is limited to a saturation value (AWWA, 1990). Therefore, Freundlich model applies best in the intermediate range of concentration values.

3.4.1.4 The Henry isotherm

The Henry isotherm is identical to the Freundlich isotherm with the distinction that n is equal to unity. Therefore the concentration on the adsorbent (i.e. the load) is directly proportional to the concentration left in solution. The Freundlich constant becomes the Henry constant K_H in [L g^{-1}] and the equation is as follows:

$$q_e = K_H C_e \tag{3.27}$$

The load on the adsorbent is plotted vs the residual concentration in the solution and the value of K_H is estimated from the slope of the straight line.

3.4.1.5 The modified Langmuir isotherm

Gu et al. (1994) briefly reviewed the modifications carried out on Langmuir isotherm. Considering the energy of adsorption as variable and dependent on surface coverage, they introduced a new parameter K_L such as (b as before):

$$q_e = \frac{Q_{mon} K_L C_e}{K_L C_e + 1} \tag{3.28}$$

with $$K_L = K' e^{-2bq_e} \quad \text{and} \quad b = \frac{\theta}{RT} \tag{3.29}$$

θ is the surface stress coefficient, R is the constant for ideal gases and T is the temperature in Kelvin. This is the "modified Langmuir isotherm". If b equals zero, then K_L is constant, equal to K', and the Langmuir isotherm is represented.

The same authors mention that it is "not always appropriate to model adsorption reactions as completely reversible or completely irreversible". Therefore, as an improvement to the adsorption-desorption model, they introduced a "hysteresis coefficient" h (between 0 and 1):

$$q_e = \frac{Q_{mon} K C_e}{K C_e + \left(\frac{C_e}{C_a}\right)^h} \tag{3.30}$$

with C_a being the equilibrium concentration of the adsorbate in the solution (after adsorption but before desorption). If h equals zero (no hysteresis) then the isotherm follows the Langmuir equation (i.e. total reversibility) and if h equals to 1, q is not dependent on C, but on C_a and the adsorption is irreversible.

3.4.2 Multicomponent solute isotherm

As mentioned in the introduction and according to Fettig (1999), the shape of the isotherm and the initial concentration influence are distinct whether the adsorption involves one or several solutes. Many isotherms obtained from humic substances adsorption onto carbon or inorganic adsorbent give evidence of this. The practice, in current research, is to separate the humic substances into several fractions. Then a single solute isotherm is applied to each of them.

The Ideal Adsorption Solute Theory (IAST) has been developed initially by Myers and Prausnitz (1965) and proposed for dilute liquid systems later in 1972 by Radke and Prausnitz. It was then applied to total organic carbon (TOC) data by Crittenden et al. (1985). The theory uses the pure-component adsorption isotherm data and the main advantage is that the adsorbed phase can be treated as an ideal solution of the adsorbed components (Ko et al., 2004). Therefore it assumes that *(i)* the liquid thermodynamic equations apply to the adsorbent phase, *(ii)* the solution in the adsorbed phase is ideal and *(iii)* the equilibrium is reached. IAST needs the adsorbate concentration to be

expressed in mol/L, which is not applicable to humic substances when using DOC as a lump index. The best fit isotherms for single components are used to calculate the spreading pressure, converted to a concentration using the ideal gas constant, the surface area of the adsorbent and the temperature (in Kelvin). The concentration of each solute on the adsorbent is then estimated by a numerical method (Newton-Raphson method in the case of the work of Ko et al., 2004). However, this fictive component analysis, which uses a non-linear regression to determine the isotherm parameters, becomes an unpractical task as the number of components is increased.

IAST remains the basis for development of modelling adsorption of multicomponent solutions. Several modifications have been made and these will be briefly reviewed in the "Modelling based on IAST theory" section of this chapter (see section 3.6).

3.4.3 Complexation and polyelectrolyte conformation models

The previously described adsorption models are valid over a small range of pH, ionic strength and concentration. Filius at al. (2000) have used a distinct approach by considering the charging behaviour of the adsorbent. The Charge Distribution Multi Site Complexation model (CD-MUSIC) described well the adsorption of fulvic acid to goethite. It assumed the surface species, the charge distribution (considering the complexation over three electrostatic planes) and the affinity constants. However, using only four species and two functional groups (carboxylic and phenolic) allowed a good simulation in this case. The model showed a low dependency on salt concentration.

Vermeer et al. (1998a, b) also studied the influence of pH and salt concentration for the adsorption of purified Aldrich Humic substances onto hematite (α-Fe_2O_3). The Self Consistent Theory (SCF) was applied considering short and long range interactions (Van der Waals, Coulombic) between the various units. The humic substances are seen as sequences of three unit types: U (uncharged), acidic units C (charged with pK=4) and P (charged with pK=10). The other units were the water and the salt ions. The units resided on discrete sites defined by a 100 layer regular lattice parallel to the adsorbent surface. Qualitative conclusions were successfully drawn but no comparative results between modelled adsorption and experimental data were shown.

Au et al. (1999) combined both surface complexation and polyelectrolyte nature of humic substances in a hybrid model called SC/SF, by dividing the system in several units (as in SCF). Electrostatic interactions and a unique non-electrostatic interaction polyelectrolyte - surface site are considered. One type of the polyelectrolyte species

reacts chemically with a proton reactive site of the adsorbent. This way, the solution chemistry was proven to be very important to model adsorption. Although good results are obtained from the complex model, the results lead more to a qualitative understanding of the process rather than a quantitative prediction of the adsorbed NOM.

In 1999, Van der Weerd et al. have also considered the humic substances as a polylectrolyte with "loops" and "tails", able to adsorb onto one or several sites (not necessarily neighbours) while still having part of the molecule in solution and being able to desorb. The adsorbate is divided into several species, each with a hydrophilic and hydrophobic part. A kinetic competitive Langmuir type equation describe the sorption. For each fraction, the affinity, the maximum adsorption and the adsorption and desorption rate constants are considered. A program NOMAD is used to resolve the set of equations by the 4^{th} order Runge-Kutta method. However, no clear explanation is given on how to determine the model parameters. Since external data were used to verify the model, very little information is given regarding the experimental conditions.

3.5 Continuous process for adsorption and analytical models

3.5.1 Introduction

Models for continuous adsorption processes have been developed, which account for a non-equilibrium state. Adsorption in a column can be considered as numerous batch operations in series and with conditions, at a particular point within the fixed bed, that vary with time. Consequently, adsorption occurs in a particular region of the bed, known as the Mass Transfer Zone (MTZ) which itself moves with time (Thomas and Crittenden, 1998). As the influent continues flowing through the column, the adsorbent is gradually consumed (saturated) along with the MTZ reaching the end of the adsorbent bed. At that final stage, the bed has reached its capacity and the contaminant to be removed is no longer eliminated from the effluent, hence a "breakthrough" at time t_B, as seen in figure 3.6 at 5% of the influent concentration. The breakthrough curve "S" shape is characteristic of an ideal adsorption system where the adsorbates molecules are small and with a simple structure (Walker and Weatherley, 1997). In practice, the operation of the column should be stopped before the breakthrough occurs at t_B.

Fettig and Sontheimer (1987a,b,c) used a short column to determine the mass transfer and diffusion (surface and pore) coefficients. The adsorbent was activated carbon and

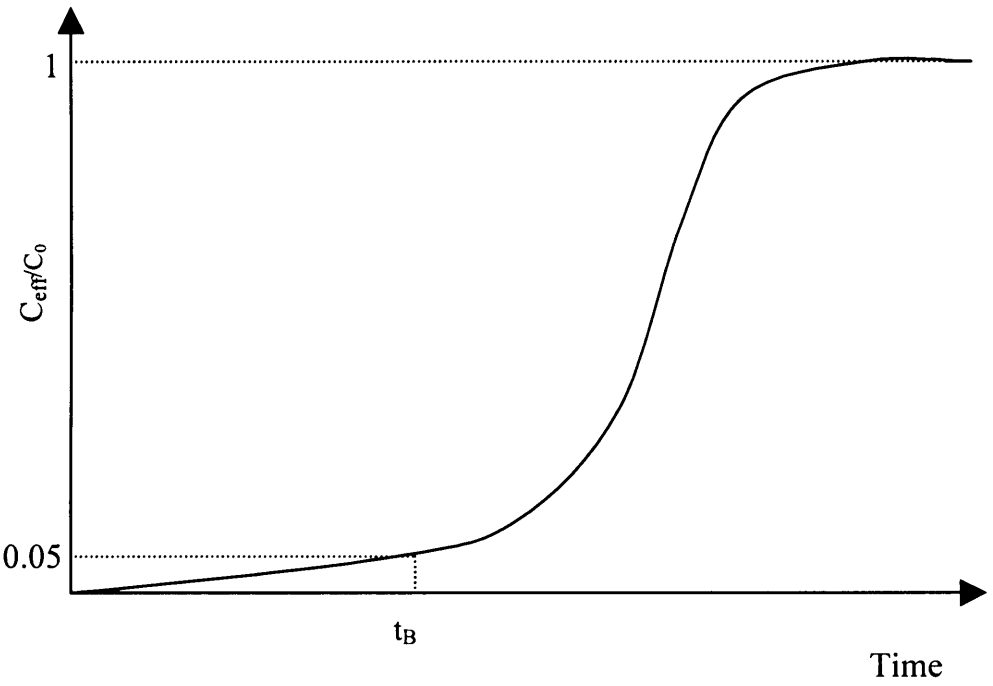

Figure 3.6 Typical shape of the breakthrough curve (column effluent concentration with time, example of breakthrough at 5% of influent concentration)

the adsorbate was fulvic acid only (low MW). Under these conditions, intraparticle diffusion seemed to control the process. Using the SCAM model (model for a multicomponent system), the minicolumn breakthrough curve was accurately predicted.

Heijman et al. (1999) used a column to assess the adsorption of NOM onto activated carbon, iron oxide and also used an ion exchange column. Both dispersion and adsorption (called here Linear Driving Force or LDF) were included in their model. The LDF had also been used in a model presented by Tien (1994) for the continuous flow adsorption study in a fixed bed. TOC was the lump index used and the selected isotherm was the Freundlich model. Other programs which "split" the NOM into several components are presented in section 3.6. Few results are published as regards continuous flow studies for NOM adsorption and modelling. General models used for single component adsorption can also be applied to humic substances. These are the Thomas equation and the Bed Depth Service Time (BDST) model. They are generally used for the engineering aspect of setting up an adsorption process system and are described in section 3.5.2.

3.5.2 *The Thomas equation*

The Thomas model predicts the concentration-time profile or breakthrough curve of the effluent. The maximum capacity of the adsorbent can be estimated which corresponds to the practical needs of an adsorption system. The model has the following form (equation 3.31 is the linearised form of equation 3.32):

$$\frac{C_t}{C_0} = \frac{1}{1+\exp\left[\frac{k_T(q_0 m - C_0 V)}{Q}\right]} \tag{3.31}$$

$$\ln\left(\frac{C_0}{C_t}-1\right) = \left(\frac{k_T q_0 m}{Q}\right) - \left(\frac{k_T C_0}{Q}\right)V \tag{3.32}$$

with C_0: Influent contaminant concentration (DOC in the present work) [mg L^{-1}]

C_t: Effluent contaminant concentration at time t (DOC in the present work) [mg L^{-1}]

k_T: Thomas constant [L min^{-1} mg^{-1}]

q_0: Maximum adsorption capacity [mg g^{-1}]

m: Mass of adsorbent [g]

V: Column throughput volume [L]

Q: Flowrate [L min^{-1}]

The Thomas model assumes Langmuir kinetics of adsorption-desorption with no axial dispersion. Therefore, it is based on a second order reaction kinetics. This is the main disadvantage of the model since adsorption is not often limited by the chemical reaction kinetics but by an interphase mass transfer (internal diffusion) (Aksu and Gönen, 2004).

3.5.3 *The Bed Depth Service Time model*

The Bed Depth Service Time (BDST) model is derived from the irreversible isotherm Adams-Bohart model which assumes that the adsorption rate is proportional to both the residual capacity of the adsorbent and the concentration of the sorbing species. It

ignores intraparticle mass transfer and external film resistance and assumes that adsorption takes place directly on the surface. Although the Adams-Bohart model was initially applied for adsorption of chlorine onto charcoal, it can describe well the column operation when the adsorbate is in the liquid phase (Aksu and Gönen, 2004). The BDST model also assumes that the adsorption capacity remains constant as the MTZ moves steadily along the column (i.e. the influent is always in contact with some "fresh" adsorbent). The main equation of the model is:

$$\ln\left(\frac{C_0}{C_B}-1\right)=\ln\left(e^{\left(\frac{K_a N_0 Z}{Q}\right)}-1\right)-K_a C_0\ t \tag{3.33}$$

The assumption on the exponential simplifies equation 3.33 (Walker and Weatherley, 1997):

$$e^{\left(\frac{K_a N_0 Z}{Q}\right)} >> 1 \quad \Rightarrow \quad \ln\left(\frac{C_0}{C_B}-1\right)=\left(\frac{K_a N_0 Z}{Q}\right)-K_a C_0\ t \tag{3.34}$$

From equation 3.34, the service time t at breakthrough is t_B and can be expressed using a linear equation:

$$t_B=\left(\frac{N_0}{C_0 Q}\right)Z-\frac{1}{K_a C_0}\ln\left(\frac{C_0}{C_B}-1\right) \tag{3.35}$$

$$t_B = aZ+b \tag{3.36}$$

with C_0: Concentration of the influent at time zero [mg L^{-1}]

C_B: Concentration of the influent at time zero [mg L^{-1}]

K_a: Adsorption rate constant [L g^{-1} min^{-1}]

N_0: Column adsorption volumetric capacity [g L^{-1}]

Z: Bed depth [dm]

Q: Flowrate [L min^{-1}]

After identifying a and b for each group of constants, equation 3.35 has become a simple relationship between the service time at breakthrough and the bed depth (equation 3.36). A group of straight lines of t_B vs Z can be plotted, each line corresponding to a fixed value of C_0/C_B (i.e. a fixed percentage removal).

The BDST model offers a simple approach and a rapid prediction of the column adsorption parameters (McKay and Bino, 1990), particularly when parameters like the flowrate or the influent concentration are changed (Ko et al., 2000). The BDST model is based on physically measuring the capacity of the bed at various percentage breakthroughs.

3.6 Adsorption numerical models based on IAST concept

As mentioned in section 3.4.2, IAST theory has been made more applicable to adsorption of humic substances and to multicomponent systems in general. Improvements have been concerned with modelling both the equilibrium and the continuous process taking place in fixed-bed columns. The equilibrium model considerations are usually used as input into a model simulating the continuous process. Fettig (1987a,b,c, 1999) has reviewed the main modifications in a useful way:

- the adsorbate mixture was divided in three components: one strongly adsorbable, one weakly adsorbable and one non-adsorbable. This fractionation is called fictive component analysis
- the Simplified Competitive Adsorption Model (SCAM) was developed to allow the use of different units in addition to mol L^{-1}; the model is similar to IAST in the case of a unique n value
- a fixed value for n was used for each component
- a logarithmic normal distribution of the adsorptive strength was assumed (Matsui, 1998, 1999)

The disadvantage of the method so far is that competition between the various components is not represented. Yuasa et al. (1997) used the IAST by splitting humic substances into 6 fractions of 6 MW ranges, and 5 adsorptive strengths. From this, a

matrix of 30 (6 x 5) components was obtained. The improvement came from the fact that competition between fractions was well represented by having various adsorptive strengths for each component. These authors used the Freundlich isotherm and the adsorptive strength K_F was generated from a log-normal distribution with a unique value being selected for the adsorptive intensity (0.273). K_F was found to increase as the molecular weight (MW) decreased. This disagrees with the general observation that low MW adsorbed less than high MW. However this result is open to discussion since only a small MW range was covered over the 6 fractions (from 1200 to 4100 Da).

Teermann and Jekel (1999) applied the Freundlich isotherm and used the value of 0.15 for n, studying the adsorption of humic substances onto β-FeOOH. The model ADSA was used, also based on IAST. The difference was that the n value was fixed meanwhile the model adjusted the K_F value to experimental data. The results were successful using DOC as a lump index.

Once the equilibrium model is accepted, it is generally applied with the Homogeneous Surface Diffusion Model (HSDM) as done by Fettig and Sontheimer (1987a,b,c). A model using this same idea is the commercial model GACMan (Granular Activated Carbon Management developed by the Water Research Centre, Swindon, UK) used as a tool to optimise adsorption processes used in the water industry on a continuous basis. This model will be used in this work and will be described in more details below.

3.7 GACMan model (Granular Activated Carbon Management)

The model GACMan (Granular Activated Carbon Management) is a software tool developed by the Water Research Centre (WRc, Swindon, UK) for the water industry. It is intended for better planning for the use, optimisation and regeneration of GAC and other adsorbents. It allows prediction of the removal of various contaminants (single or multicomponent system) by various adsorbents, using GACMan library or calibrating the model with new adsorbates and/or adsorbents. The program is written in Fortran 77. However, the code of the program is not available, hence the impossibility to modify it. Investigation is carried out from the user interface (Fortran-Windows). GACMan is based on the Ideal Adsorption Solutes Theory and on the Homogeneous Surface Diffusion concepts.

3.7.1. Assumptions in GACMan

GACMan is a Homogeneous Surface Diffusion Model (HSDM). It is developed assuming:

1. ***Rate of adsorption is diffusion-limited and local equilibrium exists at the external surface of the adsorbent.***

   This supposes that no large variation of temperature occurs in the column, hence no convection and also no eddies or dead-zone presents a resistance larger than diffusion.

2. ***Liquid-diffusion resistance occurs and is expressed using the film transfer coefficient.***

   This represents the liquid film surrounding the adsorbent grains.

3. ***The adsorbent is solid, homogeneous and spherical.***

4. ***No pore diffusion occurs and surface diffusion is the second resistance.***

   Although pore diffusion does take place in the adsorption process under study, the diffusion coefficient cannot be easily calculated or predicted. The chemical structure, size and molecular weight of a pesticide molecule may be well known and the associated diffusion coefficient can be precisely calculated. However this is not the case for humic substances which is why a lump concentration index (DOC) is used instead of the specific molecule concentration. Pore diffusion is accounted for by using a fitting parameter (called α in the model) that relates to both surface and liquid diffusion. Pore diffusion takes place to a lesser extent when studying adsorption of larger MW since the free path of the molecule in the pore is not negligible in comparison to the pore size.

5. ***Plug flow occurs throughout the adsorbent bed.***

   This is verified when working in a column where short-circuits are avoided and where the column length is far longer than its width.

6. ***In the case where several adsorbates are present, they do not interact with each other and a multicomponent system can be considered by independent equilibria.***

   By using a lump index such as DOC, the interaction between these components is ignored, although it is accepted that it will have an effect on the final adsorption result.

7. ***Axial dispersion is neglected.***

   Axial dispersion is due to molecular diffusion and turbulent mixing arising from splitting and recombining of eddies around the adsorbent particles. In the conditions of study, the flow through the column was very low and Reynolds number below 1. As a result, a definite laminar flow is expected and axial dispersion can be neglected.

It becomes obvious that these assumptions might not all be valid for the present study. This is due to the fact that GACMan has been written to simulate the adsorption of pesticides or well defined molecules onto GAC.

3.7.2 Equations used in GACMan

Explicitly, GACMan uses the equations presented below.

3.7.2.1 Transport in liquid phase (bulk)

The equations are developed taking into account the liquid phase transport (from the bulk to the surface of adsorbent, crossing the stagnant film) varying with time and axial coordinate. They are based on the material balance in a plug flow reactor, stated as:

In – Out = Transferred through liquid film around the particle

$$U(t)\frac{dc(z,t)}{dz} + \varepsilon\frac{dc(z,t)}{dt} + k_f(t)\, a_p\left[c(z,t) - c^*(z,t)\right] = 0 \qquad (3.37)$$

Where U(t) is the superficial velocity of the influent at time t, c(z,t) is the adsorbate concentration in the liquid phase, at depth z in the column, and at time t ($c^*(z,t)$ is the

same but at the adsorbent surface). k_f is the external film mass transfer at time t, a_p is the specific external surface area of the particle. This surface area is expressed below, in m^2/m^3, for spherical particles with radius R_p:

$$a_p = \frac{3\,(1-\varepsilon)}{R_p} \tag{3.38}$$

Initial condition is $c(z,t=0)=0 \quad 0 \le z \le L$ (3.39)

Boundary condition is $c(z=0,t)=c_{inf}(t)$ (3.40a)

GACMan also considers a possible non-adsorbable fraction and a biodegradable fraction. Both these fractions, respectively f_{non} and f_{bio} are input into the model by the user and are not considered as available for adsorption. Therefore, the initial adsorbate concentration is calculated and the exact concentration available for adsorption gives the new boundary condition (c_{inf} is the influent concentration):

$$c(z=0,t)=(1-f_{non}-f_{bio}) \times c_{inf}(t) \tag{3.40b}$$

3.7.2.2 Transport in solid phase

The solid phase transport varies with time and radial coordinate inside the particle. Surface diffusion is assumed to predominate, with negligible hold up of adsorbate within the pores. The accumulation on the surface at depth z, time t and radius r inside the adsorbent grain, varies with the surface diffusion coefficient D_s and is expressed by q(z,t,r), applying Fick's second law:

$$\frac{dq(z,t,r)}{dt} = D_s(t)\frac{d^2q(z,r,t)}{dr^2} = \frac{D_s(t)}{r^2}\frac{d}{dr}\left(r^2 \times \frac{dq(z,t,r)}{dr}\right) \tag{3.41a}$$

By using the general rules for the derivation of a product of two functions, the following can now be written:

$$\frac{dq(z,t,r)}{dt} = D_S(t)\left(\frac{d^2q(z,r,t)}{dr^2} + \frac{2}{r}\frac{dq(z,r,t)}{dr}\right) \qquad (3.41b)$$

The initial condition is (virgin adsorbent): $q(z,t=0,r)=0 \quad 0 \le r \le R_p$ (3.42)

Two boundary conditions:

Symmetry at centre of particle: $$\frac{dq(z,t,r=0)}{dr} = 0 \qquad (3.43)$$

At the particle surface and with ρ_p equal to the density of the adsorbent particle:

$$k_f\left[c(z,t) - c^*(z,t,R_p)\right] = \rho_p D_s \frac{dq(z,t,R_p)}{dr} \qquad (3.44)$$

Adsorbate transfers into the adsorbent particle where it accumulates ((3.44) introduced in (3.41a)):

$$k_f(t)R_p^{\,2}\left[c(z,t) - c^*(z,t)\right] = \rho_p \frac{d}{dt}\left(\int_0^{R_p} q(z,t,r)r^2 dr\right) \qquad (3.45)$$

This equation links both liquid and solid phases: liquid phase mass flow ($kg.s^{-1}$) equals the mass flow at the solid surface ($kg.s^{-1}$). Assuming there is equilibrium, the selected isotherm is introduced; three isotherms can be used in GACMan, namely the Freundlich isotherm, the extended Langmuir isotherm and the extended Redlich-Peterson isotherm. Their incorporation in GACMan is done using the following equation:

The Freundlich isotherm $$c^*(z,t) = \left[\frac{q^*(z,t)}{K}\right]^{1/n} \qquad (3.46a)$$

Note: in GACMan, Freundlich isotherm expression is

$$q(z,t) = K\ c^{n}(z,t) \qquad (3.46b)$$

The extended Langmuir isotherm

$$q^{*}(z,t) = \frac{K_L^{o} c^{*}(z,t)}{1 + a_L^{o} c^{*}(z,t)} \qquad (3.47)$$

The extended Redlich-Peterson isotherm

$$q^{*}(z,t) = \frac{K_J^{o}\ c^{*}(z,t)}{1 + b_J^{o}\ c^{*}(z,t)^{\beta''}} \qquad (3.48)$$

All previous equations correspond to a single adsorbate. However, the additional interest of GACMan is to handle the presence of several adsorbates in the same solution. For the purpose of humic substances removal, each adsorbate will correspond to a molecular range of humics. The subscript *i* represents the component investigated, out of N components. According to IAST theory (explained previously) GACMan incorporates the multicomponent isotherm and calculates the effluent concentration or load of adsorbate *i* as follows:

The Freundlich isotherm

$$c_i^{*}(z,t) = \frac{q_i^{*}(z,t)}{\sum_{j=1}^{N} q_j^{*}(z,t)} \left[\frac{n_{F,i}^{\circ}}{K_{F,i}^{\circ}} \sum_{j=1}^{N} \frac{q_j^{*}(z,t)}{n_{F,j}^{\circ}} \right]^{1/n_{F,i}^{\circ}} \qquad (3.49)$$

The extended Langmuir isotherm

$$q_i^{*}(z,t) = \frac{K_{Li}^{o} c_i^{*}(z,t)}{1 + \sum_{j=1}^{N} a_{Lj}^{o}\ c_j^{*}(z,t)} \qquad (3.50)$$

The extended Redlich-Peterson isotherm

$$q_i^{*}(z,t) = \frac{K_{Ji}^{o} c_i^{*}(z,t)}{1 + \sum_{j=1}^{N} b_{Jj}^{o}\ c_j^{*}(z,t)^{\beta_{Jj}^{\circ}}} \qquad (3.51)$$

3.7.2.3. Effluent concentration

The model is solved numerically for the bed axial distance, radial distance, and operation time dimensions. Appropriate values for the incremental step sizes of the three dimensions are chosen to ensure solution method stability. Output from the model is given as effluent liquid-phase concentrations for each adsorbate at each time

increment (if a non adsorbable fraction is present in the influent, it is added to the effluent concentration):

$$c_{eff,i}(t) = c_i(z = L, t) \tag{3.52}$$

3.7.2.4. Mass transfer coefficients

In addition to the characteristics of the media and the flow conditions, the most important aspect governing the extent of adsorption is the diffusional process. It was explained above that diffusion is considered as the major resistance to transport of the adsorbate to the location of the adsorption point. Two diffusive transports are considered:

- One is the diffusion along the adsorbent surface. The corresponding surface diffusion coefficient is $D_s(t)$. It varies with time since it depends on the influent concentration and the adsorbate load on the adsorbent surface ($q_{inf}^*(t)$) since the driving force is the concentration gradient. Porosity influences this since as it increases, more surface is available, hence a lower adsorbate flux per unit of surface area. It also depends on the diffusion in the liquid phase via the fitting coefficient α; at this stage, pore diffusion is included in surface diffusion. The numerical expression of surface diffusivity is:

$$D_s(t) = \frac{c_{inf}(t)\ D_l(t)\ \alpha\ (1-\varepsilon)}{q_{inf}^*(t)} \tag{3.53}$$

- The second diffusional transport is diffusion in the liquid phase. It depends on the temperature, T and on the fluid viscosity, μ. It also decreases as the molecular volume V_M increases. The equation for liquid diffusivity is:

$$D_l(t) = \frac{5.0624 \times 10^{-14} T}{\mu(t)\, V_M^{0.6}} \qquad (3.54)$$

- Finally and depending on the flow conditions surrounding the adsorbent grains, the travel of the adsorbate through the liquid film is based on the external film coefficient $k_f(t)$. It involves the dimentionless numbers Reynolds number, Re and Schmidt number, Sc, as well as the influent superficial velocity and the porosity. k_f is expressed as:

$$k_f(t) = \frac{U(t)}{\varepsilon} \frac{0.765\,\mathrm{Re}(t)^{-0.82} + 0.365\,\mathrm{Re}(t)^{-0.386}}{Sc(t)^{2/3}} \qquad (3.55)$$

With $k_f(t)$: external film mass transfer [m/s]

$U(t)$: superficial water velocity in bed at time t [m/s]

ε: bed porosity

3.7.3 GACMan user interface

GACMan displays four main sections accessible to the user: simulation, run, results and calibration. The flowchart in figure 3.7 represents the four sections and their corresponding input data.

Calibration in GACMan puts together the data necessary to complete the simulation. This means that data relative to the adsorbent and to the adsorbate must be available, as well as the isotherm constants relating the specific adsorbent to the specific adsorbate. In other terms, calibration of the adsorbate on the particular adsorbent must be completed. This can be done two ways: *(i)* using batch experiments where the equilibrium is reached; this will enable the estimation of constant values from the isotherm, or *(ii)* using the experimental breakthrough profile from a single filter. This involves having a dataset giving the flow, the influent concentration and the effluent concentration as a function of the time. One dataset will provide the model with the value for one constant only, the other needs to be imposed. Two datasets provide both values (for either the Freundlich or Langmuir or three datasets for the Redlich-Peterson isotherm).

Since equilibrium experiments values were performed in this work, K and n values can be directly input in equation (3.46b) for the calibration, using method *(i)*.

The next parameter of great importance is α (adimentional), which is used to calculate the surface diffusion at time t, using equation (3.53). It can be imposed or fitted to adjust the experimental data, in which case the software automatically assigns and runs the programme for the following values: 0.1, 0.14, 0.18, 0.24, 0.48 and 0.7. The best fitting α value must then be selected. In GACMan, a prediction within ±20% of the experiment data is considered as satisfactory.

The diffusion coefficient depends on the nature and conformation of the molecule, and on the solution temperature. For this reason, when calibrating a new adsorbate, GACMan requires its molecular volume ($cm^3/gmol$) as well as its pesticide critical volume (PCV in μg/L), since GACMan is used principally for simulation of pesticides adsorption. This last data (PCV) is not compulsory but only optional in case it is known. In this study and according to the GACMan userguide (1994), the molecular weight is used instead of the molecular volume which is unknown. Molecular volume is related to the chemical groups and the structure of the molecule. As for DOC and humic substances, such calculation is impossible since there is no clear definition of the molecule. Molecular weight is then accepted as a reasonable estimate.

Once estimated, the isotherm constants and α for the adsorbent/adsorbate/water type system can be stored in GACMan library, removed and used for further runs.

During the calibration and using the dataset provided, GACMan calculates the equilibrium capacity. As the contaminant (DOC for this study) accumulates on the adsorbent, it reaches its equilibrium capacity q when breakthrough occurs. Such capacity is calculated as follows:

$$q(t) = q(t - \Delta t) + \frac{Q(t) \times \left(C_{\text{inf}}(t) - C_{eff}(t)\right)}{m} \Delta t \qquad (3.56)$$

with q(t): cumulative DOC removed at time t [μg / g adsorbent]

Q(t): flow rate at time t [L/s] and t: time [s]

$C_{inf}(t)$ and $C_{eff}(t)$: influent and effluent DOC at time t [μg/L]

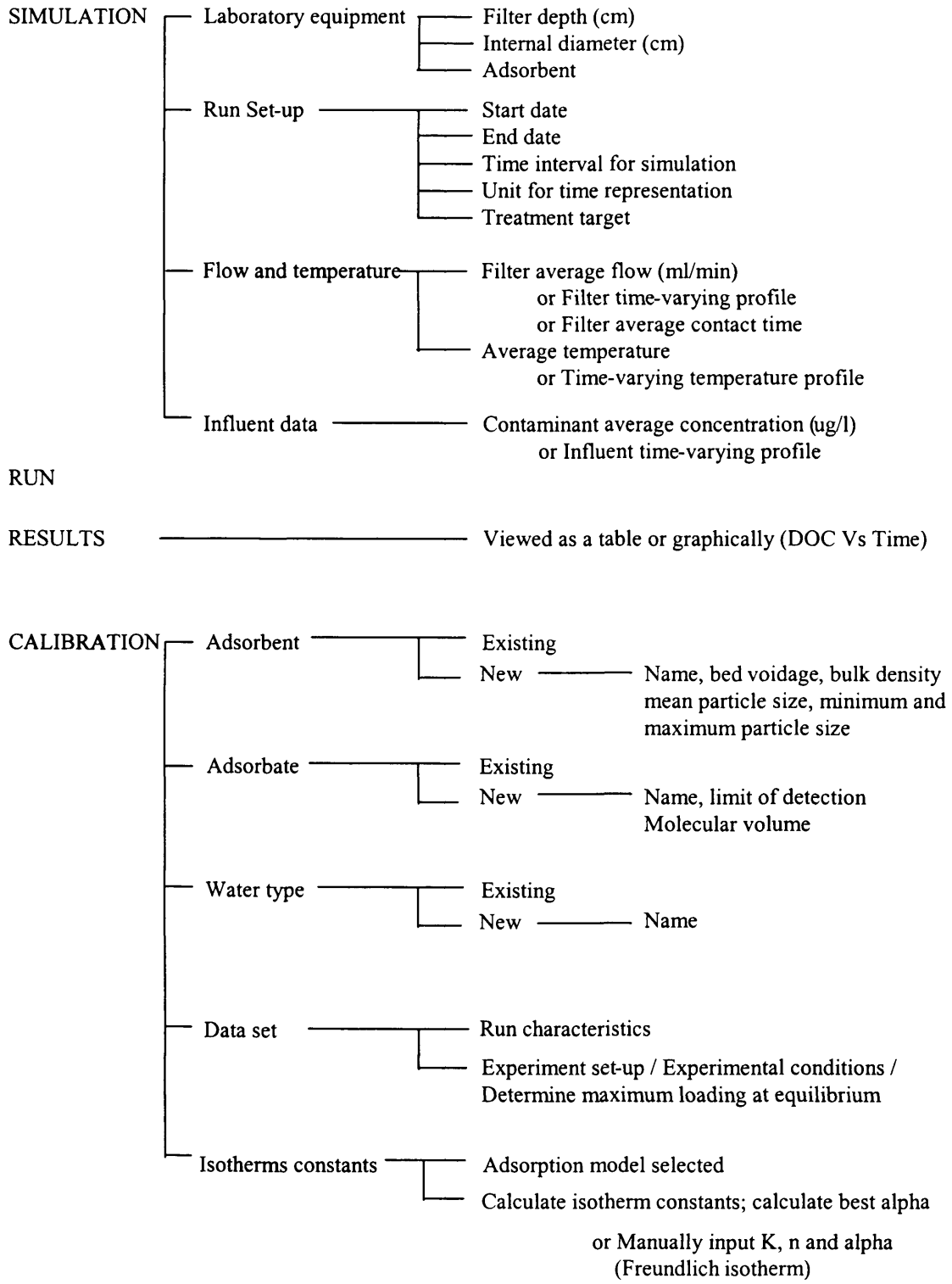

Figure 3.7 GACMan description

Δt= time step between samples

m=mass of adsorbent in the column

However for modelling purposes and since in practice, C_{eff} does not reach C_{inf}, the equilibrium capacity is approached using the following equation:

$$q(t) = A + B \times \frac{C_{eff}(t)}{C_{inf}(t)} \tag{3.57}$$

The extrapolation of $C_{eff}(t)$ to $C_{inf}(t)$ leads to the equilibrium value of q (required for calculation of the surface diffusion coefficient).

From this point, the simulation can be run for the new calibrated system.

3.8 Conclusion

Whether adsorption is favoured or not, as well as the extent of adsorption, is highly dependent on the conditions surrounding the system under study. Adsorption of humic substances is dependent on the environment. Parameters such as the pH, the ionic strength, and the presence of calcium must be considered since HS behave like both hydrophilic and hydrophobic species and short range and long range forces are involved. The steric effect and competition between various molecular weights influence the efficiency of adsorption. Adsorbents used for this purpose are GAC (commonly used) and inorganic compounds like aluminium or iron oxides. These are investigated more and more since,, although GAC has a very large surface area and a high isoelectric point, it is not always the most convenient for use on a wide range of adsorbate size. β-FeOOH has recently been investigated and coated inorganics are also emergent adsorbents, although coated activated alumina is not yet mentioned. It seems that ligand exchange is a favoured mechanism for adsorption on inorganic oxides.

As for the kinetics, models applied to single solute adsorbate can also be applied to humic substances for which much research remains to be done. In most cases studied (often on GAC), diffusion is the rate-limiting step to adsorption. The equilibrium in adsorption provides valuable information from the isotherm shape and its hysteresis.

Again due to the wide MW range of HS, isotherms are likely to be valid only on a narrow range of concentration. As for adsorption as a continuous process, general and simple equations can be used, such as the Thomas equation and the Bed Depth Service Time model. They are most useful analytical models for estimating the necessary parameters for a continuous operation.

Simulation and prediction of a continuous adsorption process can be achieved with numerical models taking the multicomponent aspects into account as well as the kinetic and most relevant isotherm model. Such models constitute a vast field for research as they can also include the competition between the adsorbates.

CHAPTER 4

MATERIALS AND METHODS

4.1 Introduction

This work is based on experimental investigation to remove the humic substances from drinking water supply using inorganic adsorbents. This chapter aims to describe the full experimental framework, including both the experimental set-up and the data monitored. It begins with a description of the humic substances, their fractionation and the parameters selected to represent the adsorption behaviour. In a second stage, interest is drawn to the adsorbents and their physico-chemical characteristics which are useful in order to understand the adsorption process. Finally, the three categories of experiments are described, the kinetics investigations, the equilibrium and the column experiments.

4.2 Selection of humic substances

Humic substances are available as powders extracted from river or lake water (aquatic humics), from peat or from soil (terrestrial humics). Ideally, river water would be used to run the experiments (real situation) but three main disadvantages lead to that option being discarded:

- Complex background of real water (i.e. many parameters not controlled)
- Quality of river water is not constant
- Difficulty to store enough water without degradation occurring (no such river water is readily available)

Therefore, it was decided to use powders. Aquatic extracts were discarded since their tedious extraction process makes them very expensive (eg. Suwanee river fulvic or

humic acids). The experiments require considerable amounts of humic substances. The best alternative was to use a commercial soil extract, commonly used for research purposes, namely the Aldrich humic acid with sodium salt (lot number H1-675-2). Technical information for this product was provided by the supplier (Aldrich, UK) and includes the elemental analysis as well as the trace analysis. The results are in chapter five for the characterisation of humic substances.

Soil HS contain more high MW than aquatic HS. Therefore, it is necessary to separate the very heavy weights to prepare the working solutions.

To prepare the initial solution, 10 g of humic acid powder were dissolved in 2 L of deionised water (equipment Elgastat Option 3 Water purifier, from Process Water Group, High Wyecombe, Bucks, UK). The flask was shaken for several minutes and a thick deposit settled. The supernatant was separated using a centrifuge (Beckman Avanti, Ireland, UK) (rotor J10) at 10000 rpm for 2.5 hours. According to Standard Methods for the Examination of Water and Wastewater (1998), Dissolved Organic Carbon (DOC) defines the organic substances under the size of 0.45 μm, as opposed to the Total Organic carbon (TOC) that includes both dissolved and suspended solids. Therefore the supernatant recovered from the centrifugation was filtered to eliminate the suspended solids. This was done progressively using the following filters: Whatman number 3 (6μm), Whatman glass microfibre GF/F (2.5 μm), GF/B (1.2 μm), GF/C (0.7 μm) and finally on a 0.45 μm cellulose acetate (Millipore type HA). The latter was soaked in 10% nitric acid overnight to prevent any of the cellulose acetate compounds from generating additional DOC in the filtrate. The recovered filtrate was the stock solution used for further fractionation.

It is known from previous studies (Tipping, 2002, Frederick, 2001) that Natural Organic Matter (NOM) such as humic substances combine with calcium before adsorption on GAC or other type of adsorbents. Therefore, the background of the solution needs to be carefully considered for bench experiments and for continuous flow studies. Using London tap water is not representative of real HS-containing natural water. It would also bias the results since a great part of the HS removal could be due to complexation and precipitation with Ca and Mg, and not to adsorption. The working solution will be adjusted to have a calcium concentration of 0.5 mmol/L to reproduce a soft water background. According to Thurman (1985), fulvic acids behave like isolated ions; therefore, the above problem should particularly concern higher molecular weights

molecules (humic acids). On the other hand, calcium influence might be lessened in the presence of iron-containing adsorbent, since for a pH below or equal to 7, Ca-NOM and Mg-NOM are too weak complexes to compete with iron (Frederick, 2001).

4.3 Fractionation

After a review of various separation methods to fractionate humic substances according to their molecular weights (see chapter 2, section 2.3.1), cost, scale of operation and availability of equipment were the decisive criteria towards the selection of the process. Ultrafiltration has been chosen and the molecular weight cut off (MWCO) selected values were 5 kDa, 10 kDa, 50 kDa and 100 kDa. The membranes were polyethersulfone (PES), Vivaflow 50 (from Sartorius Ltd, Epsom, Surrey, UK), reusable after following the cleaning and storing procedure. The pump used for this separation process was a Watson Marlow (HR flow inducer, type MHRE 200). The fractionation of the stock solution was done in 4 steps, starting with the 100 kDa (set-up is shown in figure 4.1):

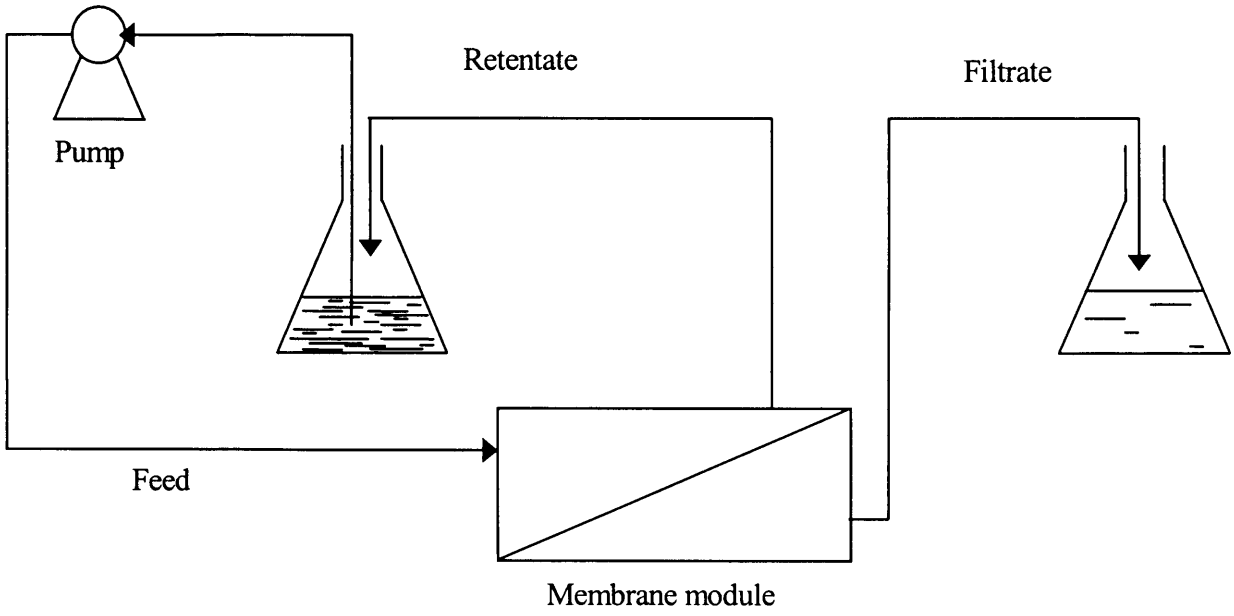

Figure 4.1. Ultrafiltration set-up

step 1 use membrane MWCO: 100 kDa

feed: stock solution

retentate: MW > 100 kDa

permeate: MW < 100 kDa

step 2 use membrane MWCO: 50 kDa

feed: MW < 100 kDa

retentate: 50 kDa < MW < 100 kDa

permeate: MW < 50 kDa

step 3 use membrane MWCO: 10 kDa

feed: MW < 50 kDa

retentate: 10 kDa < MW < 50 kDa

permeate: MW < 10 kDa

step 4 use membrane MWCO: 5 kDa

feed: MW < 10 kDa

retentate: 5 kDa < MW < 10 kDa

permeate: MW < 5 kDa

Finally five fractions are obtained:

F1: MW < 5 kDa

F2: MW = 5-10 kDa

F3: MW = 10-50 kDa

F4: MW = 50-100 kDa

F5: MW > 100 kDa

F0 is the original solution, before fractionation.

Fractions were stored in the fridge at 4 degrees, in the dark, and were used within 3 to 4 weeks. Before use, fractions were diluted with deionised water to reach a DOC around 10 mg/L. Their pH was adjusted to 7.0 (Hannah Instrument HI 9812, Fisher Scientific, Loughborough, Leicester, UK). Calcium concentration was adjusted to 0.5 mmol/L using $Ca(NO_3)_2.4H_2O$ (236.15 g/mol), analytical grade supplied by BDH.

4.4 Parameters monitored and equipment

4.4.1 Sample preparation

All samples were analysed for both UV_{254} and DOC. From these two parameters, the third one of interest, SUVA, was calculated as the ratio UV_{254}/DOC. Prior to analyses, sampling involved (for batch kinetics, equilibrium and column studies):

- Filtering 25 ml of solution through a 0.45 μm syringe filter (25 mm Millipore HA, previously soaked for 12 hours in 10% nitric acid). The influence of the filter type has been studied by comparing various filters: Millipore HA type filter (47 mm, vacuum applied), PES syringe filter and PTFE syringe filter. No significant difference was observed on UV absorbance.
- The first 5 ml of filtrate were discarded
- Approximately 5 ml were used for immediate UV absorbance measurement
- Approximately 15 ml (the rest) was stored in a 150 ml PET dark bottle (Decon washed), for DOC analysis. This fraction was immediately acidified with phosphoric acid H_3PO_4 85% (Aldrich, 85%) to pH about 2, and immediately frozen. Samples were defrosted in warm water and immediately transferred to the glass TOC tubes on the autosampler of the Carbon Analyser. Checks were carried out after four weeks storage to confirm that no leaching of organic carbon from the bottle into the sample had taken place.

4.4.2 UV_{254}

UV absorbance at 254 nm was measured on a double beam spectrophotometer (M350 double beam, Camspec Scientific Instruments Ltd, Sawston, Cambridge, UK). To avoid the imperfection of matching cuvettes when using a double beam, only one beam was

used with a 1 cm quartz cuvette. The zero was achieved with deionised water and the cuvette was regularly left to soak in concentrated hydrochloric acid as soon as the absorbance of deionised water significantly increased (due to unclear cuvette walls).

4.4.3 DOC

Dissolved Organic Carbon (DOC) analyses were performed on a Dohrman DC-80 Carbon Analyser. It uses the persulphate and UV oxidation, with an infrared carbon detector. Previous acidification and sparging (2 minutes) eliminated the inorganic carbon. Since samples were filtered on a 0.45 µm filter, DOC was measured and not TOC. The accuracy of the results is ±0.5 mg DOC/L.

4.4.4 SUVA

The Specific UV Absorbance (SUVA) index was calculated as follows (equation below is already written as equation 2.2 in chapter 2):

$$SUVA = \frac{UV_{254}}{DOC}$$

Using the unit (m^{-1}) per (mg/L), the values of SUVA range from less than 1 to 20, but below 10 is most common (see chapter 5 for the interpretation of SUVA values).

4.5 Selection of adsorbent

4.5.1 Adsorbents selected and information from suppliers

Granular Activated Carbon (GAC) is very commonly used in water treatment. However, such a general name does not correspond to a specific adsorbent since it will vary greatly according to its origin and activation. In general it is agreed that it removes some of the humic substances and therefore GAC was selected here as a reference for comparison. The particular type used here was GAC 207C, which is known to be a high activity carbon.

It is also of interest to be able to regenerate the adsorbent on-site so as to eliminate high costs associated with thermal regeneration. The new adsorbents should therefore be able to withstand high pH elevation corresponding to chemical regeneration.

New adsorbents of interest for HS removal tend to contain iron or aluminium. This idea comes from the efficiency of coagulation in removing HS (heavy MW range). Hence, the interest of applying the destabilisation and complex forming capacities to adsorbents.

From these considerations, two adsorbents were tested for these new applications. They were: activated alumina coated with iron sulphate (named AAFS 50) and iron oxihydroxide β-FeOOH (known as akaganeite). Both adsorbents are efficiently used to remove arsenic from drinking water. As a matter of comparison during the characterisation of adsorbents, non-coated activated alumina (named AA 400G) has also been used (but not for adsorption studies). General characteristics given by the suppliers are listed in table 3.1. These data will be used to compare and discuss the results further ahead.

4.5.2 Characterisation of the adsorbents

Characteristics specific to bed filtration are easily estimated from laboratory analyses. These are concerned with the media sphericity, bulk density, size distribution, porosity. Other characteristics are more adsorption specific and will be essential to applying adsorption model using isotherms; these are the surface area and the pore size distribution. Additional characteristics such as Fourier transform infrared spectroscopy (FTIR) and scanning electron microscopy (SEM) provide valuable qualitative information about the aspect of the adsorbent surface. An additional characteristic is the zero point of charge (pH_{zpc}) that gives the surface charge according to the pH, an essential piece of information in order to understand and explain the adsorption process. These analyses are described below.

4.5.2.1 Bulk density

The measurement is based on the British Effluent and Water Association (BEWA) criteria, stating that the bulk density should be the volume occupied by the media after a backwash. In this case, a known weight of media (between 20 and 25 g) was poured into a 25 ml flask and sealed. After slowly inverting the flask, the volume in the upright position was read. The weight divided by the volume gave the bulk density. Three repetitions were carried out.

Table 4.1 Adsorbents characteristics

	GAC 207C	AA (400G)	AAFS (50)	B-FeOOH
Supplier	Universal Mineral Supplies Ltd	Alcan Chemicals	Alcan Chemicals	GEH Wasserchemie
Usual use	General purpose for liquid and vapour phase	Drinking water for arsenic removal	New adsorbent	Drinking water for arsenic removal
Main component	High activity carbon	Armophous, χ and γ forms of Al_2O_3	Armophous, χ and γ forms of Al_2O_3,Coated with iron sulphate	$Fe(OH)_3$ and β-FeOOH
Size of grains	Mesh 12-30 0.5-1.4 mm	Mesh 28-48 0.32-0.56 mm	Mesh 28-48 0.32-0.56 mm	0.32-2 mm
Surface area	1050 m^2/g	350-380 m^2/g	350-380 m^2/g	100 m^2/g

4.5.2.2 Size distribution

Size distribution is determined by sieving the adsorbents with sieve sizes selected to be within the size range given by the supplier (sieves and shaker from Endecotts). Four diameters were measured: d_{10} (effective diameter), d_{50} (median diameter), d_{60} and d_{90}. They correspond to respectively 10%, 50%, 60% and 90% of the adsorbent grains in weight, being smaller than the stated diameter. Duplicates were used.

4.5.2.3 Porosity

Porosity accounts for the voidage due the stacking of adsorbent grains one over the other in a given volume. The higher the porosity the larger the voidage, i.e. little volume is occupied by the grains as opposed to a small porosity where the grains occupy most of the volume leaving little space for the water to flow. The procedure is the one

described by BEWA. The figure of interest is the bulk porosity or poured porosity ε_p (excluding the internal grain porosity). Since the media is porous, it has first been soaked and mixed with water overnight, so as to fill the pores with water. It is then dried at approximately 50°C degrees. As soon as the media can be handled as a powder (ie. when bulk water has evaporated but not the pore water). It is poured into a measuring cylinder and the unpacked volume is measured (V_1). The volume V_2 is the packed volume (after tapping the cylinder to compact the media). The volume of water V_3 (25ml) is added. After sealing the cylinder, it is inverted to help the air bubbles to escape. To ensure the elimination of air, vacuum is also applied. The volume read is V_4. Poured porosity is:

$$\varepsilon_p = \frac{V_1 - (V_4 - V_3)}{V_1} \tag{4.1}$$

V_2 is used instead of V_1 to obtain the packed porosity. Three replicates were obtained.

4.5.2.4 Grain density

Grain density corresponds to subtracting the porosity to bulk density. Its value is calculated as follows (BEWA):

$$Grain\ density = \frac{Bulk\ density}{1 - poured\ porosity} \tag{4.2}$$

4.5.2.5 Surface area

The equipment used is the Surface Area Analyser from Micrometrics Instrument Corp., model ASAP 2010. The analysis is based on the adsorption of an inert gas (nitrogen) onto a solid increasing with the pressure of the gas, at constant temperature (77 K). Degasification was done for 15 hours, at 150°C. Details of the Brunauer Emmett and Teller (BET) method are described in chapter 3.

4.5.2.6 Pore size distribution

Pore size distribution was calculated according to the Barret, Joyner and Halenda (BJH) method for the macropores (Marczewski, 2002) and according to Horvath-Kawazoe method for the micropores (Jarionec et al., 2003). Data used are the same as for BET, described in chapter 3. The instrument is the same as for the surface area analysis.

4.5.2.7 Fourier Transform InfraRed spectra (FTIR)

To compare qualitatively the organic functional groups of humic substances adsorbed on the adsorbents, a Fourier Transform InfraRed analysis was carried out. Samples were taken from the column after adsorption of various fractions of MW of HS onto the selected adsorbents. It was carried out by following Al-Ghouti's method (2004), on the FTIR Perkin Elmer Spectrophotometer RX I instrument. The samples (dry adsorbent with and without adsorbed humic matter) were dried for 18 hours at 65 degrees Celsius. A small quantity of the sample was ground with KBr and pressed by the tool provided. The disc which was formed was placed in the instrument. The disc was scanned in transmission mode through a wavelength range from 400 to 4000 cm^{-1}. Before each measurement, the instrument was run to collect the background spectrum which was then automatically subtracted from the sample spectrum (method described by Al-Ghouti, 2004).

4.5.2.8 Scanning Electron Microscopy (SEM)

Scanning Electron Microscopy gives useful information about the porosity of the adsorbent, its surface aspect and the elemental constitution of the samples. Analyses were done in the Eastman Dental Institute, University College London. Preparation of the samples is described below:

- All samples were fixed in 3% glutaraldehyde (Agar Scientific, UK) in 0.1M cacodylate buffer (CAB) for 24 hr (or longer) at 4°C.
- They were dehydrated at room temperature in a series of graded ethyl alcohols of 25%, 50%, 70%, 90% for 15 min each and 3 changes in 100% for 10 min each.
- Samples were then critical point dried by immersion in hexamethyldisilazane (TAAB Ltd, UK) for 5 min and subsequently dried in a fume hood for at least an hour.
- Particles were sprinkled onto adhesive carbon tabs (Agar Scientific, UK) attached to aluminium pin stubs.
- All samples were sputter coated with gold/palladium (Polaron E5000, Quorum Technology, UK)
- Samples were examined in a Cambridge 90B SEM (Leo, UK) operating at 15kV.

- Digital images were acquired with an I-Scan slow scan system (ISS Group, UK).

4.5.2.9 pH of Zero Point of Charge (pH_{zpc})

The pH of Zero Point of Charge (pH_{zpc}) has been estimated using the acid-base titration, following Al-Ghouti's method (2004). 24 glass erlenmeyers of 100 ml were used, previously soaked in nitric acid 10% for 24 hours. Each contained:

- 2.5 g of adsorbent
- a known amount of acid HCl (0.25 M) or base NaOH (0.25 M), from 0 to 6 ml.
- $Ca(NO_3)_2$ to reach the concentration as in the column supply solution (0.5 mmol Ca/l)
- Deionised water to bring the volume to 25 ml.

The erlenmeyers were fixed on an orbital shaker (IKA KS260 Control). Shaking went on for 24 hours at 200 rpm. The pH of the solution was then measured. Duplicate experiments were run. The largest error was ± 0.13, with a mean of ± 0.05. The surface charge σ (C/m^2) was calculated using equations described by Stumm and Morgan (1995).

$$Q = \frac{C_A - C_B + [OH^-] - [H^+]}{m} \tag{4.3}$$

$$[OH^-][H^+] = 10^{-14} \tag{4.4}$$

$$\sigma = \frac{QF}{S} \tag{4.5}$$

with C_A and C_B acid HCl and base NaOH concentration (0.25 M)

m mass of adsorbent per litre [g/L]

Q average surface charge [C.mol/g]

10^{-14} water ionic product

σ surface charge density [C/m^2]

S Surface area [m^2/g]

F Faraday [96500 C/mol]

The graph σ Vs pH was plotted. The intersection point between the σ-pH curve and the pH axis is the pH_{zpc}, i.e. the pH when the net surface charge is zero.

4.6 Kinetics investigations

The first purpose of the kinetic study was to define the time required for the adsorption process to reach equilibrium for a particular system of adsorbate-adsorbent. This was done in batch experiments. The equilibrium is reached when the rate of adsorption is equal to the desorption rate. Overall diffusion (film, surface and pore diffusion) is the limiting step. Initially, the gradient of concentration between the solution and the adsorbent surface (external and internal) is large and decreases until being null as the equilibrium is reached. This can be discussed when the adsorbate is not a single component (as a well defined pesticide molecule for example) but a multicomponent system where one component can displace another component already adsorbed or can be non-adsorbable or non-desorbable. It is assumed that the equilibrium is reached at the same time, be it for UV absorbance or DOC. Therefore, only the UV absorbance is used for this first investigation.

A fixed weight of adsorbent is mixed in a 250 ml conical flask with 250 ml of the working humic substances solution. For each adsorbent, each dose is investigated and a control (solution with no adsorbent) is used. The samples are shaken on an orbital shaker (IKA KS260 Control, Fisher Scientific) at 200 rpm. Flasks are removed after different contact times from 0 to 168 hours. Samples are filtered and analysed for UV absorbance.

A second purpose of these adsorption experiments is to fit various kinetics models to improve the understanding and to analyse the dominant process during adsorption. The results of UV absorbance decrease with increased contact time are converted to a decrease in DOC using a fixed SUVA value. The solution used was F0, i.e. the non-fractionated humic substances solution, containing the whole range of molecular weights. SUVA was assumed constant in this case. Although SUVA might vary during the adsorption and particularly at the start due to competition between the various

molecular weights, such an assumption was necessary to obtain a coherent unit for the diffusion coefficient. The diffusion coefficient would actually be different for each molecular weight and molecule configuration. The coherence of the results will confirm if the assumption is reasonable or not for the attempt to calculate the diffusion coefficient. The adsorbed DOC at time t is calculated as q_t:

$$q_t = \frac{(UV_0 - UV_t)V}{SUVA \times m} \tag{4.6}$$

with UV_0 initial UV absorbance at 254 nm [m^{-1}]

UV_t UV absorbance at 254 nm at time t [m^{-1}]

V Volume of solution 0.250 [L]

SUVA 9.5 [L/m mg]

m mass of adsorbent [g]

4.7 Equilibrium experiments (batch studies)

The purpose of these experiments is to determine the isotherms describing the humic substance adsorption onto the selected adsorbents. After characterising the humic substances, it was decided that studying molecular weights beyond 50 kDa would not bring any relevant information for realistic situation. SUVA did not change much beyond 50 kDa and aquatic humics would contain MW towards the lower range. In addition, it was shown that very high MW are actually aggregates of lower MW and Aldrich substances mainly contain MW below 20 kDa. Therefore, experiments concentrate on 3 fractions:

-fraction F1 : MW range 0-5 kDa

-fraction F2 : MW range 5-10 kDa

-fraction F3 : MW range 10-50 kDa

Solution F123 is also investigated, containing all three ranges, from 0 to 50 kDa. Each range is investigated for each adsorbent (GAC, AAFS and β-FeOOH) and duplicates

were run. This lead to 24 experiments. The orbital shaker used for this series of experiments receives 24 flasks plus one control (solution under study without any adsorbent). Hence, the possibility of running 3 experiments at a time. The experiments involved the following steps:

1. 8 Erlenmeyer flasks of 150 ml are soaked overnight in a 10% nitric acid bath, to avoid any contaminating organic carbon (analytical reagent grade, BDH from Fisher Scientific)
2. the solution is prepared so as to obtain a DOC between 10 and 15 mg/L (dilution calculated from the characterisation of HS and from the UV absorbance measurement)
3. a precise mass of adsorbent is weighed after taring the balance (Mettler AE160, ±0.1 mg) with the flask; this is done for the 8 flasks, increasing the adsorbent weight each time
4. the 8 flasks are positioned on the orbital shaker (IKA KS260 Control, Fisher Scientific) in a controlled temperature room; the temperature is 19°C ± 0.5
5. 50 ml of the solution under study is pipetted into each flask, plus in the control flask.
6. each flask is sealed with parafilm
7. the shaker is set at 200 rpm and covered so as to avoid any light influence
8. the shaker is stopped 4 days (96 hours) later
9. samples are taken and analysed as described earlier in the paragraph "Parameters monitored and equipment" of this chapter

Note: this is repeated for 2 more experiments (3 x 8 flasks + 1 control)

The amount of UV and DOC adsorbed on the adsorbent was calculated as followed, respectively:

$$q_{UV} = \frac{(UV_{Control} - UV_{sample})}{m} \qquad (4.7)$$

$$q_{DOC} = \frac{(DOC_{Control} - DOC_{sample})}{1000 * (m/50)} \quad (4.8)$$

with q_{UV}: load of UV onto the adsorbent [m^{-1}/g]

q_{DOC}: load of DOC onto adsorbent [mg/g]

$UV_{Control}$: UV absorbance at 254 nm of the control after 96 hours [m^{-1}]

UV_{sample}: UV absorbance at 254 nm of sample after 96 hours [m^{-1}]

$DOC_{Control}$: DOC of the control after 96 hours [mg/L]

DOC_{sample}: DOC of the sample after 96 hours [mg/L]

m: mass of adsorbent in the flask [g]

4.8 Column experiment (continuous flow studies)

Initially two columns of 5 cm diameter were used. This size avoids any wall effect (column diameter to grain median diameter ratio equals 54). The flow was 1.5 L/h. Supply solution was a concentrated stock solution of F123 (HS < 50 kDa), diluted 50 times and adjusted to pH 7.0. Calcium was also added to a concentration corresponding to a soft water. Ports were located at 25 cm, 40cm, 55 cm and 60 cm (effluent). This corresponds to Empty Bed Contact Time (EBCT) equal to 19, 31, 43 and 47 minutes respectively. A chart and a photograph of the rig are shown in figure 4.2.

A more comprehensive work required the continuous flow adsorption to be carried out using lower molecular weights of humic substances. It was decided to use 4 smaller columns whose diameter was 1 cm; they are later called "microcolumns" in this work. Sufficient volume of fraction F1 (<5 kDa) could then be produced to supply the columns. The flow was decreased from 1.5 L/h to 0.03 L/h. The supply solution was not produced online, but prepared by batch. The bed depth was 10 cm. The EBCT was 16 minutes in the described conditions. However, the dimensions of the columns did not respect the criteria for avoiding wall effects. By comparing the results of the adsorption on both size columns, it could be inferred that wall effects were not significant on the microcolumns (see results in chapter 9).

For these experiments, the pump was a 10 way peristaltic pump, Watson Marlow 501. The deionised water unit (for the bigger columns) was from Aqua Engineering & Equipment Inc. Deionised water was pumped to the mixing tube using a pump Watson Marlow HR Flow inducer type MHRE 200 (supplied by Fisher Scientific).

Experiments started as follows:

1. Adsorbent (used as it comes) was poured into the column to make 60 cm or 10 cm of non-packed bed, respectively for the large columns and microcolumns. This size was calculated to have Empty Bed Contact Time between 10 and 45 minutes, and to be able to reach a 100% fluidisation.

2. A backwashing system was installed so as to feed the column from the effluent port (bottom of the column) with tap water. The adsorbent bed was fluidised to 100%, until no air or fines was left (water free of particles and bubbles). GAC required the longest time for this, needing almost 12 hours. It must be noted that tap water is rich in calcium and magnesium, which might have an effect on the adsorbent surface.

3. Supply of humic substances solution was checked: introduction of the concentrated humic solution (stock solution), introduction of the correct quantities of calcium nitrate and chlorhydric acid (to adjust pH at 7.0) and diluted by the deionised water. In the case of the microcolumns, the working solution was prepared in batch (stored in the fridge) and the supply bottle was regularly topped up. The pH rarely needed adjustment for the lower MW weight fractions.

4. The backwashing system was disconnected and the normal downflow process started by switching the pumps on.

5. Time zero was counted from the moment coloured water reached the first layers of adsorbent bed.

6. Samples were taken from the ports and effluent (or effluent only for microcolumns) at designated times, in order to obtain breakthrough curves and analyse the extent of adsorption along the bed depth.

7. Samples were treated, stored and analysed as described previously.

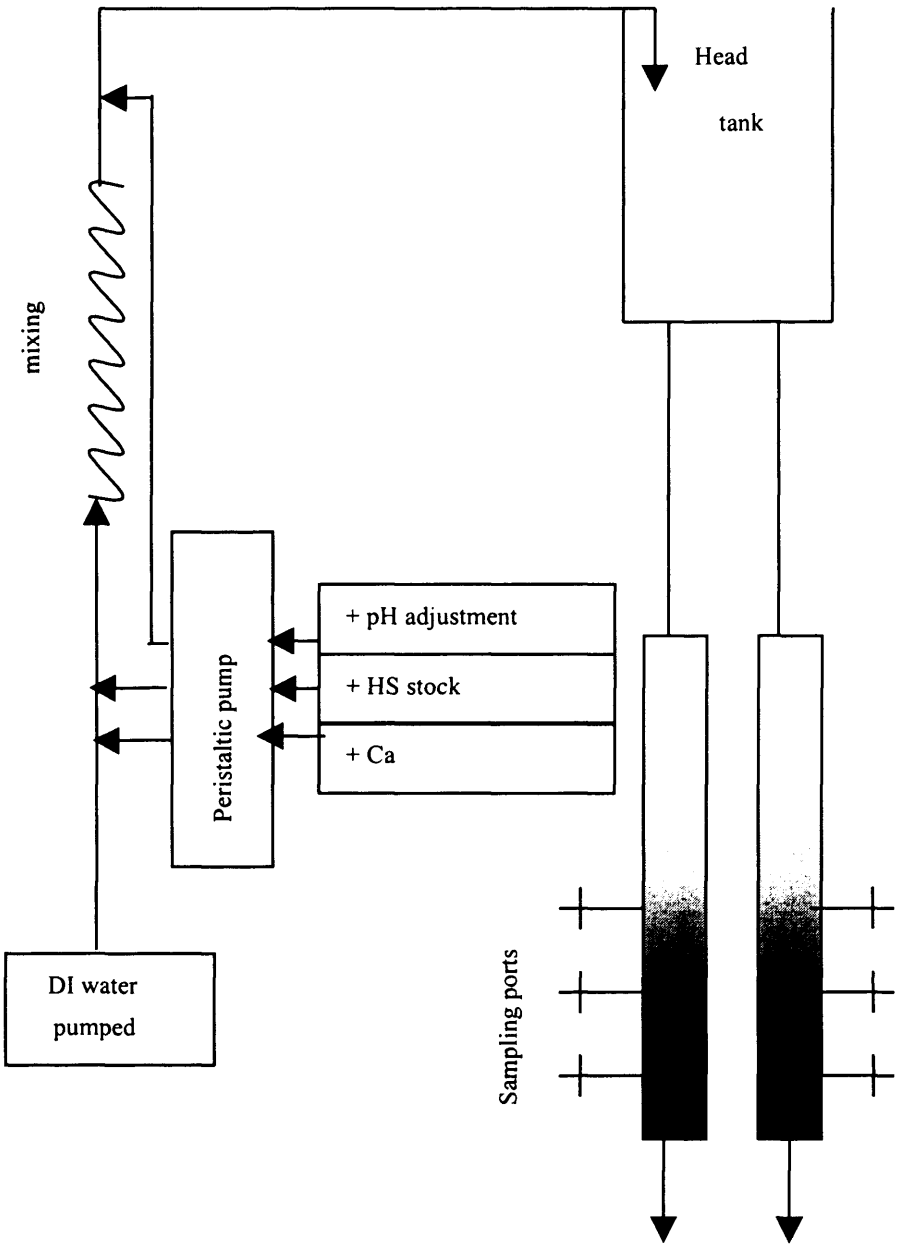

Figure 4.2 (a) Residual Experimental set-up for column studies, showing 5 cm diameter columns

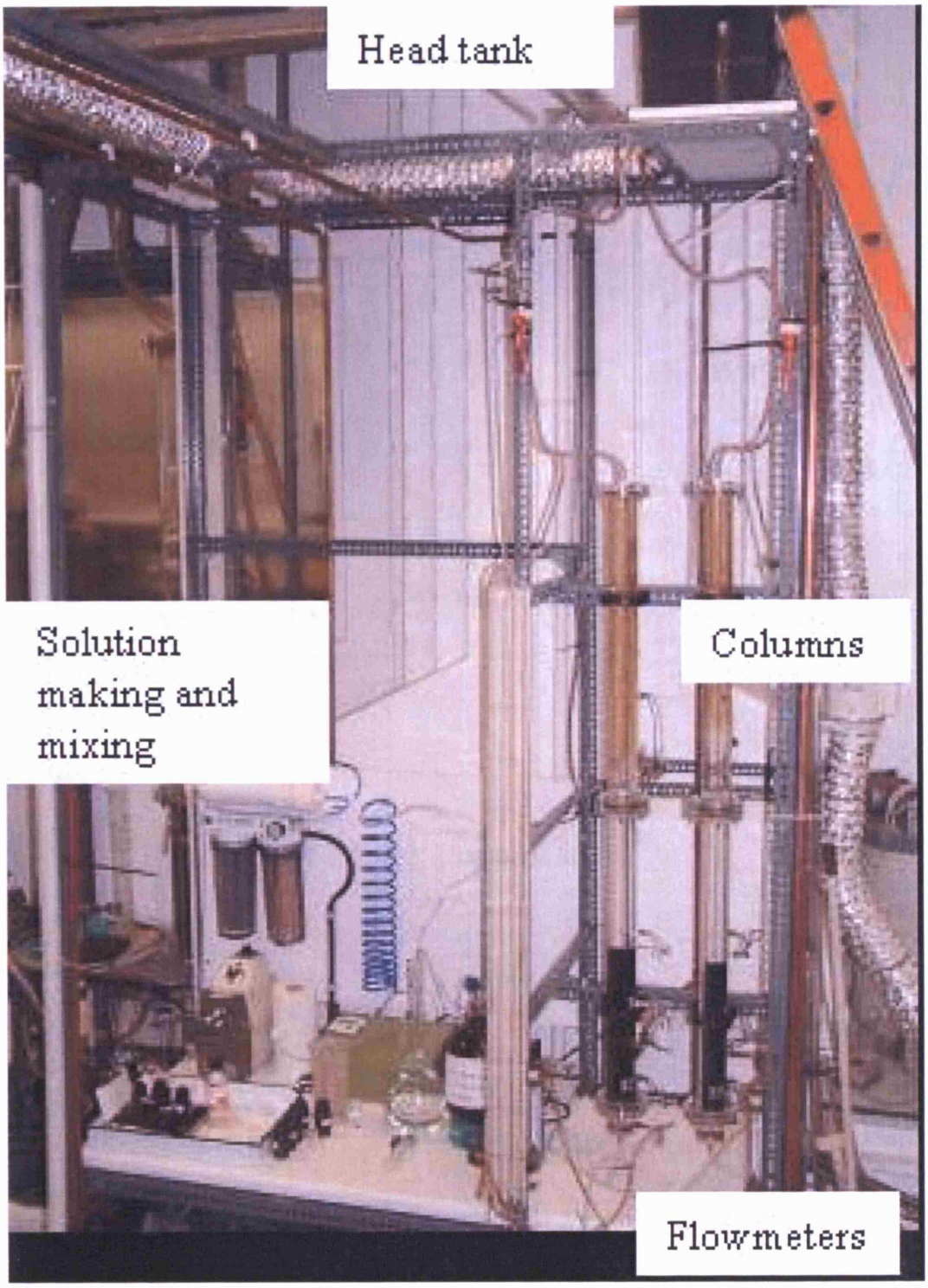

Figure 4.2 (b) photograph corresponding to figure 4.2a

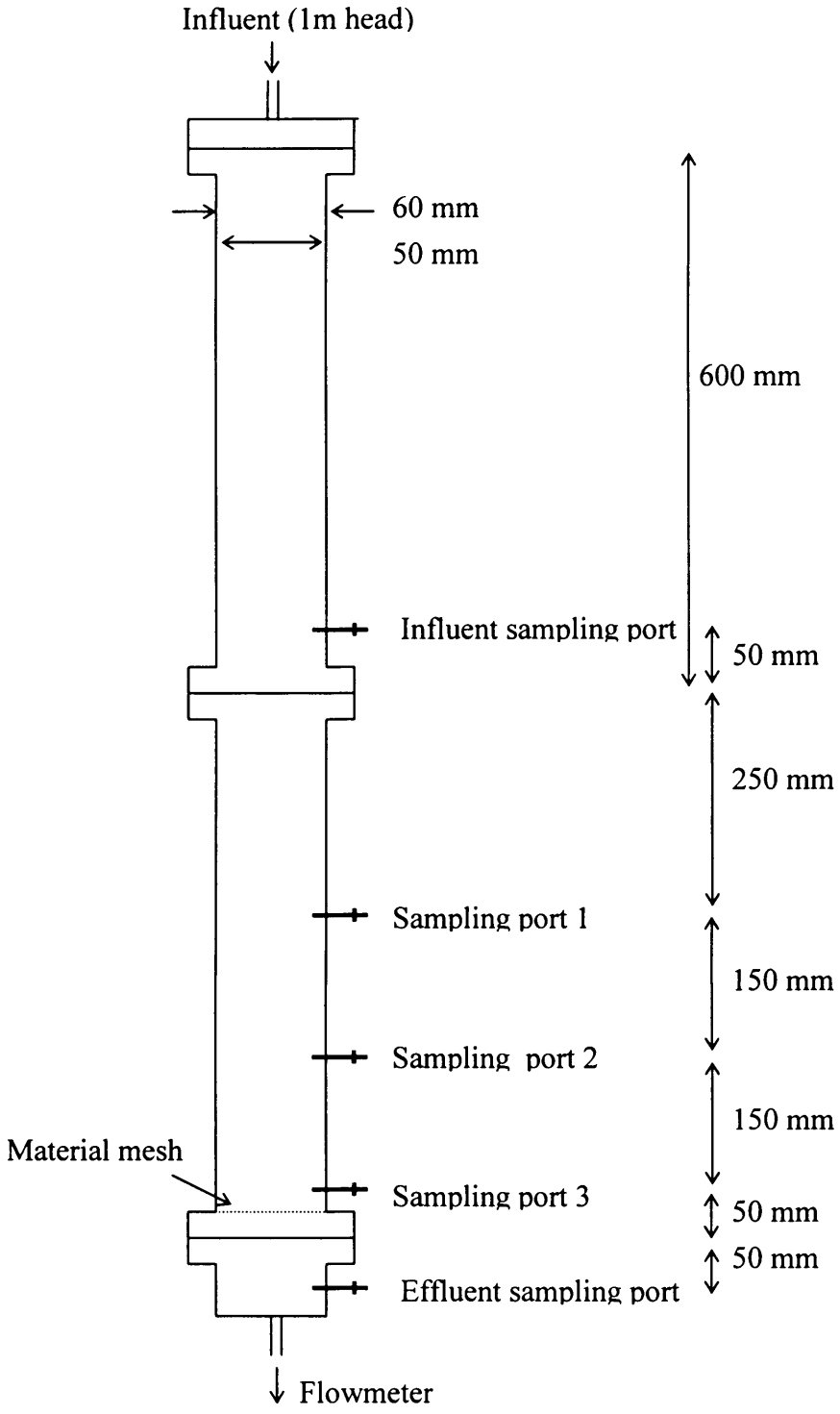

Figure 4.3 Column drawing and dimensions

CHAPTER 5

CHARACTERISATION OF ADSORBENTS AND ADSORBATES

5.1 Introduction

Adsorption can be (i) a physical process when electrostatic and coulombic attraction forces bind the adsorbate to the adsorbent, (ii) a chemical process when chemical bonds bind the adsorbate to the adsorbent and (iii) both a physical and a chemical process when both (i) and (ii) occur simultaneously. Consequently, it is of interest to describe the adsorbents both physically and chemically. The characteristics of the adsorbents are investigated in this chapter so as to provide these two aspects that will be useful in understanding, interpreting and explaining the adsorption results obtained from the experiments (kinetics, equilibrium and column studies). Four adsorbents are considered here; GAC 207C (used as a reference), activated alumina (AA), iron coated activated alumina (AAFS) and ferric oxihydroxide in its beta form (akaganeite β-FeOOH).

Fourier Transform InfraRed spectroscopy (FTIR) gives information about the functional groups in the samples. Although no quantification is applied here and no HS adsorption has yet occurred, each adsorbent exhibits its particular infrared spectrum with possibly protons and hydroxyls attached. The second chemical information is the pH of Zero Point of Charge (pH_{zpc}). This will give an indication of the surface charge of the adsorbent. Physical characteristics are the grain size distribution, density, surface area, pore size distribution and the aspect of the surface obtained from Scanning Electron Microscopy (SEM) pictures.

This chapter also details the characteristics of the humic substances used throughout the project. An important aspect to take into account is the uncertainty of the results, particularly affecting the experimental techniques and measurements. This is considered in the first part of the chapter; the difficulties and disadvantages of separation techniques are also presented. Characteristics of each fraction are analysed and

discussed to suggest the most likely conformation of the humic substances in the working solutions.

5.2 Characterisation of the adsorbents

5.2.1 FTIR

Figure 5.1 shows the FTIR spectrum of virgin GAC 207C. Constant vibrations are attributed to grains slightly too big for the analysis, which can also have shifted some of the peaks in the low frequencies. It can be noticed that all spectra (GAC, AA, AAFS and β-FeOOH) display a band between 2350 and 2310 cm^{-1} which is due to adsorption of atmospheric carbon dioxide. For GAC 207C, this band is band **b**. Band **a** at 3430 cm^{-1} is due to OH stretching, and the CO stretching of the alcohol group is found between 1160 to 1000 cm^{-1} (band **e**). Band **c** at 1550 cm^{-1} comes from the stretching of double bonds C=C in aromatic rings and from the C=O and COO^- stretching. Absorption of the C-O stretch and OH deformation is around 1450 cm^{-1} (band **d**). The basic chemistry of the surface is clearly in agreement with previous studies (Ahmedna et al., 2000) that examined several activated carbons using FTIR too.

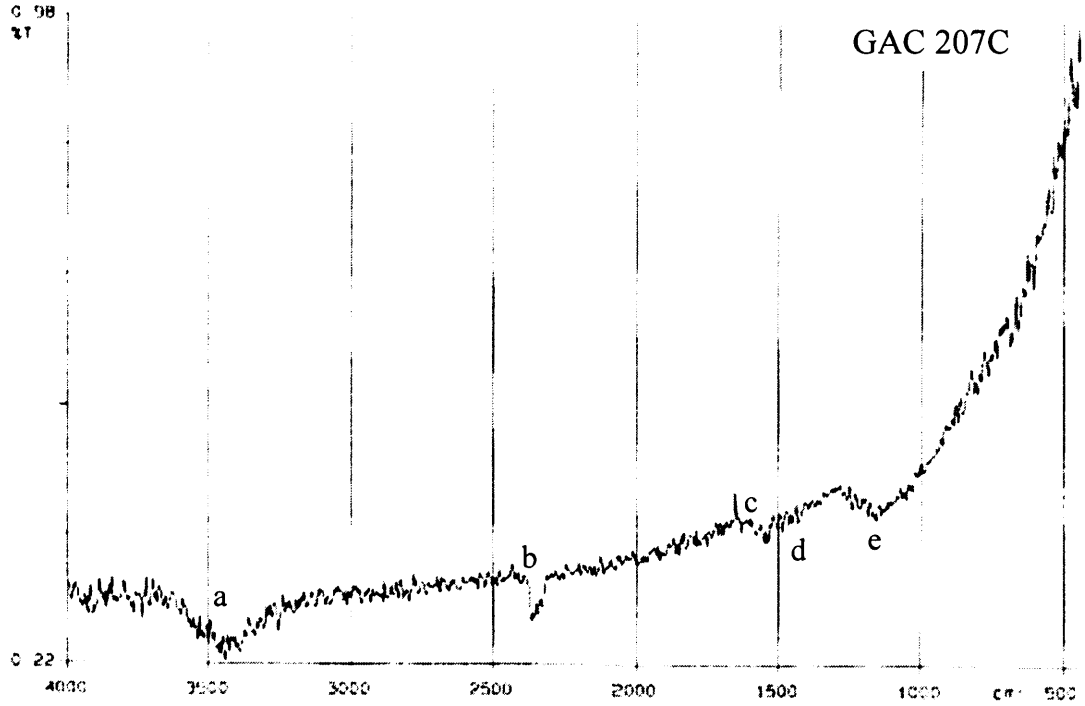

Figure 5.1 FTIR spectrum of GAC 207C

They also found two main regions of absorption; the first is between 1800 and 1540 cm^{-1} corresponding to C=O stretching, and the second region is between 1440 and 1000 cm^{-1} and assigned to C-O stretching and to O-H bending. Still according to Ahmedna et al. (2000), band shifts are most likely present due to factors such as intramolecular and intermolecular bonding, steric effect and degree of conjugation. This makes difficult the precise assignment of each small band within the above described regions, which is why the global structure is identified from the regional absorption only. Ahmedna et al. (2000) also mention several authors supporting these absorption bands assignments (for instance Bansal et al., 1988, Molina-Sabio et al., 1991) in addition of confirming the wavenumber assignments by a second method (titration of the specific functional groups on the adsorbent surface).

Iron coated activated alumina (AAFS) also presents some non-coated white patches. Hence the interest in analysing the two activated alumina FTIR spectra; the original non-coated (AA in figure 5.2) and the iron-coated (AAFS in figure 5.3). Both spectra seem very similar by displaying bands at the identical wavenumbers. An obvious difference appears at 1500 cm^{-1} and 1385 cm^{-1} where bands **f** and **g**, respectively, are clearly distinct on the non-coated alumina but difficult to distinguish on AAFS. Band **a** in the region 3600-3000 cm^{-1} is attributed to strong hydrogen bonds and hydroxyl groups stretching vibrations. These represent lattice water, M-OH (M represents a metal) and hydroxo complexes; they are noticeably more important for AAFS than for AA. Absorption of atmospheric carbon dioxide appears again at 2310 cm^{-1} (band **b**). Band **c** at 2085 cm^{-1} is an overtone of band **h** at 1075 cm^{-1}, itself due to Al=O stretching. This was well studied by Ram (2001) and corresponds to the presence of boehmite in the medium.

The small shoulder at 1950 cm^{-1} (band **d**) could be due to Fe-H bond (Socrates, 2000). However, it also appears (but less obvious) in non-coated alumina. Therefore, it is more likely to represent an overtone of the OH bending (band **h** at approximately 1150 cm^{-1}) added to the O=Al-OH angle bending (band **k** at 770 cm^{-1}) as shown by Ram (2001). It is important to notice that this absorption region is much broader in AAFS than in AA. Several bands overlap and this can only be assigned to the additional presence of the iron compounds and particularly sulphate ions and complexes which exhibit two bands in that range (**h** at 1150 cm^{-1} and **i** at 1075 cm^{-1}) (Socrates, 2000). Sulphate ions explain the very low transmission for bands **h** and **i** (5% vs around 40% for AA). They also

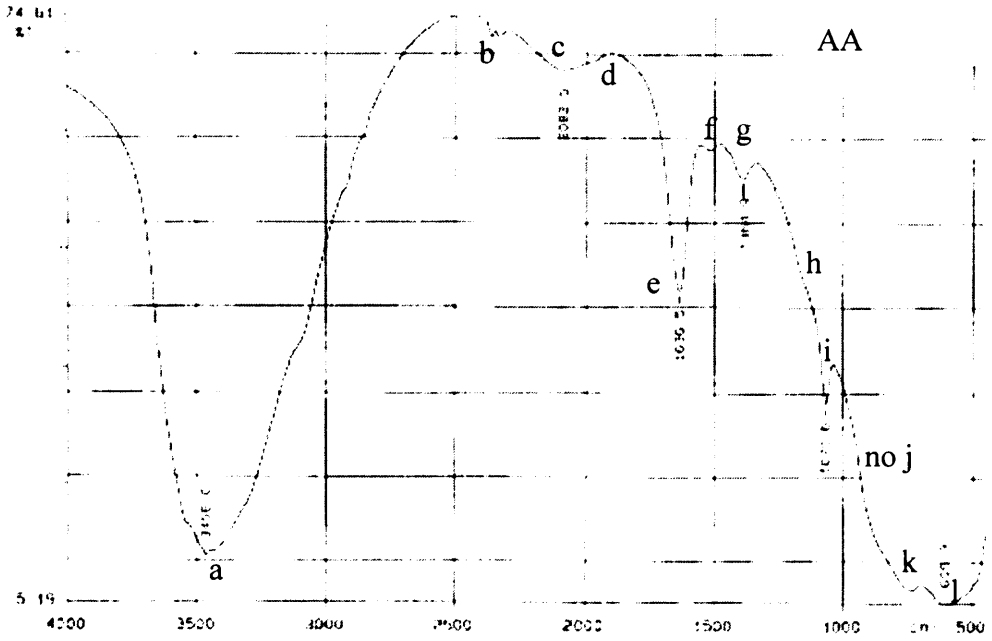

Figure 5.2 FTIR spectrum of Activated Alumina (AA)

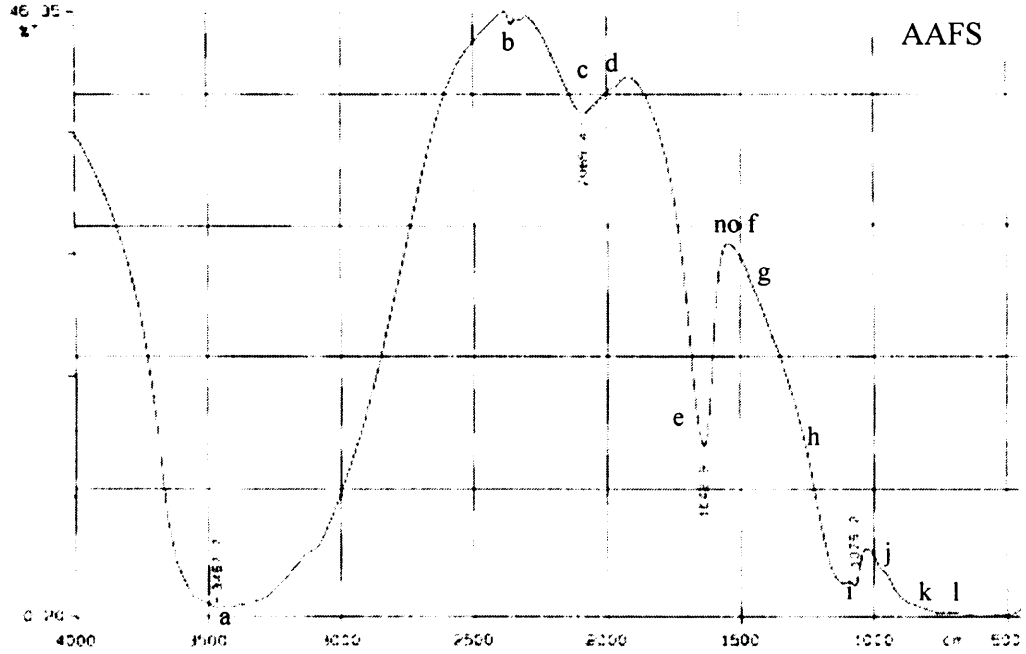

Figure 5.3 FTIR spectrum of iron coated Activated Alumina (AAFS 50)

absorb at low frequencies, although it is difficult to distinguish several bands between 680 and 580 cm^{-1} (band **k** and **l**). Band **e** at 1643 cm^{-1} is attributed to the bending of water molecule bonds H-O-H, centered on 1630 cm^{-1} (Frost et al., 2003).

It could be argued that the 1643 cm^{-1} band would represent absorption by the hydrogen bond to aluminium. However, this occurs in the region 1910-1675 cm^{-1} and it would be expected to be stronger in AA compared to AAFS where numerous aluminium sites would be replaced by iron sites. Absorption band **f** at 1500 cm^{-1} is due to carbonyl compounds and band **g** at 1385 cm^{-1} is attributed to carbonate ions in the presence of iron (Socrates, 2000, Chorover et Amistadi, 2001). Band **g** is small on AA with 54% transmission (AA contain a small proportion of iron oxide) and stronger on AAFS with 25% transmission only, due to the iron content of the coating. The adsorbents have not been treated prior to FTIR analyses, but the exact previous treatment by the manufacturer is not known. It is assumed that CO adsorption and CO_3 complexes formation took place before FTIR analyses. Band **j** at 980 cm^{-1} on figure 5.3 is attributed to sulphate absorption in η-Al_2O_3 , as recognised by Pradhan et al. (2000). They also mention an abundant review of transition aluminas FTIR spectra. Characteristic vibrations were found to be at 3860-3400 cm^{-1} (OH stretching from hydroxyls and hydrate water), 1654 cm^{-1} (H-OH bending), 1119 and 980 cm^{-1} (sulphate absorption) and 606 cm^{-1} (Al-O vibrations), all of these also found in the present aluminas.

From this analysis, it is confirmed that the iron coating on the activated alumina is mainly iron sulphate. Al-H or Fe-H bonds are not obviously present. It is also clear that the hydroxyl groups strongly bond to the surface via Al-OH bonds and hydrogen bonds formed on the surface oxygen atoms, hence a strong presence of hydroxo complexes.

The spectrum of β-FeOOH is shown in figure 5.4. As for the AAFS, OH stretching and H bonds absorb in the range of 3600 to 3000 cm^{-1} (band **a**, very broad). Fe-H bonds absorb around 2000-1900 cm^{-1} (band **b**) and the H-O-H bending mode absorbs at 1610 cm^{-1} (band **c**).

Comparing bands **f** and **g** on AA spectrum, β-FeOOH displays two bands at similar wavenumbers: band **d** at 1480 cm^{-1} and band **e** at 1340 cm^{-1} that should be attributed to carbonyl compounds and carbonate ion CO_3^-. Absorption bands **f** (1100 cm^{-1}) and **g** (1060 cm^{-1}) are attributed to aquo- and hydroxo-complexes absorbing between 1200 and

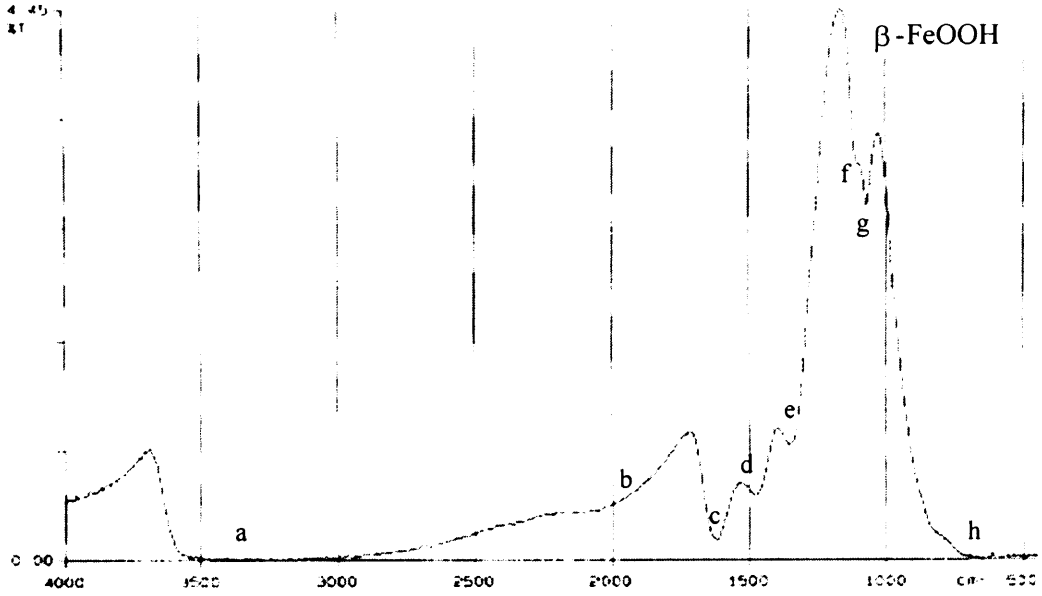

Figure 5.4 FTIR spectrum of Ferric Oxihydroxide (β-FeOOH)

600 cm^{-1} (Socrates, 2000). Usual characteristics of the akaganeite structure are two absorption bands around 690 cm^{-1} (band **h**) and 430 cm^{-1} (Delyanni et al. 2001). However, absorption bands below 700 cm^{-1} are not clear here and these bands are difficult to identify, most likely due the weak transmittance in the presence of water in the hydrophilic ferric oxihydroxide. For this akaganeite β-FeOOH, the hydroxyl OH is the dominant absorbing group.

5.2.2 Point of Zero Charge

Adsorbents are neutral compounds although their surface can be electrically charged according to the surface functional groups and to the pH of the water they are in contact with. FTIR has supplied details about the surface groups present at the surface of the media. This can now be completed by estimating the evolution of the surface electrical charge with the addition of a strong acid or base, i.e. with the modification of the pH. This will give an indication as to possible adsorbent/adsorbate behaviours towards adsorption. The graphs showing the evolution of the surface charge with the pH appear on figures 5.5, 5.6 and 5.7 for GAC, AAFS and β-FeOOH respectively.

Looking at the three graphs, the immediate difference between the adsorbents is the basic character of GAC compared to the acid character of the iron-containing media. In figure 5.6, dissolution of AAFS occurs for a pH under 3.8 and the curves becomes very

steep (Atkinson et al., 1967). Dissolution also affects β-FeOOH in acidic conditions even if from figure 5.7, the slope is not as steep as for AAFS. As a consequence, a low pH indicates a highly dissolved compound, hence no adsorption surface available to adsorb the humic substances. Therefore, data corresponding to pH below 3.8 are not used on these graphs.

Each graph shows two curves, corresponding to two different ionic backgrounds. First, the background was identical to that of working solution without the humic subtances. For this, calcium nitrate was added to deionised water to a concentration of 0.5×10^{-3} mol/L. The second curve was obtained by using potassium chloride instead of calcium nitrate, as described in the method presented by Al-Ghouti (2004).

When calcium nitrate is used, the points of zero charge are at pH 10.6, 5.0 and 5.4 for GAC, AAFS and β-FeOOH respectively. These values are very close to the pH values before any addition of acid or base, which were 10.8, 5.4 and 5.8 for the same compounds particularly taking into account the error on pH to be ±0.1. It shows that only very few protons needed to be added to reach the pH_{zpc}. Therefore, the surface was initially slightly negative. The pH_{zpc} values both iron compounds are similar. This is attributed to the iron presence since in general, alumina have a higher pH_{zpc} values. Boehmite is part of the activated alumina and as an aluminium oxihydroxide, it has some similarities with iron oxihydroxide (β-FeOOH); Fe^{3+} can actually replace Al^{3+} in the boehmite crystal lattice (Sposito, 1995) which explains that their zero point of charge are very close.

As soon as the media are immersed in water (with $Ca(NO_3)_2$ or KCl), hydration takes place. From the previous characterisation technique (FTIR spectroscopy), functional groups in each media have been detected and the hydroxyl group OH in particular was strongly present in each adsorbent analysed. Therefore, hydration of the adsorbents can lead to the surface charge considering the OH group as follows in equations 5.1 to 5.2:

AAFS:	$Al\text{-}OH_2^+$	$Al\text{-}O^-$	Al-OH	(5.1)
β-FeOOH:	$Fe\text{-}OH_2^+$	$Fe\text{-}O^-$	Fe-OH	(5.2)
GAC:		$C\text{-}OO^-$	C-OH	(5.3)

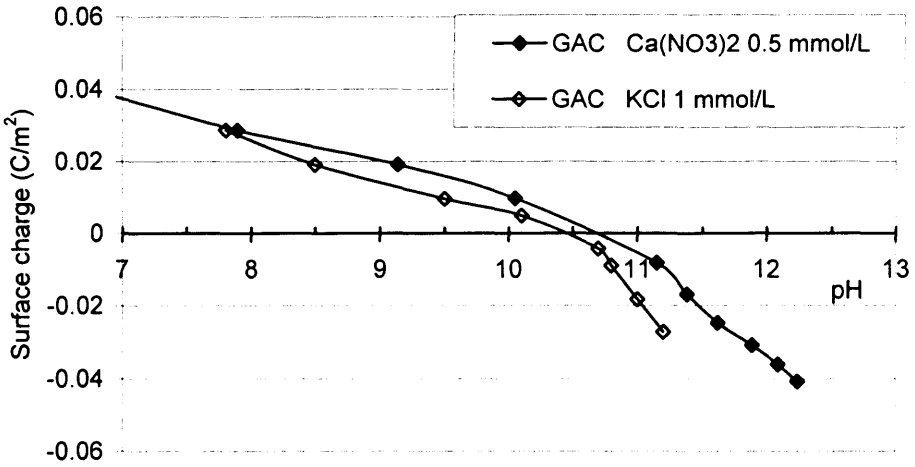

Figure 5.5 Surface charge of GAC. pH_{zpc}=10.7 ($Ca(NO_3)_2$) and 10.4 (KCl)

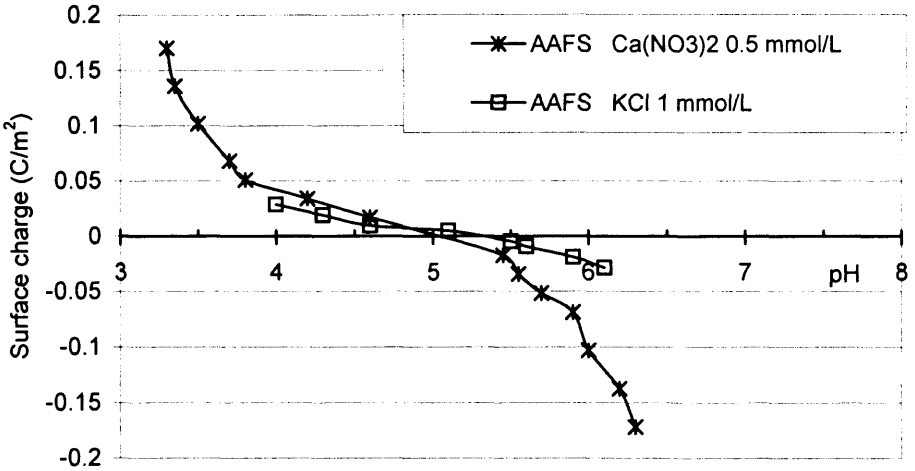

Figure 5.6 Surface charge of AAFS. pH_{zpc}=5.0 ($Ca(NO_3)_2$) and 5.3 (KCl)

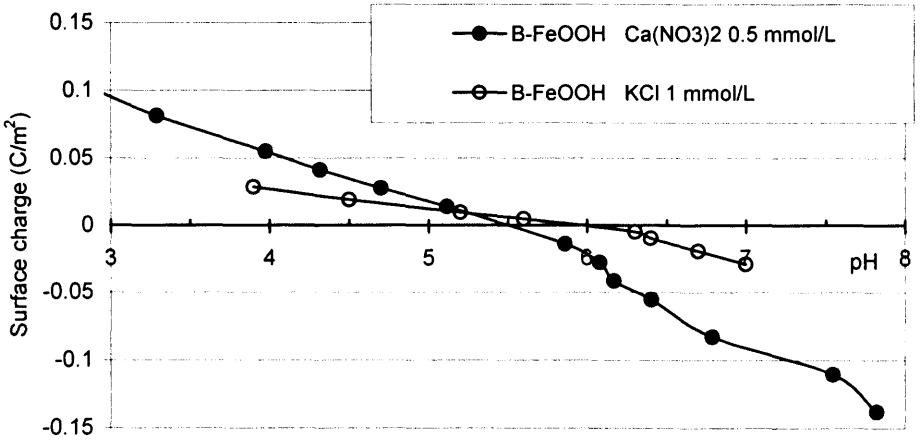

Figure 5.7 Surface charge of β-FeOOH. pH_{zpc}=5.5 ($Ca(NO_3)_2$) and 5.9 (KCl)

The hydroxyl groups of oxihydroxide Metal-OOH provide both acidic and basic functionalities to the media. As for the GAC, its basic functionality is dominant.

When adding the GAC to deionised water only, the pH was raised from 5.5 to 10.9. This pH increase is evidence of either the adsorption of the protons on the GAC surface or of the release of the hydroxyl groups from the surface. Comparatively, the addition of AAFS to deionised water only slightly decreased the pH, which was attributed to the deprotonation of AlOH. The pH slightly increased for β-FeOOH in the same conditions. Since the surface was also negative at pH 5.8, it can be interpreted that some FeO^- sites re-associated to become FeOH.

The equations below (5.4, 5.5 and 5.6) show the chemisorption of calcium on AAFS and β-FeOOH. These were originally suggested by Sposito (1995) for the adsorption of lead on aluminium compounds. For the present application, two assumptions are made: the behaviour of Ca^{2+} is similar to Pb^{2+}, and these reactions are valid for iron instead of aluminium. Hence calcium replaces the protons on the surface and aluminium (AAFS) can be swapped for iron (β-FeOOH):

$$AlOH + Ca^{2+} \leftrightarrow AlOCa^{+} + H^{+} \quad (5.4)$$

And possibly displacement of two protons:

$$AlOH + Ca^{2+} + H_2O \leftrightarrow AlOCaOH + 2H^{+} \quad (5.5)$$

$$2AlOH + Ca^{2+} \leftrightarrow (AlO)_2Ca + 2H^{+} \quad (5.6)$$

Calcium concentration was 5×10^{-4} mol/L and a pH of 5.3 corresponds to proton concentration of 5×10^{-6} mol/L. If one calcium ion would displace one or two adsorbed H^+, then the pH should decrease significantly. Protons are likely to be re-adsorbed by the surface through "ion-pair formation or aluminol (AlOH) group" (Sposito, 1995). Adsorption of calcium near a metal oxide negative surface is also cited by Jolivet (2000). Particularly when using the same electrolyte $Ca(NO_3)_2$, Jolivet (2000) found the pH_{zpc} of hematite to decrease from 8.5 to 6.5.

Therefore, it can be concluded that calcium ions have adsorbed on the surface, shielding the negative charges. As a consequence, calcium did not act as an indifferent electrolyte.

This will have a consequence on the humic substances adsorption. Should some calcium remain unbound to the humic substances, it is then free to adsorb on the adsorbent. Such phenomenon was observed by Sander et al. (2004) when they measured the force between two oxide surfaces using atomic force microscopy (AFM). They found the calcium ion was used to bridge the two surfaces. If Ca^{2+} is adsorbed on the medium, it can either screen the adsorption site and inhibit HS adsorption, or act as a ligand between the organic matter and the adsorbent, thereby increasing the adsorption.

These experimental pH_{zpc} values did not agree with several of those reported values. For example, pH_{zpc} for η alumina is 6.5 (Goyne et al., 2004) up to 10.4 for boehmite (from electrokinetic data measuring the streaming potential, compiled data by Sposito, 1995). However, those aluminas were not iron-coated and the pH of non-coated alumina (AA) was measured to be 10.2. More recently, Peng et al. (2005) measured the pH_{zpc} of pillared bentonite to be 5.5, in presence of calcium, which is similar to the values in this study. For the ferric oxihydroxides, a value of 5.8 also seemed low compared to Teermann and Jekel's value (pH_{zpc}=8.0) in 1999, although the compound came from the same supplier (Wasserchemie, Germany). For an iron oxihydroxide, Kanungo (1994) measured a pH_{zpc} equal to 7.0. However in that case the crystallite form was not mentioned. It might have been ghoetite which is a more common form of the iron oxihydroxide than akaganeite (β form). These results correspond with calcium acting as mentioned above, i.e. decreasing the pH_{zpc}.

For GAC, reported pH_{zpc} values vary from 2.1 to 9.7 according to the activation treatment and origin of the GAC (Li et al. 2002). The present GAC 207C has a higher pH_{zpc}, and is more basic, confirmed by a domination of OH groups detected from the FTIR spectroscopy.

To confirm these results, the surface charge of the adsorbents was measured using a different electrolyte at a higher concentration, namely potassium chloride KCl at 0.001 mol/L. This new concentration brings the same amount of charges since K^+ is monovalent and Ca^{2+} is divalent. However, using KCl instead of $Ca(NO_3)_2$ has only brought a slight change in pH_{zpc} values. pH of the zero point of charge has shifted from 5.0 to 5.3 for AAFS and from 5.4 to 5.9 for β-FeOOH. This confirms the role of calcium in decreasing the apparent surface charge of the iron compounds due to its affinity for the surface. Figure 5.6 and 5.7 show a larger slope of the curve for the calcium nitrate electrolyte, which also confirms that calcium nitrate was not an

indifferent electrolyte. pH_{zpc} of GAC has shifted from 10.6 with $Ca(NO_3)_2$ down to 10.4 with KCl, showing a different behaviour from the two other adsorbents. The GAC surface was also slightly negative initially (pH=10.8). However, in this case, the surface has the same sensitivity towards calcium nitrate and potassium chloride (curves are parallel in the pH region close to pH_{zpc}). The increase of pH_{zpc} with calcium nitrate is attributed to anion adsorption (nitrate), as observed by Jolivet (2000).

During the adsorption studies (kinetics, equilibrium and column studies), all experiments were carried out at pH 7.0. Therefore, the GAC surface is positive with +0.04 C/m^2. An estimation of the iron compound surface charge was made using a four degree polynomial function (R^2=0.996) and the results at pH 7.0 were –0.5 C/m^2 for AAFS and –0.1 C/m^2 for β-FeOOH.

5.2.3 Physical characteristics of the adsorbents

Table 5.1 shows the bulk density, grain density, porosity and median size of the adsorbents. These are average values and the standard deviation is also given. GAC is known for its low bulk density which is confirmed here, in agreement with the large porosity. Presence of iron increases the density and β-FeOOH is the denser of the adsorbents.

Poured porosity represents the voidage before the occupied volume starts to compact under the weight of both the grains and the water column. For the four analysed adsorbents, it is around 50%, which means that the grains occupy only half of the volume. Hence, grain density is expected to be about twice as large as bulk density. This agrees with the first two rows of data in table 5.1. GAC poured porosity would be expected to be the highest due to bigger grains, although this can be compensated for by the shape of the grains which are mostly "torn-broken" for GAC compared to "angled" for the other adsorbents (description from Fair et al. 1968). GAC and aluminas (coated and non-coated) have similar porosity when taking into account the uncertainty of ± 0.01 on the last digit. Activated carbon porosity is mainly internal and not measured by poured or packed porosity. Therefore, at this stage, it is difficult to reach any reliable conclusion about GAC porosity compared to aluminas. Complementary results will be brought from nitrogen adsorption studies (section 5.2.6.2).

However, it is clear that the β-FeOOH is much less porous than GAC and aluminas. Porosity, on activated media, comes from heating the material at high temperatures. Artificial preparation of β-FeOOH does not involve such an activation step (Bailey et al., 1993). Instead, it is precipitated from $FeCl_3$ solution aged a few hours, which leads to rod shape crystals. Therefore, the "absence " of activation is considered to be responsible for the less porous structure. However, it is interesting to compare it with the packed porosity. Packed porosity is much smaller than poured porosity for the ferric oxihydroxide, showing how compactable this media is (loss of almost 20% of the poured porosity). This is likely to bring a large variation in the porosity of the adsorbent bed and on the adsorption capacity, particularly when submitted to the weight of the water column. It can also reflect the attrition effect on the media.

As regards the diameters, values are read from figure 5.8 showing the cumulative grain size distribution. Three diameters are considered; d_{10} (generally used to describe filtering media), d_{50} and d_{90}, respectively meaning that 10%, 50% and 90% of the adsorbent weight is below the corresponding size. This choice allows a qualitative estimation of the distribution of grain sizes. Both aluminas are very similar with a narrow grain size distribution, centered on 0.41-0.42 mm. This is justified since both are supplied as grain sizes in the range 0.32 - 0.56 mm, as from the supplier's information sheet (Alcan Chemicals). According to the supplier's data (GEH Wasserchemie), β-FeOOH's grain sizes are spread from 0.32 to 2 mm. However, it seems that these are mainly below 1 mm, which is likely to be due to the friability of this medium. GAC also has a broad grain size range, uniformly spread and centered on 0.91 mm.

5.2.4 Scanning Electron Microscopy (SEM) images

SEM images of the adsorbents are shown on figures 5.9, 5.10, 5.11 and 5.12 for GAC, AA, AAFS and β-FeOOH respectively. The torn edges of the grains of GAC also show the internal "holes". Its internal structure can be recognised as graphite type layering of carbon sheets (Thomas and Crittenden, 1998). Pores created from the activation process and the extensive debris account for the friability of this adsorbent. Micropores that constitute most of the GAC porosity are not visible using this technique. Considering the scale, mesopores and macropores cannot be seen on the photographs (sizes above 2.5 nm).

Table 5.1 Bulk characteristics of the adsorbents

Adsorbent	GAC	AA	AA-FS	β-FeOOH
Bulk density (kg/L)	0.44	0.70	0.89	1.32
Grain density (kg/L)	0.90	1.46	1.78	2.26
Poured porosity	0.51	0.52	0.50	0.42
Packed porosity	0.46	0.48	0.47	0.34
Effective diameter (d_{10}) (mm)	0.63	0.33	0.33	0.36(*)
Median diameter (d_{50}) (mm)	0.91	0.42	0.41	0.56
d_{90} (mm)	1.15	0.5	0.5	0.94

(*) 0.36 mm was the minimum measured size value

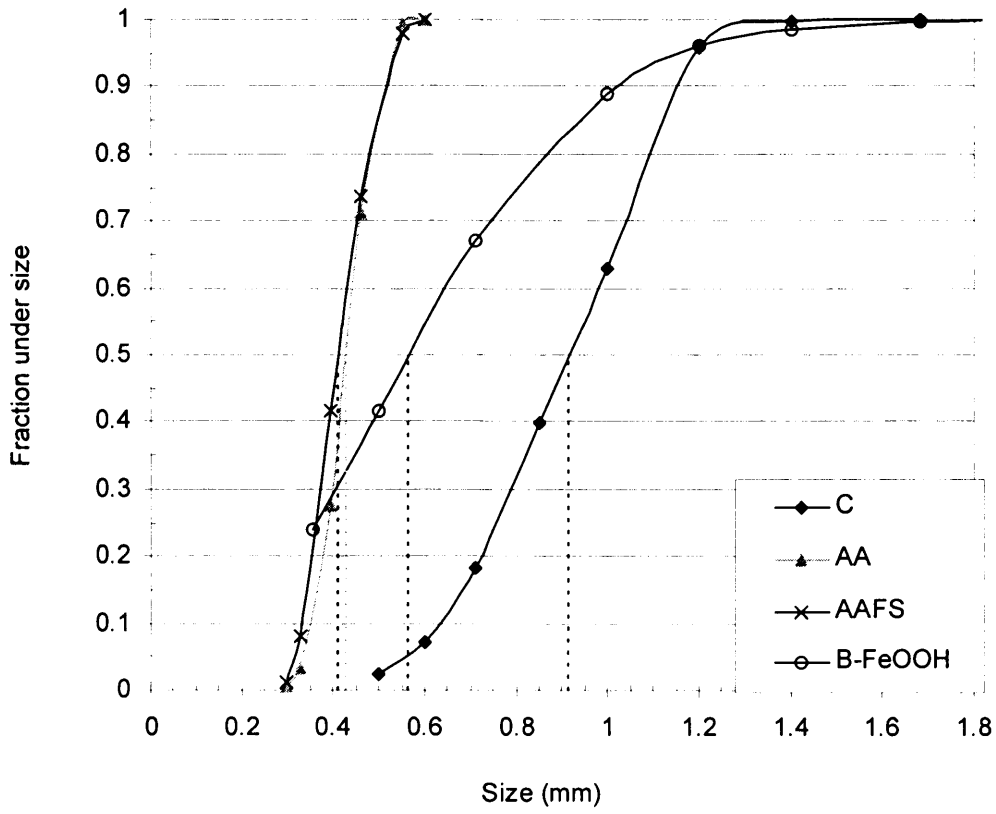

Figure 5.8 Adsorbents' size distribution obtained from sieving analyses

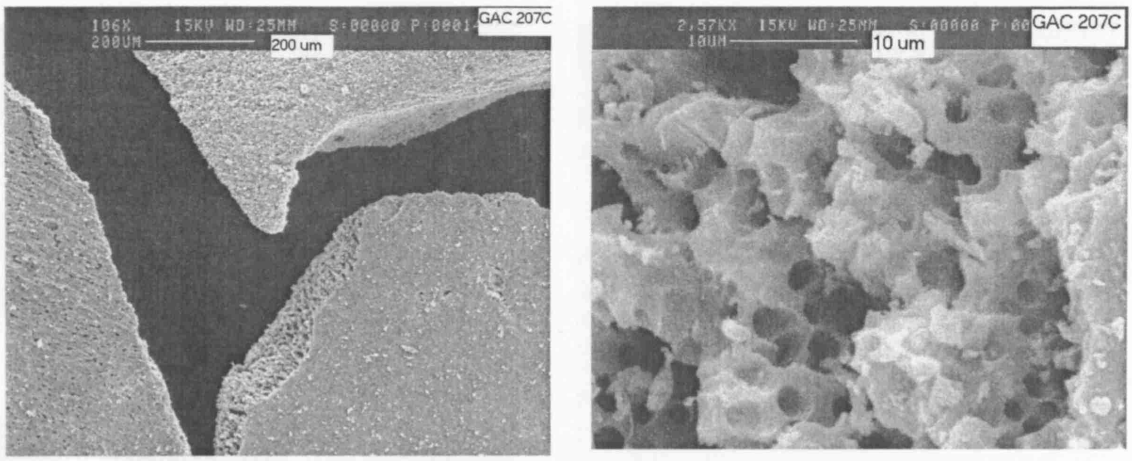

Figure 5.9 SEM images of the GAC (magnifications x 100 and x 2500)

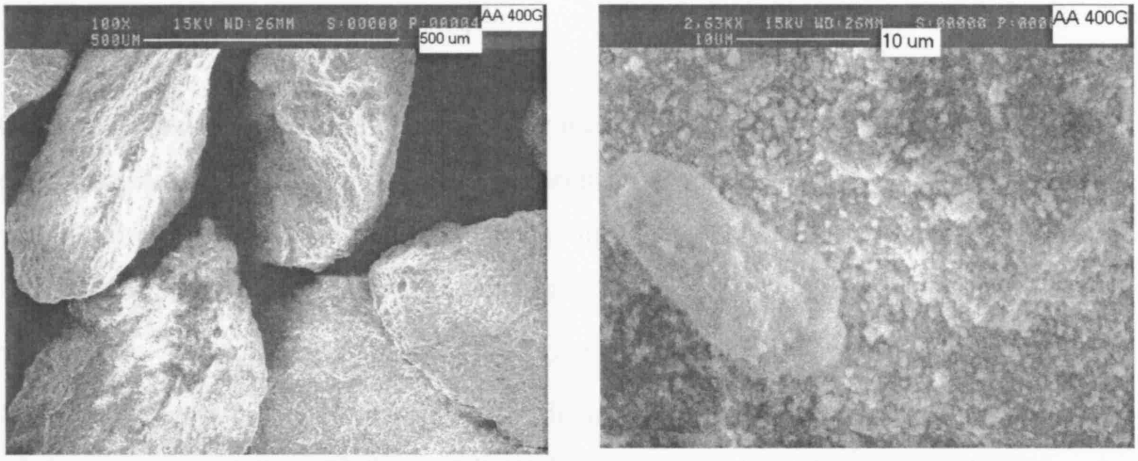

Figure 5.10 SEM images of the AA (magnifications x 100 and x 2500)

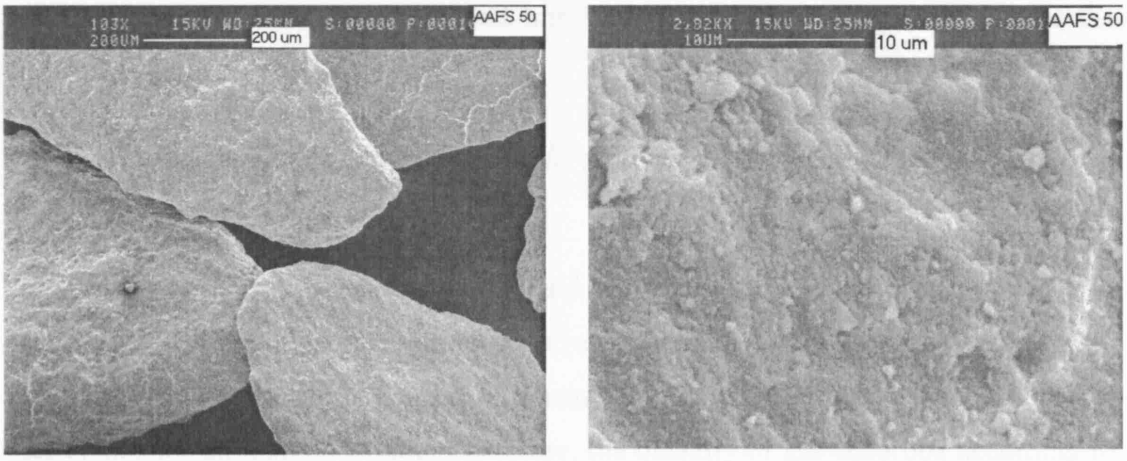

Figure 5.11 SEM images of the AAFS (magnifications x 100 and x 2500)

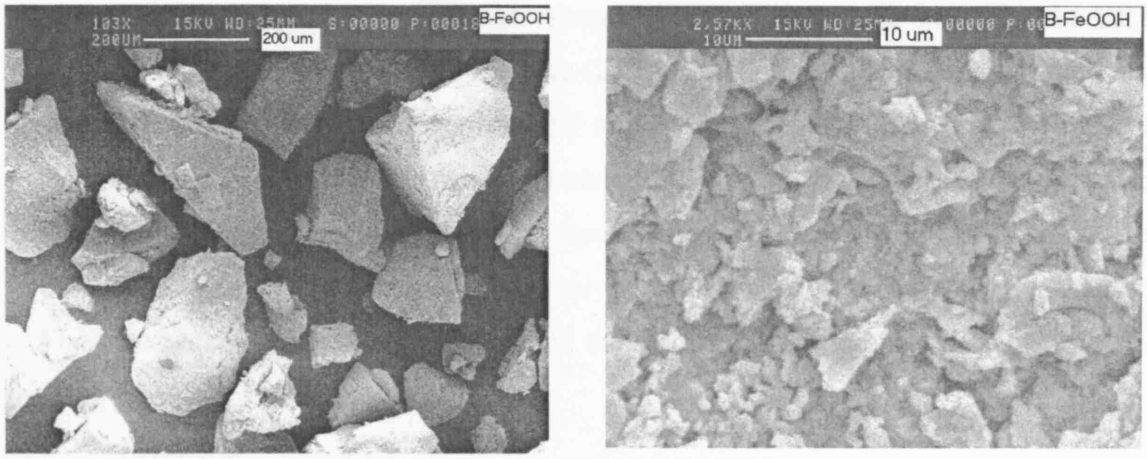

Figure 5.12 SEM images of the β-FeOOH (magnifications x 100 and x 2500)

Grains of alumina and coated alumina show identical angled shape. AA's surface is less even than AAFS's, probably due to its bareness. Oppositely, AAFS appears smooth with a uniform coating. On the bigger scale, only few cracks or holes are visible which suggests the surface area to be mainly external.

The surface of β-FeOOH appears smooth with an abundance of debris due to its high friability. The scale does not allow one to distinguish the characteristic rod-cigar shape of akaganeite crystallites (β form of FeOOH) as described by Bailey et al. (1993) and Randall et al. (1999). A SEM picture similar to figure 5.12 was obtained by Deliyanni et al. (2001). However only Transmission Electron Microscopy (TEM allowing a larger scale to observe nanometers) provided him with measurement of 2 to 6 nm for the crystallites size.

5.2.5 Characterisation of the adsorbents by physisorption of an inert gas

5.2.5.1 Introduction

An inert gas such as nitrogen has a small and stable molecule. Therefore, it will tend to accumulate within the porous structure of an adsorbent when its partial pressure is increased. It will also desorb when the pressure is decreased since no chemisorption takes place for an inert adsorbate. Therefore, the quantity of gas adsorbed according to the pressure applied, together with the characteristics of the gas, enable the porosity of the adsorbent to be measured. Various ways of using the data provided from such an

adsorption-desorption experiment correspond to several analytical tools like the BET analysis, the t-plot, Barret-Joyner-Halenda (BJH) and Horvath-Kawazoe (HK) methods. The first two provide data regarding the surface area (external and internal) of the medium under study. The last two (BJH and HK) give information about the pore size distribution (PSD). These analyses are described in the literature review (see section 2.6.2 in chapter 2). Results from these analyses are given and analysed in this chapter. They are necessary in order to understand the results of adsorption experiments on HS using these adsorbents.

5.2.5.2 Adsorption – desorption isotherms

5.2.5.2.1 Isotherm shape and hysteresis

The isotherms characterise the adsorbents by describing how their adsorption sites are filled as the partial pressure of the inert gas increases and how they empty when the pressure is decreased. Everett (1958, cited by Thomas and Crittenden, 1998) showed that the hysteresis loop is a good indicator of the pore shape. When the adsorbent surface is in contact with the adsorbate, a change in the free energy takes place and the surface tension decreases to minimise this change. As surface tension decreases under adsorption forces (London and Van der Waals), a meniscus is formed between the two sides of the pore (in the case of a gas being adsorbed). The energies necessary for condensation and vaporisation of the gas and the size of the pore or capillary, define the shape of the hysteresis loop.

Figures 5.13a to c show the isotherms, respectively for GAC, for non-coated and coated aluminas (AA and AAFS) and for β-FeOOH. The adsorption branch is compared to the several isotherm types presented in the literature review, a concave shape indicating a favourable adsorption and an unfavourable adsorption if the curve is convex (respectively types I and III in figure 3.3, chapter 3). For GAC, the isotherm is related to type I, and the slight upwards part, at relative pressure close to one, shows the presence of wider pores, but these are not dominant. Most of the gas adsorption occurs at relative pressure below 0.1. The smallest pores are filled and adsorption hardly occurs beyond that point as the isotherm is rising very slowly. This is proof of a small size of pores where no condensation occurs. The volume of the pores is more important than the area in such a situation. Hysteresis is hardly visible for GAC 207C due to the fact that adsorption and desorption occurs almost at the same pressure. In turn, this means that vaporisation heat (on desorption branch) following condensation (adsorption branch) is

low. This is attributed to small pore volumes, i.e. micropores. Therefore, it is concluded that the pores of GAC are mainly in the microporous range, with a slight proportion in the mesoporous range. Micropores are slit-shaped (type D according to figure 3.5 in chapter 3), associated with the small and horizontal hysteresis loop shape (Rouquerol et al. 1999).

Both aluminas present similar isotherm shapes, type II, i.e. the hysteresis starting as soon as pressure is decreased. The inflexion point on the adsorption branch occurs very early suggesting that the first monolayer is reached at low pressure. Then new layers adsorb, followed by condensation. The curve becomes almost vertical as the relative pressure reaches the unity. This means that a very large volume of gas can condense on the surface and this is possible only if the pore volume is large (larger than in the first example for GAC). Hence, the pore size is larger, mainly in the mesoporous range. A macroporous range would show a much steeper slope as pressure equals unity. The pore size covers a broad range since the slope was steadily increasing until 90% of the relative pressure was reached. Hence the pore size is in the micro and mesoporous range. The immediate hysteresis confirms that desorption is slow and a low pressure has to be imposed so as to move the gas away from the surface. From the hysteresis shape, both aluminas have parallel plates and slit shape pores, closed or connected with other pores and forming a network. These plates correspond to the crystal layer structure of boehmite and η-alumina (Sposito et al., 1995).

The shape of the ferric oxihydroxide isotherm is rather ill-defined. It corresponds best to type IV with a very slow filling of the mono and multilayers. β-FeOOH is saturated from a relative pressure of 0.7 and no more inert gas is adsorbed beyond this pressure. The start of the adsorption branch is similar to that for the aluminas and pore size distribution should be fairly similar. The ferric oxihydroxide does not show a sudden increase at high relative pressure which could mean that no condensation occurs in the mesopores. However this is contradicted by the large hysteresis since desorption occurs only when relative pressure has decreased to 0.5. It appears that the adsorbate (N_2) has little affinity for this adsorbent and interactions adsorbate-adsorbate dominate (Doan, 2001). This hysteresis shape is related to type E. The shape of the pores is classified as an "ink-bottle" shape. These are also interconnected. This isotherm is very similar in shape and values to the one shown by Deliyanni et al. (2001), for both adsorption and desorption for the same adsorbent.

(a)

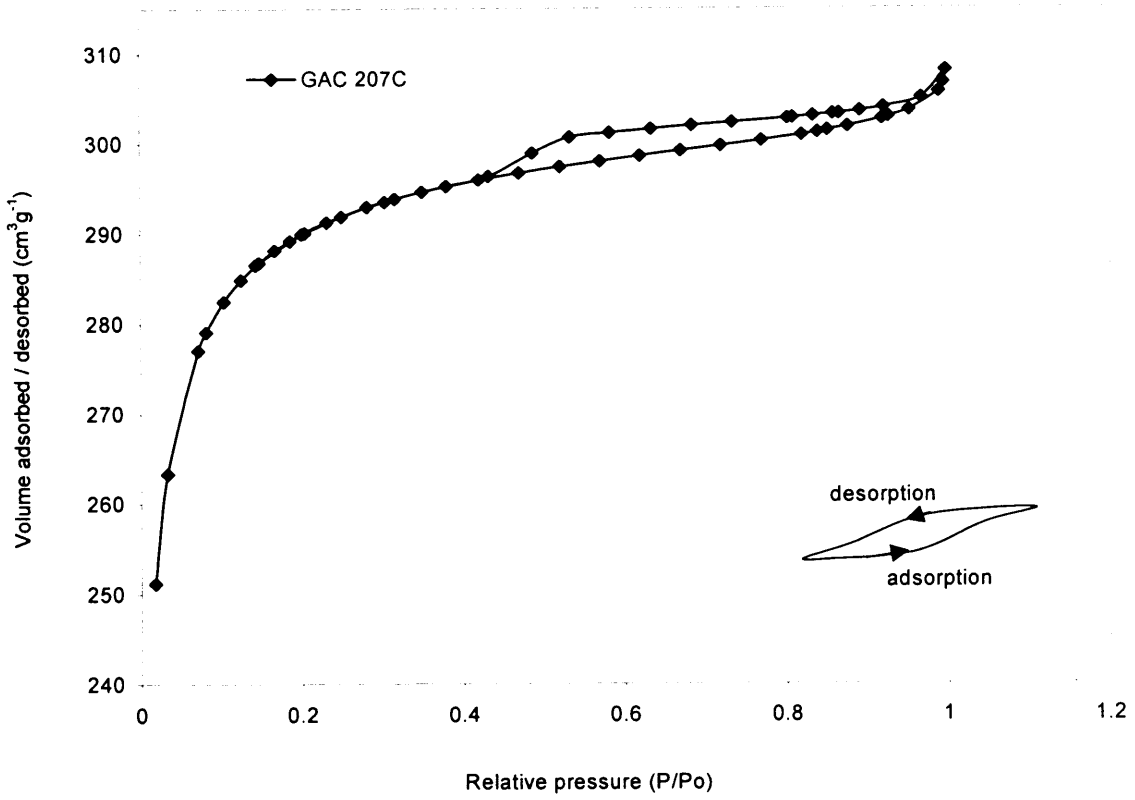

(b)

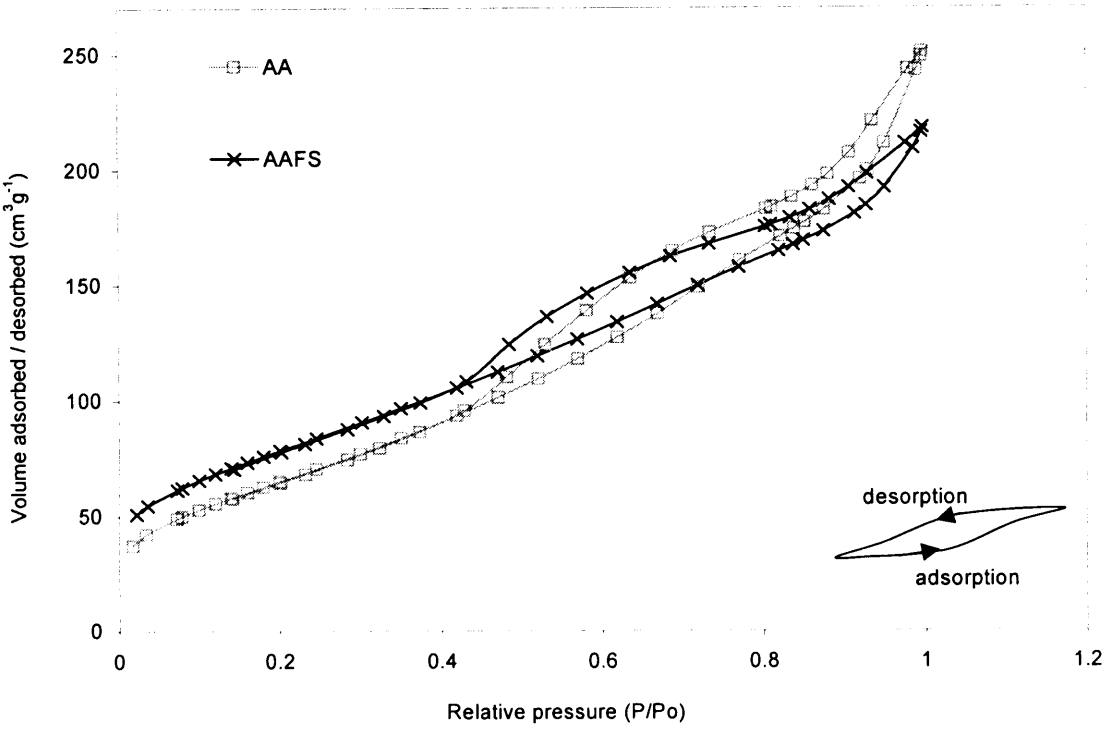

Figure 5.13 Isotherm and hysteresis for (a) GAC (b) AA and AAFS (c) β-FeOOH

(c)

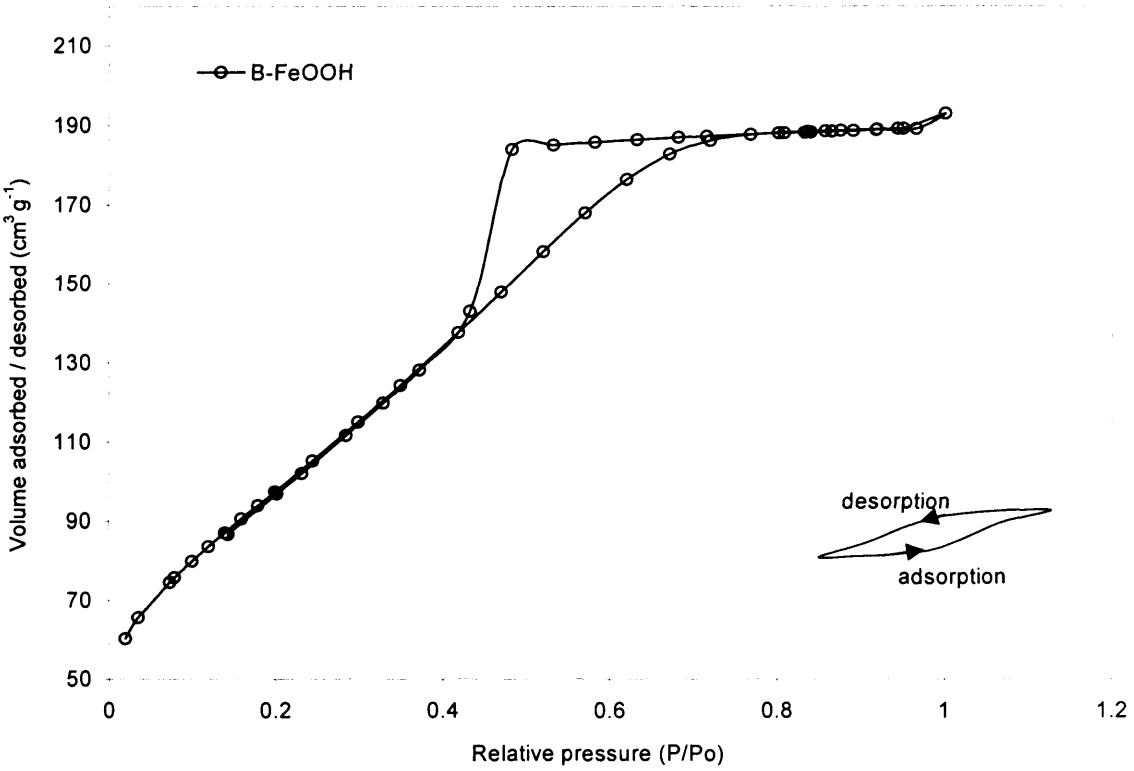

Figure 5.13 Isotherm and hysteresis for (a) GAC (b) AA and AAFS (c) β-FeOOH

5.2.5.2.2 Surface area

When the previous described isotherms are obtained and for each adsorbent, the surface area (S_{BET}) is then calculated according to the method described in section 2.6.2 (chapter 2) and considering the relative pressure between 0.05 and 0.2 only. GAC 207C has a surface area of 980 m^2/g, less than the value stated by the supplier (1050 m^2/g), but closer to the surface area of another coconut based GAC of 1026 m^2/g (Aracheandio, 2002). This difference is likely to be due to the points considered for calculation of S_{BET}. For example, considering two additional points (relative pressure of 0.017 and 0.033), S_{BET} becomes equal to 1009 m^2/g. The large surface area agrees with the graphitic sheet structure observed from the SEM images (figure 5.9, magnification 2500).

The surface area of the non-coated (AA) and coated (AAFS) aluminas are estimated to be 243 and 286 m^2/g respectively. The supplier's information sheet states that AA has a larger surface area than AAFS (respectively 350-380 and 220 m^2/g). This can be attributed to the method of calculation of S_{BET}. In particular, eliminating the fine powder prior to analysis would decrease the surface area.

For the ferric oxihydroxide, the measured surface area was 360 m^2/g as compared to 280 m^2/g reported by Teermann and Jekel (1999) using the same adsorbent. This adsorbent is very friable and a large proportion of powder has been included in the sample, raising its surface area. However, Bakoyannakis (2003) gave similar results for akaganeite with the surface area equal to 330 and 358 m^2/g on two samples.

5.2.5.3 The t-plot

The t-plot method is used to compare the shapes of the isotherms as well as to estimate the external and microporous surface area. The volume of nitrogen gas adsorbed is plotted against t, the thickness of the adsorbed layer, as described by Harkins and Jura's equation (equation 2.15 in chapter 2). The equation is valid if micropores are filled and if condensation has not yet occurred. Details of the t-plot method to estimate the micropore area are given in chapter 2.

Figure 5.14 shows the t-plots for the adsorbents GAC, AAFS and β-FeOOH. AA is not shown for clarity of the graph as it was very similar to AAFS. The grey shaded area shows the range of the adsorbed layer thickness (0.35-0.5 nm). From the slope and the y intercept, the external surface area (i.e. the surface area of pores larger than micropores in this case) and the micropore volume are respectively estimated. From this, the micropore area is then calculated by subtracting the external surface to S_{BET} (total area estimated in the previous section of this chapter).

The dotted line shows a high intercept for GAC corresponding to a large micropore volume (0.16 $cm^3\ g^{-1}$). The external surface area is calculated to be 168 m^2/g vs 812 m^2/g for the micropore area. For AAFS, the intercept is slightly negative which leads to non-existent micropore volume. The micropore area calculation leads to 2.34 m^2/g, almost insignificant compared to the GAC. The intercept is largely negative for β-FeOOH and leads to a negative micropore volume and surface area. The external area is actually greater than the total surface area (S_{BET}) which suggests that points within the range of condensation might have been considered in the calculation, although relative pressure was less than 0.4 (from the isotherms, condensation started at about 0.4). Such negative values have been previously reported when the adsorbent has little microporosity, although the Harkins and Jura equation is usually more reliable than De Boer equation for this (Marczewski, 2002). In this case, the external area is considered

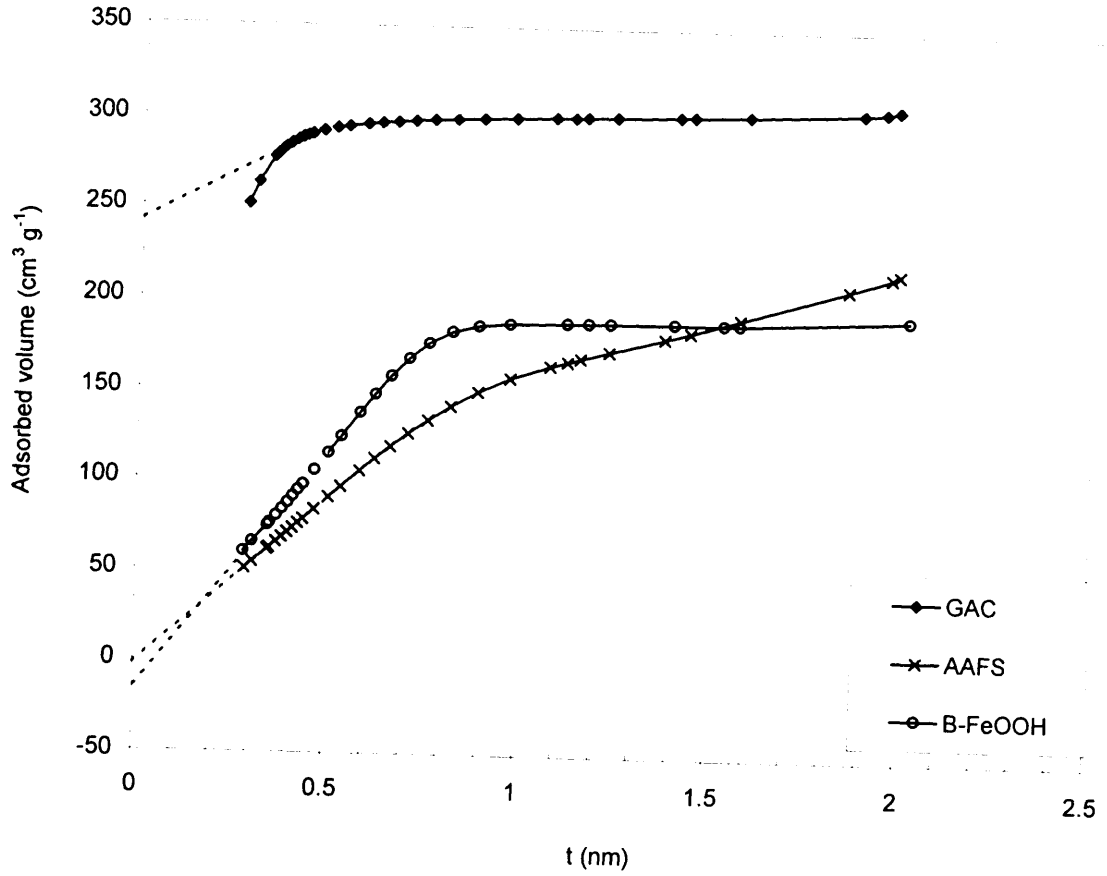

Figure 5.14 t-plot for the adsorbents by Harkins and Jura method (AA not shown for clarity; AA was similar to AAFS)

equal to S_{BET} since the larger value from the t-plot would only represent the limitations of the mathematical calculation (Marczewski, 2002).

It can be concluded that both iron compounds do not have any microporosity as opposed to GAC where the porosity is constituted of microporosity at 83%. The calculated information is summarised in table 6.2 (section 6.7).

5.2.5.4 Pore size distribution; BJH and HK methods

Figures 5.15, 5.16 and 5.17 show the Pore Size Distribution (PSD) for GAC, AAFS and β-FeOOH respectively, using both Barret-Joyner-Halenda (BJH) and (Horvath-Kawazoe (HK) methods. The BJH method is valid for mesopores only, whereas HK methods considers micropores only (detailed in chapter 2, section 2.6.3 and by Marczewski, 2002 and Jarionec et al., 2003). Hence it is of interest of using both complementary methods as mentioned by Lastoskie (1994). The grey shaded area on the

graphs represents the limit between micropore and mesopores. Such a limit is not strictly defined and lies between 2 nm and 2.5 nm (down to 1 nm according to Montgomery, 1985).

It should also be remembered that the BJH method assumes open-ended cylindrical pores which explains the size description in terms of "diameter". HK methods assumes slit shape pores, hence the size description in terms of "width". However, only GAC and AAFS have slit-shape pore, and none of the adsorbents has cylindrical pores. Therefore, discrepancies might occur between the model and reality, which means that the results are to be considered with caution. In addition, PSD is calculated from the desorption branch by the BJH method whereas the adsorption branch is used by HK calculations.

The striking feature on each of these graphs (5.16, 5.17 and less obvious on figure 5.15) is the presence of a peak around 3-4 nm for the BJH method, but no peak in that range for HK method. This may be due to *(i)* the different branch used in each method (adsorption or desorption); Marczewski (2002) actually observed no peak when using the adsorption branch by BJH method, due to discrepancies between the model pore shape and the real pore shape, and *(ii)* the values beyond 2-2.5 nm by HK method are considered to be less reliable since they are beyond micropores size and HK method considers micropores only.

For the GAC (figure 5.15), both methods provide complementary information. The microporous range is clearly dominant over the mesoporous range, although the smallest detectable pore width is 1.13 nm. The associated differential volume is 0.35 $cm^3g^{-1}nm^{-1}$ and covers all widths below 1.13 nm. From the BJH curve, a small peak around 3.5 nm suggests the existence of mesopores. This is in agreement with 17% of the area being external. However, if adapting the scale of the y-axis, the peak corresponding to the smaller pore diameter is far more important, confirming again the dominant microporous domain. From the HK method, 93% of the porosity is microporous.

For AAFS (figure 5.16), a certain amount of micropore volume seems to exist between approximately 1.3 and 2 nm width. The t-plot did suggest a small amount of microporous area. However, the volume is more important than the area in that low size range, thereby making the micropore area data doubtful. Nevertheless, the median

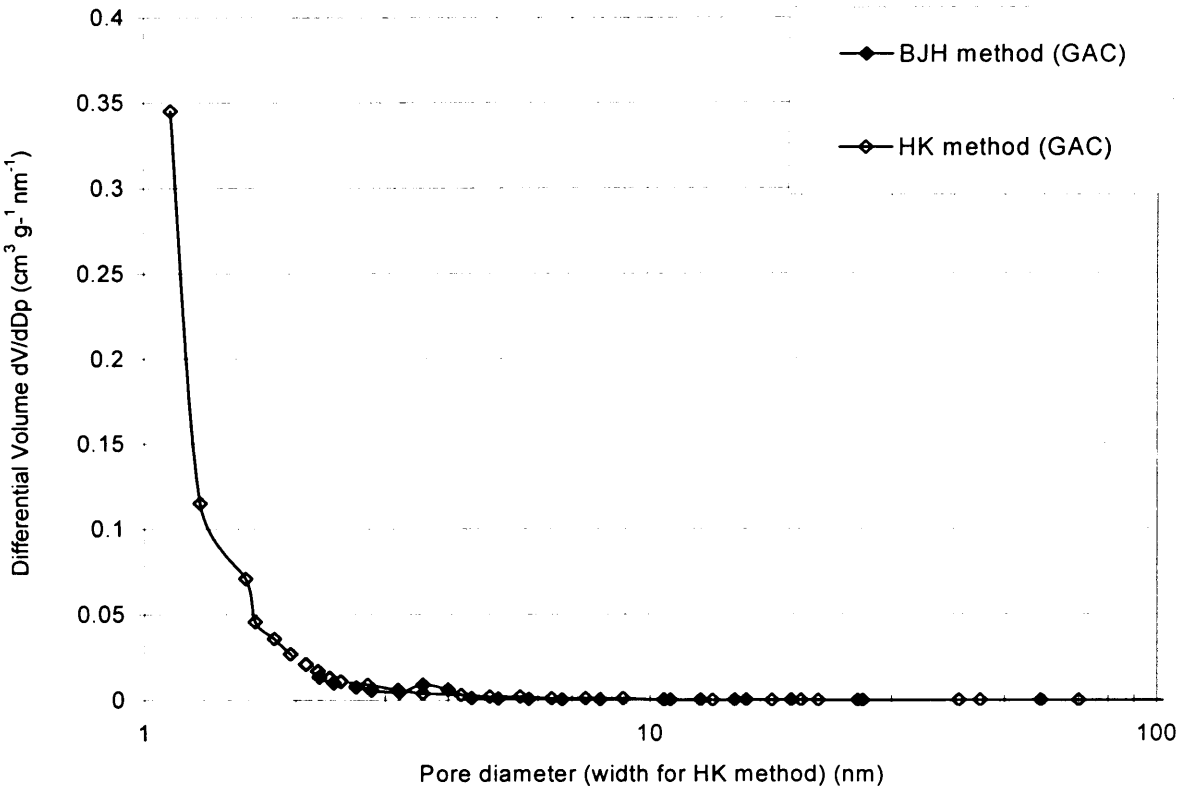

Figure 5.15 GAC Pore size distribution by BJH and HK methods

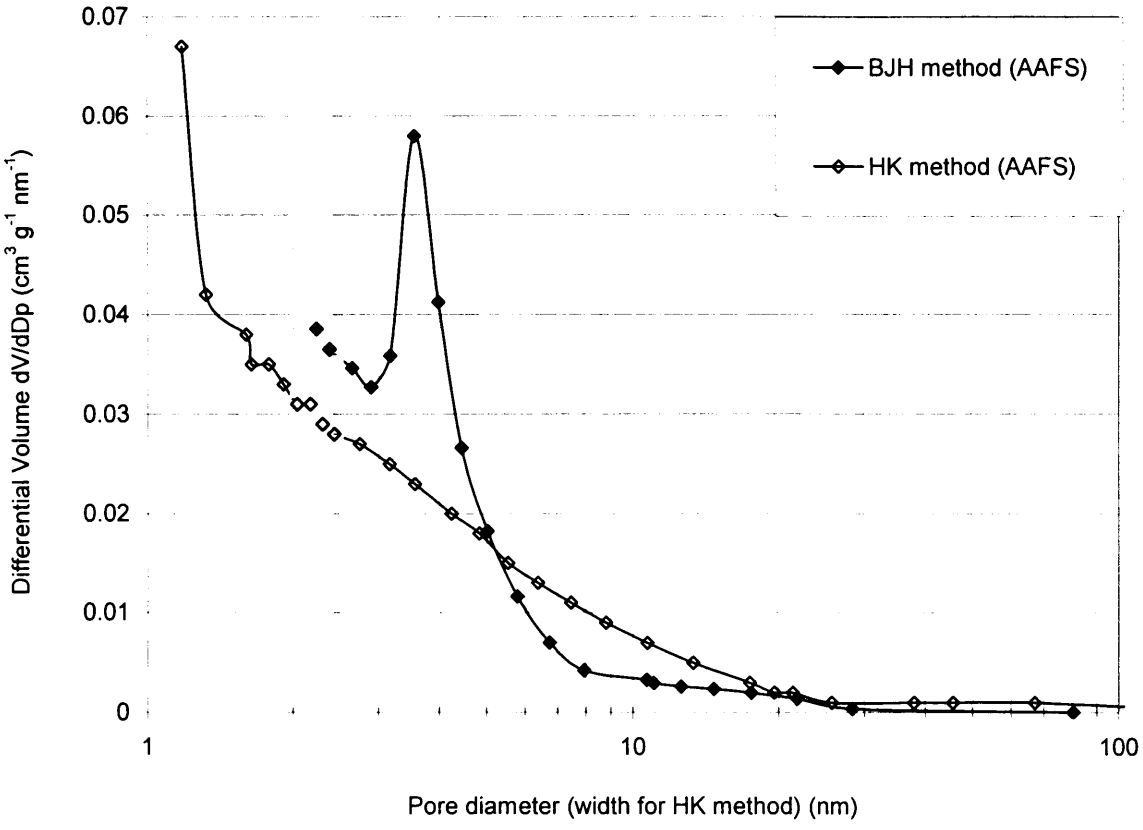

Figure 5.16 AAFS Pore size distribution by BJH and HK methods

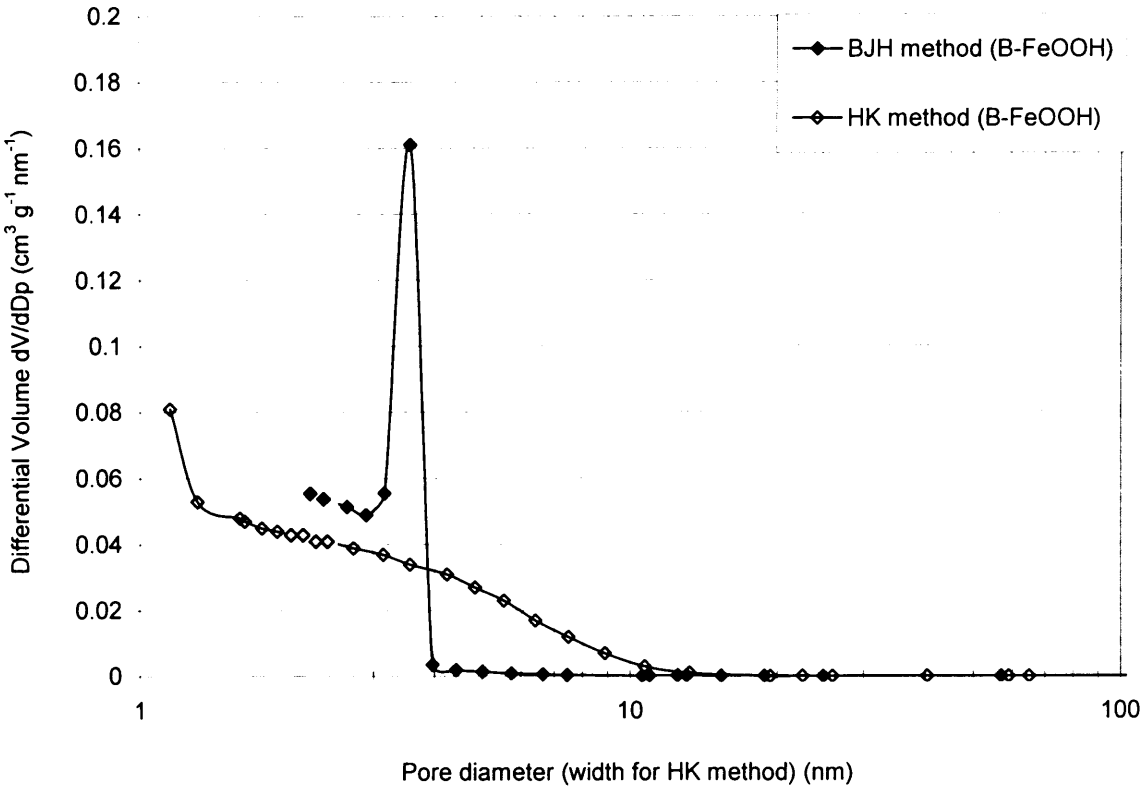

Figure 5.17 β-FeOOH Pore size distribution by BJH and HK methods

diameter from HK method is at 2.2 nm, which stands at the limit of the micro-mesopore range, and the micropore volume is 33% of the total volume. The BJH curve shows a peak at 3.5 nm and pore diameters extending to beyond 10 nm. The mesopore range is dominant for AAFS as suggested by the previous analyses.

Pore size distribution of β-FeOOH is also difficult when considering the HK method indicating the presence of micropores (45% of porosity is microporosity) and the t-plot results indicating the absence of micropores. The PSD is rather similar to the AAFS's. The most obvious feature is the high narrow peak at 3.5 nm. A smooth "bump" is visible on the HK curve too, which confirms the unique mesopore size for this iron adsorbent. This very identical characteristic was observed by Bakoyannakis et al. (2003) on akaganeite too. The same authors identified the pores of the triple hydroxide $Fe(OH)_3$ to be smaller, down to 1 nm. The present adsorbent also contains $Fe(OH)_3$, which is likely to explain the smaller pores. The fact that no micropore volume could be associated to the iron-containing adsorbents is probably due to the difficulty of using the t-plot in the presence of low microporosity. Although BJH method is not strictly reliable under mesoporous size, it should still be considered as an indicator. Then, as such, it

clearly indicates the presence of micropores. The HK method confirms that the pore volume remains low as it is 0.30 cm^3/g for β-FeOOH vs 0.48 cm^3/g for GAC and considering that the iron oxihydroxide is approximately three times denser that GAC.

5.2.5.5 Adsorbents characteristics summary

The data obtained from the previous analyses are summarised in table 5.2 below. They include the non-coated alumina, mainly for comparison purposes to relate the role of iron coating in the adsorbent characteristics. Such coating seems to have increased the external surface area available for adsorption. It might have occurred through cracks within the coating or during a different activation treatment of the alumina itself. Pore size has decreased but remained in the mesoporous range.

Table 5.2 Data obtained from nitrogen gas physisorption to characterise the adsorbents

	GAC 207C	**AA**	**AAFS**	**β-FeOOH**
S_{BET} (m^2/g)	980	243	286	360
t method				
micropore area (m^2/g)	812	0	0	0
micropore volume (cm^3/g)	0.37	0	0	0
external area (m^2/g)	168	243	286	360
BJH method				
pore diameter at peak value (nm)	3.5 (very weak) 2.2 (very strong)	3.5 (medium)	3.5 (medium)	3.5 (narrow and strong)
HK method				
median pore width (nm)	1.13	7.24	4.55	2.38
maximum pore volume (cm^3/g)	0.48	0.39	0.34	0.30
micropore volume (%<2.5 nm)	94	26	36	51

5.2.6 Summary

From the analyses carried out to characterise the adsorbents, it can be concluded that GAC is physically and chemically very different from the iron adsorbents. Although the FTIR has shown that the hydroxyl group was the main surface group on the three adsorbents, the zero point of charge showed that GAC is basic and positively charged at pH 7.0, whereas AAFS and β-FeOOH are more acidic and slightly negatively charged at neutral pH.

As for the physical characteristics, the alumina is the only adsorbent to have a narrow grain size distribution. The ferric oxihydroxide is far denser than the GAC (alumina is intermediate). The large surface area on GAC compared to the iron adsorbents (respectively 980 m^2/g and between 240 and 360 m^2/g) corresponds to the SEM images showing the numerous cavities in the GAC sheet structure. The iron adsorbents appeared fairly smooth with only a few cracks.

All porosities are about 0.5 although these are differently distributed according to the media. From the nitrogen adsorption, GAC has a very large internal surface area and microporosity, but little mesoporosity. Conversely, iron compounds have no microporosity, according to the t-plot analyses, and exhibit mainly mesoporosity. However, both pore size distribution methods (BJH and HK) disagreed with this conclusion regarding the iron compounds. It is calculated that a large proportion of the porosity is actually a microporous volume. This also corresponds with other findings (Bakoyannakis et al., 2003) studying ferric oxihydroxide. Since the ferric oxihydroxide has a very narrow pore size distribution around 3.5 nm, the presence of microporosity remains unclear as the border between micro and mesoporosity is around 2.5 nm. However, such a narrow pore size distribution might bring a specific behaviour during the adsorption of humic substances.

5.3 Characterisation of the adsorbates (HS)

5.3.1 Uncertainties on parameters measured

5.3.1.1 Systematic and experimental uncertainties

Parameters used to characterise humic substances are (as described in chapter four, "Materials and Methods") the UV absorbances at 254 nm, the Dissolved Organic

Carbon, the ratio of UV to DOC, SUVA. Uncertainty is calculated on these three indicators:

- Uncertainty on UV absorbance reading

The instrument is accurate at ± 0.001 cm^{-1} ($\Delta UV_{instrument}$). The reading for deionised water (used for setting the system to zero absorbance) has been found to vary from 0.048 to 0.053 cm^{-1}; this brings an uncertainty of 0.005 cm^{-1} ($\Delta UV_{experimental}$) due to manipulation (cleaning cuvette, temperature factor, ageing of the UV lamp, sampling). The experimental error is taken as constant, although in most cases it should depend on the value measured itself. However, ±0.005 cm^{-1} covers the experimental error range as seen from figure 5.18; after 20 repetitions, measurements are within the Lower and Upper Warning Limits (LWL and UWL), equal to the mean ± 0.003 (twice the standard deviation). These limits are suggested by the Standard Methods for Examination of Water and Wastewater (1998). From the same source, the accumulated uncertainty (ΔUV) is calculated using a combination of each uncertainty:

$$\Delta UV = \sqrt{(\Delta UV_{instrument})^2 + (\Delta UV_{experimental})^2} \qquad (5.7)$$

$$\Delta UV = \sqrt{(0.001)^2 + (0.005)^2}$$

$$\Delta UV = 0.005 \quad cm^{-1}$$

- Uncertainty on DOC

The instrument precision is ±0.5 mg L^{-1}. Experimental uncertainty (filtering, dilution due to acidification) is estimated to be ±0.1 mg L^{-1}. Again this uncertainty is set as constant since it is estimated and intended to be the maximum error:

$$\Delta DOC = \sqrt{(\Delta DOC_{instrument})^2 + DOC(\Delta UV_{experimental}{}^2)} \qquad (5.8)$$

$$\Delta DOC = \sqrt{(0.1)^2 + (0.5)^2}$$

$$\Delta DOC = 0.5 \quad mgL^{-1}$$

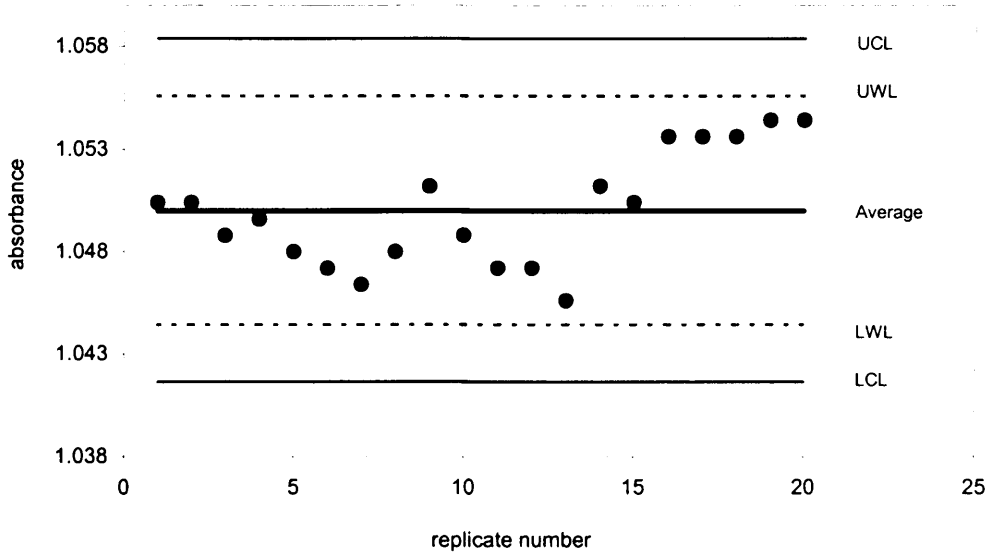

Figure 5.18 Reproducibility of UV absorbance reading at 254 nm
(UCL / LCL for Upper / Lower Critical Limit; UWL / LWL for Upper/Lower Warning Limit)

- Uncertainty on SUVA

SUVA is a function depending on UV and DOC. By using the derivation of such function (UV/DOC) and taking the limit, the error is calculated as:

$$\Delta SUVA = \left| \frac{(\Delta UV \times DOC) - (UV \times \Delta DOC)}{DOC^2} \right| \tag{5.9}$$

Later in this chapter, figure 5.22 compares values of UV absorbance, DOC and SUVA, before adsorption batch studies and after 4 days (e.g. UV/UV_0), using a bar chart. The graph shows individual measured values for the three parameters (one value for each fraction and batch a or b when available). The error bar is calculated as the difference between the largest possible value and the measured value as expressed below:

$$\Delta\left(\frac{UV}{UV_0}\right) = \left(\frac{UV + 0.005}{UV_0 - 0.005}\right) - \frac{UV}{UV_0} \tag{5.10}$$

$$\Delta\left(\frac{DOC}{DOC_0}\right) = \left(\frac{DOC + 0.5}{DOC_0 - 0.5}\right) - \frac{DOC}{DOC_0} \tag{5.11}$$

$$\Delta\left(\frac{SUVA}{SUVA_0}\right) = \left(\frac{SUVA + \Delta SUVA}{SUVA_0 - \Delta SUVA}\right) - \frac{SUVA}{SUVA_0} \tag{5.12}$$

5.3.1.2 Relative uncertainty

Relative uncertainty is calculated as a percentage:

For UV: $\frac{0.005}{UV} \times 100$

For DOC: $\frac{0.5}{DOC} \times 100$

For SUVA: $\frac{\Delta SUVA}{SUVA} \times 100$

Using evaluations for 24 samples (including values before and after 4 days adsorption), the mean and standard deviation of the relative uncertainties are:

For UV	1.3% ± 0.8	(maximum observed error 3.8%)
For DOC	5.9% ± 2.1	(maximum observed error 11.0%)
For SUVA	4.7% ± 2.3	(maximum observed error 10.0%)

5.3.1.3 Mean and standard deviation

When displaying average results instead of individual results, the uncertainty is replaced by the standard deviation. This is the deviation calculated over the total of the samples (entire population), since the number can be two only on some occasions. It is calculated from Excel with the function "STDEVP" and applied to the SUVA values in figure 5.19 below.

5.3.1.4. Consequence of freezing

So far in the literature consulted, no method is mentioned to store samples for DOC analyses. Freezing the samples in high density polyethylene dark bottles was tested in this work. Five samples analysed immediately after sampling and acidifying were compared to the same samples acidified and frozen for four weeks. The results are shown in table 5.3.

After freezing and in each case, the DOC is lower than before (-0.246mg/l ±0.06 on average) and appears to be a systematic error rather than being dependant on initial DOC. This is unexpected since using plastic bottles was thought to bring about leaching

Table 5.3 Effect of freezing samples on DOC results

DOC sample not frozen (NF) mg L^{-1}	DOC frozen sample (4 weeks) (F) mg L^{-1}	Difference brought by freezing (F-NF) mg L^{-1}
1.983	1.826	-0.157
1.767	1.538	-0.229
6.593	6.371	-0.222
3.921	3.632	-0.289
2.563	2.229	-0.334

of carbon into the solution. In addition, the difference is well below ±0.5 mg/l (uncertainty on DOC). Therefore, it cannot be attributed specifically to freezing. The repetitive decrease in DOC is most likely due to the degradation of the samples, as humic substances are not completely refractory but exhibit very slow biodegradation. As a consequence, it was decided that freezing the samples for storage during four weeks or less has no consequence on the DOC.

5.3.2 Characteristics of humic fractions

Humic substances are separated in 3 ranges of molecular weights: 0-5 kDa, 5-10 kDa and 10-50 kDa. The molecular weights above 50 kDa were discarded. Fractions were separated by ultrafiltration and respectively called F1, F2 and F3 (F12 includes both F1 and F2, F123 includes F1, F2 and F3). Before and after using them for equilibrium adsorption studies, their UV absorbance and DOC were measured on the control solution to calculate SUVA (as described in chapter 4). The results appeared in figure 5.19 as averages and deviation (SUVA values actually spread from 0.8 to 11.3). Fraction F1 has the lowest SUVA values, about 2 initially. F2 has a SUVA of about 5.8 and F3 a SUVA of 8.3. As the molecular weight increases, SUVA rises. This is expected since aromatic content increases with the MW and aromatic organic structure (particularly phenolic groups) absorb UV at 254 nm (see table 2.2 and section 2.2 in chapter two). The same tendency is valid for four day old solution (ageing is analysed in the next section). The difference between F1 and F2 is more important than between F2

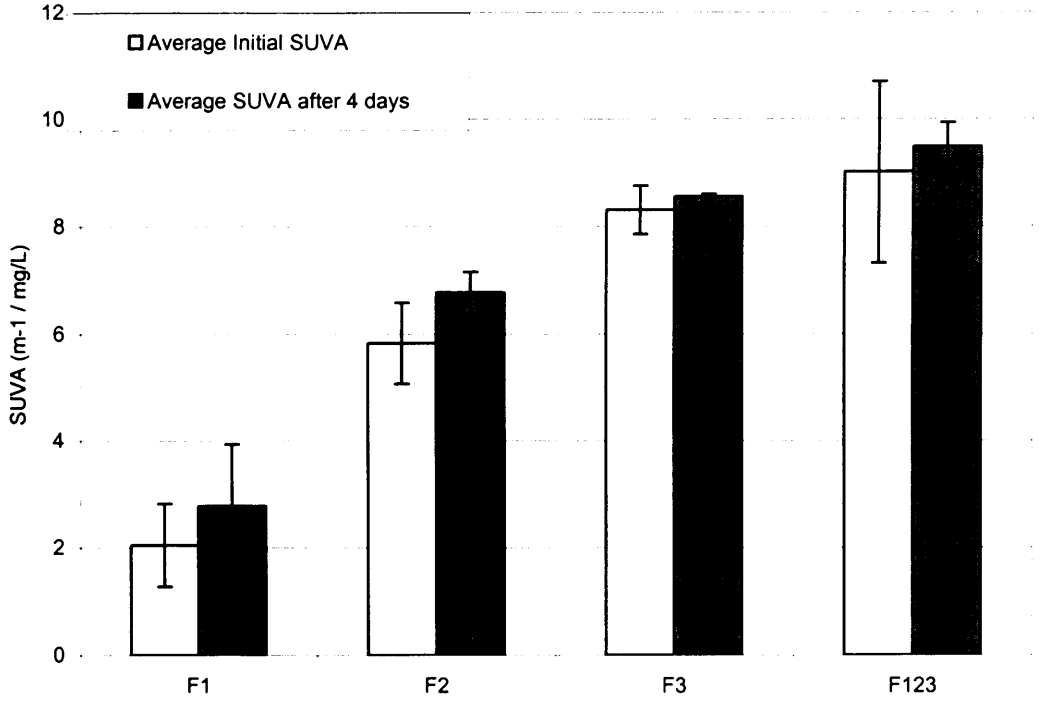

Figure 5.19 SUVA values for each fraction and for the complete solution, original and after 96 hours; standard deviation also represented

and F3. This means that F3 characteristics are closer to F2 than F2 to F1. Therefore, it is deemed acceptable to interpret the MW of F3 to be nearer to 10 kDa than to 50 kDa. On the other hand, SUVA increases again slightly in F123, although it would be expected to have a value between F1 and F3. However, the standard deviation range (error bar) would include the SUVA figure of F3. It is then assumed that in this case, SUVA of F123 is similar to SUVA of F3.

For the same Aldrich humic substances and based on weight averages, other authors reported MW of 4.1 kDa (Chin et al., 1994, Bob and Walker, 2001) and 14.5 kDa (Beckett et al., 1987). More recently, Wall and Chopin (2003) found the same substances, largely purified, reaching MW above 100 kDa. Different preparation of the solution and separation techniques make the results difficult to compare.

Separation techniques used here are the centrifugation (10000 rpm i.e. 18600g) and ultrafiltration polyethersulfone (PES) membranes. Aggregation might have occurred during centrifugation. Cameron et al. (1972) showed aggregation of HS leading to very high MW in the deposit of the centrifuge tube (ultracentrifugation). Aggregation would

also occur in the liquid phase if the centripetal force is high enough to reduce the diffusive layer around the humic molecules so as to reach a stable aggregate, but not strong enough to make it settle. Aggregates of the colloidal size (a few nm to 1μm) would remain in the liquid to be ultrafiltered and they are likely to be stabilised through hydrophobic interactions and H-bonds (Sutton and Sposito, 2005). During ultrafiltration, Egeberg (2002) showed a high retention by PES membrane in particular. In the present conditions of study, conformation of humic substances is more likely to be elongated rather than globular (see discussion in next section). In this case, the size rejected by the membrane can be smaller than the stated membrane molecular weight cut-off (MWCO). Acidification of the solution before UF would enable the separation to be closer to the MWCO (standards are produced using globular protein molecules). Two consequences arise: *(i)* the permeate might be less concentrated than expected and *(ii)* maximum MW in permeate might be smaller than stated by the MWCO. From the separation techniques here, aggregation has probably taken place, explaining why F3 corresponds to the main fraction.

As a summary, for the following molecular ranges: below 5 kDa, between 5 and 10 kDa and between 10 and 50 kDa, SUVA value is respectively less than 4, about 6 and about 8. These results are in agreement with Kitis et al.'s data (2002) who studied a river water using a different UF membrane and found SUVA to be less than 4.5 for MW less than 3 kDa, SUVA about 5.5 for MW between 3 and 30 kDa and SUVA about 7 for MW above 30 kDa. They also agree with Allpike et al. (2005) who measured a SUVA approximately equal to 5, corresponding to 61 % of molecular weights between 4 and 10 kDa.

On figure 5.19, the deviation from the mean is relatively more important for F1, showing that it was more difficult to reproduce similar F1 solutions, compared to F2 and F3 (low deviation for F3 after 4 days is due to only 2 values available and close to one another). Two explanations can be given: *(i)* non quantified binding of HS on the membrane occurs at each step of ultrafiltration; since F1 is the fraction bearing the most ultrafiltration steps, it suffers a greater accumulated effect of such binding and *(ii)* quick degradation of F1.

From this graph, it could also be inferred that F3 represents F123 well. However, such conclusion is not straightforward. SUVA gives the qualitative information about the type of humic substances but does not give any quantitative information. Values of

UV_{254} absorbance and DOC must be considered. The following figures show the UV and DOC ranges for the three humic fractions and the complete solution F123:

F1 ranges:	UV = 0.179-0.434 cm^{-1}	DOC = 11.7-20.3 mg L^{-1}
F2 ranges:	UV = 0.480-0.859 cm^{-1}	DOC = 9.1-13.3 mg L^{-1}
F3 ranges:	UV = 1.197-1.460 cm^{-1}	DOC = 13.6-19.0 mg L^{-1}
F123 ranges:	UV = 0.534-1.199 cm^{-1}	DOC = 5.8-10.6 mg L^{-1}

Considering that F1 represents low MW, UV absorbance of about 0.4 cm^{-1} is high and so is the DOC of 20.3 mg L^{-1}. On the other hand, a low DOC was obtained for F123 but for F3, DOC reached 19 mg L^{-1}, almost like F1. As a consequence, characterising the humic solution by only SUVA or DOC or UV absorbance is not sufficient. Two parameters out of three are needed (SUVA, DOC, UV).

The fact that SUVA values for F3 and F123 are similar can be due to the proportion of F3 in F123, which is confirmed from figure 5.20. The difficulty in reproducing the same solution (a and b) is shown again here. However, trends are similar. F3 is clearly dominant in both solutions and F1 contributes by its DOC (striking in solution a). Nevertheless, the properties of F1 influence the adsorption and are of utmost interest, since aquatic humic will more closely resemble F1. From the distribution of F1, F2 and F3 in F123 shown in figure 5.20, it seems that ultrafiltration membranes have been more selective in solution a compared to solution b, where SUVA for F1 and F3 are closer in value. This is attributed to the very beginning of the preparation as problems were experienced with centrifugation for solution b. Filtration and ultrafiltration presented more resistance due to the high MW still present in the centrifuged solution.

The humic substances solutions contain solids smaller than 0.45 µm, i.e. dissolved solids. From Aldrich technical data, the powder used here contains the following elements:

- Elemental analysis:

C	39.03 %
H	4.43 %
N	0.68 %

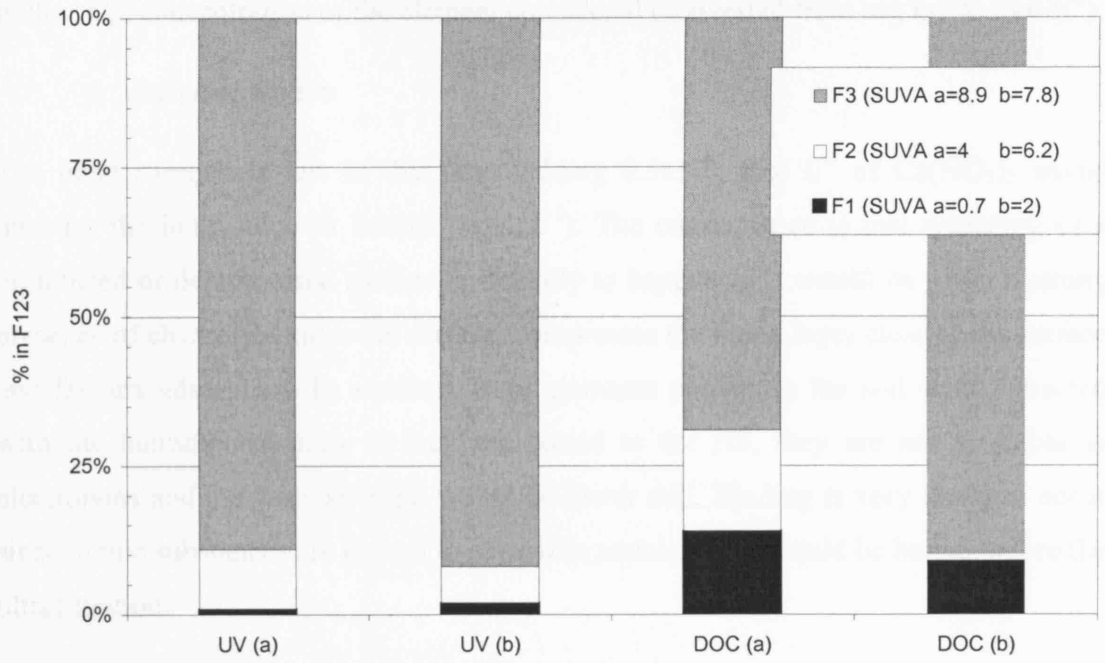

Figure 5.20 Contribution of F1, F2, F3 to F123 represented by the distribution of UV absorbance and DOC in solution F123

- Trace analysis:

Na	7670 mg kg^{-1}
S	2500 mg kg^{-1}
Fe	1300 mg kg^{-1}
Ca	1200 mg kg^{-1}
Mg	1091 mg kg^{-1}
P	215 mg kg^{-1}
Li	3 mg kg^{-1}

The concentration in trace elements corresponds to 1.4 mg L^{-1}. If trace elements are present as ions in the solution, the ionic strength I can be calculated as follows (assuming Fe as Fe^{2+} and P as PO_4^-):

$$I = \frac{1}{2}\sum_i C_i z_i^2 \tag{5.13}$$

$$I = 5.22 \times 10^{-5} \ mol \ L^{-1}$$

with C_i : concentration of the element considered (converted from mg $kg^{-1}$to mol L^{-1})

z_i: charge of the ion

The ionic strength is low in this case (adding $0.5x10^{-3}$ mol L^{-1} of $Ca(NO_3)_2$ would increase the ionic force to $1.5x10^{-3}$ mol L^{-1}). The consequence is that screening of a protonised or deprotonised surface is unlikely to happen as it would do when a strong presence of electrolyte hides the surface, compresses the liquid layer close to the surface and favours adsorption. In addition, trace elements present in the soil were extracted with the humic substances. If they are bound to the HS, they are not available as electrolytes and the ionic strength would be lower still. Binding is very likely to occur since humic substances are known to solubilise metals. They would be bound before the ultrafiltration.

Solution F123 has about 6.9 mg L^{-1} of organic carbon (see figure 5.21). Therefore, trace elements binding correspond to a metal/mineral associated every 5 carbon atoms (1.4 mg trace elements for every 6.9 mg C).

Preparation of the solution F123 eliminates the suspended solids and molecular weights above 50 kDa. The composition of the working solution F123 is shown in figure 5.21. The Total Dissolved Solids (TDS) include humic substances and calcium nitrate added for hardness adjustment (118.075 mg L^{-1} of $Ca(NO_3)_2.4H_2O$ were added). Humic substances correspond to only 18.3 % of the TDS. Of these humics, 28 % correspond to organic carbon (as DOC). It is much lower than the 39.03% stated by Aldrich. The loss of carbon comes from the loss of the high carbon content matter through centrifugation and ultrafiltration. It agrees with Montgomery (1985) relating that, in soil, humics contain more carbon than fulvics which have a lower MW. Since ultrafiltration eliminated the higher MW, carbon proportion should also decrease. On the other hand, Wall and Choppin (2003) found 50-60% of the original powder to be ashes in the same product (Aldrich humic acid), down to 5% after purification of the powder. Therefore, the inorganic carbon should constitute the main proportion of "others".

Most interestingly, water is still present in the TDS when hydrated calcium nitrate has been added. It is agreed that HS are mainly constituted of water (up to 80% according to Wilkinson et al. 1999). These 27 mg of bound water did not evaporate at 105°C. Calcium associates with humic substances to form complexes which can be larger than

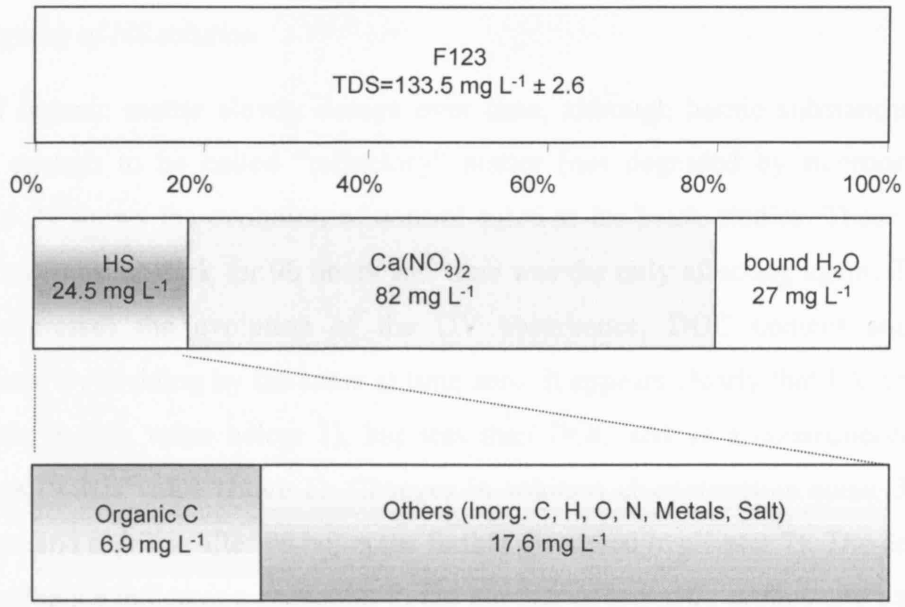

Figure 5.21 Composition of working solution F123

0.45 µm as confirmed during preliminary filtration experiments (André, 2003). Calcium is used as a ligand in the humic molecules. From figure 5.21, nitrate ions are a major constituent of the working solution.

Therefore, it was confirmed that nitrate ions do not interfere with UV absorbance measurements. These ions serve as electrolytes to transport electrons. The ionic strength brought from calcium nitrate addition is $1.5*10^{-3}$ mol mg L^{-1}, thirty times the ionic strength calculated from the trace elements. It is still low and unlikely to significantly compress the diffusive layer surrounding the humic molecule. From the literature, aggregation was observed at higher ionic strength (Balnois et al. 1999, Wall and Choppin, 2003) but seemed to depend more on the type of humic substances. During the diffusion process, the hydrodynamic resistance due to this layer will limit the kinetics and needs to be considered in the "Kinetics" section (chapter 6).

It is known that aquatic NOM have a high content of non-humic material (carbohydrates, carboxylic and amino acids, hydrocarbons) which can reach 50-70% of the DOC or lower (10%) for high DOC upland water (Lambert, 1992). However, regarding the present humic substances, it is unknown whether or not the non-humic material has been eliminated and it will be assumed that only humic and fulvic acids are present in solution.

5.3.3 Ageing of HS solution

Natural organic matter slowly decays over time, although humic substances degrade slowly enough to be called "refractory" matter (not degraded by microorganisms). Figure 5.22 shows the evolution of control solution for batch studies. Those solutions were shaken in the dark for 96 hours and time was the only affecting agent. The y-axis value expresses the evolution of the UV absorbance, DOC content and SUVA, normalised by dividing by the same at time zero. It appears clearly that UV absorbance decreases (y-axis value below 1), but less than DOC and as a consequence, SUVA increases (y-axis value above 1). Changes in solution characteristics occur during the first days and stabilise after 96 hours (as further discussed in chapter 7). The decrease of UV absorbance indicates a reduction in the number of aromatic groups and particularly phenolic groups (representing higher MW). Consequently, a DOC decrease is also observed. The decrease in the aromatic groups number is a valuable aspect of the adsorption since they govern the natural organic matter activity and favours trihalomethane formation (Kim and Yu, 2005).

However, a reduction of the DOC is also attributed the degradation of lower molecular weights which themselves hardly absorb at 254 nm. The overall tendency results in a larger decrease in DOC and increase in SUVA. This behaviour does not seem to apply to fraction F3 whose characteristics remain unchanged, although this result is not very reliable as only two values were available.

Ageing of such solutions has been observed before under different conditions. Kulovaara (1996) observed an easier degradation of fulvic and humic acids under UV irradiation. UV absorbance decreased more than DOC. The contrary is observed here, when the HS do not receive any UV radiation. Either a temperature of 19°C was high enough to break some of the aliphatic structure of F1, or a microbiological growth has occurred, starting to mineralise the HS. The latter is more likely since the solution itself provides nutrients (via trace elements) and the equipment was not sterilised. As observed, the degradation is very slow. This agrees with Filip and Kubát (2001) who noticed the difficulty of degrading aromatics from soil since they were bound to minerals, hence little decrease in aromatic concentration, whereas aliphatic content was observed to decrease, i.e. were degraded.

Ageing of the solution has an additional consequence which is the changing quality of supply solution to the columns when studying the continuous flow adsorption. Figures 5.23, 5.24 and 5.25 show that the difference in DOC can be up to 2 mg/L. This will need to be considered when interpreting the results. During a single run, the absorbance slightly decreases with time. This is confirmed by the decrease in DOC too, which is small when considering the error. Consequently, SUVA does not significantly change over a column run. It is worth mentioning here that a microbial growth is still likely even if degradation of HS does not take place due to slow kinetics.

5.3.4 Size and conformation of humic substances

Many parameters influence the size and conformation of HS in solution. First and as said above, it is likely that the isolation procedure brings defects in the quality of the substances. However, it is necessary to accept these modifications to enable study of the humics under a controlled environment (fresh water provides a complex environment, not systematically available and not constant in quality). Relevant concepts are hydrophobicity, ionic strength, pH, MW, membrane pore sizes, all influencing size, conformation, diffusion and possible aggregation of humic molecules. They have been discussed in chapter 2 and can be applied to the particular case of this study.

5.3.4.1 Hydrophobicity

The parallel between hydrophobicity and a harmful effect has been drawn by Kim and Yu (2005). The hydrophobic compounds have a high OH and phenolic group content which increases their ability to form cancerigenous compouds (THM). Conversely, the group COOH which is hydrophilic, leads to less THM formation. Separation based on the hydrophobicity instead of MW brings the following fractions (Bolto et al., 2002): very hydrophobic acid (VHA), slightly hydrophobic acid (SHA), hydrophilic charged (Char) and hydrophilic neutral (Neut). VHA correspond to high MW since UV_{254} decreases significantly as they are removed. Bolto et al. (2002) analysed the same Aldrich humic substances and found:

VHA=40% DOC

SHA= 5 % DOC

Char=10 % DOC

Neut=45 % DOC

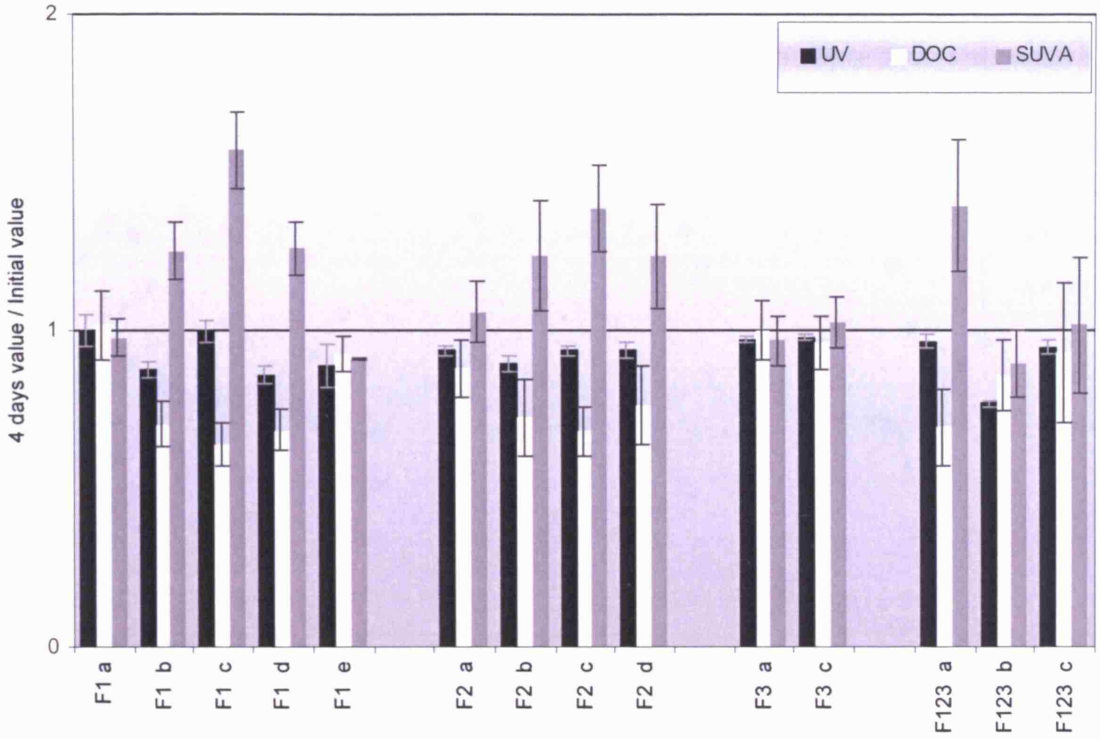

Figure 5.22 Ageing of solutions (ratio shows increase/decrease of UV / DOC / SUVA of fractions after 4 days)

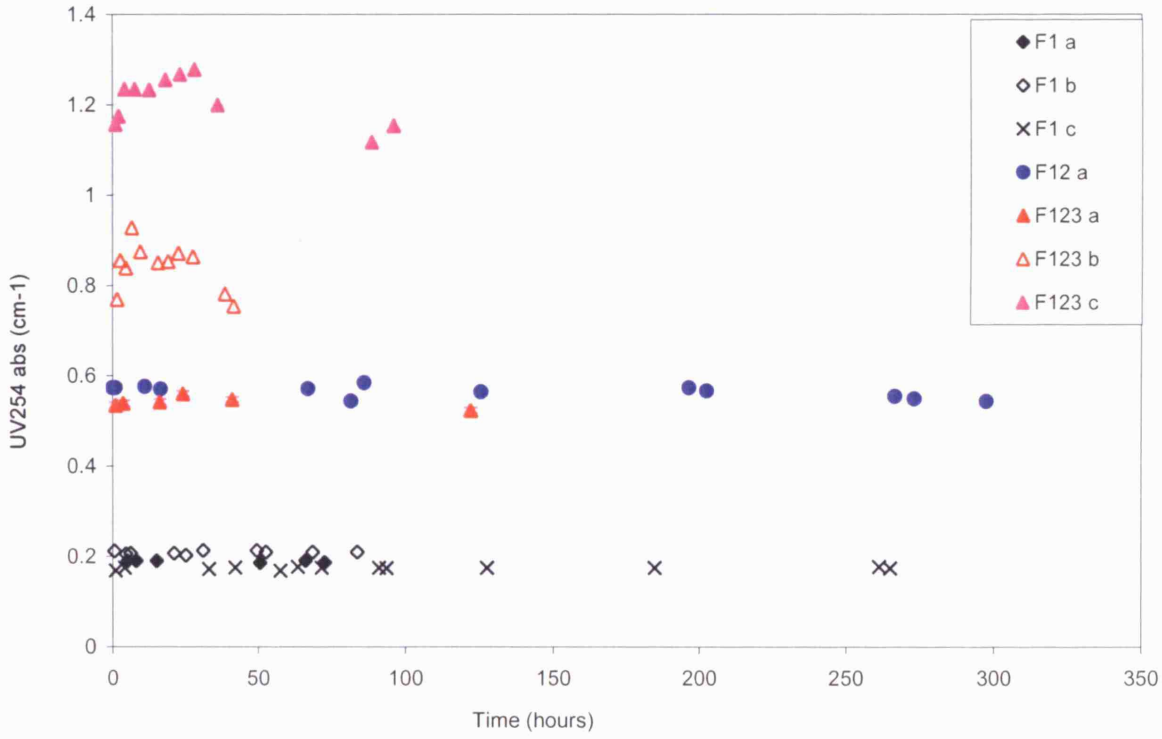

Figure 5.23 Evolution of column influent for UV_{254} absorbance

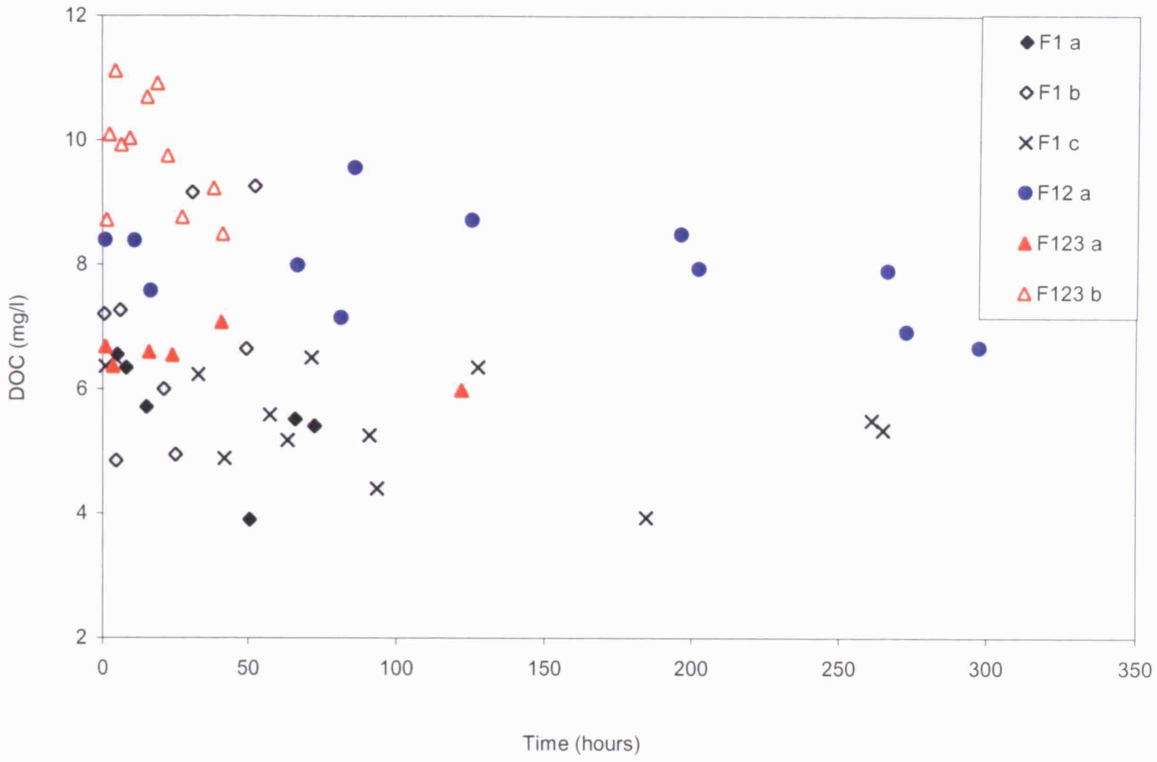

Figure 5.24 Evolution of column influent for DOC

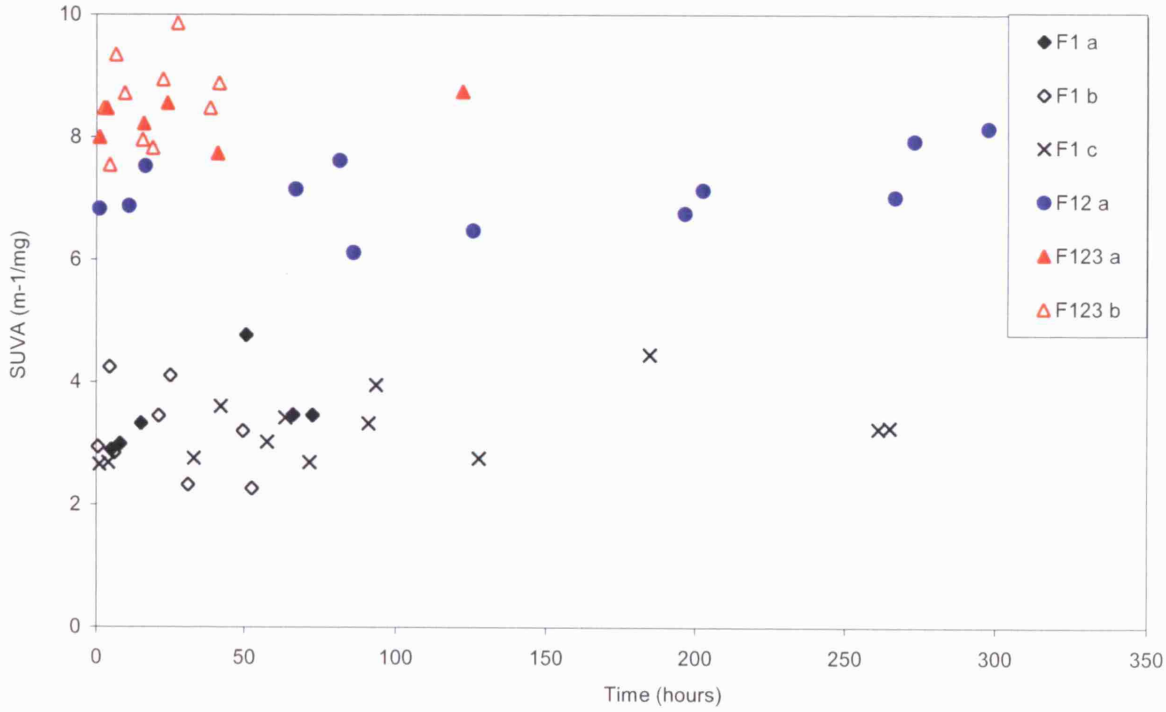

Figure 5.25 Evolution of column influent for (a) UV absorbance (b) DOC and (c) SUVA

In addition, Kitis et al. (2002) could relate MW and hydrophobicity via SUVA. It appeared that hydrophilic HS had SUVA below 4 and hydrophobic HS had a higher SUVA, between 5 and 6. It can be concluded that F1 is a hydrophilic fraction, probably charged. F2 and F3 correspond to hydrophobic compounds, and also probably neutral hydrophilic compounds, due to their high contribution to the DOC.

5.3.4.2 Ionic strength and pH

After dissolving 5 g/L of humic substances in deionised water the pH was above 7. After dilution and addition of hardness, pH was adjusted to 7.0. Ionic strength is low ($1.5*10^{-3}$ mol L^{-1}). Such conditions are favourable to metal binding (Tipping, 2002). Calcium was also shown to strongly bind HS too (André, 2003). The low ionic strength does not obviously influence the intermolecular aggregation as mentioned above.

On the other hand, a high pH causes the HS to extend (or uncoil from a coiled structure at low pH) exposing the deprotonised groups to the water. This behaviour is increased at low ionic strength since negative charges are not screened by other ions and this increases intramolecular repulsion. Therefore, in the present conditions, it is expected that the humic substances will be elongated, deprotonised and will exhibit negative charges.

5.3.4.3 Membranes pore sizes

Ultrafiltration separates sizes from about 2 nm to 0.1 µm. The correspondence of MW to sizes has been suggested by Ratnaweera (1999) and also by Thorsen (1999). On average they say: 5 kDa corresponds to 2 nm, 10 kDa to 3.1 nm, 50 kDa to 7.4 nm. Since HS are likely to be extended, the pore size represents a maximum for the smaller dimension of the molecule. This shows that separation is also influenced by pH. The separation is likely to rely on the structure rather than the charge of the molecules, since the membrane is hydrophobic but negatively charged (characteristic of PES membranes).

5.3.4.4 Size and MW

A UK Geological Survey of aquatic humic acid (cited by Wilkinson et al. 1999) was found to have an average radius of gyration between 1.5 and 5 nm for an average MW of 20 kDa (weight based). Radius of gyration was calculated from the diffusion coefficient (Cameron et al., 1972). The results were 1.5 nm, 2 nm, 3.2 nm, 4.2 nm respectively for 2.6 kDa, 4.4 kDa, 12.8 kDa and 23.8 kDa. This corresponds to the pore

size of the relevant membrane for 5 kDa and 10 kDa. Following this reasoning, F2 has a size between 2 and 3.1 nm and F3 between 3.1 and 7.4 nm (size for MWCO), although closer to 4.2 due to MW being closer to 10 than to 50 kDa and to the UK geological survey aquatic humic acid characteristics. These figures are only arbitrary estimates which will be useful when analysing the adsorption according to adsorbent pore sizes.

5.3.4.5 Likely conformation of HS

It is concluded that conformation of humics in fractions F1, F2, F3, F12 and F123 are extended and ionised. In addition, Lead et al. (2000) found the diffusion coefficient to vary very little with ionic strength or pH. This gives evidence of a rigid structure for these substances. Aggregation (as opposed to coiling) increases the size of the structure leading to a higher diffusion coefficient. Therefore at pH 7, HS are not strongly aggregated but rather forming a superstructure as defined by Piccolo (2001). This kind of aggregation associates sub-units by weak hydrophobic forces (Van der Waals, electrostatic repulsion, Pi-Pi bonds) and H bonds and leads to higher MW. It explains why F3 is the main constituent of the solution used in this work. This is supported by the fact that the origin of the humic substances, more than the ionic strength, influences the association of more simple molecules and it corresponds to the soil extracts which are known to be more hydrophobic.

5.3.5 Summary

From the characteristics analysed for the separated fractions, we can conclude that:

- Humic substances under study have an extended conformation and are ionised
- Gyration radius for each fraction is as follows:

  F1 1.5 – 2 nm

  F2 2 – 3.1 nm

  F3 3.1—7.4 nm (but closer to 4.2 nm)

- Humic substances are bound to metals and minerals (traces elements and added calcium) and weakly aggregated under hydrophobic forces and H bonds
- Separation techniques (likely centrifugation and definitely ultrafiltration) has brought defects in the original MW distribution
- Ageing of the solution has influenced batch studies but not column studies.

5.4 Conclusions

The previous analyses give clear characteristics of the three adsorbents to be used in this work and of the humic substances to be adsorbed.

The common feature of the adsorbents is the presence of surface hydroxyl groups which will enable adsorption to take place. The surface of GAC is basic and positive at neutral pH but slightly negative on both AAFS and β-FeOOH, hence a more favourable adsorption of humic substances onto the activated carbon. As for the porosity, GAC is mainly microporous, with a very large surface area. The presence of microporosity on β-FeOOH is unclear, since different methods give different results. However, it is concluded that microporos ity is most likely to be present on the iron compounds. The area available for adsorption on AAFS and β-FeOOH is small compared to the GAC. But, this must be related to the size of the adsorbate which are unable to penetrate micropores, hence inhibiting adsorption onto GAC. The porous structure agrees well with the SEM photographs that show the sheet structure of GAC and its numerous cavities in contrast with the iron compounds which appear smooth with only a few cracks.

The humic substances represent the adsorbate, most likely with an extended conformation and ionised (deprotonised). They are bound to metals present in the original HS extract powder and also bound to calcium added to the working solutions. This should favour their adsorption via the ligand exchange mechanism. These HS are also aggregated together under weak forces which can be broken when adsorption is more favourable. Gyration radius was estimated for the three fractions F1 (< 5 kDa), F2 (5-10 kDa) and F3 (10-50 kDa), from 1.5 nm for the lightest, up to 7.4 nm for the heaviest MW. It must be kept in mind that the ageing of the HS solution alters the MW distribution, which might have influenced the kinetic and batch studies but not the column studies.

CHAPTER 6

KINETIC STUDIES

6.1 Introduction

The literature review has shown that humic substances could be adsorbed on GAC and iron compounds according to their molecular weight. In most occasions, the maximum adsorption capacity of the adsorbent is not fully used since the system does not reach the equilibrium, as for example during a continuous flow process. On the other hand, the extent of adsorption depends on initial and final states and on the path used to reach this final state (Weber et al., 1991). Various mechanisms of adsorption simultaneously take place on this path, each of which has a specific resistance to adsorption. The overall kinetics of the process are limited by the largest resistance. Therefore, it is essential to know which mechanism is dominant since the slowest mechanism imposes the kinetics of adsorption. For this, several kinetics models (detailed in chapter three) should be tested and that is the scope of this chapter.

The iron-containing adsorbents can be compared to iron-containing coagulants. These act chemically by a charge cancellation mechanism which enables flocculation to take place (gathering of the suspended solids). As a consequence of the iron ion valence (+II or +III), chemical adsorption is also considered to take place in the cases considered by this study. This was mentioned as the "chemical feature" of the humic acids adsorption on iron oxides by Tombácz et al. (2004). Therefore, the first type of model will consider the adsorption sites as chemical species reacting with the adsorbate. Three models are tested here: the pseudo-first and -second order models, which consider the adsorbent as a homogeneous surface. The third is the Elovich equation model which is based on a heterogeneous surface of the adsorbent (Al-Ghouti, 2004).

The intraparticle diffusion and external diffusion models will also be tested. They represent a type of models which draw attention to microscopic mechanisms of mass transport. In addition the "Homogeneous Surface Diffusion Model" (HSDM) will also be tested since it corresponds to the GACMan simulation programme used for column studies. The HSDM model is presented in detail in Chapter three (literature review).

Kinetics are influenced by numerous parameters (pH, temperature, adsorbate concentration, adsorbent quantity, mixing speed) and it is helpful to investigate the influence of each parameter on the adsorption rate. However, such work is not carried out in detail here. The purpose of this chapter is to compare the importance of each adsorption mechanism under the conditions of study (set for the whole range of study) for the three systems "adsorbate-adsorbent"; HS-GAC, HS-AAFS and HS-βFeOOH, by fitting the best kinetics model. To apply the above mentioned models, adsorption should not be limited by external mass transfer. Therefore, the reactor is well mixed (CSTR) and, in addition, two mixing speeds are compared.

Finally, an error function will allow an estimate to be made of how well the models fit the experimental data. Consequently, the best model can be selected although it is possible that different models fit at different stages of adsorption.

The study is performed on fraction F123 which includes molecular weights up to 50 kDa. The concentration left in the flasks (non-adsorbed humic substances) is measured by UV_{254} absorbance. However, for consistency throughout the model tested, a concentration unit should be used instead of an absorbance unit. From figure 5.19 in chapter five, the average SUVA of solution F123 was estimated at 9.5 which was assumed to remain constant. Hence, the concentration in dissolved organic carbon (DOC mg L^{-1}) is obtained by the ratio UV_{254}/SUVA. As a consequence, low MW, which have a high DOC but little absorbance, might be wrongly considered as removed under this assumption. This will be taken into account during the interpretation. The working temperature is 20°C and the initial pH 7.0. The electrolyte was $Ca(NO_3)_2$ and added at 0.5×10^{-3} mol/L.

6.2 Influence of the mixing speed

Whether the process involves chemi- or physisorption, mass transfer occurs first to bring the adsorbate from the bulk solution close to the adsorbent external surface. Mixing should also provide *(i)* a uniform distribution of the adsorbate in the solution and *(ii)* the adsorbate with as much chance as possible to get in contact with the adsorbent, i.e. to keep the adsorbent suspended in solution, "showing" its surface for adsorption to the humic substances. However, a vigorous mixing can also have a negative impact by breaking the adsorbent grains subject to friability. None of the literature reviewed in this work referred to this problem although some authors used a mixing speed of 400 rpm (Cheung et al. 2000) or 1100 rpm (Lazaridis et al. 2003). During this work, qualitative experiments showed that the solution in the flasks quickly became very turbid above 300 rpm. Therefore, attrition obviously occurs beyond that mixing speed and adsorption parameters are modified (particularly the surface area of the adsorbent). The diffusion process is also altered under these new conditions for internal and external adsorbent surfaces. As a consequence, the best fitting models could be wrongly attributed.

Two mixing speeds were investigated here: 200 rpm and 300 rpm. From visual observation, the adsorbents were all well suspended at 200 rpm in a 100 ml Erlenmeyer flask as used for the equilibrium studies. This was the minimum speed for a complete suspension, therefore minimising the attrition for a maximum contact between the adsorbent and the adsorbate. However, in the 250 ml Erlenmeyer flasks, used for the kinetics study (containing proportionally more adsorbent), 200 rpm did not allow the suspension of the iron compounds due to their higher density compared to GAC. The minimum speed for a complete suspension in these conditions was 300 rpm. The evolution of the load (adsorbate quantity adsorbed onto the adsorbent in mg DOC per g of adsorbent), vs time, is shown in figures 6.1, 6.2 and 6.3 respectively for GAC, AAFS and β-FeOOH, comparing the two mixing speeds.

On each graph, the curve for 300 rpm is well above the curve for 200 rpm. The initial slope is also larger. This feature shows that the load on the adsorbent increases faster at 300 than at 200 rpm. Strong mixing decreases the thickness of the boundary layer surrounding the adsorbent grains where transport occurs by film diffusion. Although the diffusion itself is not affected by the mixing, a thinner film will lead to a shorter

distance to be diffused through. External mass transfer coefficient will be calculated in section 6.8.

For the three adsorbents, the curve at 200 rpm is smooth, showing a very slow approach to equilibrium. This is specific to humic substances and has also been noticed by other authors. For example, Zhang and Bai (2003) concluded that several days were necessary to reach the equilibrium at neutral pH. In their study, they used chitosan-coated granules to adsorb humic substances (sodium salt Aldrich HS powder, which is similar to the one used in this study), and compared the results at various pHs. The results showed a drastic effect of the pH on the time needed to reach equilibrium. At around a pH of 12, several days were needed to attain equilibrium. Another example is presented by Wu et al. (2002) who also used chitosan-encapsulated carbon to adsorb Aldrich humic substances and concluded that equilibrium was reached after 4 days. Humic substances are made of big molecules and although they are not well defined, their size implies that they diffuse slowly. This gives time for reconformation of the molecules on the adsorbent surface and brings a change in the adsorption sites availability, and hence an increased time to reach equilibrium.

Equilibrium is reached when both adsorption and desorption occur at the same rate (relevant particularly for physi- rather than for chemisorption). Considering that humic substances do not represent a single component but rather a multicomponent adsorbate as discussed in the chapter describing humic substances (Chapter five), at equilibrium adsorption-desorption is very likely to occur. This was indeed observed by Gu et al. (1996b) when they used Suwanee River Fulvic Acid (SRFA). SRFA competed very strongly with other organic matter (model organic compounds such as polyacrylic acid PAA) during adsorption on iron oxide. They clearly observed a displacement of the PAA by the SRFA. Preferential adsorption is a phenomenon that is also shown in this work when SUVA was evaluated for adsorption processes in chapter eight (during the continuous flow studies).

In figures 6.1 to 6.3, the time scale was cut for clarity and the amount of DOC adsorbed on the adsorbent (i.e. the load in mg DOC/g adsorbent) at 200 rpm is not much less than at 300 rpm, particularly for GAC. Respectively for GAC, AAFS and for β-FeOOH, the load after 240 minutes were 0.49, 0.59, 0.56 mg DOC/g compared to 0.50, 0.68 and 0.70 mg DOC/g at 300 rpm. Consequently, it appears that the mixing speed does not affect the equilibrium of adsorption to a great extent. This was also found by

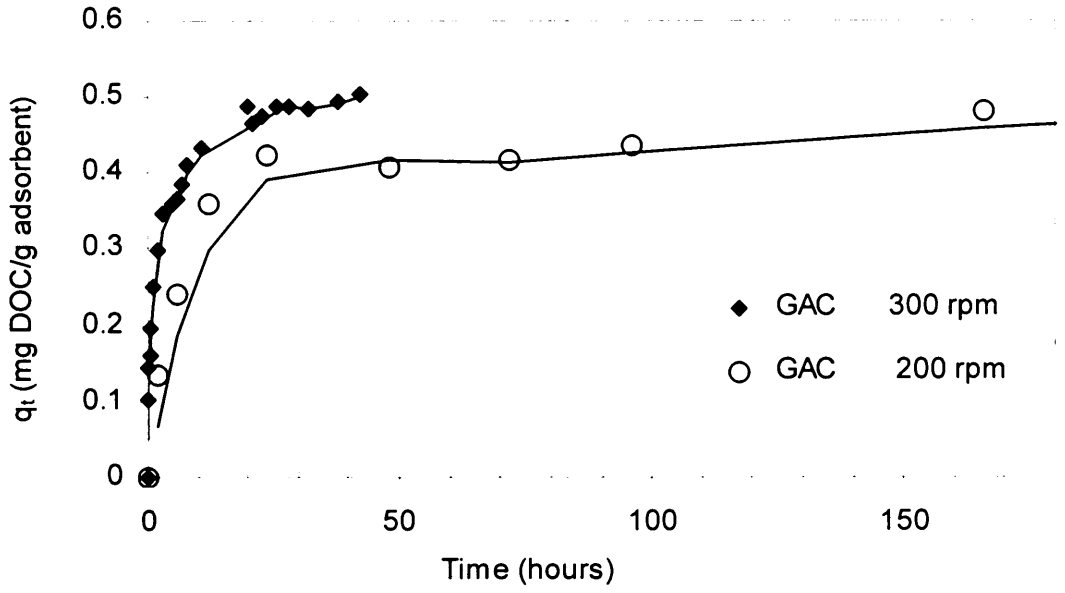

Figure 6.1 Influence of the mixing speed on DOC load on GAC vs Time; Experimental conditions: 250 ml of F123, SUVA=9.5. At 200 rpm; 2.3 g GAC and $(UV_{254})_0$=0.457 cm^{-1}, at 300 rpm; 2 g GAC and $(UV_{254})_0$=0.582 cm^{-1}

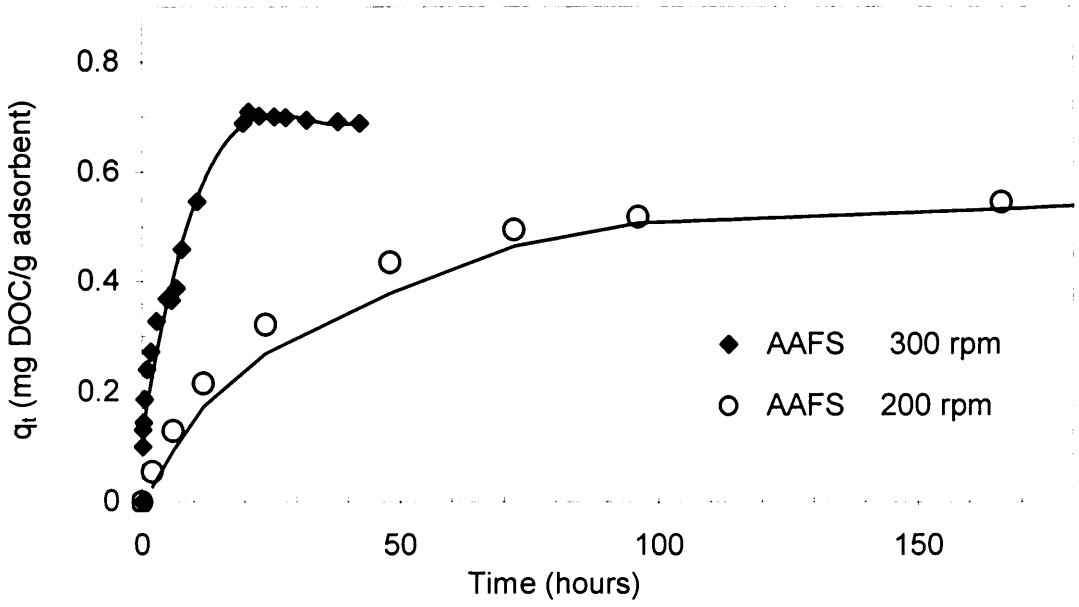

Figure 6.2 Influence of the mixing speed on DOC load on AAFS vs Time; Experimental conditions: 250 ml of F123, SUVA=9.5. At 200 rpm; 2.3 g AAFS and $(UV_{254})_0$=0.508 cm^{-1}, at 300 rpm; 2 g AAFS and $(UV_{254})_0$=0.582 cm^{-1}

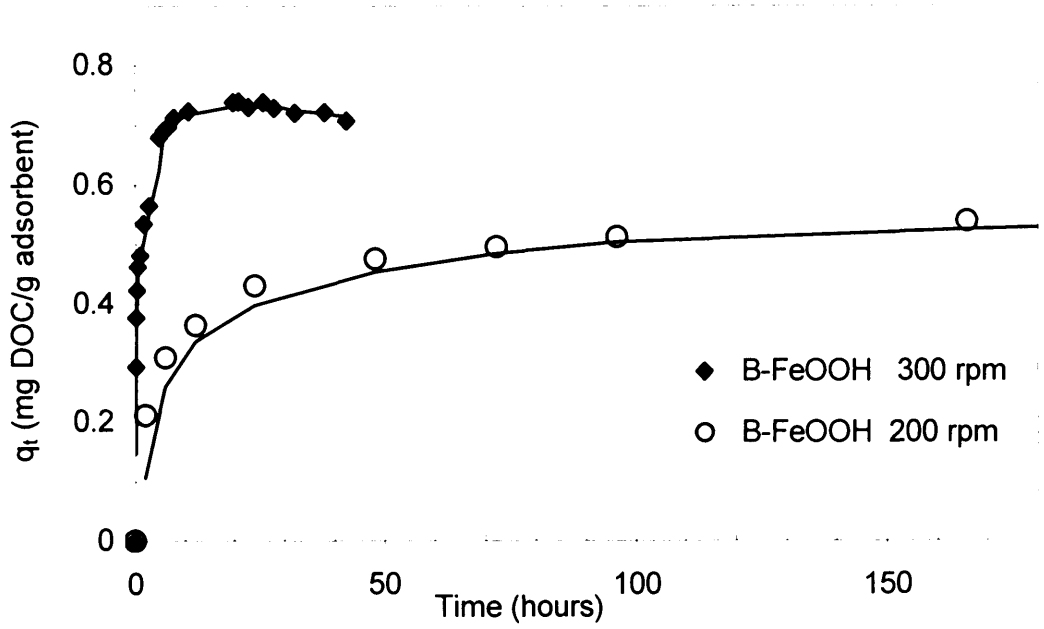

Figure 6.3 Influence of the mixing speed on DOC load on β-FeOOH vs Time; Experimental conditions: 250 ml of F123, SUVA=9.5. At 200 rpm; 2.3 g β-FeOOH and $(UV_{254})_0$=0.508 cm^{-1}, at 300 rpm; 2 g β-FeOOH and $(UV_{254})_0$=0.582 cm^{-1}

Al-Ghouti (2004) whose studies showed that adsorption of dyes onto diatomite reached found the almost similar equilibrium loads after several hours at 200 or 400 rpm. The authors also mixing speed to have an irregular effect on the adsorption process. From figures 6.2 and 6.6, it is also clear that the equilibrium is reached quicker at 300 than at 200 rpm. This is less obvious on figure 6.1 and it corresponds to the GAC being principally microporous.

According to Badruzzaman et al. (2004), the mixing speed does not influence the extent of adsorption if the principal resistance to adsorption is due to intraparticle transport. This is expected since the mixing does not affect the liquid flow within the pore. The same authors found that particle size distribution, bed porosity and Reynolds number (hence mixing speed) can be used to minimise the external film diffusion but that these do not have any impact on internal mass transport, as observed in figure 6.1.

At 300 rpm, the curves are not smooth, indicating that adsorption is not only external transport limited but that a more complicated process is involved. During the first few minutes, strong instantaneous adsorption occurs which slows down as the curves detach

from the y-axis. The various stages of this process will be detailed in section 6.6 (intraparticle diffusion). Among the three adsorbents and at low mixing speed, AAFS showed the least affinity for the HS with no instantaneous adsorption at all at 200 rpm. This is seen from figure 6.2 where the curve does not follow the y-axis (0.1 mg DOC/g AAFS at 2 minutes) and as opposed on figures 6.1 (0.3 mg DOC/g GAC at 2 minutes) and 6.3 (axis (0.56 mg DOC/g β-FeOOH at 2 minutes) where a strong slope proves faster adsorption of the humic substances GAC and β-FeOOHthan on AAFS. This difference between AAFS and GAC is less apparent at 300 rpm. Therefore, it is suggested that external transport limits the adsorption process on AAFS at 200 rpm. Although adsorption is greater on β-FeOOH than on AAFS, external transport plays a large role as seen from the large difference between the two curves (200 rpm and 300 rpm in figure 6.3). This is in agreement with the fact that these two iron compounds have mostly an external surface.

In addition, the three curves at 300 rpm seem to suffer a shift after about 6-7 hours. From the experimental point of view, this corresponded to a difficult filtration of the sample. The mixed solutions were very turbid and the filter retained a great quantity of adsorbent powder, at the same time increasing the resistance to filtration. This was due to a large attrition of the media and had two negative consequences. First, the increased resistance to filtration meant that the powdered media acted as an additional filter. Therefore, the measured absorbance of the sample is likely to be lower than the true absorbance and as a result, a higher load is calculated. Second, the breakage of the adsorbents grains in the solution modifies the surface area which is inversely proportional to the radius of a spherical particle (Hiemenz, 1986). From this, the adsorption is largely favoured if it is principally external (macro and mesoporosity). As a consequence from attrition, the results beyond 6.65 hours (sample at 399 minutes) will not be used in the calculations. Such an important issue is not mentioned in the literature and would deserve more attention in future studies.

It is interesting to notice at this point that the increase of surface area is equivalent to the addition of more adsorbent. This was mentioned by Al-Ghouti (2004) who investigated the adsorption of methylene blue onto diatomite. He observed an increase in the external diffusion coefficient when the adsorbent mass was increased under the same experimental conditions. McKay et al. (1986) suggested that this was due to the increase in surface area, which confirms the above observations.

For the GAC, the mixing speed has less influence than for the iron compounds. Therefore, the mass transfer through the external boundary layer is unlikely to offer the greatest resistance to adsorption. Since the available sites for adsorption on GAC are mainly internal (microporosity), internal transport is likely to play a greater role and this is detailed in the relevant "Intraparticle diffusion" (section 6.6).

It was decided to use the 300 rpm mixing speed for the kinetic studies, as compared to 200 rpm, on the assumption that external transport is not limiting the adsorption process. It also enabled to focus on the intraparticle diffusion which is commonly agreed as a major resistance to HS adsorption (Fettig and Sontheimer, 1987a,b,c, Wu et al. 2002, Fettig, 2005). At this speed, the data beyond 399 minutes are not used due to the strong impact of adsorbent attrition. Although equilibrium is reached slowly for HS adsorption, kinetic models can be used before completion of equilibrium.

6.3 The pseudo-first order model

The pseudo-first order model considers that the adsorption rate (load in milligram of humic substances adsorbed per gram of adsorbent) varies proportionally with the number of sites remaining free at time t, before reaching the equilibrium, hence the term "first order". It is as comparing the adsorption sites consumption (site occupied by the adsorbate) with a first order chemical reaction. Such variation is expressed in equation 3.4 in chapter 3 and it is illustrated in figures 6.4, 6.5 and 6.6 respectively for GAC, AAFS and β-FeOOH. The graphs include experimental points up to 399 minutes as explained above.

A common feature on the three graphs is the division of each plot into three sections representing different stages of adsorption. A first section up to 10-15 minutes, then a second section between 15 and 165 minutes and finally a third section beyond 165 minutes can be distinguished. These are shown in figures 6.4, 6.5 and 6.6 by three different linear regressions fitting each of the three periods of time named (i), (ii) and (iii). In the first section (i), adsorbate molecules bind to the active sites on the surface and this is the first stage of adsorption. Then the second stage of adsorption (ii) corresponds to the filling of the monolayer (Ho and Mc Kay, 1999; Cheung et al., 2000). The last stage (iii) is the slow establishment of the equilibrium.

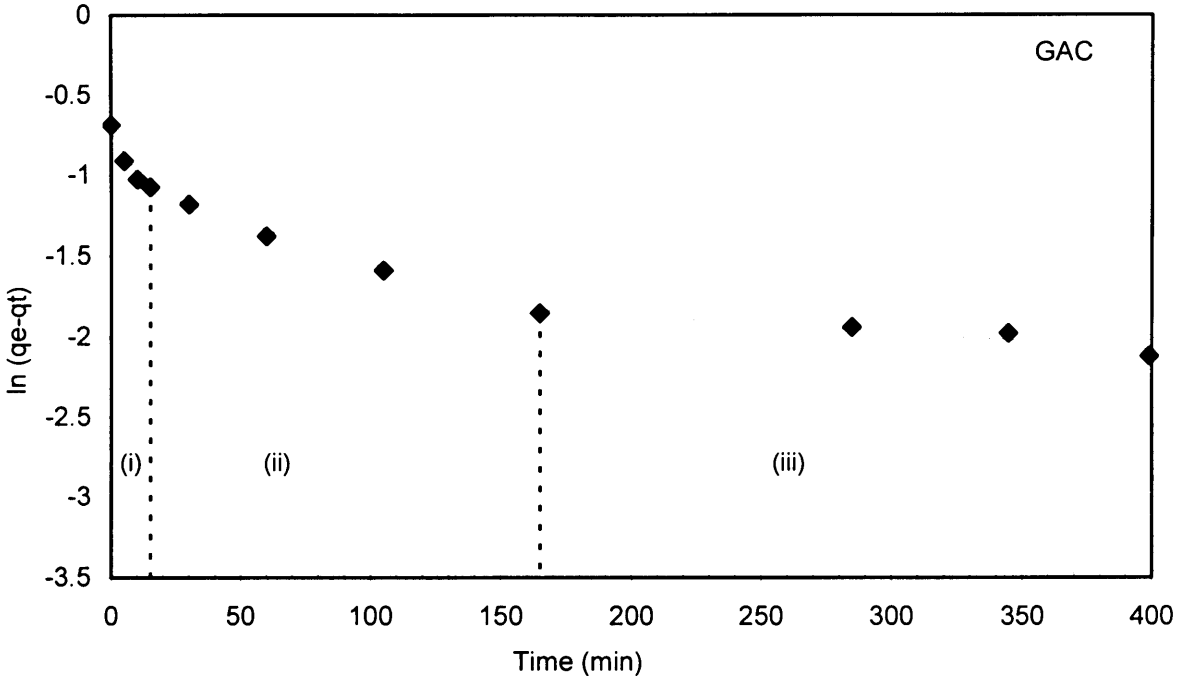

Figure 6.4 The pseudo-first order model for GAC

Experimental conditions: 250 ml of F123, SUVA = 9.5, 300 rpm, 2 g GAC, $(UV_{254})_0 = 0.582\ cm^{-1}$, $k_1 = 0.031\ min^{-1}$

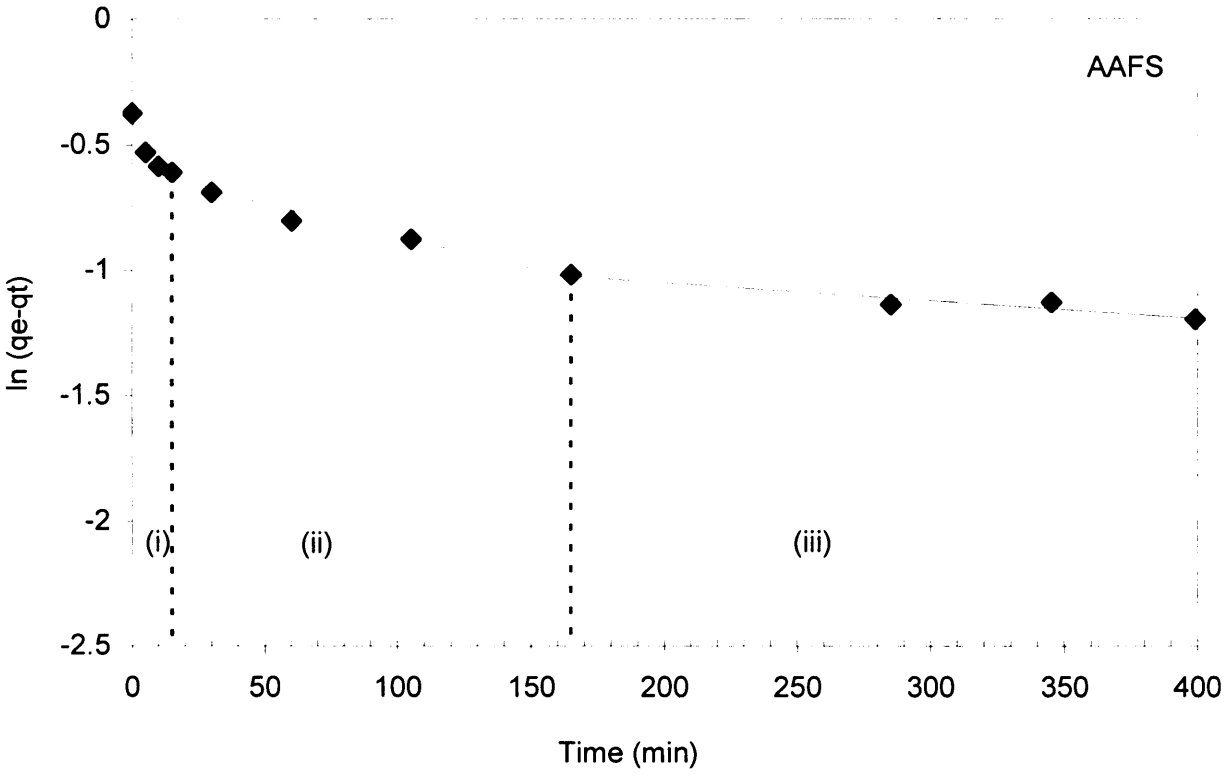

Figure 6.5 The pseudo-first order model for AAFS

Experimental conditions: 250 ml of F123, SUVA = 9.5, 300 rpm, 2 g AAFS, $(UV_{254})_0 = 0.582\ cm^{-1}$, $k_1 = 0.0017\ min^{-1}$

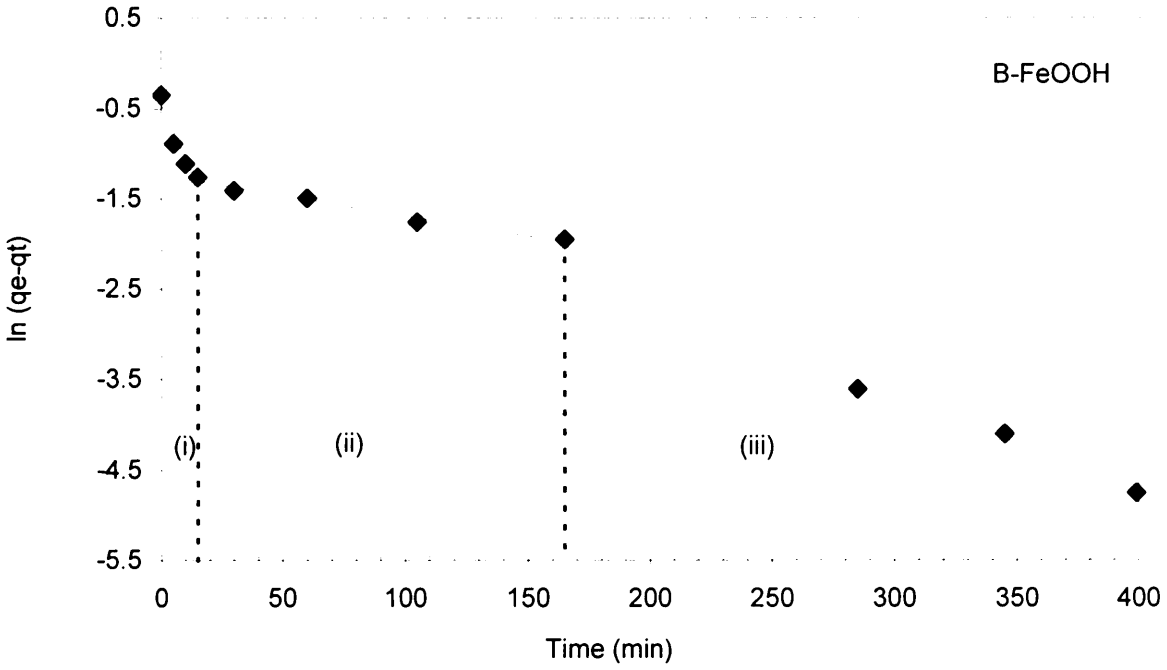

Figure 6.6 The pseudo-first order model for β-FeOOH

Experimental conditions: 250 ml of F123, SUVA = 9.5, 300 rpm, 2 g β-FeOOH, $(UV_{254})_0 = 0.582\ cm^{-1}$, $k_1 = 0.0095\ min^{-1}$

However, the pseudo-first order model includes all steps of adsorption and does not account for any mechanism. In that sense, the model should cover the three sections.

The first stage is completed quickly after about ten minutes. This also agrees with Wu et al. (2002) who identified the first stage to be less apparent for humic acid adsorption onto chitosan compared to dyes adsorption. According to those authors, the first stage of adsorption lasted less than 5 minutes. This indicates that instantaneous adsorption of HS onto these adsorbents is limited for two possible reasons: *(i)* the sites available for immediate adsorption are limited in number and *(ii)* the immediate adsorption becomes hidden by another mechanism. Reason *(i)* is coherent with the fact that the pseudo-first order model assumes the surface to be homogeneous, which means that all sites are equally active. In this case, the Elovich equation should fit better since it assumes a heterogeneous surface. The second reason *(ii)* is valid since after approaching the external surface, the adsorbate species should diffuse inside the pores to occupy the internal surface. This is why Wu et al. (2002) called the first stage the "external surface adsorption". For the intraparticle transport, more time is required to diffuse into the pores, hence limiting the adsorption rate.

From each graph representing the pseudo-first order model, the coefficient k_1 can be calculated using equation 3.6 given in chapter 3. This corresponds to the rate constant value over the whole range of adsorption. As explained above, the rate of adsorption varies according to the limiting stage (instantaneous, monolayer filling or slow filling towards equilibrium).

Table 6.1 gives the k_1 values together with the calculated equilibrium load $q_{e,calc}$. This load can be compared to the experimental equilibrium load (mg DOC/g adsorbent). From the k_1 values, it seems that overall rate of adsorption is the largest on β-FeOOH. The low value for GAC and AAFS reflects the fact that instantaneous adsorption is not as intense.

Table 6.1 Parameters for the pseudo-first order model

	k_1 min^{-1}	$q_{e,calc}$ (mg/g)	$q_{e,exp}$ (mg/g)	R^2
GAC	0.0031	0.356	0.504	0.8537
AAFS	0.0017	0.556	0.689	0.8583
β-FeOOH	0.0095	0.434	0.706	0.9675

It is observed in general that the pseudo-first order model is not valid for the whole range of data. Particularly experimental data for stage one of adsorption (external surface or instantaneous adsorption) do not correspond with the linear line. As a consequence, $q_{e,calc}$ (y-axis intercept) does not correspond to the experimental equilibrium load. For β-FeOOH, stage (iii) of adsorption appears with a much steeper slope. This fast increase in the load could correspond to the breakage of the grains allowing for more surface area and creating a second stage (i) adsorption. It could also mean that the pseudo-first order model is not suitable for the system HS - β-FeOOH and that the monolayer filling is not really happening. This model is likely to fit better if considering a multi-pseudo first order model corresponding to each stage, as suggested by Al-Ghouti (2004).

6.4 The pseudo-second order model

Similarly to the pseudo-first order model, the pseudo-second order kinetic model compares the adsorption process to a second-order chemical reaction. The rate of consumption of the adsorption sites is proportional to the square of the available number of sites left (see equation 3.7 in chapter three). Resolution of the equation has shown that the parameters of the model are obtained from the plot t/q_t vs t. These plots appear on figures 6.7, 6.8 and 6.9 respectively for adsorption onto GAC, AAFS and β-FeOOH.

The model covers well the data range up to 399 minutes for the three adsorbents, although the fitting is not so good for the first ten minutes when instantaneous adsorption occurs. This represents an improvement to the pseudo-first order model where the range of data was split into three stages. Results for the parameters calculated with this model are shown in table 6.2.

The initial adsorption rate h is the highest for β-FeOOH which indicates the intense instantaneous adsorption. This model appears more suitable than the pseudo-first order model to represent the adsorption of fraction F123 on the whole time range on these adsorbents. Particularly, the calculated equilibrium value for the load on β-FeOOH is very close to the experimental value. The regression coefficients are also high. However, the calculated and experimental loads do not agree well for AAFS, as the instantaneous adsorption is not well represented.

These results do not agree with Chang and Juang's results (2004). The authors also tested the pseudo-first and second order models to represent the adsorption of humic substances. They used a different adsorbent (chitosan) and found that the pseudo-first order model better fitted the experimental data. Overall, the equilibrium loads were much higher (from 20 to 245 mg/g) and the rate constant k_2 smaller (0.011 to 0.008 g/mg.min). However, direct comparison is difficult since no working pH is mentioned. The same observation was made by Wu et al. (2002), where a similar study was conducted at pH 6.4 which is likely to explain the enhanced adsorption when compared with this present study. Here, the pH is neutral and it has been shown that this is not the optimum value. For example, Teermann and Jekel (1999) compared the adsorption of humic substances onto β-FeOOH at four pH values (5, 6, 7 and 8). The load gradually increased from 20 to 50 mg DOC/g β-FeOOH as the pH decreased from 8 to 5. This is

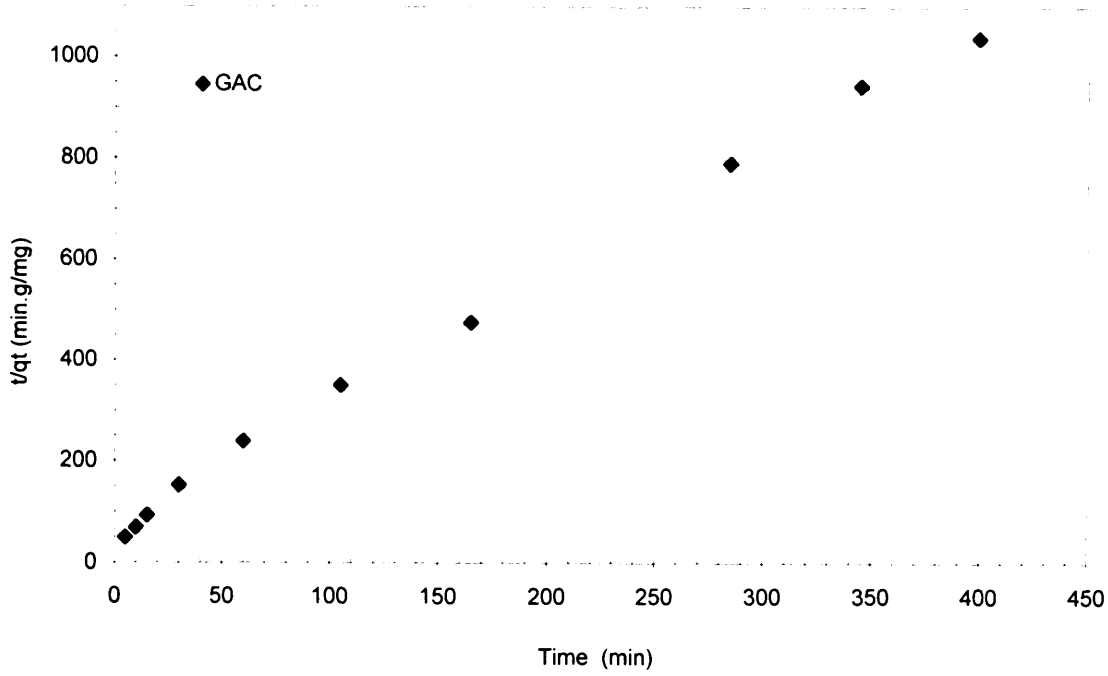

Figure 6.7 The pseudo-second order model for GAC

Experimental conditions: 250 ml of F123, SUVA = 9.5, 300 rpm, 2 g GAC, $(UV_{254})_0 = 0.582\ cm^{-1}$, h = 0.0157 mg/(g.min), k_2 = 0.0993 g/(mg.min)

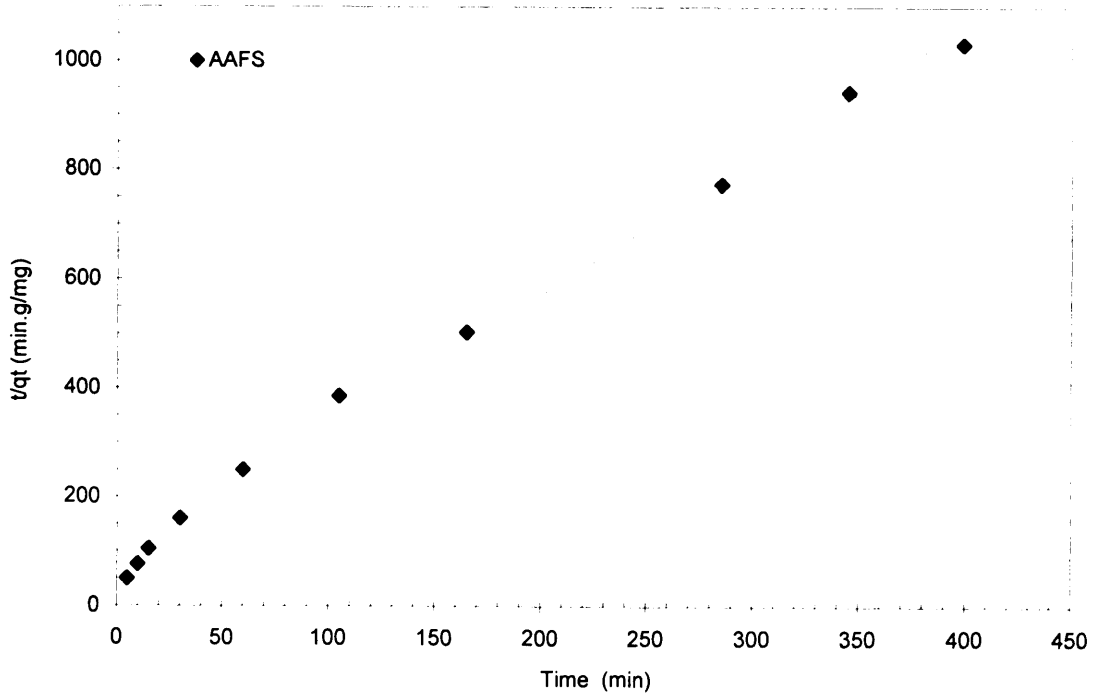

Figure 6.8 The pseudo-second order model for AAFS

Experimental conditions: 250 ml of F123, SUVA = 9.5, 300 rpm, 2 g AAFS, $(UV_{254})_0 = 0.582\ cm^{-1}$, h = 0.129 mg/(g.min), k_2 = 0.0785 g/(mg.min)

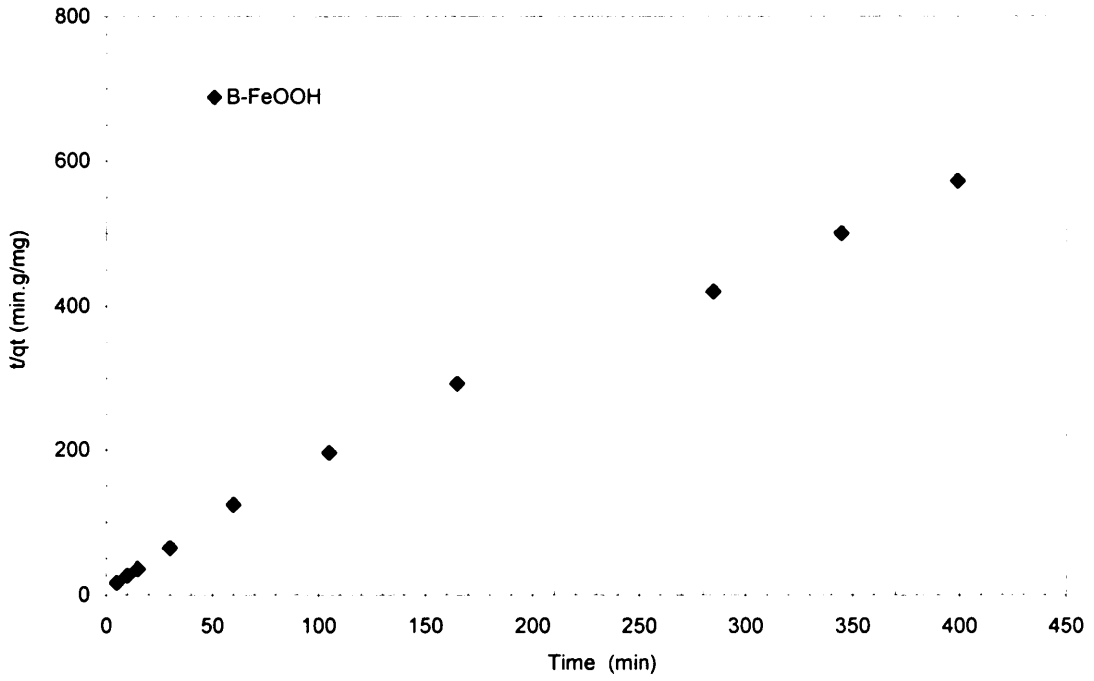

Figure 6.9 The pseudo-second order model for β-FeOOH

Experimental conditions: 250 ml of F123, SUVA = 9.5, 300 rpm, 2 g β-FeOOH, $(UV_{254})_0 = 0.582\ cm^{-1}$, h = 0.368 mg/(g.min), k_2 = 0.0715 g/(mg.min)

Table 6.2 Parameters for the pseudo-second order model

	h mg/(g.min)	**k_2** g/(mg.min)	**$q_{e,calc}$** mg/g	**$q_{e,exp}$** mg/g	**R^2**
GAC	0.0157	0.0993	0.398	0.504	0.9972
AAFS	0.0129	0.0785	0.405	0.689	0.9943
β-FeOOH	0.0368	0.0715	0.717	0.706	0.9928

explained by the charge neutralisation under addition of Fe(III) at a pH of 5.5-6 and that is particularly exploited for coagulation of organic matter (AWWA, 1990).

6.5 The Elovich equation

The model using the Elovich equation generally considers adsorption to be principally chemisorption occurring on a heterogeneous surface. This is the main difference with the two previous models that considered the surface to be homogeneous. The Elovich equation was initially developed for gas adsorption.

The application of the Elovich equation is shown in figures 6.10, 6.11 and 6.12 respectively for the adsorption of fraction F123 of HS onto GAC, AAFS and β-FeOOH. At first glance the model appears to fit well the experimental data for GAC and AAFS but appears not to be as applicable for β-FeOOH. Data taken into account for the model are the one beyond 5 minutes of adsorption and up to 399 minutes as before. The model is valid only for a time longer than the time rate constant t_0. Therefore, the initial points should not be taken into account. According to Cheung et al. (2000), a first trial and error method is applied to obtain the linear plot. Then a and b, in equation 3.12, can be calculated. In turn t_0 is calculated (equation 3.13) and checked against the first estimated value. In this work, the trial and error process was carried out by estimating t_0, then calculating a, b and t_0 and continuing the procedure until the best match was obtained between both t_0 values. The assumption of applying the Elovich equation at t larger than t_0 must be checked as suggested by Wu et al. (2002). Application of the model beyond 5 minutes time leads to values for t_0 equal to 1.86 minute for GAC, 2.88 minutes for AAFS and 0.19 minutes for β-FeOOH. These three values are well below 5 minutes, therefore the assumption is valid.

The Elovich equation applies for the whole range of data. According to Wu et al. (2002), this indicates that the adsorption mechanism, for the system under study, is that of chemisorption. Particularly for the iron coated alumina and the ferric oxihydroxide, the cation Fe(III) is expected to play a role in adsorption via a ligand exchange mechanism (Tipping, 2002). Consequently, a better correlation (R^2 is 0.9553) would be expected for this iron adsorbent in particular. However, the low correlation can be due to the attrition of the ferric oxihydroxide which might have occurred significantly before the 399 minutes as indicated by the early appearance of ferric oxide colour in the

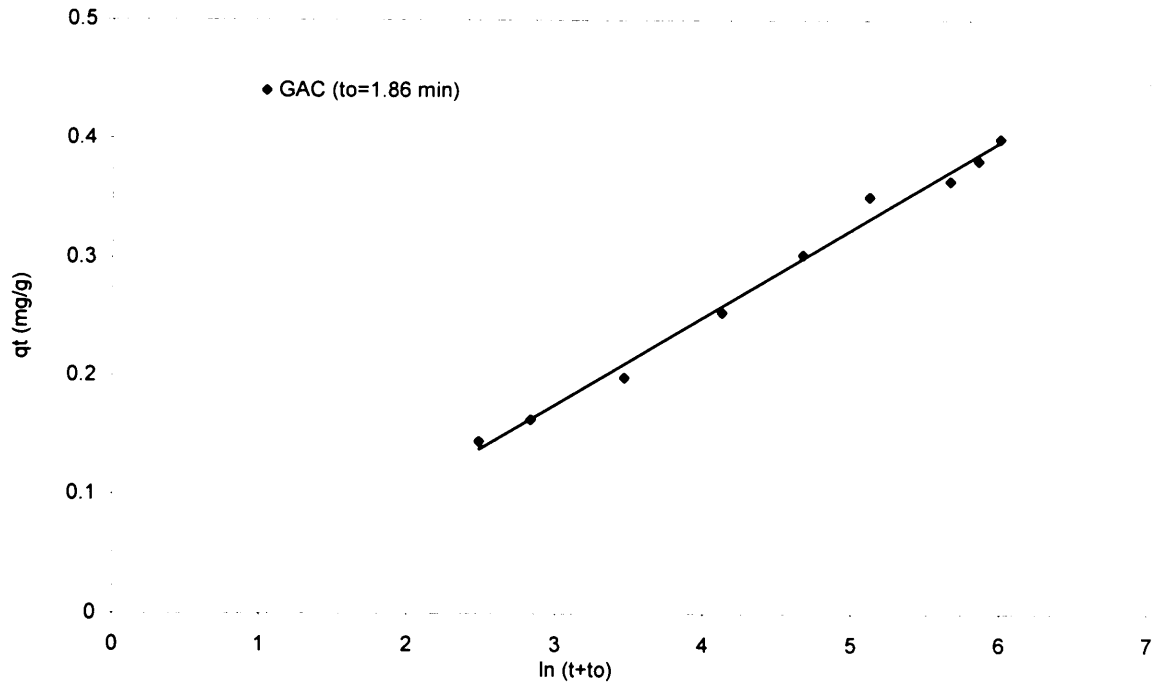

Figure 6.10 The Elovich equation for GAC

Experimental conditions: 250 ml of F123, SUVA = 9.5, 300 rpm, 2 g GAC, $(UV_{254})_0 = 0.582\ cm^{-1}$, b = 14.12 g/mg, a = 0.047 mg/(g.min)

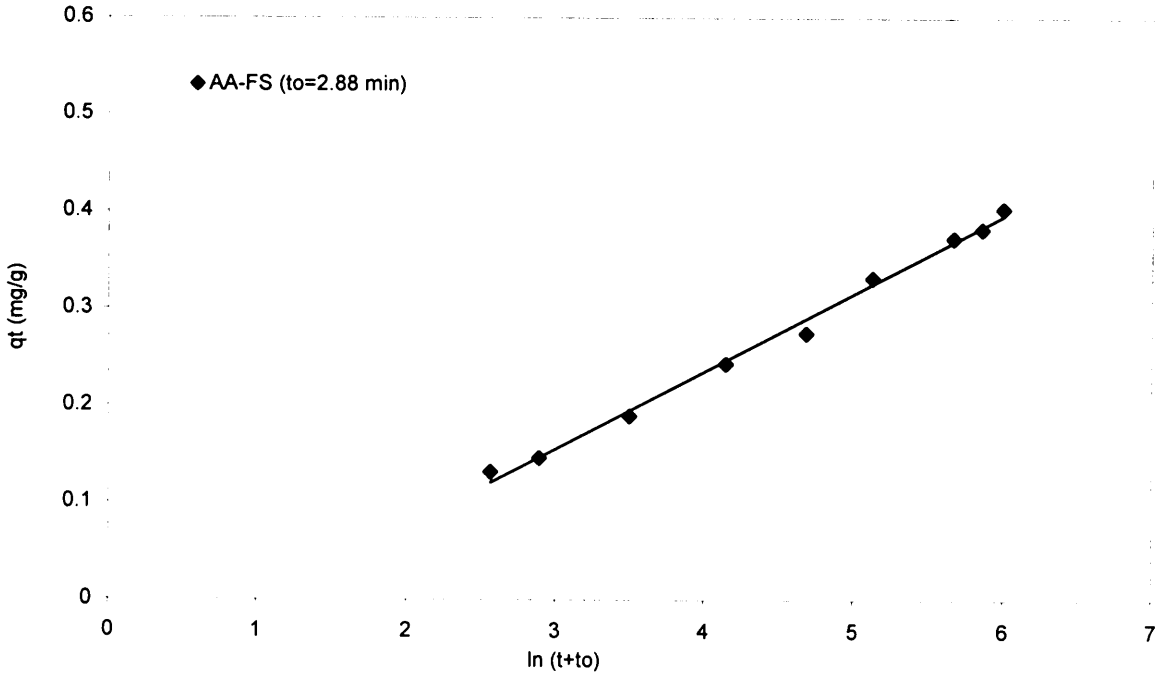

Figure 6.11 The Elovich equation for AAFS

Experimental conditions: 250 ml of F123, SUVA = 9.5, 300 rpm, 2 g AAFS, $(UV_{254})_0 = 0.582\ cm^{-1}$, b = 13.31 g/mg, a = 0.035 mg/(g.min)

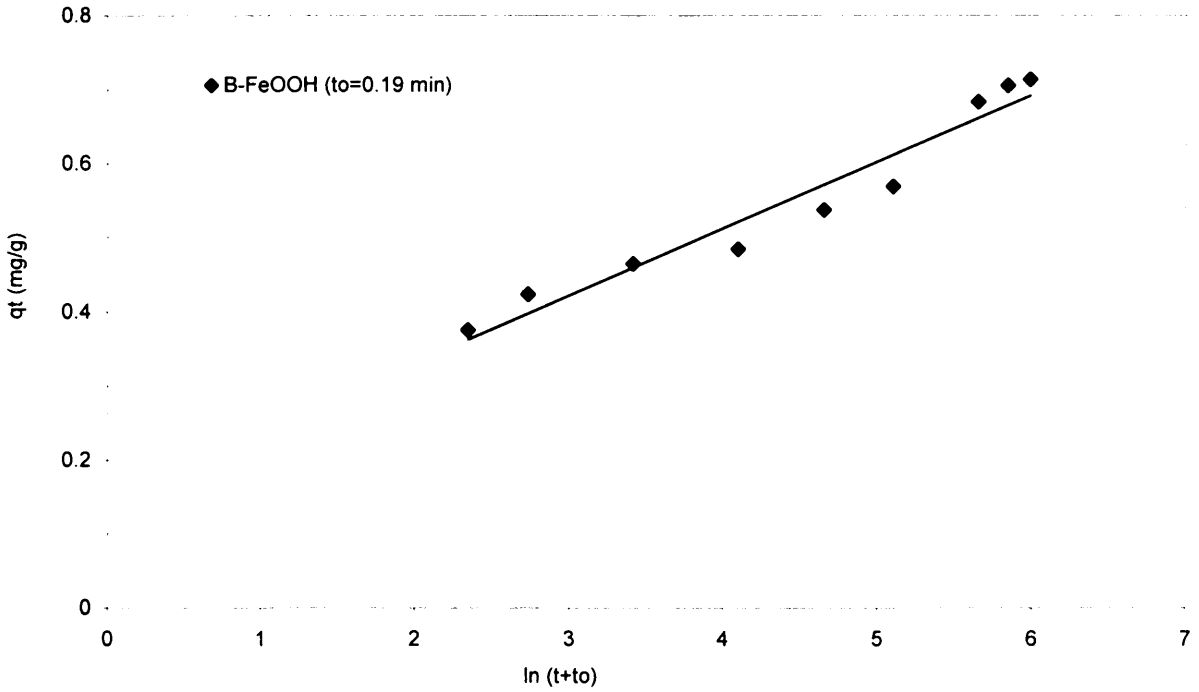

Figure 6.12 The Elovich equation for β-FeOOH

Experimental conditions: 250 ml of F123, SUVA = 9.5, 300 rpm, 2 g β-FeOOH, $(UV_{254})_0 = 0.582\ cm^{-1}$, b = 11.23 g/mg, a = 0.522 mg/(g.min)

Table 6.3 Parameters for the Elovich equation

	b g/mg	**a** mg/(g.min)	**t_0** min	**R^2**
GAC	13.51	0.039	1.86	0.9939
AAFS	12.48	0.028	2.87	0.9956
β-FeOOH	11.10	0.485	0.19	0.9553

solution. In this case, the last three points could be uncertain and may explain the poorer fitting on figure 6.12. On the other hand, ligand exchange might involve preferentially a certain molecular weight and this would alter the value of the sample absorbance and the DOC. In other terms, a selective adsorption can make fitting a unique model more difficult since each molecular weight is likely to adsorb at different rates.

It appears that more sites would be available on GAC than on β-FeOOH. This is not consistent with the equilibrium experimental q_e that clearly shows a higher adsorption on β-FeOOH after 399 minutes (0.504 mg/g on GAC vs 0.706 mg/g on β-FeOOH). It was shown in the previous chapter that GAC and β-FeOOH do not adsorb the same molecular weight range of HS. Therefore, it is unreliable to consider an absolute number of adsorption sites. In fact, since humic substances correspond to large molecules, it is possible that one molecule adsorbs onto several sites. In this case, the number of sites would be a number without any real application unless a number of sites per humic molecule or per mg of DOC would also be known.

The parameters for the Elovich equation are presented in table 6.3, as calculated from equations 3.12 and 3.13. a is the Elovich constant (mg/g.min) indicating the rate of adsorption. t_0 is the time constant. b is an indicator of the number of available sites for adsorption (Al-Ghouti, 2004).

The time constants in table 6.3 are rather low. Al-Ghouti (2004) obtained about the same range or less (less than a minute) but studied the adsorption of dye molecules, smaller than humics. However, Wu et al. (2002) investigated the adsorption of the same humic substances and obtained higher values (about ten minutes). The fact that time constants are low enhances the applicability of the Elovich equation, particularly for β-FeOOH.

More models should be tested to better describe the several aspects of the adsorption of humic substances. Agbenin and van Raig (1999) cited Aharoni and Sparks (1991), suggesting that the Elovich equation is actually one of several diffusion expressions with slow kinetic reactions. From such comment, it is interesting to test two diffusion models as is discussed in the following section.

6.6 The intraparticle diffusion model

The intraparticle diffusion model provides the initial rate of diffusion by plotting the load of humic substances (mg DOC/g adsorbent) as a function of the square root of the time (q_t vs $t^{1/2}$). This is depicted in figure 6.13 for the whole experimental data set, including the time when attrition was very significant ($t^{1/2} > 20$ $min^{1/2}$). As mentioned in section 3.5.3.4, three distinctive stages of adsorption were observed. These were attributed to the following stages (Lorenc-Grabowska and Glyglewicz, 2005, Wu et al., 2002); *(i)* adsorption occurs on the external surface only, in stage *(ii)* a gradual adsorption takes place, limited by intraparticle diffusion and in stage *(iii)* the final equilibrium is reached. According to Fick's laws, the diffusion is driven by the concentration gradient between the liquid and solid phases. As the gradient decreases, so does the diffusion rate, hence the slow attainment of equilibrium.

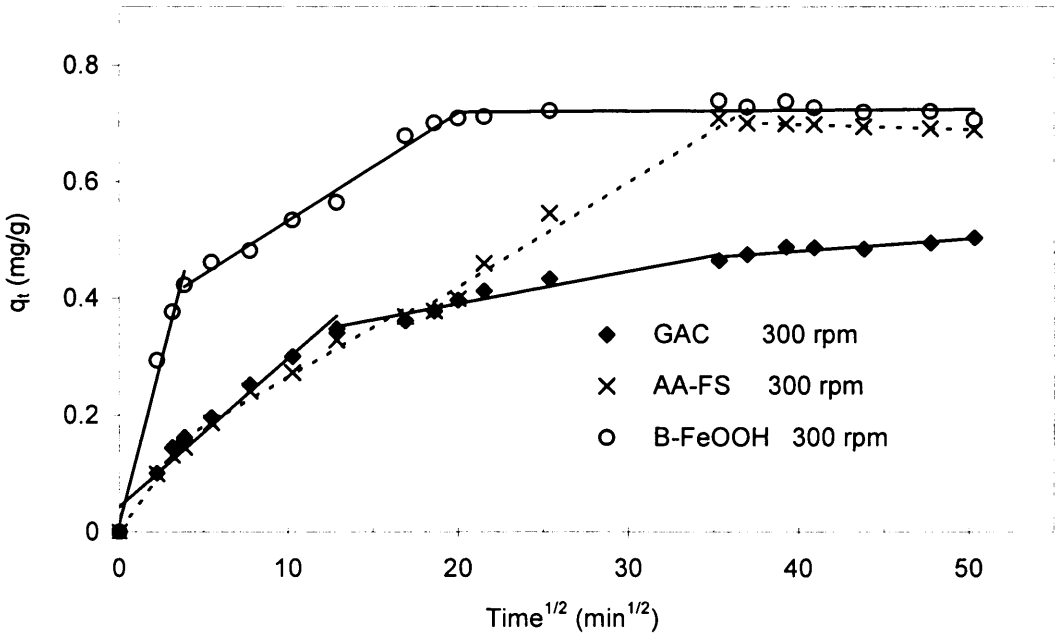

Figure 6.13 The intraparticle diffusion model for adsorption of HS (F123) onto GAC, AAFS, β-FeOOH. Experimental conditions: 250 ml of F123, SUVA = 9.5, 300 rpm, 2 g adsorbent, $(UV_{254})_0 = 0.582$ cm^{-1}

From figure 6.13, stage one occurs quickly compared to the two other stages, which is in agreement with the work carried out by Wu et al. (2002). These authors also found the first stage to take under 5 minutes when using similar humic substances. This is true for the three adsorbents used in this study, although instantaneous adsorption on the external surface of β-FeOOH is noticeably more important than on GAC or AAFS. Instantaneous adsorption is detected from the slope at the origin (in figure 6.13). The larger the slope, the more active the external adsorption sites. In this case, the data reflect particularly the adsorption of the heavy molecular weights and not the light ones since the SUVA was measured to decrease during the first stage of adsorption. Numerical values for SUVA are presented in the chapter relating to the adsorption in the columns (figures 8.4, 8.5, 8.6, 8.9, 8.12, 8.13 and 8.14).

Figures 6.14, 6.15 and 6.16 represent the intraparticle diffusion model data for GAC, AAFS and β-FeOOH respectively. Calculation of the model parameters is carried out over the range of data covered in stage two of adsorption. It corresponds to the range where attrition is not obviously significant (i.e before 399 minutes). However, the whole set of data is shown for two reasons; firstly it confirms that the model does not apply for the data beyond 399 minutes (20 $min^{1/2}$) and secondly, it enables the comparison of two mixing speed. At 200 rpm, the external transport can be the limiting factor in the adsorption process.

It is clear that the intraparticle diffusion model fitted from stage two of adsorption and does not apply to the initial and final stages of adsorption. When the adsorption process starts, only transport and attachment should be considered, but not the rearrangement of the adsorbed molecules (due to re-conformation) and not the slow adsorption (Avena and Koopal, 1999). This also explains well the fact that the model cannot be applied towards the equilibrium stage since competition and displacement (i.e. rearrangement of the adsorbed molecules and slow adsorption of others) are known to take place when the adsorbate is made of a wide range of molecular weights (Gu et al., 1996a,b).

Wu et al. (2002) found that this same model applied to the full range of data, however the first stage was not taken into account. In addition their study did not investigate adsorption beyond 300 minutes, which is equivalent to stage two of adsorption for this study (17.3 $min^{1/2}$). Zhang and Bai (2003) applied this model from the time zero to 100 minutes (10 $min^{1/2}$) and without considering the initial stage of adsorption. The quantities of humic substances adsorbed on chitosan coated granules were lower than

values estimated in this study by nearly ten fold, although the pH was more favourable (6.5). For these two examples, the intraparticle diffusion model was applied and therefore proves its applicability for the adsorption of humic substances on different kinds of adsorbents. This is expected since the adsorbents are made of micropores as well as meso and macropores. In particular for GAC, 93% of the porosity is within micropores. The data obtained here show very similar trends to the data presented by Zhang and Bai (2003). However, stage one of adsorption, as described above, should not be neglected since adsorption also takes place on the external surface, particularly on β-FeOOH.

In equation 3.25 (literature review in chapter three), x_i is proportional to the diffusion film thickness or boundary layer and x_i units are also in mg/g. Table 6.4 shows that x_i values (from 0.099 to 0.347 mg/g) are significant compared to q_t values (maxima range between 0.504 and 0.506 mg/g) at 300 rpm, which means that intraparticle diffusion is controlling the overall adsorption when a significant amount of HS has already adsorbed onto the external surface. The value of k_p is the lowest for adsorption on GAC, followed by AAFS and k_p is the largest for β-FeOOH. This suggests that the intraparticle diffusion is occuring faster on the iron compounds than on GAC. This can be justified by the lesser travel necessary to reach the internal surface when the adsorbent is less microporous, as compared to a very microporous medium such as GAC. This was also mentioned by Ding et al. (2006) when modelling the natural organic matter (NOM) effect on adsorption of atrazine on GAC, particularly where it involved site competition and pore blockage.

The first stage of the adsorption process represents the instantaneous adsorption which could be hindered only by a vigorous mixing, itself bringing about the attrition of the media. The difficulty in reproducing the instantaneous adsorption by the intraparticle diffusion model will appear more clearly when comparing the model fitting to experimental data.

Figures 6.14 to 6.16 also show the intraparticle diffusion model applied to data representing the adsorption experiment under a slower agitation speed. Since the agitation speed affects only the external boundary layer, the intraparticle diffusion coefficient should not vary when the mixing speed is altered. From the slopes in figures 6.14 to 6.16, the effect of agitation speed is small for GAC (slope almost similar in the last stage). It can be concluded that the intraparticle diffusion is a dominant mechanism

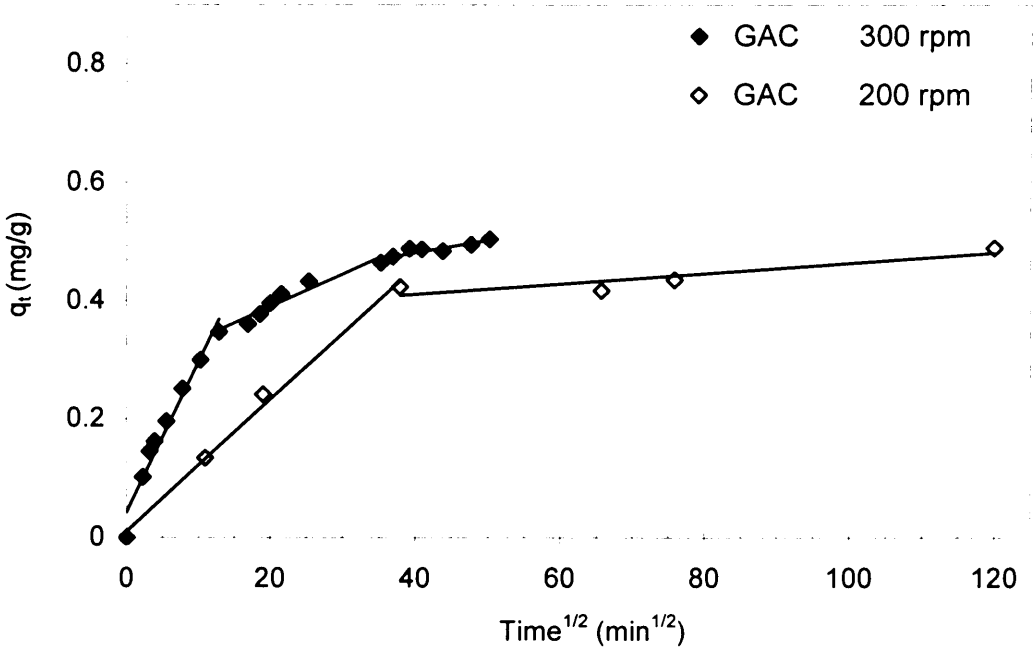

Figure 6.14 The intraparticle diffusion model for GAC;
Experimental conditions: 250 ml of F123, SUVA = 9.5, 300 rpm, 2 g GAC, $(UV_{254})_0 = 0.582\ cm^{-1}$

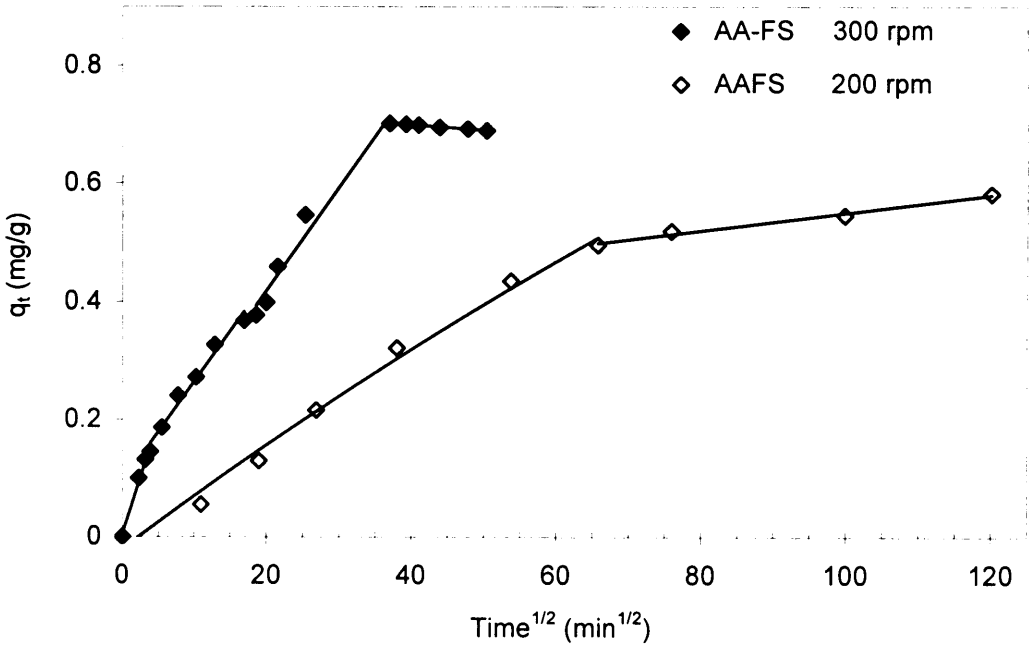

Figure 6.15 The intraparticle diffusion model for AAFS;
Experimental conditions: 250 ml of F123, SUVA = 9.5, 300 rpm, 2 g AAFS, $(UV_{254})_0 = 0.582\ cm^{-1}$

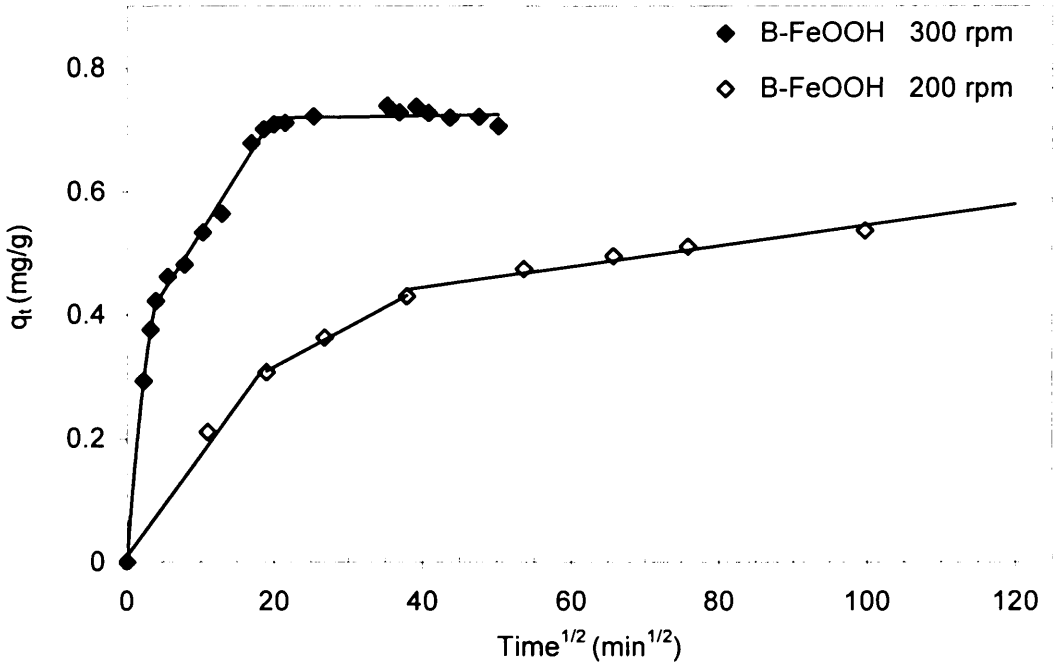

Figure 6.16 The intraparticle diffusion model for β-FeOOH;
Experimental conditions: 250 ml of F123, SUVA = 9.5, 300 rpm, 2 g β-FeOOH, $(UV_{254})_0 = 0.582\ cm^{-1}$

Table 6.4 Parameters for the intraparticle diffusion model (300 rpm)

	k_p mg/(g.min$^{1/2}$)	x_i mg/g	R^2
GAC	0.0139	0.1332	0.9441
AAFS	0.0157	0.0995	0.9797
β-FeOOH	0.0186	0.3475	0.9814

over external diffusion and mass transfer. This agrees with the microporosity of GAC. The situation is different for the iron compounds since they do not have any microporosity as read from table 6.2 (actually very close to zero) but principally meso- and macroporosity. This explains why the two lines are not parallel on figure 6.15 and 6.16 as it was for GAC in figure 6.14. For meso- and macroporosities, the boundary layer surrounds most of the available area for adsorption. Therefore, eddies resulting from the agitation affect the concentration gradient close to the surface and have a large influence on the quantities adsorbed. It is concluded that for the iron-compounds, the intraparticle diffusion is not the main resistance to mass transfer. A second mechanism is likely to be dominant. Intraparticle diffusion can also be slowed down or even inhibited due to large molecules being instantaneously adsorbed and blocking access to the micropores for the adsorption of smaller molecules. This is true for large HS (gyration radius up to 5 nm from the chapter "Characterisation of HS") and micropores (diameter smaller than 5 nm). In that case, a different diffusion model would apply better.

The intraparticle diffusion coefficient can be calculated from the fractional approach (also used by Streat et al. 1995, Al-Ghouti et al., 2005). The equation (3.16) is derived from Fick's law and the corresponding plot is shown in figure 6.17. The slope of the lines is equal to ($\pi^2 D/r^2$) where r is the radius of the adsorbent grains. The intraparticle diffusion accounts for both internal surface and pore diffusion, which is called the effective diffusivity by Streat et al. (1995). Although it is likely that either surface or pore diffusion will dominate over the other, it is difficult to separate one from the other by fitting experimental data because the models produce fits of similar quality (Badruzzaman et al., 2004). This is partly due to the inability to measure the actual mean diffusion path length (Ding et al., 2006).

The calculated diffusion coefficient D represents the average of non-adsorbed HS since measurements are based on the concentration left in solution. This is not a concern if the adsorbate is monocomponent (i.e. only one model of molecule). However, in this case this factor is very important since the molecular weights of the humic substances have a broad range (0-50 kDa) and the adsorbate is multicomponent. Avena and Koopal (1999) describe this coefficient as an "apparent diffusion coefficient", likely to be lower than the true D value of the adsorbing fraction. These observations agree with the K_f values obtained from the isotherms (see chapter 7) that clearly show that GAC adsorbs lower

molecular weights and iron compounds adsorb heavier molecular weights. Therefore, higher MW remain in solution when using the GAC compared to a smaller proportion when using AAFS or β-FeOOH. Consequently, the diffusion coefficient value corresponds to bigger molecules in the case of GAC and is likely to be underestimated (adsorbed particles are smaller with a higher diffusion coefficient D).

Further investigation would be necessary to confirm such hypothesis, particularly studying narrower MW fractions of humic substances. Intraparticle diffusion coefficient values for fraction F123, as calculated from the slopes on figure 6.17, are also given below:

On GAC $D = 9 \times 10^{-11}$ m^2s^{-1}

On AAFS $D = 4.91 \times 10^{-12}$ m^2s^{-1}

On β-FeOOH $D = 8.34 \times 10^{-11}$ m^2s^{-1}

D values for GAC and β-FeOOH are very close but the value is much lower for AAFS. The difference is possibly due to the molecular weights selectively adsorbed onto the adsorbent. This result is also coherent with figure 6.13 where it clearly appears that adsorption onto AAFS and β-FeOOH takes place to a similar extent but much more slowly on AAFS and without any instantaneous adsorption. The first stage of adsorption actually influences D value in figure 6.17 and in particular, it affects the slope, hence there is a higher D value for diffusion in β-FeOOH.

Weber et al. (1991) specified that the diffusion coefficient in the liquid phase is affected by factors such as the size, configuration and chemical structure of the molecule as well as by the solvent viscosity and molecular structure. According to the same authors, the diffusion coefficient is also affected by resistances encountered at the interface of the liquid phase-adsorbent surface, such as accumulated molecules and drag forces. Attrition of the adsorbent inevitably causes hydrodynamic disturbances around the adsorbents thereby affecting the value of D. The attrition phenomenon is suggested to explain the peculiar shape of the curve for AAFS in figure 6.13. The curve follows the one for GAC for the first and most of the second stage of adsorption. Then at approximately 20 $min^{1/2}$, adsorption on AAFS increases again well above the curve for GAC.

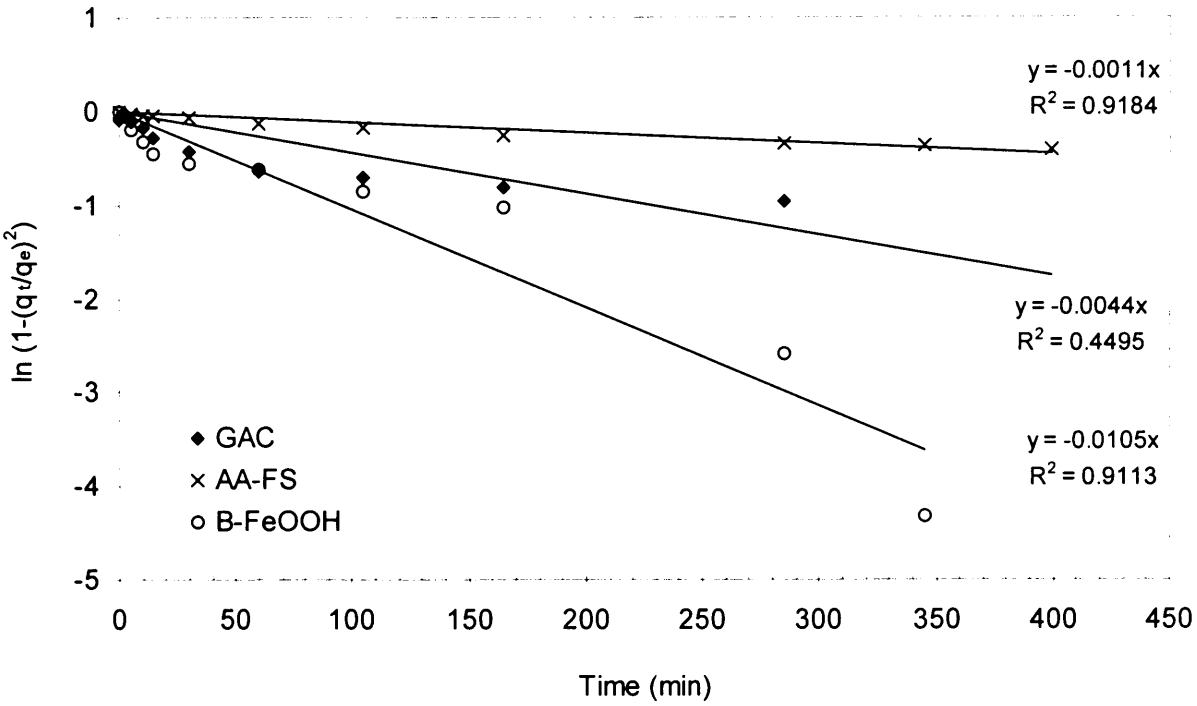

Figure 6.17 Intraparticle diffusion coefficients calculation. Values used are; for GAC, r = 0.45 mm and D = 9 x 10^{-11} m^2s^{-1} ; for AAFS, r = 0.21 mm and D = 4.91 x 10^{-12} m^2s^{-1}, for β-FeOOH, r = 0.28 mm and D = 8.34 x 10^{-11} m^2s^{-1}

It is suggested that attrition releases the iron coating on AAFS (from Scanning Electronic Microscopy photographs shown in appendix). Therefore, adsorption process can start again with a stage one on the bare alumina. This also corresponds to the plot for AAFS on figure 6.15. The initial slope is stage one of adsorption (between 0 and 10 $min^{1/2}$) and a second steep slope, parallel to the first one is observed between 20 and 36 $min^{1/2}$.

However, the good agreement for D on GAC and β-FeOOH allows D to be considered between 8.34 and 9x10^{-11} m^2s^{-1}. This is still more reliable when considering that GAC and β-FeOOH had the opposite affinity towards HS adsorption as regards the MW. Therefore the cited figures can be considered as a reliable range of the intraparticle diffusion coefficient for these humic substances.

This also agrees fairly well with values calculated by Avena and Koopal (1999) for the same HS. The coefficient was equal to 6x10^{-11} m^2s^{-1} and 9x10^{-11} m^2s^{-1} for an electrolyte concentration of 0.003 M and 0.03 M respectively (using KNO_3). In this work, the electrolyte used, $Ca(NO_3)_2$, was found to influence the calcium complexation with the

humic substances. However, the nitrate concentration was 0.001 M, still below Avena and Koopal's value. A higher concentration of electrolyte usually increases the diffusion coefficient due to molecular shrinkage. A different working pH influences the diffusion coefficient value since at low pH, the humic molecules tend to coil and diffuse quicker and Avena and Koopal (1999) worked at a pH of 3.9. Conversely, a higher pH causes the humic molecules to uncoil, stretching their structure. The consequence would be a slown down diffusion as suggested by Zhang and Bai (2003). Other factors may be responsible for the high diffusion coefficient which in this case may be the presence of the calcium ion in the solution. Calcium can form complexes with humic substances. These complexes together with electrostatic type attraction, cause the organic molecules to coil. In turn, such coiling tends to exclude the water which reduces the size of the adsorbate. As a consequence, the adsorbate diffuses quicker towards the adsorbent.

As a conclusion, the intraparticle diffusion model applies well to the systems studied here, but not over the whole range of data. The calculated diffusion coefficient is between 8.34 and $9x10^{-11}$ m^2s^{-1} representing molecular weights up to 50 kDa.

6.7 The external diffusion model

The external diffusion model is based on the assumption that the adsorbent surface is bare. Hence at time zero, $\ln(C_t/C_0)$ equals zero too. The concentration of humic substances C is represented by the DOC. The equation corresponding to this model is plotted on figure 6.18. The y-axis value is represented by $\ln(UV/UV_0)$ instead of $\ln(C_t/C_0)$ since the ratio (UV/DOC), i.e. SUVA value, is assumed to remain constant. Points up to ten minutes are taken into account to calculate the slope and the external mass transfer coefficient. This corresponds to the instantaneous adsorption that was observed to take place strongly on β-FeOOH.

Calculated external mass transfer coefficients are shown in table 6.5, together with the parameters needed for their calculation (using equation 3.19 and 3.20 in chapter 3). It is clear that the external mass transfer coefficient is the largest for β-FeOOH, which is perhaps overestimated. However, the values for GAC and AAFS are very comparable to Fettig and Sontheimer's value (1987c) of 0.81×10^{-5} ms^{-1}. This is a slightly lower value compared to this study and it might be due to the different technique used for the coefficient estimation. They used a minicolumn assuming that over a short bed depth,

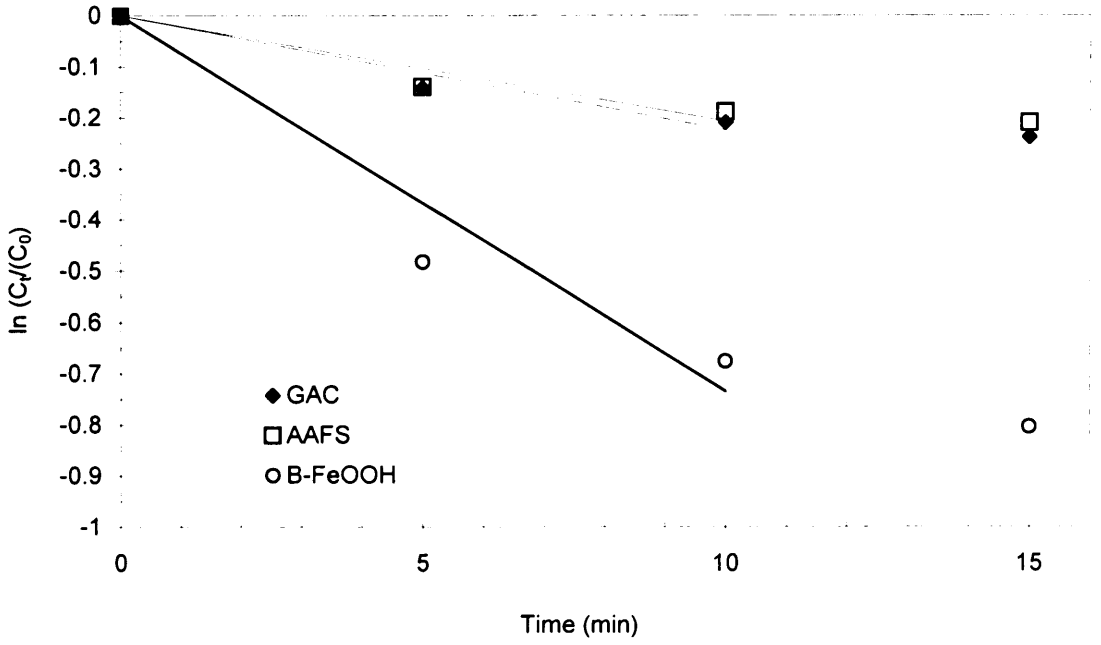

Figure 6.18 External mass transfer coefficient calculation.

Values used; for GAC, $k_f = 1.25 \times 10^{-5}$ ms^{-1}, for AAFS, $k_f = 1.05 \times 10^{-5}$ ms^{-1} and for β-FeOOH, $k_f = 7.54 \times 10^{-5}$ ms^{-1}

Table 6.5 External mass transfer coefficient calculation (k_f) (slope from figure 6.18)

	Slope (min^{-1})	**A/V=6m/(ρd_m)** (m^2/m^3)	**k_f** (ms^{-1})	**R^2**
GAC	-0.0224	29.97	1.25×10^{-5}	0.95
AAFS	-0.0207	32.8857	1.05×10^{-5}	0.91
β-FeOOH	-0.0734	16.2337	7.54×10^{-5}	0.93

the external mass transfer is the main resistance since no internal diffusion or attachment has yet occurred. In this work, the agitation of the media is likely to increase the external mass transfer from the very start of the process, hence increasing k_f. The calculation was performed the same way, but Fettig and Sontheimer (1987a, b and c) also added a correction factor for the external surface area and took into account the non-adsorbable fraction $C_{non\ ads}$ in the term $\ln(C_t/C_0)$ which became $\ln[(C_t-C_{non\ ads} / (C_0-C_{non\ ads})]$, leading to an overall decrease of k_f. Although the mass transfer depends on the hydrodynamic conditions, the fluid velocity and the porosity, it is not expected to vary with the molecular weight of the adsorbate. This also explained why these two authors observed little difference in k_f for components of different adsorbabilities (different MW of HS). From this comment, it is reasonable to think that k_f values are a good representative of the whole range of MW covered in this study.

GAC and AAFS behave similarly as regards the external mass transfer. k_f values for β-FeOOH might be overestimated due to the modified hydrodynamic environment around the particles. A strong shear causes significant attrition of this compound, thereby producing more smaller grains and more microscopic eddies. It can be assumed that the high external mass transfer is mainly due to the increase of microturbulence. This is a field of study that would deserve more attention since it is not mentioned in the literature relating the adsorption of organic matter onto friable adsorbents.

The following figures 6.19, 6.20 and 6.21, show the influence of the mixing speed on the external diffusion model, respectively for adsorption on GAC, AAFS and β-FeOOH.

Oppositely to the internal diffusion model, the mixing speed is expected to influence greatly the external diffusion. However, if it has no influence, it indicates that the external diffusion transport does not play a great role in the adsorption. As seen in figure 6.19, a speed of 200 rpm results in a lower adsorption rate during the first minutes of the process only and the results quickly tends to similar values with 200 or 300 rpm. This confirms that external resistance is not the main resistance on GAC and this was expected from the very large microporosity. On figures 6.20 and 6.21, experimental points for 200 rpm are well above the curve for 300 rpm. This indicates a slower external diffusion at lower mixing speed. For the iron compounds, the external diffusion represent a large resistance, which agrees with their mesoporosity.

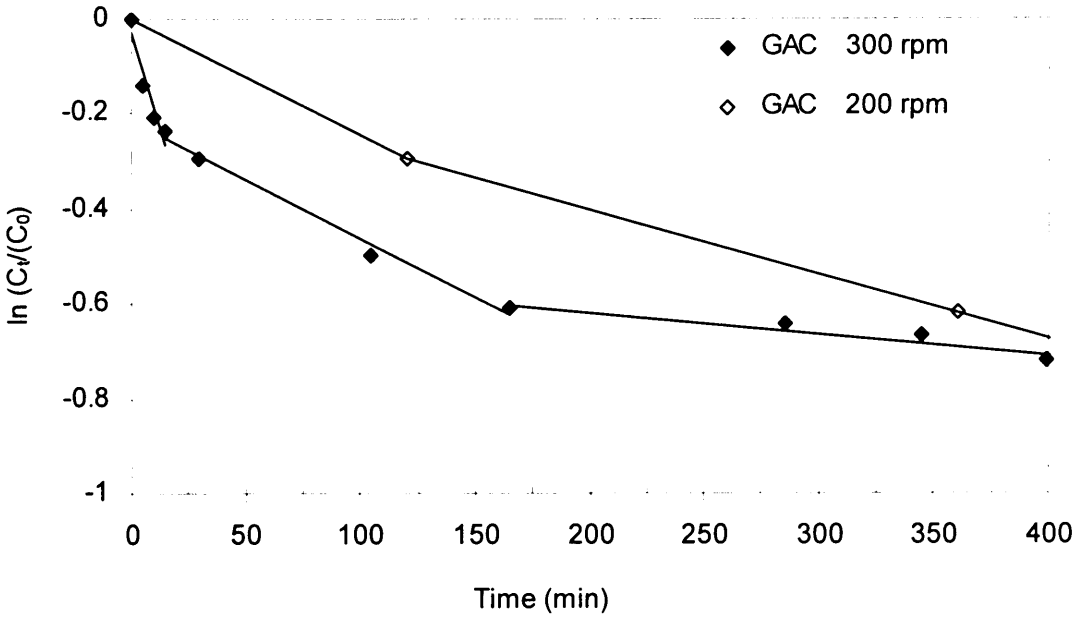

Figure 6.19 The external diffusion model for GAC, at two mixing speeds

Experimental conditions: 250 ml of F123, SUVA=9.5. At 200 rpm; 2.3 g GAC and $(UV_{254})_0$=0.457 cm^{-1}, at 300 rpm; 2 g GAC and $(UV_{254})_0$=0.582 cm^{-1}

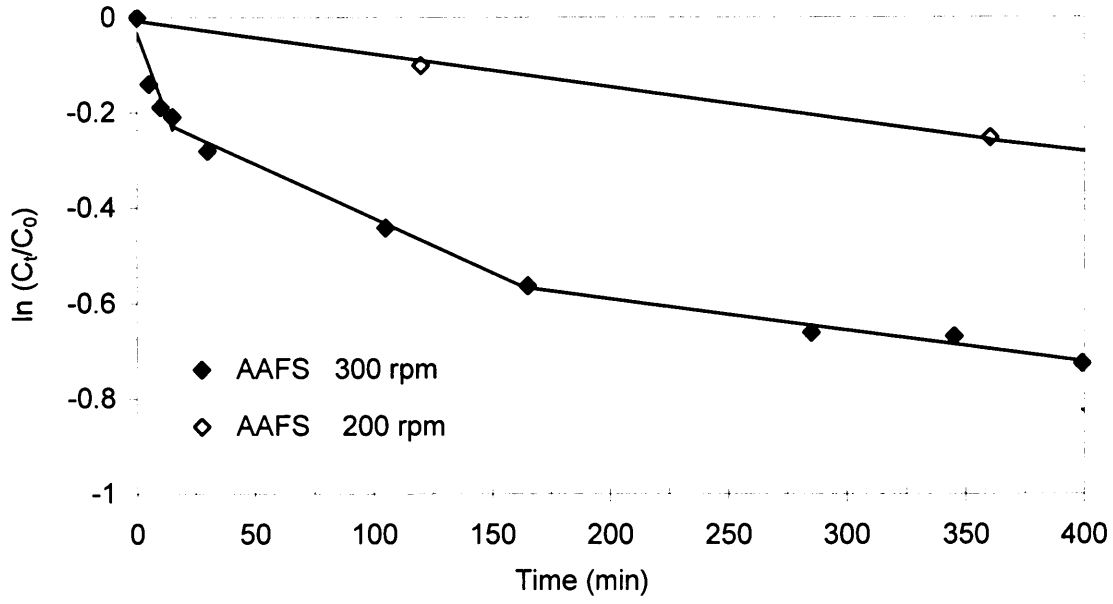

Figure 6.20 The external diffusion model for AAFS, at two mixing speeds

Experimental conditions: 250 ml of F123, SUVA=9.5. At 200 rpm; 2.3 g AAFS and $(UV_{254})_0$=0.508 cm^{-1}, at 300 rpm; 2 g AAFS and $(UV_{254})_0$=0.582 cm^{-1}

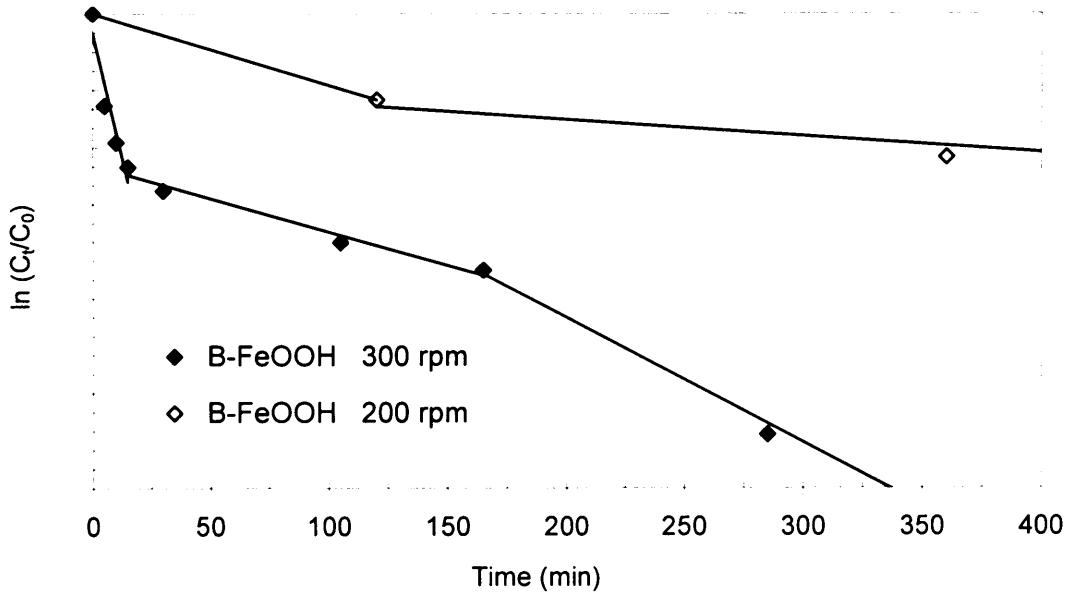

Figure 6.21 The external diffusion model for β-FeOOH, at two mixing speeds

Experimental conditions: 250 ml of F123, SUVA=9.5. At 200 rpm; 2.3 g β-FeOOH and $(UV_{254})_0$=0.508 cm^{-1}, at 300 rpm; 2 g β-FeOOH and $(UV_{254})_0$=0.582 cm^{-1}

6.8 Comparisons between modelled and experimental data

For each kinetics model for a specific adsorbents/adsorbate system, calculations of the parameters were carried out in the above sections. The following step is to compare the tested models with the experimental data. As explained earlier, the time period beyond 399 minutes brings uncertainties with regards to the interpretation of the data, due to attrition of the media. For complete application of the models, two graphs, displaying the load vs time are shown for each adsorbent (figures 6.22 to 6.27). The first graph shows the model applied over the whole range up to 2600 minutes (43 hours) and the second graph applies up to 399 minutes only. The first graph shows the deviation of the model over a long time period (e.g. the external diffusion model indicates a final load of 0.77 $mg.g^{-1}$ when maximum experimental load is 0.57-0.6 $mg.g^{-1}$). The second graph is important in examining the fitting of the model in the very early stage of adsorption, particularly when instantaneous adsorption occurs (stage one).

For each graph, the function F corresponding to the error is calculated as stated in equation (6.1), as expressed by McKay (2001). It actually corresponds to an extension

of the Sum of Squared Errors often used to estimate the error (Cheung et al. 2001, Chen et al. 2001) and corresponds to the square of the standard deviation as expressed by Chang and Juang (2004).

$$F = \frac{1}{m}\sum_{j=1}^{m}\left(\frac{q_{\exp} - q_{calc}}{q_{\exp}}\right)^2 \qquad (6.1)$$

where m is the number of data, q_{exp} is the experimental load, q_{cal} is the load calculated by the model and using the parameters calculated from tables 6.1, 6.2, 6.3, 6.4 and 6.5 respectively for the pseudo-first order, pseudo-second order, Elovich equation, intraparticle diffusion and external diffusion models. The F value provides a numerical value to interpret the goodness of fit of a given mathematical model to the experimental data (Cheung et al., 2001). Consequently, the smaller the F value, the better the model.

The fitting of models to experimental data for adsorption on GAC are shown on figures 6.22 and 6.23. The Elovich equation fitted the experimental data best and was applied to the whole range of data. The external diffusion model overpredicts the adsorption, probably due to the fact that by assuming external diffusion to limit the process rate, the slowness of internal diffusion is omitted. The pseudo-first order model under-predicts the adsorption over the whole range. The pseudo-second order model predicts well the adsorption only until 399 minutes, i.e. before attrition has become significant.

It is interesting to see that the intraparticle diffusion model does not give the best prediction. This was unexpected for GAC since the presence of a highly developed microporous structure is thought to affect the internal diffusion, hence limit the adsorption. The value of F (error) for the intraparticle model over the whole range of data is 0.0886, vs 0.0027 for the Elovich equation (30 times less) and 0.0264 for the pseudo-second order model. Cheung et al. (2001) reported error values between 10^{-4} and 10^{-2} for kinetic models when studying the sorption of cadmium ions onto bone char, which is a much lower range of errors than those identified in this study. On the other hand, to compare this F value with the standard deviation SD (SD is one hundred times the square root of F), SD is 29%, 5% and 16% respectively for the intraparticle, the Elovich equation and pseudo-second order model. It is concluded that the errors in this study are very large. Chang and Juang (2004) obtained SD between 2.7% and 6.6% for

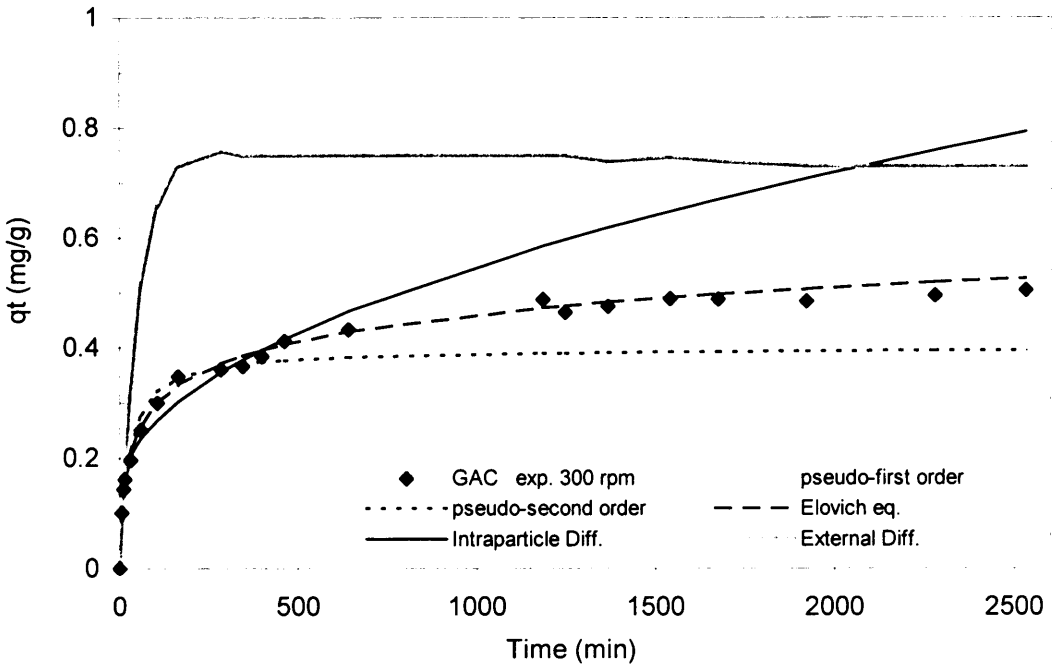

Figure 6.22 Adsorption onto GAC over the whole range of data

Experimental conditions: 250 ml solution F123, SUVA = 9.5, 300 rpm, 2 g GAC, $(UV_{254})_0 = 0.582\ cm^{-1}$.

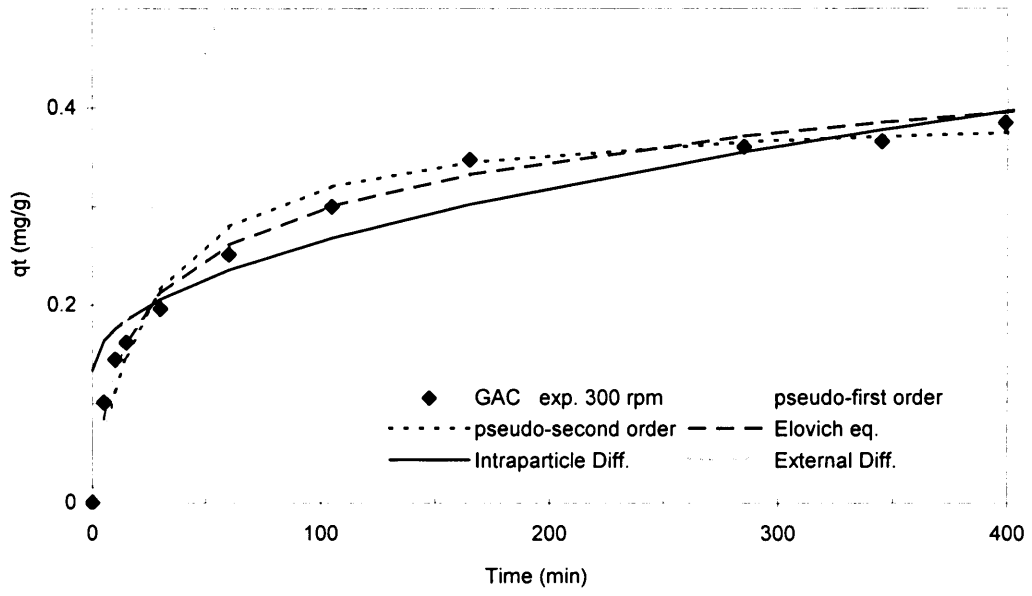

Figure 6.23 Adsorption onto GAC until 399 minutes only. Experimental conditions as in figure 6.22 (the curve for the external diffusion model is cut due to the scale)

the adsorption of humic acid on chitosan and activated clay, using kinetic models. However, the only parameter measured was UV absorbance (218.5 nm), which represents mainly the high MW since low MW hardly absorb UV at 218.5 nm. The last two models (the Elovich equation and the pseudo-second order model) also predict best the adsorption rate at the very beginning of the process. Wu et al. (2002) found that humic substances adsorption was better represented by the intraparticle model. They used chitosan-encapsulated carbon. However their range of study was between 5 and 240 minutes which corresponds to the good fitting range of the same model in this study.

The intraparticle diffusion model largely overpredicts the load beyond 400 minutes. Therefore, it becomes obvious that another mechanism could be controlling the adsorption process. Internal diffusion is likely to be less important as micropores are plugged by the adsorbed humic substances (Ding et al., 2006). This is more valid at this pH (7.0), when the molecules take on an extended conformation. As mentioned above, the Elovich equation represents diffusion together with a slow chemical reaction. It is suggested that this reaction corresponds to the competition of the various molecular weights for adsorption and to the displacement of some of them.

The models fitting for the adsorption onto AAFS are shown on figures 6.24 and 6.25. It is clear that no single model fits the whole range of data. This indicates that several mechanisms may occur and present variable resistances over time. In particular, the intraparticle model works well for the beginning of the adsorption but shows very large deviations from experimental data after 1000-1500 minutes. During stage two of adsorption (where intraparticle is likely to limit the process), the Elovich equation is the best model. The pseudo-second order model works well when equilibrium is reached.

For this particular adsorbent, the difficulty in predicting the load seems to be associated with attrition. Before attrition, AAFS behaves very much like GAC regarding the adsorption of humic substances. But when attrition becomes significant (from about 400 minutes to 1500 minutes), the intraparticle diffusion model is the only suitable model until most of the humics have disappeared from the solution and the equilibrium load is at its maximum (about 95% is adsorbed). At this stage, the external diffusion model fits the data best which corresponds very well to the limiting external diffusion due to the low concentration gradient in the liquid phase.

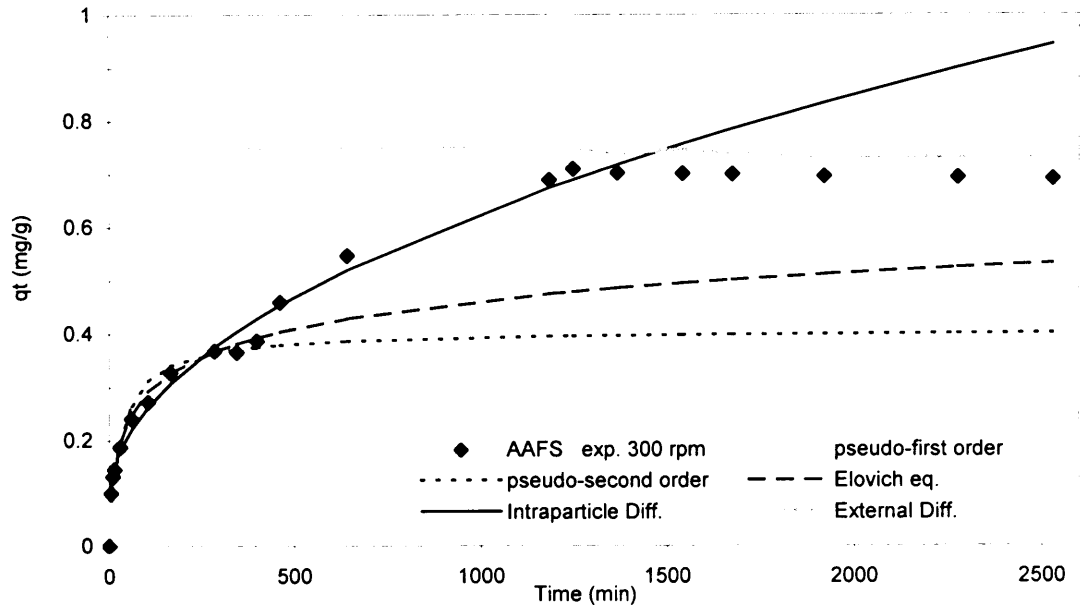

Figure 6.24 Adsorption onto AAFS over the whole range of data

Experimental conditions: 250 ml of F123, SUVA = 9.5, 300 rpm, 2 g AAFS, $(UV_{254})_0 = 0.582\ cm^{-1}$

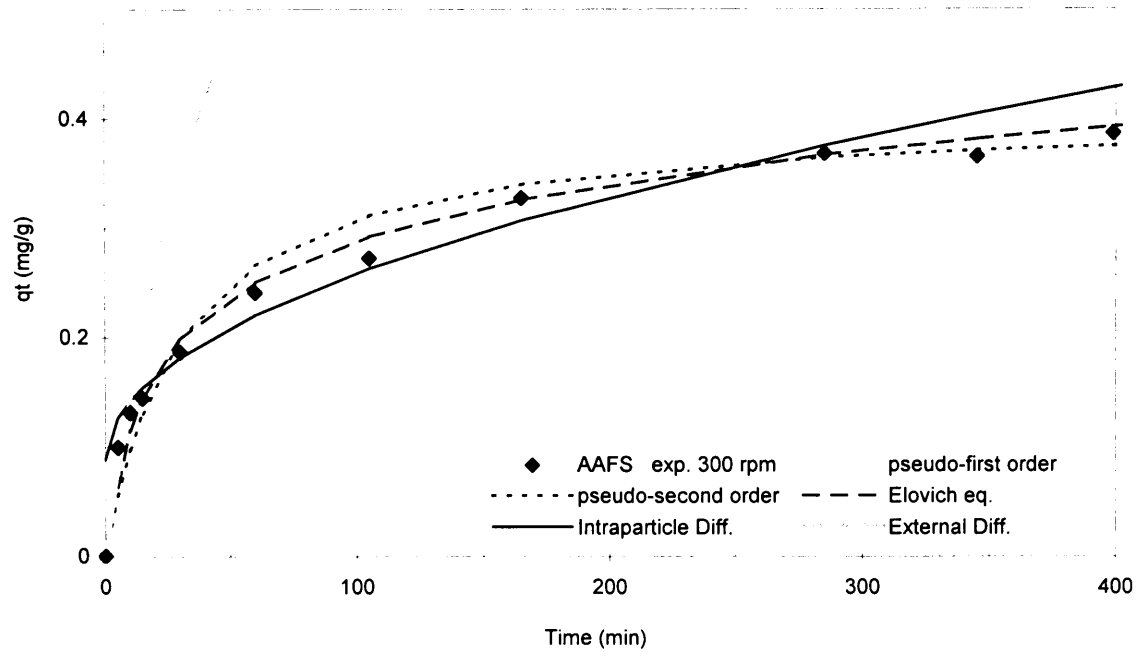

Figure 6.25 Adsorption onto AAFS until 399 minutes only. Experimental conditions as in figure 6.24 (the curve for the external diffusion model is cut due to the scale)

Overall the best model for adsorption onto AAFS is the intraparticle diffusion model. However, the error value F is never less than 0.02 which is very large when compared to to 0.002 for GAC and 0.008 for β-FeOOH. This indicates that none of the models is able to represent well the adsorption of humic substances onto AAFS. It is then likely that the process is controlled by different mechanisms at different stages of adsorption.

The comparison of models fitting to experimental data for the adsorption of humic substances onto β-FeOOH is represented on figures 6.26 and 6.27. The instantaneous adsorption at the beginning is best represented by the Elovich equation. It is likely to correspond to a chemical reaction of the humic molecules with the most active site since this model assumes a heterogeneous surface. It might involve mainly the parts of the molecules where the calcium ion is involved and such a hypothesis could be further explored by measuring the calcium content during the first stage of adsorption.

The intraparticle diffusion model is the second best fitting model justified by the presence of micropores, as for AAFS. Intraparticle diffusion is also expected to take place, although to a lesser extent than on GAC.

When the attrition takes place a sudden increase of the load appears and this is when the intraparticle model fits best. Overall the intraparticle model is not the best due to the deviation from experimental data over time. The Elovich equation is best, reflected in the low F value (0.00254) or a standard deviation of 5% (a very reasonable value according to Chang and Juang, 2004). It is concluded that a unique model cannot describe the adsorption of HS onto β-FeOOH. The intraparticle diffusion seems to control the process initially, followed by a mechanism corresponding to the Elovich equation. However, this also corresponds well with the mechanism of diffusion associated with chemical reaction in the Elovich equation model since Agbenin and van Raij (1999) mentioned that the Elovich equation is one of several diffusion expressions with slow chemical reactions.

The last figure 6.28 represents the values of the error F when considering the model over the whole range of data. It shows immediately the interest of the Elovich equation for each adsorbent. The intraparticle model is the second best for the iron compounds and it seems to represent the attrition of these adsorbents. The second best model for adsorption on GAC is the pseudo-second order model. The expected intraparticle diffusion is most likely to be hindered by plugging of the pores. Recent studies by Choy

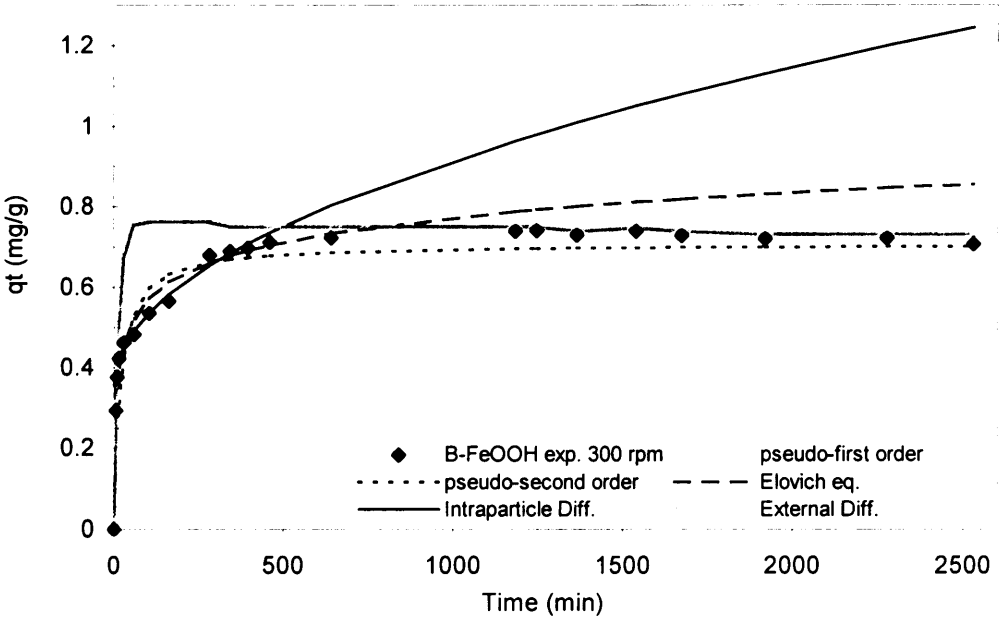

Figure 6.26 Adsorption onto β-FeOOH over the whole range of data
250 ml solution F123, SUVA = 9.5, 300 rpm, 2 g β-FeOOH, $(UV_{254})_0$ = 0.582 cm^{-1}

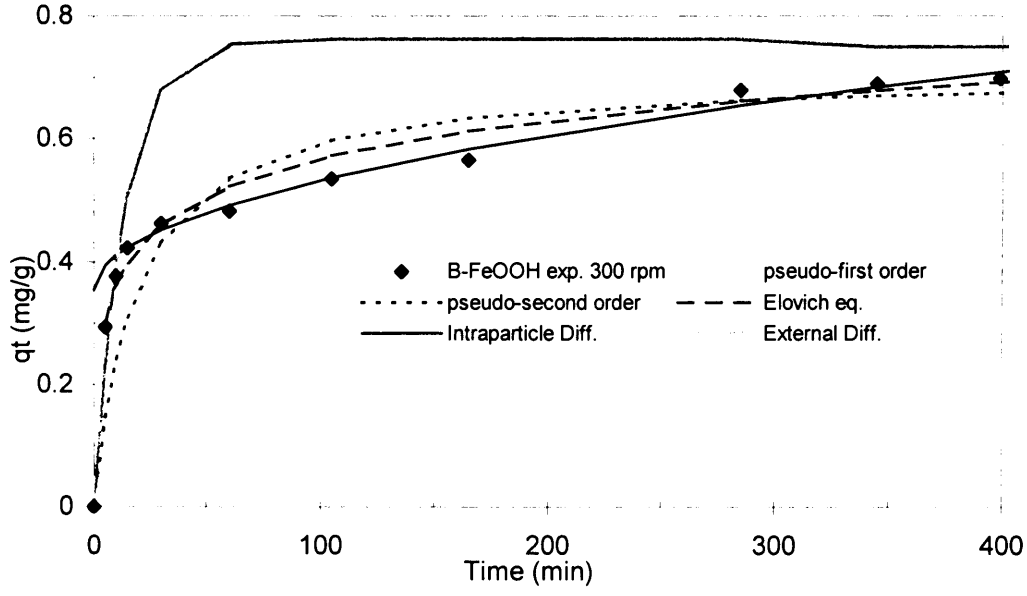

Figure 6.27 Adsorption onto β-FeOOH until 399 minutes only (experimental conditions as in figure 6.26)

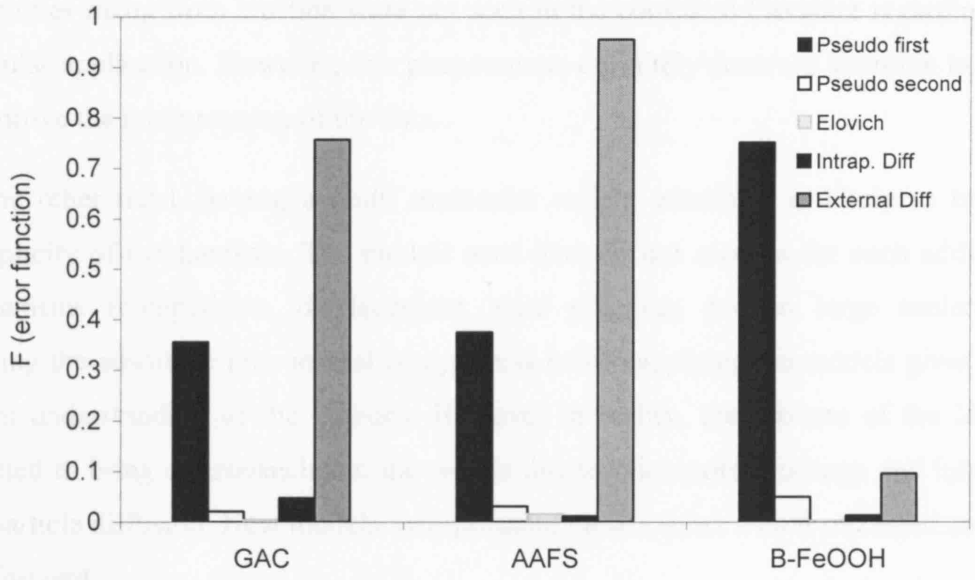

Figure 6.28 Error values (from function F) for each adsorbent and adsorption model

et al. (2004) showed that using a multicomponent system still resulted in discrepancies, which they attributed to micropore blockage and inhibited intraparticle diffusion. In contrast, the pseudo-first order model is not satisfactory and neither is the external diffusion model. The latter predicts adsorption well over the maximum load, as a result of the high k_f value (see table 6.5) calculated from the high initial adsorption rate.

6.9 Conclusions

The kinetic analyses bring evidence that intraparticle diffusion is a major mechanism in adsorption of HS onto AAFS and β-FeOOH. It is also a major mechanism for adsorption onto GAC although the large proportion of micropores corresponds to a larger proportion of pores being blocked by big molecules thereby diminishing this model's application.

It is important to notice that, particularly on AAFS, the dominant mechanism varies starting with the adsorption being limited by internal diffusion, then diffusion accompanied by a chemical reaction and later by external diffusion. External diffusion also represented well the adsorption onto β-FeOOH when the equilibrium was reached, due to the limiting concentration gradient.

Difficulties rising from attrition were not seen in the consulted literature regarding this particular application. However, this phenomenon definitely deserves attention in order to improve the interpretation of the data.

On the other hand, having a multi molecular weight adsorbate is likely to bring a multiplicity of mechanisms. The models used here do not account for such additional mechanisms (competition, displacement, pore plugging due to large molecules). Splitting the adsorbate into several components before applying the models gives more insight understanding of the kinetics. However in reality, the mixture of the MW is expected to bring discrepancies in the results due to micropore blockage and inhibited intraparticle diffusion. New models incorporating these factors would represent an ideal way forward.

CHAPTER 7

ADSORPTION IN A BATCH SYSTEM

7.1 Introduction

The results of the kinetic studies, shown in the previous chapter, indicated that equilibrium is reached in four days when the adsorbent (GAC, AAFS or β-FeOOH) is mixed with the humic substances solution. Therefore, results presented in this chapter correspond to equilibrium analyses performed, using a centrifuge at 200 rpm, after four days contact between the adsorbate (humic substances) and the above cited adsorbents.

The batch studies described in this chapter concentrated on single adsorbent behaviour using the isotherm, and were also extended to multicomponent adsorption. The isotherm represents the variation of adsorption with concentration of adsorbate in bulk solution, hence a graph was produced of the DOC load (milligram of DOC per gram of adsorbent) vs the residual DOC (milligram per litre). Two additional conditions must be met to obtain the isotherm; these are *(i)* the equilibrium must be attained and *(ii)* the temperature must be constant. Where the adsorption is reversible, the equilibrium is a dynamic equilibrium with desorption and adsorption taking place at the same rate once the adsorbent has reached its adsorption capacity (AWWA, 1990).

In this chapter, the classification of the isotherms is first introduced and will be used to interpret the results. Then adsorption models selected (Freundlich, Langmuir and Henry models) to calculate the theoretical adsorption capacities are presented. Finally, the results are discussed in sections corresponding to each fraction and show the degree to which each fraction F1, F2, F3 is removed on each adsorbent in the absence of the other fractions. It will be observed that for F123, i.e. a multicomponent adsorbate, the adsorption behaviour proves the importance of competition between several fractions. For each of them (F1, F2, F3 and F123), the shape of the isotherm is first examined to

qualitatively describe the adsorption behaviour, followed by the application of adsorption models to fit the experimental data.

The results show the isotherms for both DOC and UV absorbance at 254 nm. All experiments were run in duplicate and were found to be reproducible. These batch studies together with kinetic studies give essential information as regards to the feasibility of adsorption in a continuous flow context (column studies) where equilibrium conditions are not reached.

7.2 Isotherms classification

The isotherms represent the concentration of the adsorbate left in solution versus the load of adsorbate on the adsorbent. The shape of the isotherm is compared to Brunauer et al.'s isotherm classification (1940), shown in figure 3.3 in chapter 3 (literature review). Although the shapes were obtained for gas adsorption, it can be extended for adsorption from a liquid state, replacing the pressure (x on the graph) by the concentration (Giles et al., 1960).

The isotherms are examined in three regions as shown in figure 7.1:

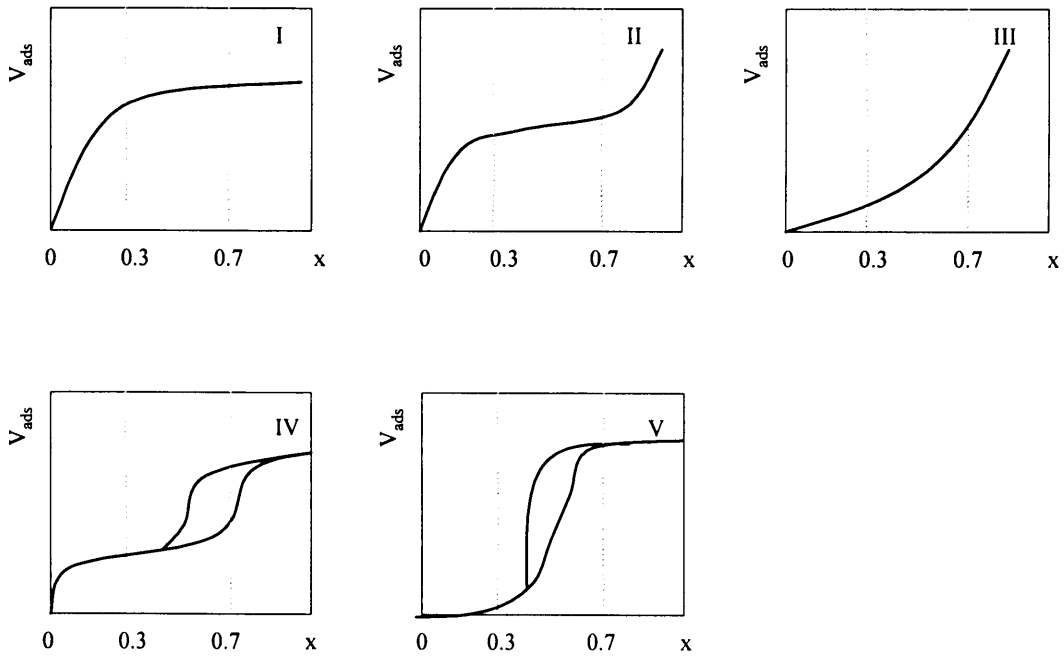

Figure 7.1 Type of adsorption isotherms in each region of adsorption (adapted from Brunauer et al.,1940)

- $0<x<0.3$ low pressure or low concentration
- $0.3<x<0.7$ intermediate pressure or concentration
- $0.7<x<1.0$ maximum pressure or high concentration

A steep slope in the first region of adsorption (see x between 0 and 0.3 for isotherms of type I, II or III in figure 7.1) indicates a strong interaction between adsorbate and adsorbent. Conversely a shape as isotherm type III or V represents a weak adsorbate-adsorbent interaction. These shapes III and V show the adsorption to be delayed until a significant solution concentration is reached. This corresponds to a low affinity of the adsorbate for the adsorbent.

The second region indicates the possibility of multilayer adsorption and this is where the multiplicity of inflexion points, associated with the filling of new layers (Weber, 1972), can be observed. A new layer can be started before completing the previous ones. In that case, the equilibrium condition involves several types of surfaces, in the sense of number of layers of molecules on each surface site (Weber, 1972). It is equivalent to say that a distribution of energies takes place on the surface, which in turn means that the surface is heterogeneous. Consequently, this multilayer adsorption can also be the result of a wide pore size distribution, particularly in the case of type (II) isotherm of the Brunauer et al.'s classification (see figure 7.1 above) (Thomas and Crittenden, 1998).

The last region of the isotherm is indicative of the availability of high-energy sites (Chen and Snoeyink, 1987). If only few of them are available, the adsorption slows down and the isotherm slope decreases to become a plateau. It means that the surface does not present any heterogeneity towards adsorption energy (Ebie et al., 2001). If the slope still increases in the last region III (type II isotherm), adsorption sites present a large heterogeneity indicative of a wide distribution of pore sizes, with condensation occurring in the larger pores (Thomas and Crittenden, 1998).

7.3 Adsorption models

The equilibrium (with or without reversibility) represents a thermodynamically stable adsorbent-adsorbate system with a minimum energy level (Montgomery, 1985). Several

equations or models are available that describe the progress of adsorption onto an adsorbent. A good model fitting enables better understanding of the adsorption process according to the model assumptions. It also allows to predict the extend of adsorption for a given system and to design installations to remove a given contaminant (humic substances here).

Three models are considered here: Langmuir, Henry and Freundlich. These models are reviewed and detailed in sections 3.4.1.2, 3.4.1.3 and 3.4.1.4 of chapter 3. It is important to insist on the range of validity of the model since this aspect of model fitting is often not taken into account (model fits well according to the experimental conditions of study). For example, it can be noticed that studies are often carried out at a pH between 4 and 6 (Teermann and Jekel, 1999, Chi and Amy, 2004) which is the optimum range for humic substances adsorption. However, this does not represent the reality of a water with a pH nearer to 6 – 8. Tipping (2002) also insisted on the research needs for studying HS adsorption at neutral pH. The three selected models have been described in chapter 3 (literature review). Therefore, only the basic assumptions are mentioned here:

- The Langmuir model: Adsorption is limited to one layer, corresponding to a unique type of site and unique energy. As a consequence, it is likely to be valid for a single adsorbate (a well defined molecule) or a very homogeneous adsorbent or only at low coverage for a heterogeneous adsorbent. Relevant equations are 3.23 and 3.24 in chapter three. Relevant parameters are K_L (Langmuir constant), Q_m (monolayer capacity).

- The Freundlich isotherm: Adsorption sites present a distribution of energy. Therefore, sites are suitable for different adsorbates or for the same adsorbent in different conditions (pH, ionic strength, etc.). The most energetic sites are occupied first and as adsorption increases, less energetic sites are used. It allows multilayers to be formed.

  Parameters to be considered are K_F (Freundlich constant, indicating the capacity of adsorption), 1/n (indicating the intensity of adsorption). If the slope 1/n of the linearised isotherm is equal to 1, then the model is equivalent to the Henry model (third model selected in this work). If it is greater than 1, it means that a small increase in the adsorbate residual concentration brings a large increase in the load. In such a situation, it is likely that a phenomenon different from adsorption is

taking place (as said before, condensation or precipitation). However, the removal of the adsorbate from the solution is still accounted for as adsorption. The capacity of adsorption is estimated from the isotherm experimental points. After selecting the point representing the adsorbent concentration of 1g/L (or by using a linear regression between points near 1 g/L), the corresponding experimental load is used as the adsorption capacity. This value of 1 g/L is arbitrary; it is a mean to compare this parameter between the various adsorbents and humics fractions.

- The Henry isotherm: This model is equivalent to the Freundlich model when the parameter 1/n is equal to 1. The parameter, instead of Freundlich constant, becomes Henry constant K_H. The load on the adsorbent increases directly with the concentration which is most likely when the availability of adsorption sites is not a limiting factor. Therefore the Henry model is usually valid at low coverage.

At low residual concentration, the three models are equivalent. At high coverage, phenomena different from adsorption occur, such as precipitation and condensation (Tipping, 2002, Thomas and Crittenden, 1998).

A first linear plot using the model equation is compared to the "trendline" (function in the Excel programme) fitted to the experimental data. This trendline gives a correlation coefficient R^2. The model fitting is shown in the cases where R^2 is larger than 0.5.

7.4 Fraction F1 (<5 kDa)

7.4.1. Isotherm for F1

Adsorption of fraction F1 is shown on figures 7.2 and 7.3, respectively for UV_{254} and for DOC. Adsorption on each media is shown.

F1 adsorption differs greatly according to the adsorbent. Although UV_{254} absorbance is low (characteristic of low MW of humic substances), trends for UV and DOC are similar. GAC largely adsorbs F1 whereas iron compounds do not. Details are investigated below.

The two striking features in UV (figure 7.2) and DOC (figure 7.3) isotherms are *(i)* the difference in the first region (where low residual concentration) and *(ii)* the low loads on iron compounds compared to GAC.

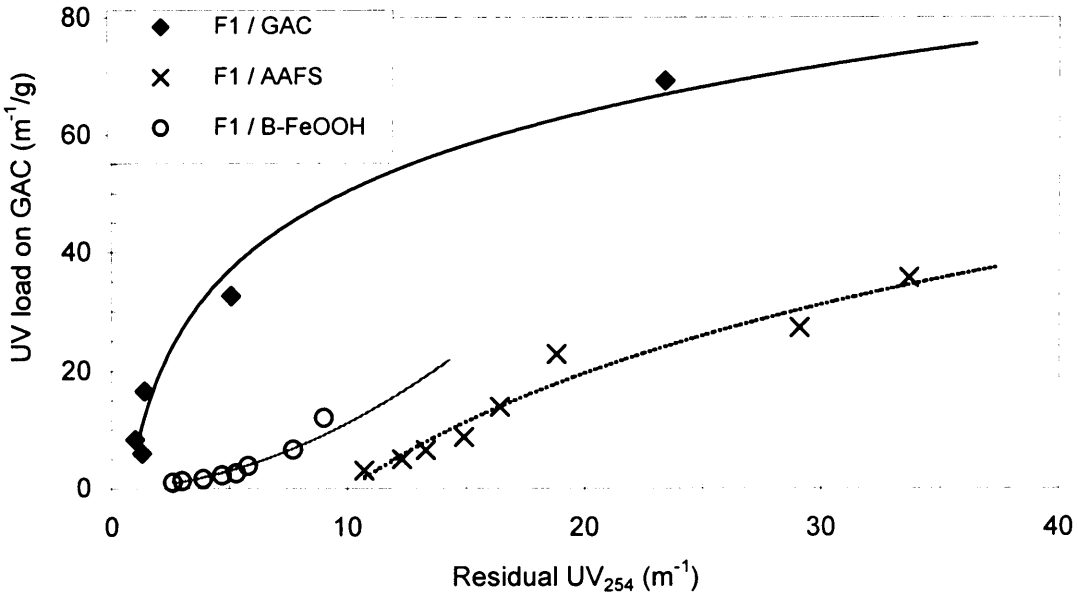

Figure 7.2 Adsorption of F1 on the GAC, AAFS and β-FeOOH, for UV_{254}. (experimental points and trendlines).

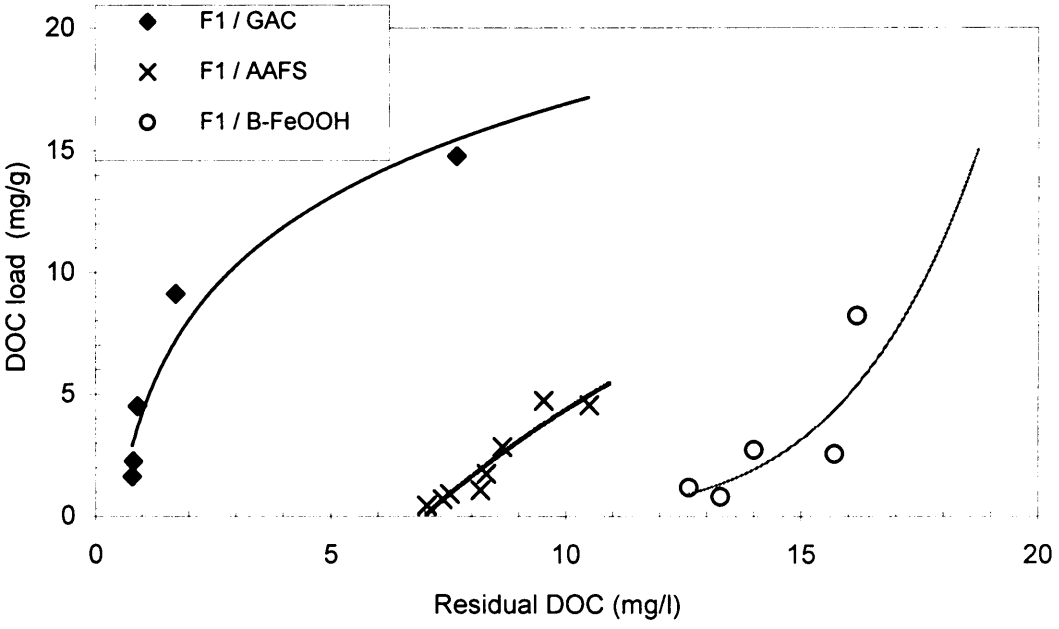

Figure 7.3 Adsorption of F1 on the GAC, AAFS and β-FeOOH for DOC. (experimental points and trendlines).

The first region indicates how strong the interactions are between the adsorbate and the adsorbent. Filius et al. (1997) also related the increase of the slope at low concentration to the number of active functional groups involved in the binding. The high load on GAC from a very low residual concentration (see figure 7.3) shows the strong affinity of the lowest MW for the GAC surface. In chapter five, it was shown that F1 could be classified as a hydrophilic fraction (Kitis et al., 2002). However, fulvic acids are generally part of the hydrophobic substances and hydrophilic matter refers to the substances with a MW below 500 Da (Drever, 1994). Since it contains MW up to 5 kDa, F1 covers a range of both hydrophilic and hydrophobic humic substances (Thurman, 1985). The tendency of F1 to adsorption is equivalent to F1 "escaping" from the water, which confirms its dominant hydrophobic aspect.

Cook and Langford (1998) showed the fulvic acids to be very functionalised with many carboxylic groups and aliphatic structures. At pH 7, they loose their protons and since GAC is highly positive (pH_{zpc} is 10.7), strong links are favoured. Filius et al. (2000), investigated the MW around 1000 Da and found that outer sphere coordination becomes more important than inner sphere coordination when pH increases, due to a surface increasingly more negatively charged, hence a stronger repulsion between the humics and the surface. At neutral pH, GAC is positive and complexation might occur more through the inner sphere corresponding to a high affinity of F1 for the surface, favouring a strong adsorption. On iron compounds, the pH_{zpc} is between 5.0 and 5.5, hence these adsorbents acquire a negative surface at pH 7. Ionised fulvic acids face repulsion when approaching the surface. In this case, Vermeer et al. (1998a) mention the specific interactions such as ligand exchange, accompanying coulombic forces. On positive mineral surface (where surface still bears most of the hydroxyl groups), the ligand exchange is the most common humic substances adsorption process (Tipping, 2002). Parfitt et al. (1977) gave evidence of the following scheme in equation 7.1 (S represent the mineral surface and R the humic molecule) where the ligand exchange takes place with the hydroxyl that have not deprotononised:

$$\equiv SOH \quad + \quad R-COOH \quad \Leftrightarrow \quad \equiv S-OCOR \quad + \quad H_2O \qquad (7.1)$$

However, since the surfaces, in this study, are negative, non-specific interaction are also to be considered. These are the long range forces also called "dispersive forces" (Everett, 1988). They include Van der Waals forces, London and Keesom forces and involve dipole-dipole interactions between permanent and induced dipole.

The AAFS grains were initially brown with white spots where the iron coating was not complete and left the Al_2O_3 surface bare. By the end of the experiments, the whole surface of the grains was dark brown due to the humic substances adsorption. This was equally mentioned by Chen and Snoeyink (1987) who, in addition, observed the white core of the alumina grains. From such observations, it can be concluded that the adsorption is mainly external. Although according to those authors, pores with a 7 nm width were too small for HS heavier than 1000 Da. However, this finding is contradicted by more recent studies (De Wit et al., 1993, a, b, Avena et al., 1999). They actually estimated the size of low molecular weight humic substances (1000 Da) to be approximately 0.75 nm, which would enable them to diffuse into 7 nm wide pores. A suggested cause of the low adsorption on AAFS is that the low microporosity is not accessible for low MW of F1.

As mentioned in chapter five, gyration radius R_G of a molecule represents the radius of the sphere swept by the same molecule when turning on itself. R_G of F1 molecules (or entities with sub-units) is between 1.5 and 2 nm. GAC is mainly microporous with most pores smaller than 2.2 nm and a median pore size of 1.13 nm. Conversely, AAFS and β-FeOOH are mainly mesoporous (>2.5 nm) but present little microporosity too. At these sizes, F1 is able to enter most pores of the three adsorbents under study, but the smallest pores of GAC remaining unaccessible. For GAC, this corresponds well with the second region of adsorption on the isotherm. Figures 7.2 and 7.3 show a slow approach to a plateau and assuming this level corresponds to saturation, the isotherm is of type I in the Brunauer et al.'s classification (see figure 7.1). It indicates a favourable adsorption from its concave shape (Weber, 1972) and that a monolayer is completed, when the media is mainly microporous (Thomas and Crittenden, 1998).

For the iron compounds, adsorption does not take place immediately (particularly for β-FeOOH) although pore size is not a limiting factor. Therefore, only a few adsorption sites are favourable to adsorption of low MW (different energy of adsorption involved). If considering the dissociation constants for alumina (Kummert and Stumm, 1980):

$$AlOH_2^+ = AlOH + H^+ \quad pKa_1=7.4 \quad (7.2)$$

$$AlOH = AlOH^- + H^+ \quad pKa_2=10.0 \quad (7.3)$$

Where pKa_1 (subscript "a" stands for "acid" for the dissociation of the proton) is equal to $-\log Ka_1$, Ka_1 being the first dissociation constant of $AlOH_2^+$ (equation 7.2), and similarly for pKa_2 (equation 7.3). The pK is the pH for half dissociation (Tipping, 2002).

At pH 7, and using AAFS, where white patches of bare alumina are exposed (the coating does not cover 100% of the surface), the surface presents positive charges. Consequently, it can attract HS and this explains the high loads on AAFS compared to β-FeOOH. Although the pH_{zpc} values suggest otherwise (AAFS more negative at pH 7 than β-FeOOH), fulvic acids are likely to be attracted to local charges, such as the initially non-covered alumina white patches (Al^{3+}) and Fe^{2+} and Fe^{3+} (ferrous/ferric sulphate coating).

Low adsorption on the ferric oxihydroxide is also likely to be due to relatively few sites being favourable for adsorption of low MW humic substances. Other authors (Vermeer et al., 1998a, Namjesnik-Dejanovic et al. 2000, Chi and Amy, 2004) mentioned a steep slope of the isotherm in the low concentration region, using different iron oxides (hematite, goethite and quartz respectively for the authors cited). However, the main difference was the pH_{zpc} which was approximately 7.5, leading to a positive surface even at neutral pH for each of the three studies mentioned. As the pH increased to 8, the slope decreased and the interaction, initially of coulombic nature, became more and more specific (ligand exchange) and non-specific (dispersive forces). Since they studied a wide range of concentration (residual concentration up to 250 mgL^{-1}), the strong intermolecular repulsion, within the solution, causes the HS to reach for the surface. This is probably the reason for the adsorption observed on β-FeOOH, occuring only at high residual concentration. Zhou (1996), Schroth and Sposito (1997) also observed a low adsorption on kaolinite with a pH_{zpc} of about 5. This strenghtens the idea that the electrostatic effect does not control the adsorption in the conditions of this work. However, strong adsorption via ligand exchange, by inner sphere coordination, can also take place where positive charges are available on the iron mineral.

Adsorption might also take place on the dissolved media. This is mentioned by Seida and Nakano (2000) whereby the hydroxide dissolution promotes the coagulation of humic substances on the media. This is likely to happen on ferric oxihydroxide at pH 7. On the other hand, the attrition of the media is rarely mentioned (never mentioned in the literature cited above) although it is an inherent and clearly occuring phenomenon in a batch study where external diffusion limitation is avoided by mixing the system adsorbent-adsorbate system. The solution with the ferric oxihydroxide and the coated alumina (although less) became very much of a "ferric" colour after few hours. When filtering the sample (0.45 um), the filter was unequivocally iron brown in colour. Therefore, should the humic substances have reacted with the dissolved iron or adsorbed on the powder, they would be retained on the filter. Consequently, they would be counted as adsorbed matter on the adsorbent and a high load would be observed even at low residual DOC. The low loads prove that this was not the case (up to 7 to 13 mgL^{-1} residual DOC for AAFS and β-FeOOH). Therefore, medium dissolution cannot be considered as an explanation for low adsorption.

The second interesting feature on figures 7.2 and 7.3 is the difference between the adsorption load on the iron compounds when comparing UV_{254} and DOC. A residual UV_{254} beyond 10 m^{-1} is necessary before adsorption takes place on AAFS whereas on β-FeOOH, residual UV_{254} needs to be approximately 2.5 m^{-1} only. This is attributed to the SUVA value. SUVA was 0.9 for F1 used on β-FeOOH versus 3.4 for F1 used on AAFS, due to the difficulty in making solutions with identical characteristics for consecutive experiments. It indicates that the solution has a high DOC but a low UV absorbance, as seen from the residual concentrations on both graphs. It particularly shows that F1 could be subdivided much further in more MW ranges. This was actually selected by most of the authors mentioned in this work since aquatic NOM are usually smaller than 5 kDa (Thurman, 1985, Fettig, 1999a, Fettig and Sontheimer, 1987c, Teermann and Jekel, 1999). However, it was shown in chapter five that low molecular weight humic substances are difficult to store since decomposition of the solution was observed after a few days (decomposition is not generally mentioned in the literature consulted). In addition, it is also impractical to make large quantities of solution to scale up any bench study, due to the cost of isolating low MW aquatic NOM. These reasons justify that as the NOM molecular weight decreases, the more difficult is the study of the adsorption.

As a conclusion, it appears necessary to have a positive surface for adsorption of low MW humic substances, which occurs only for GAC in this study. In addition, the high microporosity of GAC provides a large surface for adsorption, as long as pores are not blocked by heavy MW humic substances. This does not happen on the iron compounds, which have, in addition, a very definite negative surface. It is then only from a high solution concentration that adsorption is observed since the deprotonised humic substances repel each other. Consequently they approach the adsorbent surface. In this situation, the most likely mechanism for adsorption is the outer-sphere complexation by the long range Van der Waals forces. Such a mechanism was suggested by Chi and Amy (2004) when only few adsorption sites are available. This is the case here since the iron compounds globally have a negative surface at neutral pH. Therefore, it seems likely that the interaction involves principally the non-ionised groups of the iron compounds with the functional group of F1, and to a lesser extent the inner-sphere coordination via positive charges on the mineral surface.

7.4.2 Model fitting for Fraction F1

Models fitting is shown below on figure 7.4 for fraction F1. Langmuir model was not applicable since no trend of linearity was observed between C_e/q_e vs C_e. This indicates that the Langmuir assumptions (as from Weber, 1972) are not respected, i.e. the energy of adsorption is not constant, adsorption might occur over more than one layer and interaction between adsorbed species can take place. It also corresponds to the isotherms showing no sign of a plateau. The Henry model applied for the GAC only (but fitting is not good). On the range of concentration studied, only the Freundlich model could be applied to the three adsorbents, although the fitting for β-FeOOH was not good either. Parameters corresponding to the three models are given in table 7.1.

It is clear that this fraction is hardly adsorbable on AAFS and β-FeOOH. A high residual DOC must be reached in the solution to observe a low adsorption on those media. The delay in adsorption was more obvious for DOC than for UV_{254}, giving evidence that only the higher molecular weights of F1 (close to 5 kDa) are adsorbed on the iron compounds. Adsorption capacity (table 7.1) confirms this particularly on β-FeOOH. In this case, since the initial DOC was high (16.17 mg/L due to the difficulty in reproducing exactly the same solution from one experiment to another), adsorption would be expected to be high under the accumulation of HS on the surface. This does not happen and the adsorption capacity is only 0.43 mg/g, compared to 9.11 and

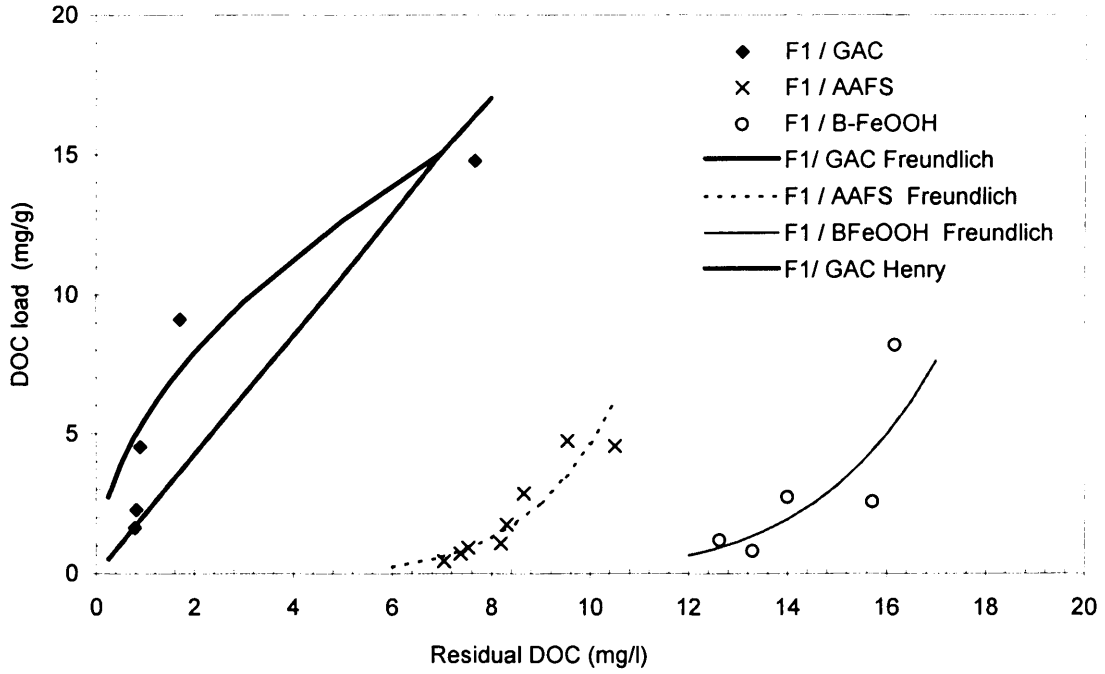

Figure 7.4 Fitting of adsorption models to experimental points for F1 on GAC, AAFS and β-FeOOH (the Langmuir model not applicable, the Henry model not applicable for AAFS and β-FeOOH).

Table 7.1 Isotherm parameters for F1 on GAC, AAFS and β-FeOOH

F1		Freundlich model			Langmuir model		Henry model
Adsorbent	Initial DOC (mgL^{-1})	K_F ($mg\ g^{-1}$). ($mgL^{-1})^n$	1/n	Adsorption Capacity (*) ($mg\ g^{-1}$)	b ($L\ mg^{-1}$)	Q_{mon} ($mg\ g^{-1}$)	K_H ($L\ g^{-1}$)
GAC	10.48	5.55	0.51	9.11	<0	<0	2.121
AAFS	10.96	$<10^{-2}$	5.75	2.55	<0	<0	n.a.
B-FeOOH	16.99	$<10^{-2}$	0.71	2.73	<0	<0	n.a.

(*) experimental load (DOC mg/g of adsorbent) after 96 hours, in experiments where the dose was of 1 g adsorbent/L

2.55 mg/g respectively on GAC and AAFS, when the initial DOC was much lower (approximately 10 mg/L).

Teermann and Jekel (1999) studied the adsorption of the same humic substances onto β-FeOOH. A delay in adsorption was also observed. In particular, when the solution contained a high proportion of low MW, a minimum residual of 7 mg DOC/L was the starting point of adsorption. However, the initial DOC was higher (37 mg/L) and in general, the adsorption capacities were much higher than in this study, up to 45 mg/g.

This means that a non-adsorbable fraction was also present in the adsorbate, corresponding to approximately 20% of the initial concentration (7 out of 37), also in agreement with 20% of the MW below 1000 Da. It must be stressed that the pH_{zpc} of their β-FeOOH was 8 and not 5.5 as measured here. The isoelectric point was measured by zeta potential ζ, which might give a result slightly different from the point of zero charge since the precise location of the shear plane where ζ is measured, is difficult to define (Everett, 1988). However the difference would not be as large as 2.5 pH unit. Teermann and Jekel (1999) do not give any information regarding the solution the ferric oxihydroxide was in; for example, the presence of ions could compress more or less the boundary layer limiting the shear plane, increasing the potential, hence giving a higher ζ. However, Chang et al. (1997) mention that the reported range for the pH_{zpc} of iron oxides is around 6-9. This makes the value in this study acceptable since the pH_{zpc} had increased from 5.5 to 5.9 when using a different electrolyte (KCl instead of $CaNO_3$). Zhou et al. (2001) used goethite to adsorb a natural organic matter from surface water, with a DOC of 24.2 mg/L. A high adsorption was obtained, particularly with the MW between 500 and 11000 Da. The lower MW were also non-adsorbable. However, in their study and on a narrow MW range between 1250-3750 Da, the Langmuir model fitted the isotherm well. This confirms that fitting one model or another is specific to the system under study, and in particular the adsorbent characteristics will define how diverse the adsorption sites can be.

From Al-Ghouti (2004), 1/n value (multiplied by 100) corresponds to the percentage of sites having a similar energy (the Freundlich model assumes the existence of a distribution of the sites energy). It could be interpreted that at a higher 1/n value, the same reasoning is applicable and all sites are similar. This corresponds to a homogeneous surface. However, it disagrees with the fact that Langmuir model did not

strictly fit the isotherm, although it is a model that assumes the adsorbent surface to be homogeneous, as opposed to the Freundlich model. The interpretation of 1/n should perhaps be considered separately for GAC and the iron compounds:

- on GAC, 1/n is equal to 0.5 (table 7.1) indicating a wide range of sites corresponding to different energies of adsorption. However, the 1/n value would be higher if the delay in adsorption were not taken into account since initially the load increases sharply. This sharp start leads to a concave isotherm. The short delay shows that adsorption is observed from a residual DOC of approximately 0.7 mg/L. This DOC is attributed to the non-adsorbable fraction of fraction F1. As a consequence, it can be concluded that on GAC, the adsorbable fraction of F1 is strongly adsorbed and for the adsorbable part of F1, the surface would be more homogeneous, hence there is the possibility of applying the Henry model.

- The high 1/n value on AAFS (5.75), on the other hand, is due to a slow increase in adsorption, followed by a very sharp increase for the solutions with a high residual DOC. This leads to a convex isotherm shape. The similar shape for the isotherm on β-FeOOH leads to a similar conclusion although the 1/n value is not very high (0.71). The very long delay in adsorption shows that whatever the energy of the adsorption sites, they do not present any affinity to humic substances molecules below 5 kDa until a high solution concentration causes other mechanisms to take place. The Henry model did not apply for any of these adsorbents, although high values of 1/n should correspond to a homogeneous surface (according to Al-Ghouti, 2004, the higher the slope, the more similar the energies of adsorption). It can be interpreted that F1 is quasi non-adsorbable on these adsorbents.

Yuasa et al. (1997) observed that GAC adsorbed the lower MW of humic substances better than high MW. They suggested that each fraction studied could be further divided in subfractions with different adsorbabilities. However, when modelling adsorption, Fettig et al. (1985) obtained no better results by fractionating the MW up to 5 kDa into more than 3 fractions with respective adsorbabilities nul, medium and high. It can be concluded that F1 could be subdivided in 2 or 3 sub-fractions for modelling purposes.

7.5 Fraction F2 (5-10 kDa)

7.5.1 Isotherm for F2

SUVA of fraction F2 was between 6 and 7 m^{-1}/mg/L, corresponding to MW between 5 and 10 kDa. Figures 7.5 and 7.6 show the adsorption isotherms of F2 on the three media, respectively for UV_{254} and DOC. It is immediately noticeable that the isotherms shape are very different from F1. In this case, iron compounds adsorb F2 whereas GAC is not so efficient an adsorbent.

Examining the first region of adsorption, it is clear that UV_{254} is adsorbed immediately on β-FeOOH. However, for the DOC a slight delay is observed on figure 7.6 and the isotherm resembles more closely to type IV in figure 7.1. This indicates that the heavier molecules of F2 (the one which absorb UV) are removed more efficiently on β-FeOOH than the lighter ones of F2. For both UV and DOC, a sharp start of the isotherms on both iron compounds contrasts with the low slope for GAC.

The GAC has mainly micropores and the above observation agrees with Li et al. (2003). They studied MW up to 1800 Da and concluded that carbon with a larger mesoporous volume had a higher adsorption capacity for larger MW natural organic matter. By extending such a result to MW above 5 kDa, it can be inferred that GAC would adsorb F2 better, with a higher proportion of mesopores and perhaps some macropores. It was shown by Othman et al. (2000) who found that a GAC ("Picactif"), with most pores smaller than 2.7 nm, demonstrated the lowest adsorption capacity, compared to another GAC ("APSC") with most pores larger than 2.7 nm, that showed the largest capacity.

It also becomes apparent that for efficient adsorption, interaction of HS with iron compounds at pH 7 is possible only for MW above 5 kDa. Fraction F2 tends to "escape" from the water more than fraction F1 due to less ionisable groups (less carboxylic groups than in F1 as defined in chapter 5). Humic substances in fraction F2 are too big to diffuse into micropores and need meso- or macropores, present in iron compounds, to be adsorbed efficiently. However, it is also possible that the number of sites used for adsorption is the same as for F1. In such a situation, having one heavy MW humic molecule adsorbed has more consequence on the residual concentration than having a small MW molecule adsorbed. This prediction can be illustrated by figure 7.7 and two possibilities are suggested: *(i)* one heavy molecule occupies one site and as a consequence, adjacent humic molecules are repulsed towards the solution and *(ii)* the

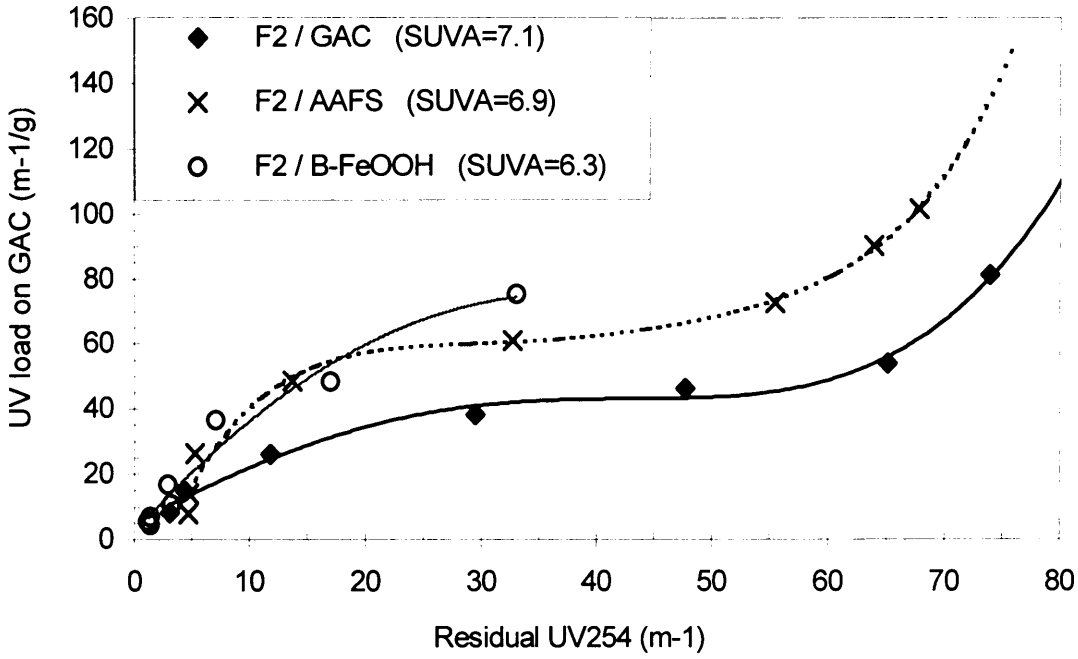

Figure 7.5 Adsorption of F2 on the GAC, AAFS and β-FeOOH, for UV_{254}. (experimental points and trendlines).

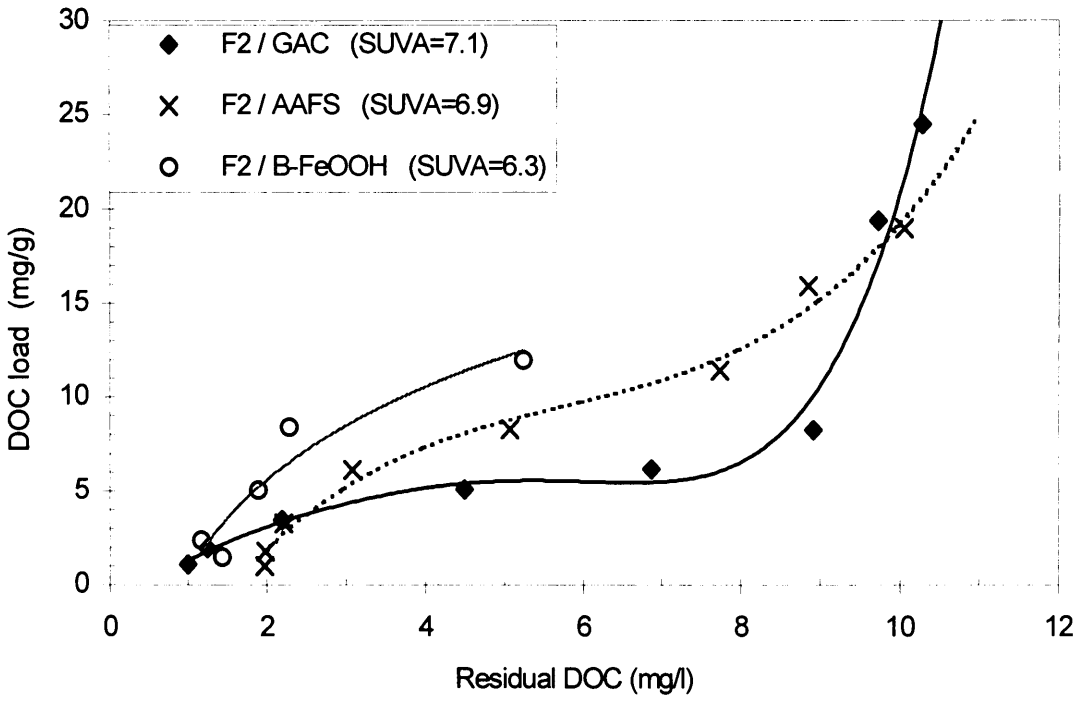

Figure 7.6 Adsorption of F2 on the GAC, AAFS and β-FeOOH, for DOC (experimental points and trendlines).

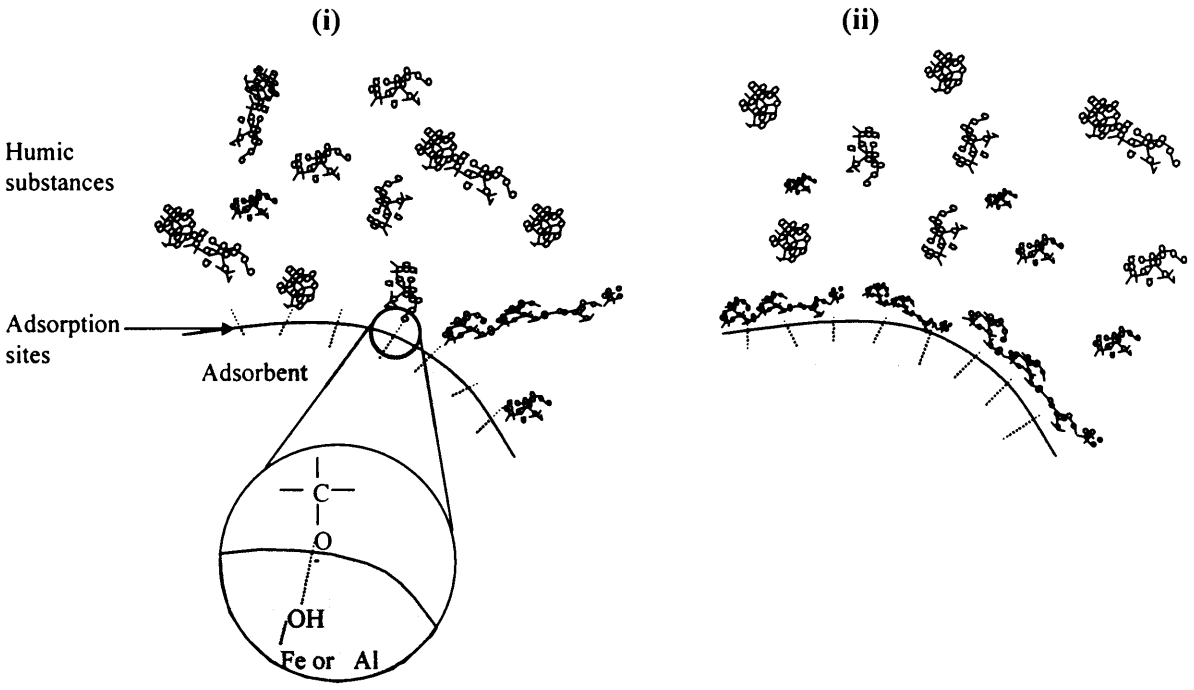

Figure 7.7 Different configurations for humic substances adsorption

humic molecule occupies several sites.

Vermeer et al. (1998a) found that when increasing the pH, the thickness of the hydrodynamic layer of adsorbed humic substances decreased but the hydrodynamic diameter of the humic substances in solution increased. The interpretation brings to favour situation (ii) above, where the adsorbed humic substances are flattened upon adsorption. Should this be the only adsorption mechanism, the load would be expected to decrease significantly since few HS molecules would occupy most adsorption sites. However, the quantities adsorbed did not decrease considerably. Therefore, this mechanism of adsorption is not exclusive. It can be concluded that configuration (i) above also happens, with part of the humic molecules still protruding into the solution.

Actually, the number and the steric arrangement of the functional groups of NOM influences the adsorption processes. Illés and Tombácz (2004) showed, using FTIR and NMR analyses, that ortho-positioned carboxyls and/or hydroxyls may form complexes with iron oxide surfaces through the ligand exchange mechanism.

Analysing further the isotherm, it appears that for both AAFS and GAC, it resembles type II in figure 7.1 (two inflexion points), with a sharp rise of the load when the

residual DOC increases. It indicates that adsorption takes places beyond a monolayer. In the third region of adsorption (high residual DOC), the high concentration of humic substances brings a modification in their behaviour. Since the pH of the solution is 7, humic substances tend to lose their protons and therefore can strongly repel each other and "escape" onto the positive surface of GAC. In turn, the GAC becomes saturated and the load increases steeply. This also indicates that the heavier MW either displace lighter MW or plugs the pores, since UV_{254} load increases a lot, which corresponds to high MW removal. The greater adsorption of heavier MW also corresponds to the higher content of phenolic groups. Gu et al. (1995) and Evanko and Dzombak (1998) showed that the maximum adsorption of carboxylic groups occurred at low pH (acidic), while it occurred at a higher pH (5-7) for phenolic groups. Therefore, it is expected to increase the adsorption of heavy MW (more phenolic groups) as the pH increases beyond acidic values. It agrees well with the present situation for iron compounds for which adsorption has become favourable as compared to unfavourable for fraction F1. Filius et al. (2000) illustrate the adsorption of phenolic groups on the negative surface in equations 7.4 and 7.5 below (Φ represents a phenolic group):

$$FeOH^{-0.5} + \phi\ C-OH \longleftrightarrow H-FeO^{0}.....H.....^{-0.5}O-C\phi \qquad (7.4)$$

or

$$FeOH^{-0.5} + \phi\ C-OH \longleftrightarrow FeOH_2^{+0.3}.....^{-0.8}O-C\phi \qquad (7.5)$$

Through this distribution of charges, part of the positive charge of the proton is attributed to the surface plane and H bonds can be formed between the humic substances and the proton (Filius et al., 2000).

This charge distribution was part of their "Charged Distributed Multi Site Complexation" model (or CD-MUSIC) approach to describe the adsorption of fulvic acids onto goethite. With this model, the charging behaviour of the adsorbent in the presence of fulvic acids could be described assuming that pH_{zpc} is equal to the pK_a of the protonation of goethite. This means that at the zero point of charge, half of the goethite is dissociated, hence the charge –0.5 of FeOH in equation 7.4 and 7.5 (pK_a is the pH value for half dissociation).

The limit for adsorption on GAC must also consider the pore size of this adsorbent. The external surface of GAC is small compared to its internal surface (168 vs 812 m^2/g). As a consequence, HS with a high molecular weight are expected to adsorb less than HS with a small MW. Since it was also shown earlier that GAC pores are mostly smaller than 2 nm and that the size of humic substances in F2 was likely to be more than 2 nm, GAC is not likely to adsorb fraction F2 well.

The external surface of GAC is much less present than on iron compounds (168 m^2/g compared to 286 and 360 m^2/g for AAFS and β-FeOOH respectively). Therefore, adsorption of bigger molecules on AAFS and β-FeOOH is more favoured than it was for F1. In addition to the size consideration, the enhanced adsorption is also due to the phenolic groups (more present on heavier MW fractions) not losing the protons as easily as the carboxylic groups. Illustration of this phenomenon is explained by the pK_a values corresponding to the dissociation of formic acid (carboxylic acid) and phenol according to equations 7.6 and 7.7 below (Φ represent the phenolic ring C_6H_5) (Tipping, 2002):

$$HCOOH \longleftrightarrow HCOO^- + H^+ \qquad pK_a = 3.8 \qquad (7.6)$$

$$\phi - OH \longleftrightarrow \phi - O^- + H^+ \qquad pK_a = 10.0 \qquad (7.7)$$

At pH 3.8, half of the carboxylic acid is dissociated and becoming more so as pH increases, whereas the pH needs to reach 10.0 to have half of the phenol dissociated. Therefore at pH 7, the carboxylic groups of HS are mostly ionised as hardly any phenolic groups are dissociated. Therefore, on the negative surface, less repulsion occurs as more phenolic groups are involved. Also, the adsorption of the high MW humic substances is more likely to result in a higher load since only part of the molecule can be adsorbed, leaving free sites for others but contributing to a high proportion of UV and DOC removal.

7.5.2 Model fitting for Fraction F2

Figures 7.8, 7.9 and 7.10 show the model fittings for fraction F2 (5-10 kDa) onto GAC, AAFS and β-FeOOH respectively. Corresponding parameters are shown in table 7.2.

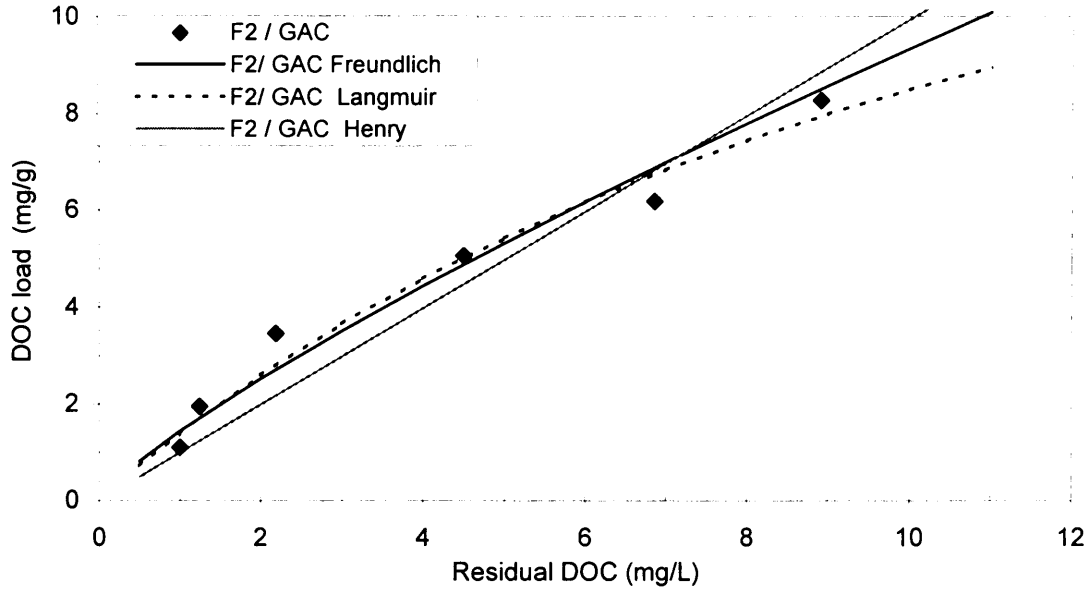

Figure 7.8 Fitting of adsorption models to experimental points for F2 on GAC.

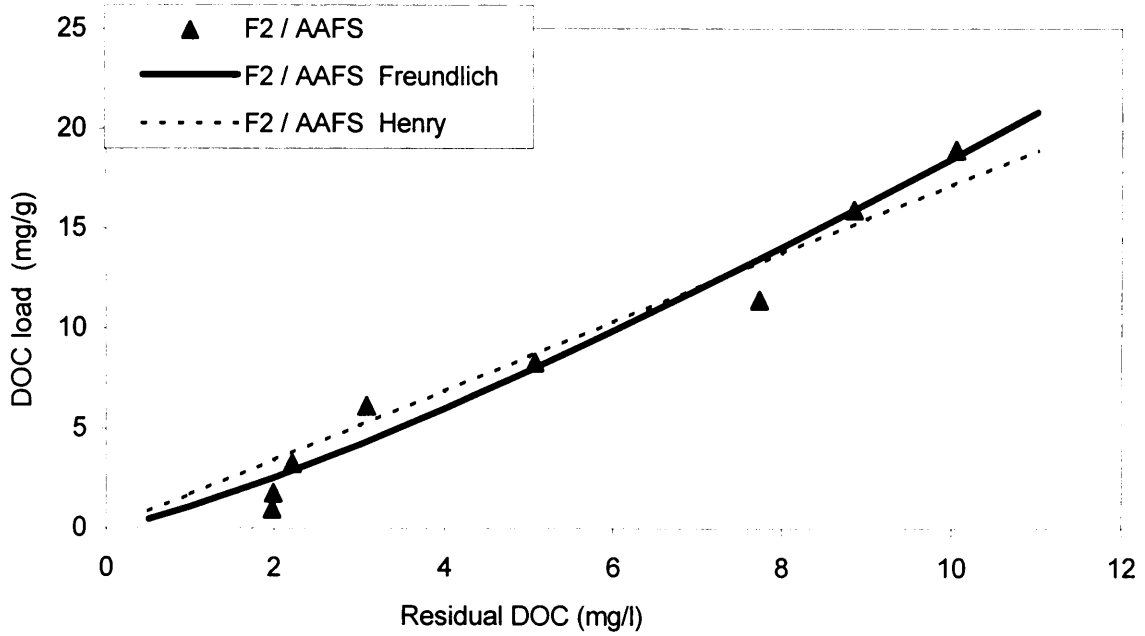

Figure 7.9 Fitting of adsorption models to experimental points for F2 on AAFS Langmuir model not applicable).

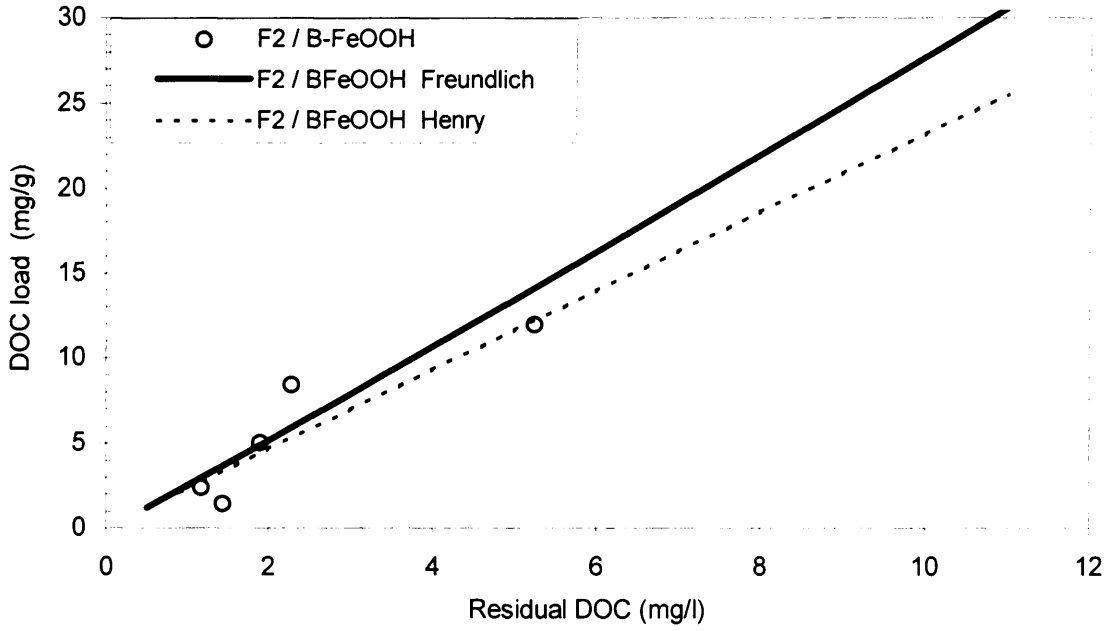

Figure 7.10 Fitting of adsorption models to experimental points for F2 on β-FeOOH (Langmuir model not applicable).

Table 7.2 Isotherm parameters for F2 on GAC, AAFS and β-FeOOH

F2		Freundlich model			Langmuir model		Henry model
Adsorbent	Initial DOC (mgL^{-1})	K_F ($mg\ g^{-1}$). ($mgL^{-1})^n$	1/n	Adsorption capacity ($mg\ g^{-1}$)	b ($L\ mg^{-1}$)	Q_{mon} ($mg\ g^{-1}$)	K_H ($L\ g^{-1}$)
GAC	11.25	1.44	0.81	5.66	0.08	19.57	0.9938
AAFS	10.93	1.08	1.23	7.18	<0	<0	1.7183
B-FeOOH	7.08	2.50	1.05	5.02	<0	<0	2.3221

(*) experimental load (DOC mg/g of adsorbent) after 96 hours, in experiments where the dose was of 1 g adsorbent/L

The three models, Langmuir, Freundlich and Henry can be applied successfully to GAC. However none of the models represent the complete range of data, which is likely to be due to additional surface creation (Teermann and Jekel, 1999) and a precipitation on the surface beyond adsorption phenomena (Tipping, 2002, Thomas and Crittenden, 1998). As for F1, a slight delay is observed and adsorption is obvious from a residual DOC of 0.7 mg/L.

On AAFS, the Langmuir model did not fit the experimental data while the Freundlich and Henry models were successfully applied. As for fraction F1, the adsorption delay (due to the non-adsorbable fraction) is not well represented by any of the models. The Freundlich model showed that it is the best model to describe the adsorption of fraction F2 and it can represent a complete range of MW if taking into account a non-adsorbable part of the humic substances, using the concept of fractionation into different adsorbabilities in the computer models (Fettig and Sontheimer, 1987c, Teermann and Jekel, 1999).

On β-FeOOH, results are very dispersed. On the range of DOC studied, Freundlich and Henry's model fitting are similar, but become distinct as the residual DOC increases. It is difficult to draw any conclusion as to which model is the best since the DOC range illustrated in figure 7.10 is small.

Comparing K_F and 1/n values for F1, it is clear that K_F decreases for GAC and the slope 1/n increases, indicating that the energy of adsorption is more uniform. On the iron compounds, K_F and the adsorption capacity increase. This indicates that adsorption is favourable on these adsorbents and the phenomenon takes place according to mechanisms (i) and (ii) in figure 7.7, involving both short and long range forces (Filius et al., 2000, Weber et al., 1991). On the other hand, 1/n approached unity which agrees with the fact that the Henry model could be applied, particularly for β-FeOOH.

7.6 Fraction F3 (10-50 kDa)

7.6.1 Isotherm for F3

Adsorption isotherms of fraction F3 are shown on figures 7.11 and 7.12, respectively for UV_{254} and DOC. The distinctions between GAC and the iron compounds are more obvious than for F2. Also, by comparing figures 7.2 to 7.11 and figures 7.3 to 7.12, the

adsorption tendencies between F1 and F3 seem to have reversed. The first region of the isotherm is sharp on AAFS, indicative of strong adsorption. On β-FeOOH, the isotherm is slightly convex for DOC and definitely concave for UV (figure 7.11). On GAC, the convex shape of the isotherm is very definite and indicates that adsorption is not favoured (Weber, 1972) due to little affinity between high MW humics and GAC.

As for F1 and F2, adsorption starts when the residual DOC is larger than 0.7 mg/L (between 0.5 and 1 mg/L). Since this delay does not appear when analysing UV residual (figure 7.11), the minimum DOC corresponds to non-UV absorbing organic matter, i.e. low MW humic substances. Hence, F3 also contains a non-adsorbable fraction although the MW is above 10 kDa. This is attributed to the experimental separation method which leaves some low MW in F3 since the membrane MWCO (Molecular Weight Cut Off) is actually a MW distribution.

As explained in the previous sections for F1 and F2, adsorption of humic substances on negative surfaces was attributed to specific interactions and non-coulombic forces (dispersive). Vermeer et al. (1998a) observed a strong affinity between humics and iron oxide at a pH as high as 9, but there again, the iron oxide surface was positive since the pH_{zpc} of the hematite was equal to 8.9. The load is not higher than for F2, although the initial DOC was higher (13.6 mg/L for F3 versus 10.9 and 7.1 mg/L for F2, on AAFS and β-FeOOH respectively). The load of F3 on the iron compounds reached a maximum of 7 mg/g when it was above 10-15 mg/g for F2. The adsorption schemes suggested in figure 7.7 remain valid as the MW increases. In particular, situation (ii) in figure 7.7 justifies a decrease in the load when high MW molecules occupy several adsorption sites.

On the other hand, DOC load on GAC is low in the three regions of adsorption (below 4 mg/g) which is explained by its microporosity. Most of the GAC structure is advanced and porous compared to the iron compounds. Inaccessibility to sites was justified for F2, and it becomes more valid as the MW increases. Since MW above 10 kDa are expected to be around 4 nm, they cannot access any of the GAC pores since the adsorption process is based on diffusion of HS molecules and only very little external surface is available for their adsorption.

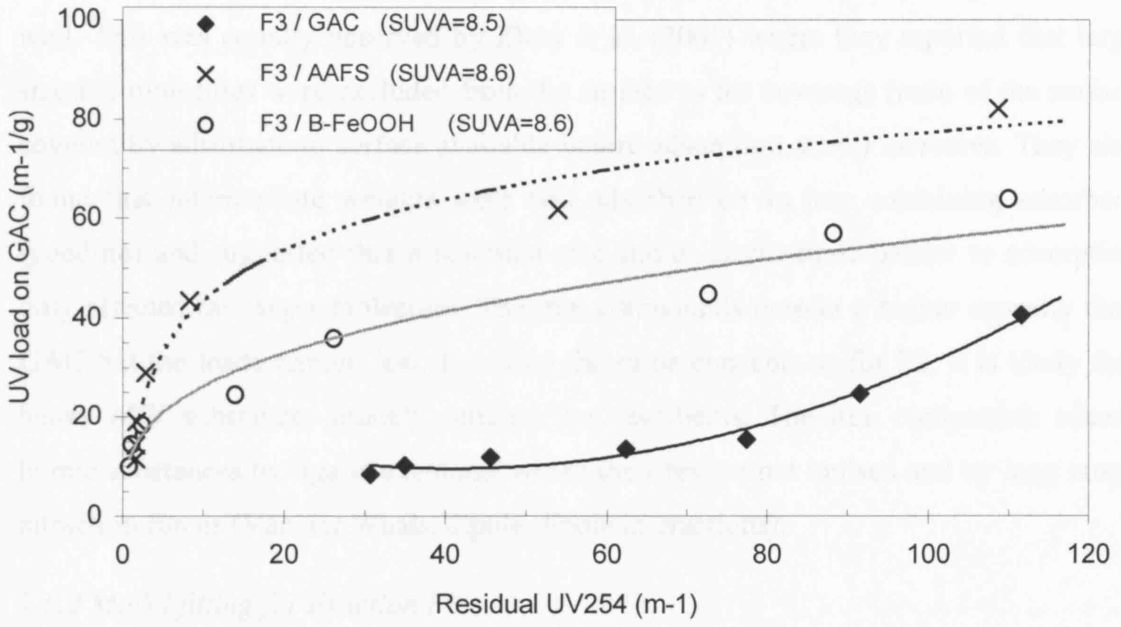

Figure 7.11 Adsorption of F3 on the GAC, AAFS and β-FeOOH, for UV_{254}. (experimental points and trendlines).

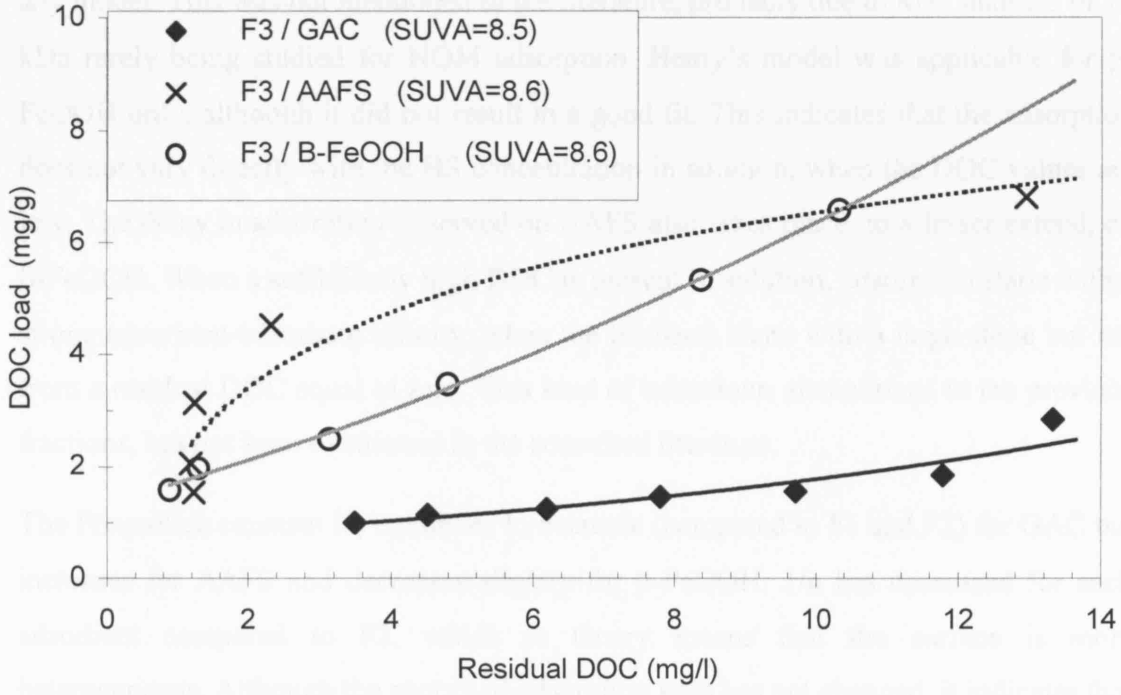

Figure 7.12 Adsorption of F3 on the GAC, AAFS and β-FeOOH, for DOC. (experimental points and trendlines).

To summarise F3 adsorption, none of the media studied adsorbs the very heavy MW well. This was equally observed by Zhou et al. (2001) where they reported that large size HS molecules were excluded from the surface as the coverage (ratio of the surface covered by adsorbate to surface available before adsorption starts) increases. They also found that intermediate weights were best adsorbed on an iron containing adsorbent (goethite) and suggested that a potential size and/or electrostatic barrier to adsorption only affected the larger molecules. The iron compounds present a higher capacity than GAC but the loads remain low. By using the same concepts as for F2, it is likely that heavy MW substances quickly saturate the adsorbents. The iron compounds adsorb humic substances by ligand exchange where the sites are not ionised and by long range attraction forces (Van der Waals, dipole-dipole interactions).

7.6.2 Model fitting for Fraction F3

Figures 7.13, 7.14 and 7.15 show the fitting of adsorption models for adsorption of F3 onto GAC, AAFS and β-FeOOH respectively and parameters values are also shown in table 7.3. The Langmuir and Freundlich models represent well the adsorption. However, as observed in the previous fractions, the delay on AAFS cannot be properly handled by any model. This was not mentioned in the literature, probably due to MW above 5 or 10 kDa rarely being studied for NOM adsorption. Henry's model was applicable for β-FeOOH only, although it did not result in a good fit. This indicates that the adsorption does not vary directly with the HS concentration in solution, when the DOC values are low. The delay in adsorption observed on AAFS also takes place, to a lesser extend, on β-FeOOH. When a sufficiently high DOC is present in solution, adsorption starts with a strong adsorbent-adsorbate affinity, when the isotherm starts with a large slope but not from a residual DOC equal to zero. This kind of behaviour, also noticed in the previous fractions, has not been mentioned in the consulted literature.

The Freundlich constant K_F continues to decrease (compared to F1 and F2) for GAC but increases for AAFS and decreases slightly for β-FeOOH. 1/n has decreased for each adsorbent compared to F2, which in theory means that the surface is more heterogeneous. Although the energy of adsorption sites has not changed, it indicates that as the MW increases, the energy of adsorption seems to become a parameter of less importance. This is likely to be due to the effect represented on figure 7.7, insisting on the increasing importance of long distance forces with the MW. For example for AAFS,

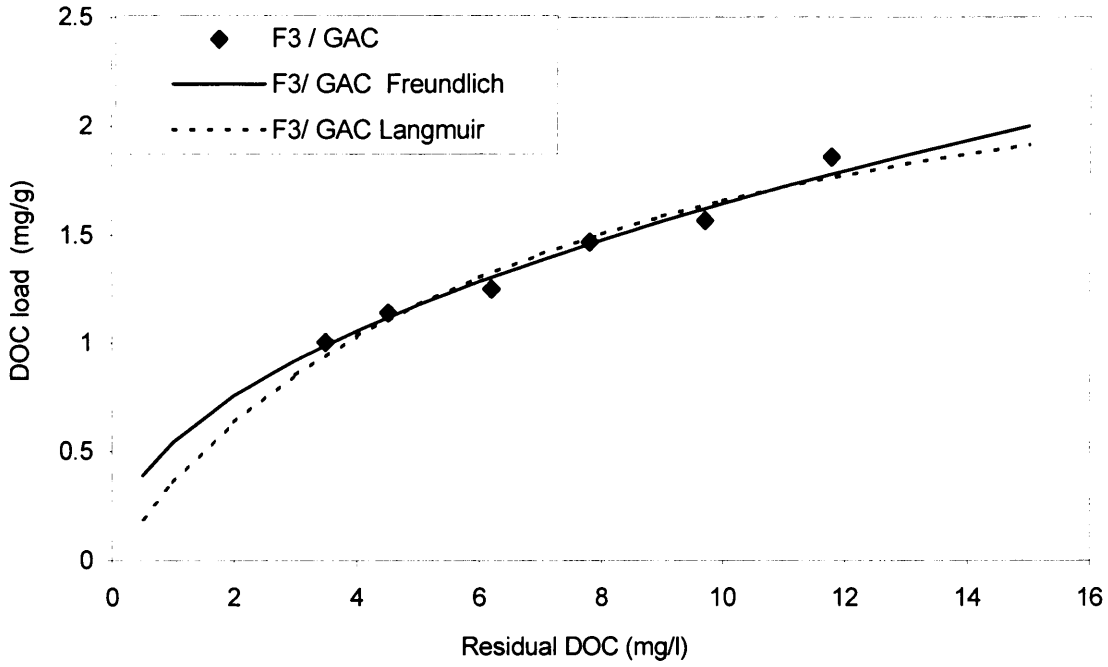

Figure 7.13 Fitting of adsorption models to experimental points for F3 on GAC (Henry not applicable).

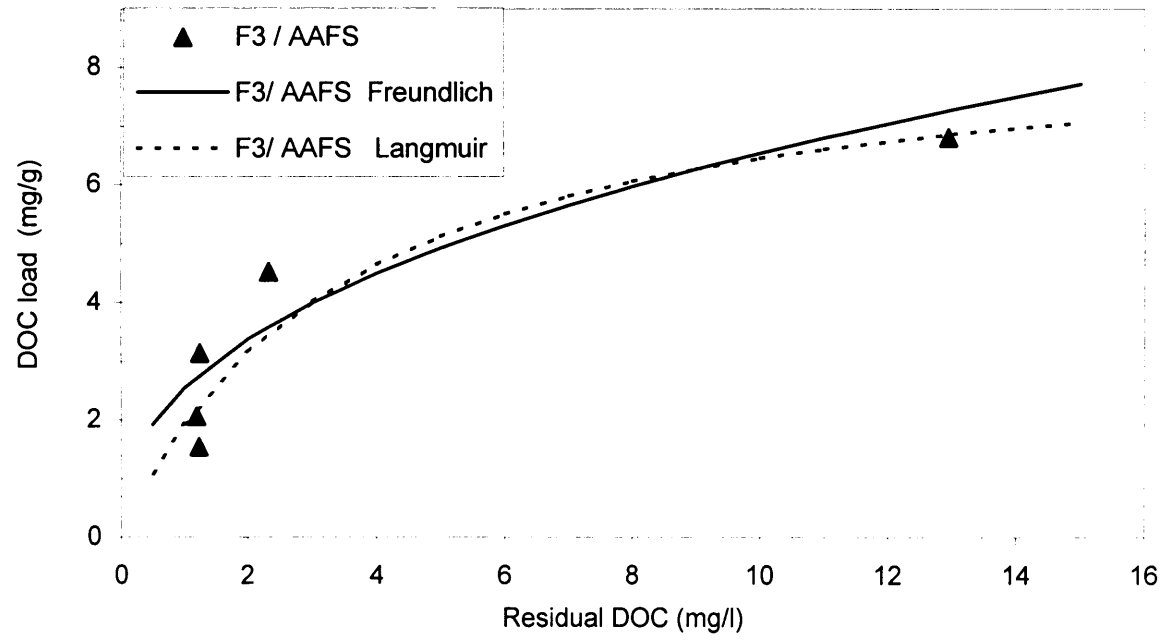

Figure 7.14 Fitting of adsorption models to experimental points for F3 on AAFS (Henry not applicable).

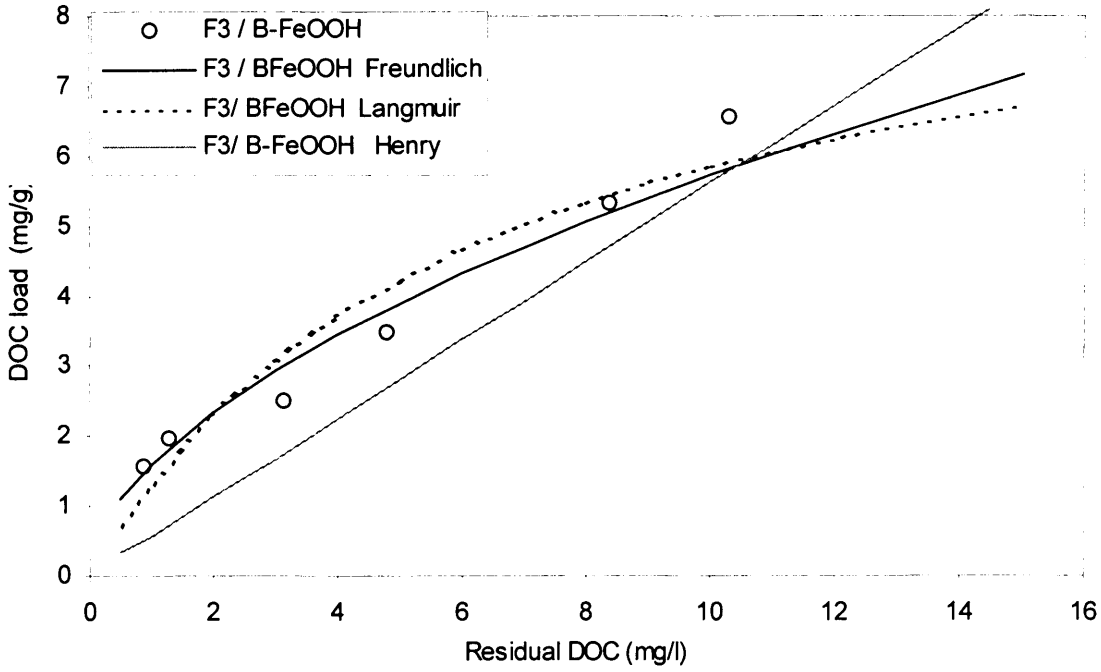

Figure 7.15 Fitting of adsorption models to experimental points for F3 on β-FeOOH

Table 7.3 Isotherm parameters for F3 on GAC, AAFS and β-FeOOH

F3		Freundlich model			Langmuir model		Henry model
Adsorbent	Initial DOC (mgL^{-1})	K_F ($mg\ g^{-1}$). ($mgL^{-1})^n$	1/n	Adsorption capacity ($mg\ g^{-1}$)	b ($L\ mg^{-1}$)	Q_{mon} ($mg\ g^{-1}$)	K_H
GAC	13.65	0.54	0.48	1.86	0.15	2.77	n.a.
AAFS	13.61	2.55	0.41	5.45	0.29	8.71	n.a.
β-FeOOH	13.61	1.60	0.55	4.64	0.16	9.56	0.6651

(*) experimental load (DOC mg/g of adsorbent) after 96 hours, in experiments where the dose was of 1 g adsorbent/L

1/n is 0.41 compared to 1.23 for F2. It shows that as residual DOC increases by 100%, the load increases by 41% (123% for F2) and a high concentration of HS molecules needs to compress the layer around the adsorbent grains for adsorption to occur and Van der Waals forces to become more significant. Ligand exchange takes place close to the surface and long range forces dominate when the surface high energy sites (chemical or electrostatic adsorption, Weber et al., 1991) are occupied.

This also agrees with De Laat and van der Heuvel (1995) who worked out that during polyelectrolyte adsorption, an electrostatic barrier retarded adsorption, depending on the salt concentration and on the polyelectrolyte MW. They concluded that the intermediate MW would adsorb better than high MW as is observed here (comparing adsorption capacities of F2 and F3). This is confirmed by adsorption capacity values, higher for F2 than for F3 and for each adsorbent.

The precipitation of humic substances on the iron compounds is supported by the value of Q_{mon} for the Langmuir model, being larger for β-FeOOH and AAFS than for GAC. In these experiments, no distinction is made between precipitation and adsorption since only the residual DOC is measured and the difference between this and the initial DOC is considered as adsorbed. However, since Henry's model does not apply for GAC and AAFS and does not give good results for β-FeOOH, it is likely that adsorption is not the only phenomenon taking place. Precipitation or association of the adsorbate close to the adsorbent surface is possible but must be preceded by adsorption to generate the high surface or interface concentration (Weber et al., 1991).

7.7 Solution F123 (0-50 kDa)

7.7.1 Isotherm for F123

Solution F123 has not been fractionated and therefore covers the humic substances MW from 0 to 50 kDa. Figures 7.16 and 7.17 show the adsorption isotherms of F123 adsorption on GAC, AAFS and β-FeOOH, respectively for UV_{254} and DOC. SUVA values of F123 are around 9, very close to SUVA values of fraction F3 that was 8.6. Consequently, it is expected that F123 will exert a similar adsorption to F3.

By comparing figures 7.12 and 7.17, trends are effectively similar in the first and second regions (between 0 and 3 and 3 and 6 mg/L of residual DOC mg/L respectively)

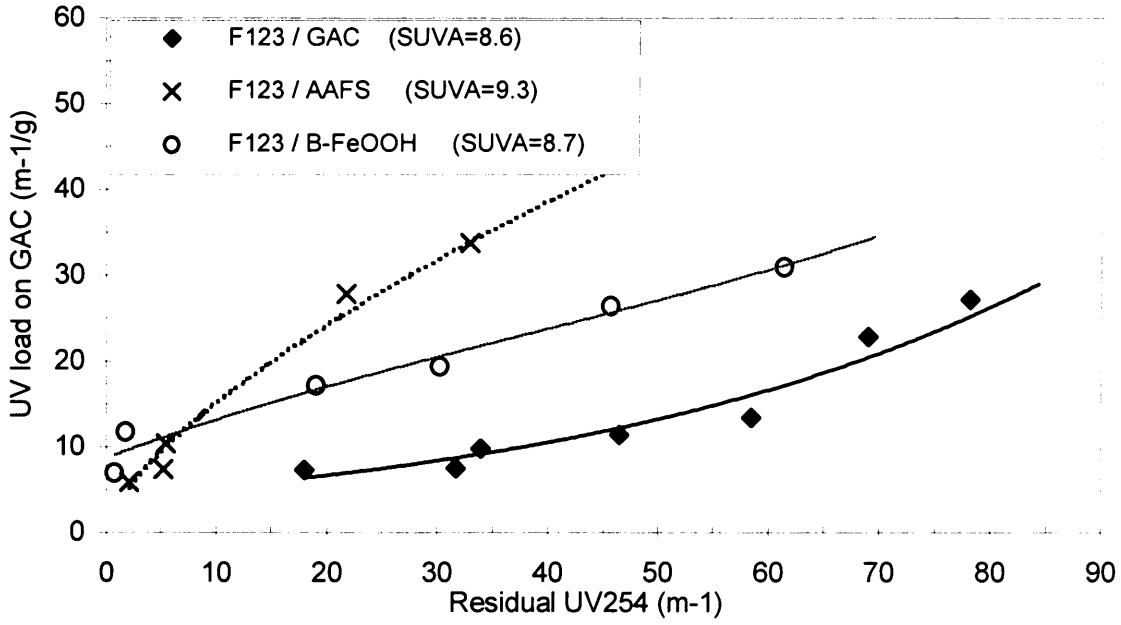

Figure 7.16 Adsorption of F123 on the GAC, AAFS and β-FeOOH, for UV_{254}. (experimental points and trendlines).

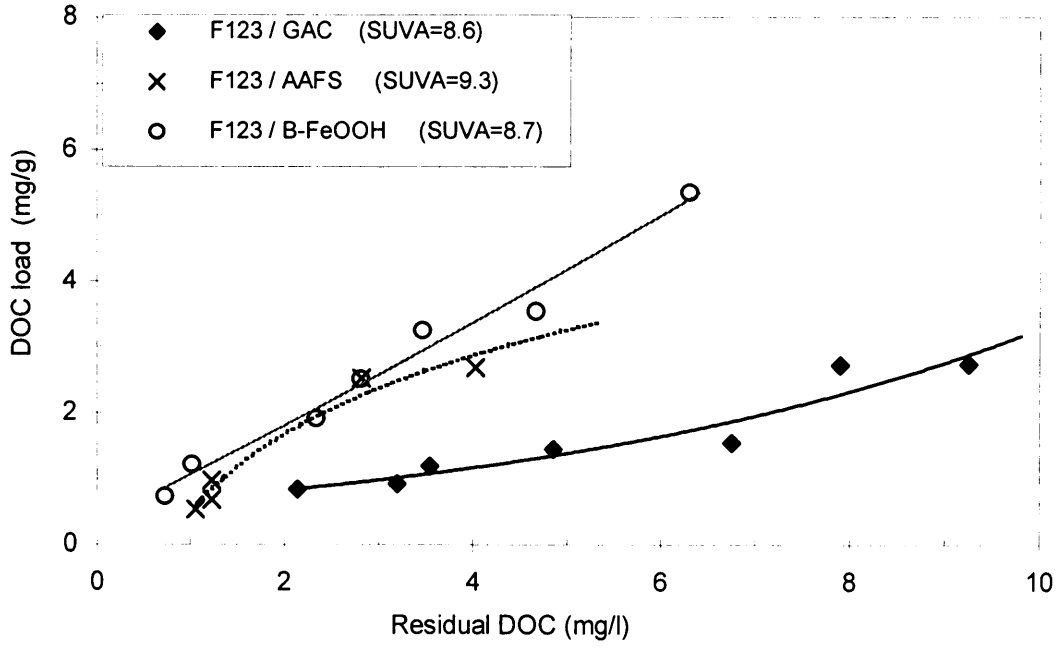

Figure 7.17 Adsorption of F123 on the GAC, AAFS and β-FeOOH, for DOC (experimental points and trendlines).

of the isotherms. However, two features are distinctive; (i) the later region of adsorption (beyond 6 mg/L of residual DOC) on GAC and (ii) the loads achieved on AAFS and β-FeOOH.

On GAC, the load increases faster than it did for F3 on the same range of residual DOC, as well as for the UV isotherm. At low residual DOC, the isotherm shape is similar to F3 showing very little adsorption. As the residual DOC increases, F123 appears to adsorb more than F3. The difference is due to the intermediate and low MW which strengthens the idea that the lower the MW, the better the adsorption on GAC.

As for AAFS and β-FeOOH, the isotherm shapes are similar to the isotherms for adsorption of fraction F3 (figure 7.12). The loads are slightly less on AAFS and slightly more on β-FeOOH. It can be concluded that F123 behaves like F3. Therefore, the very heavy MW (above 10 kDa) occupy the adsorption sites or displace the lighter MW initially adsorbed. Competition and displacement have been mentioned by several authors; Fettig (1999a) found an adsorptive fractionation of Natural Organic Matter on the basis of molecular size; Gu et al. (1996 a, b) compared the adsorption of Suwanee River fulvic acids to lower MW organic acids (phtalic and salicylic acids) and concluded that NOM displaced weakly bound adsorbate when adsorption sites were limited. The steric arrangement of heavy MW molecules makes difficult the binding by interaction between iron oxide and functional groups of HS. Consequently, long range forces are involved for high loads of organic matter on the adsorbents.

7.7.2. Model fitting for Solution F123

Figures 7.18, 7.19 and 7.20 show the fitting of various adsorption models for the adsorption of the complete solution of humic substances (F123, mixture of F1, F2 and F3) on GAC, AAFS and β-FeOOH respectively. Corresponding parameters are shown in table 7.4.

The three models represent well the adsorption on GAC in the low residual range of DOC, but not as well in the higher range. On the iron compounds, Henry's model represents well the adsorption data on only a very narrow range of residual DOC. Vermeer et al. (1998a) investigated the adsorption of Aldrich Humic Substances on hematite; the average MW was 23 kDa. Good adsorption was obtained. This was attributed to a larger initial DOC (24.2 mg/L), probably related to a high pH_{zpc} (8.5

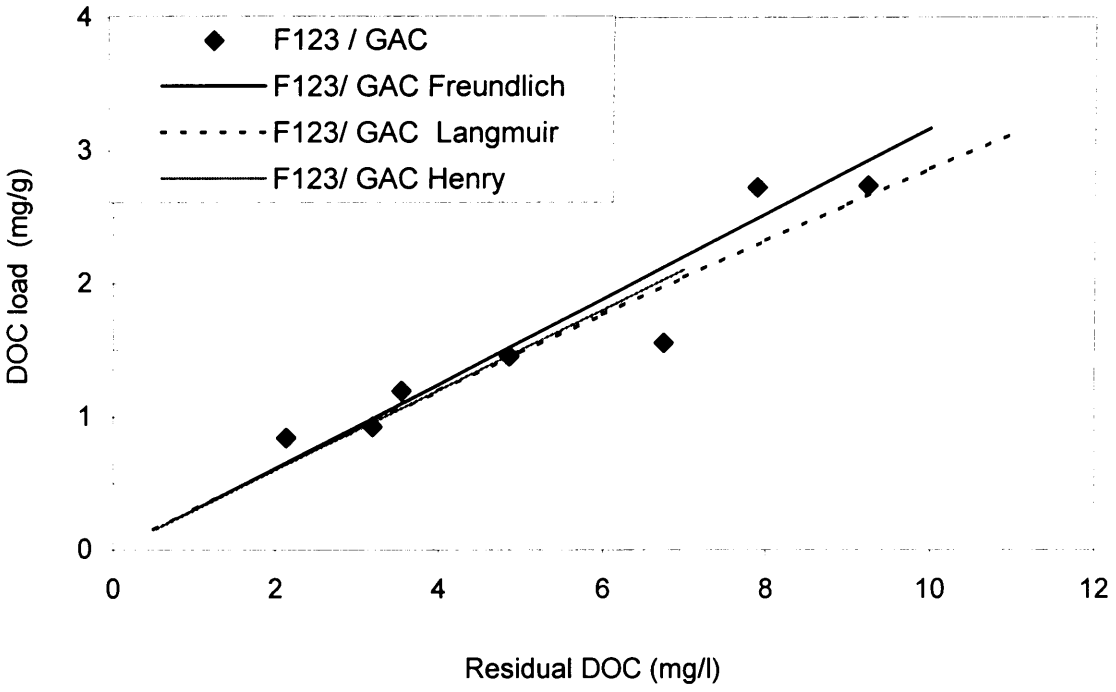

Figure 7.18 Fitting of adsorption models to experimental points for F123 on GAC.

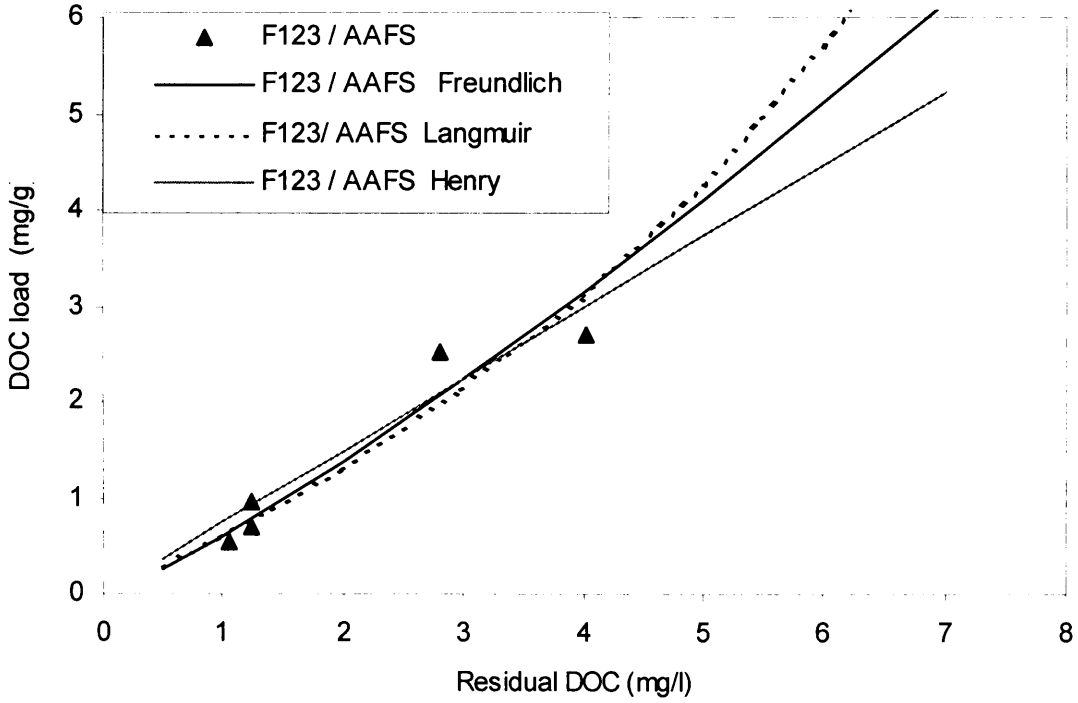

Figure 7.19 Fitting of adsorption models to experimental points for F123 on AAFS (Langmuir shown although b and Q_{mon} <0).

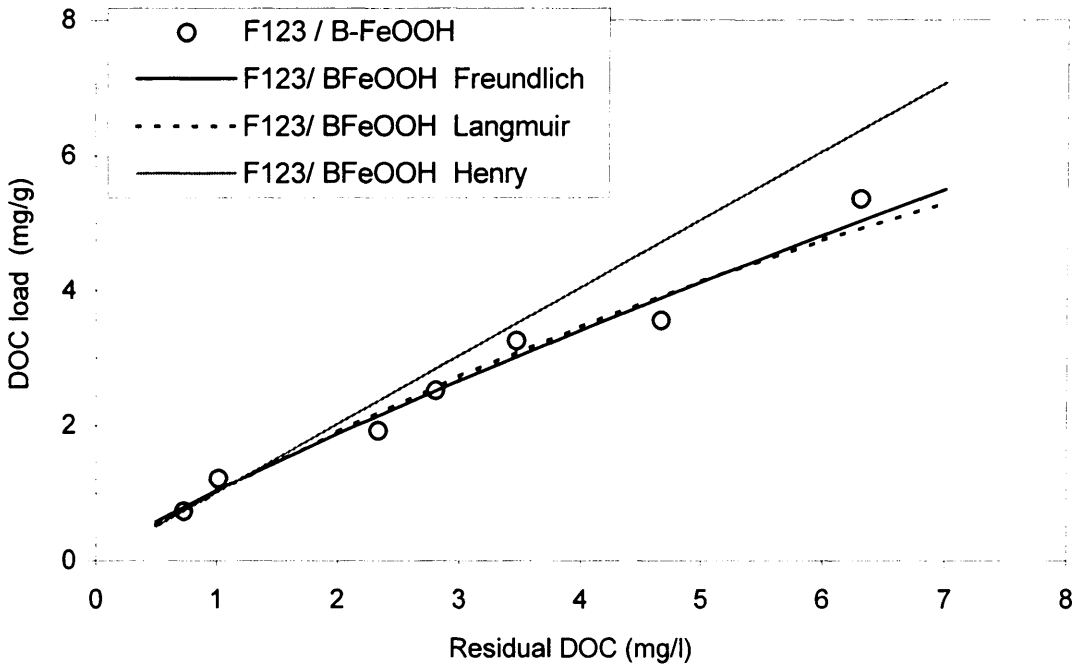

Figure 7.20 Fitting of adsorption models to experimental points for F123 on β-FeOOH.

Table 7.4 Isotherm parameters for F123 on GAC, AAFS and β-FeOOH

F123		The Freundlich model			The Langmuir model		The Henry model
Adsorbent	Initial DOC (mgL^{-1})	K_F ($mg\ g^{-1}$). ($mgL^{-1})^n$	1/n	Adsorption capacity ($mg\ g^{-1}$)	b ($L\ mg^{-1}$)	Q_{mon} ($mg\ g^{-1}$)	K_H
GAC	10.64	0.30	1.02	2.72	0.007	41.49	0.30
AAFS	5.43	0.60	1.20	2.75	<0	<0	0.75
β-FeOOH	8.44	1.04	0.86	3.49	0.06	18.18	1.01

(*) experimental load (DOC mg/g of adsorbent) after 96 hours, in experiments where the dose was of 1 g adsorbent/L

approximately) and to a higher salt concentration. The latter was 0.01 M, however it was KNO_3 and not calcium. It is likely that by using calcium, the adsorption would have increased to a value still higher than 40 mg/g at a residual concentration of 10 mg DOC/L. This value is close to the value obtained by Teermann and Jekel (1999). This tends to confirm that the high pH_{zpc} is favourable for high adsorption capacity.

K_F values decreased for the iron adsorbents when compared to K_F for F2 and F3. This means that the role played by fraction F1 (very low adsorbability on these adsorbents, with K_F almost equal to zero) is not negligible in F123, although the SUVA value was close to SUVA for fraction F3. For adsorption on GAC, K_F is at its lowest and competition between initially adsorbed low MW and higher MW is taking place. Heavier MW have been shown to displace adsorbed light MW (Gu et al. 1996b). At high residual DOC (beyond 5 mg/L), the load is only 1.5 mg/g approximately whereas it was 14 mg/g for F1. It also shows that the heavy MW are largely represented in F123 and do not have an opportunity to find a suitable surface for adsorbing on GAC. The load increases faster as the residual DOC increases, which can also be attributed to the adsorbed substances generating additional surface for adsorption. Increase of surface can also be attributed to calcium humates/fulvates surface precipitation (Teerman and Jekel, 1999). Heavy MW find some meso or macroporous surface to adsorb onto. This was already observed by Vermeer et al. (1998b). They described a fractionation of the HS upon adsorption, the larger MW remaining on the adsorbent and the smaller remaining in solution.

This would happen particularly at the surface of a non-microporous adsorbent as is β-FeOOH. Teerman and Jekel's findings (1999) actually strengthened this point when they modelled the adsorption of HS onto β-FeOOH using IAST. They imposed 1/n value to be 0.15 and it was necessary to make K_F vary over a large range, from 0 (non-adsorbable) to 300 (very adsorbable) to fit the experimental data.

From table 7.4, 1/n values are close to 1, indicating a narrow distribution of the energy of adsorption of F123 on the three media and the surface is quasi-homogeneous towards solution F123. Q_{mon} on GAC is also higher than on β-FeOOH although the external surface on GAC is quasi non-existent. This seems to confirm that additional surface for adsorption is generated. On the other hand, and for all adsorbents, K_F and K_H are almost equal, which correspond to 1/n being close to 1. This means that the isotherm is linear and appropriate for situations where adsorption increases with the concentration when

the load is low (Weber et al., 1991). Agreement between the Freundlich and the Henry models is observed up to approximately 6 mg DOC/L. Beyond this value, the phenomenon of adsorption is not the only one to occur and it is suggested that the adsorbent grains act as a core onto which the humic substances concentrate under hydrophobic characteristics.

7.8 Comparisons of model parameters between F1, F2, F3 and F123

The parameters estimated for Freundlich, Langmuir and Henry models are represented respectively in figures 7.21, 7.22 and 7.23. The Freundlich model, which allows for a distribution of energy of adsorption, is the only model applicable to each system adsorbent/adsorbate system. The adsorbents are most likely to present a heterogeneous surface, viz. a high tortuosity in GAC, and uneven distribution of the local charges on the iron compounds. In addition, variations of natural organic matter in weight and organic functions is expected to adsorb with different energies. These two aspects justify the applicability of the Freundlich model. However, from figure 7.21, heterogeneity of the surface becomes less obvious as the MW increases and the adsorption energy is then more uniform (1/n is closer to 1). The possibility of using K_F as an indicator of adsorption capacity is confirmed with both parameters following similar trends (units are different). It is also clear that the presence of F1 influences the behaviour of F123 (see figures 7.21a and 7.21c). Figure 7.21c shows the adsorption capacity compared to the original DOC measured by the control. The affinity of F1 for GAC becomes clear when observing the small difference between the original DOC and the adsorption capacity. For β-FeOOH, the very large difference indicates the low affinity of F1 for this iron compound.

From figure 7.22, the Langmuir model is generally not suitable, hence the confirmation that adsorption of humic substances requires a heterogeneous surface with a distribution of sites energy. F1 is particularly refractory to such a model, which is probably due to being the closest in MW to the non-adsorbable fraction (very low MW).

The Henry model applies to most cases and broadly follows the trend of the Freundlich model (see figure 7.23). F2 shows regular behaviour on each adsorbent and the influence of F1 and F3 appears in the K_H values for F123.

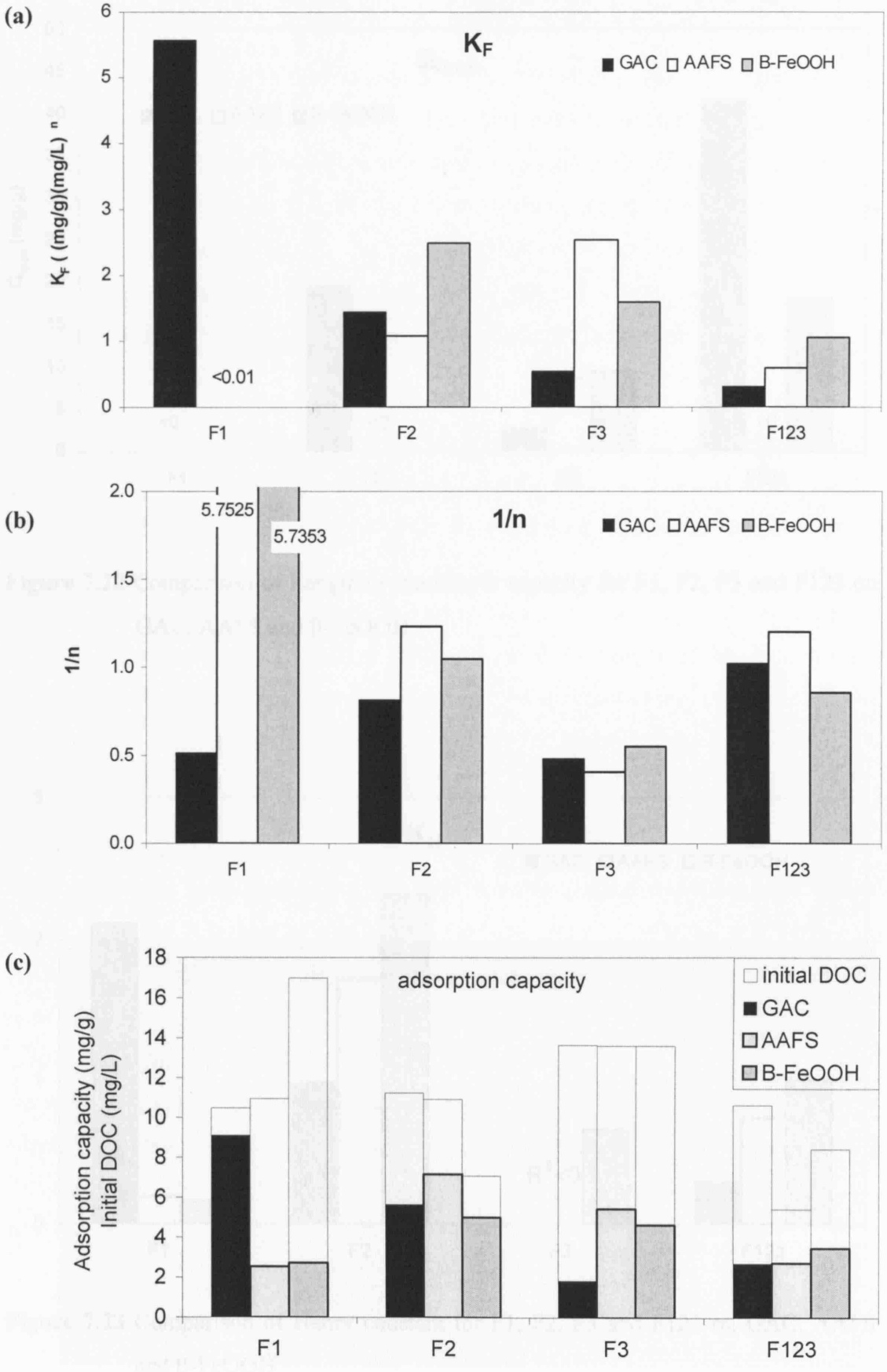

Figure 7.21 Comparison of Freundlich parameters for F1, F2, F3 and F123 on GAC, AAFS and β-FeOOH: **(a)** K_F, **(b)** 1/n and **(c)** adsorption capacity

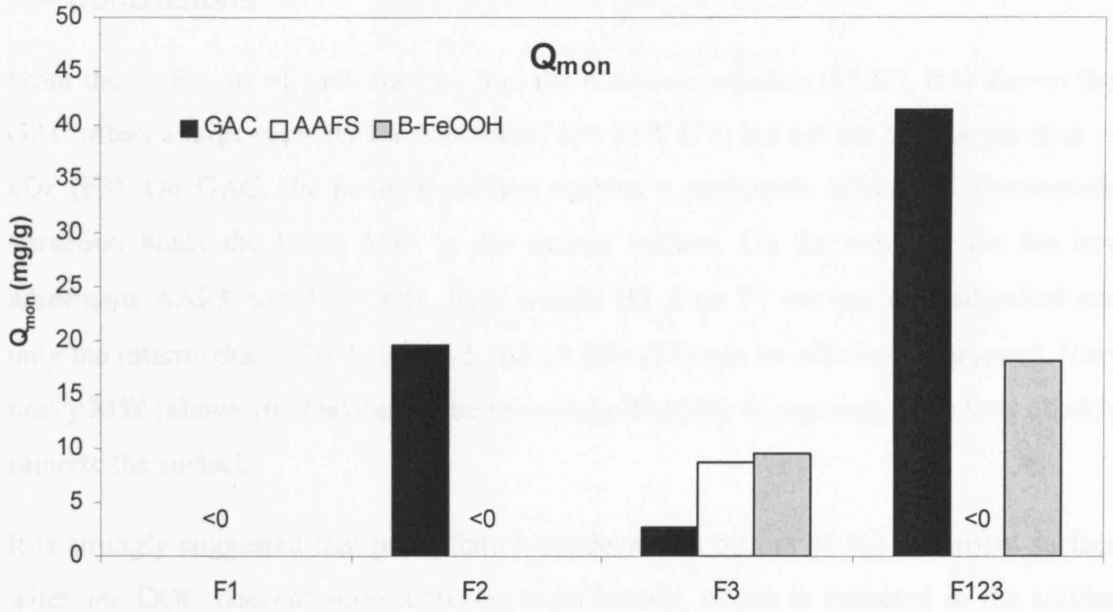

Figure 7.22 Comparison of Langmuir monolayer capacity for F1, F2, F3 and F123 on GAC, AAFS and β-FeOOH

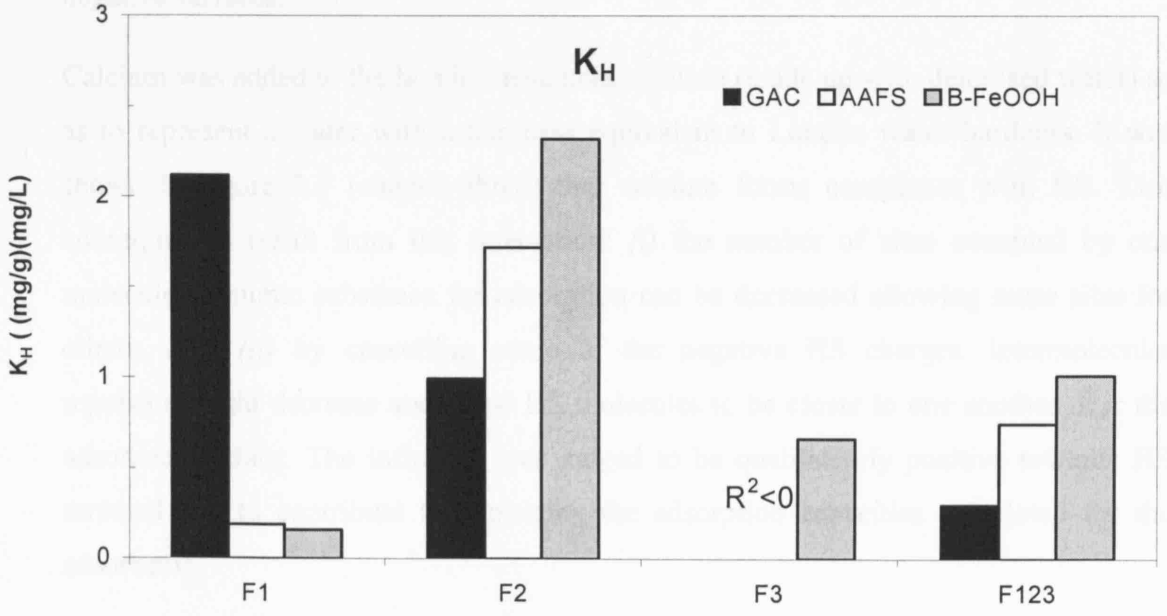

Figure 7.23 Comparison of Henry constant for F1, F2, F3 and F123 on GAC, AAFS and β-FeOOH

7.9 Conclusions

From the isotherms of each fraction and the complete solution (F123), it is shown that GAC offers a large capacity for removal of low MW (F1) but not for MW larger than 10 kDa (F3). On GAC, the positive surface enables a coulombic effect and electrostatic attraction binds the lower MW to the carbon surface. On the contrary for the iron adsorbents AAFS and β-FeOOH, light weight HS from F1 are not well adsorbed and only the intermediate MW between 5 and 10 kDa (F2) can be efficiently removed. Very heavy MW (above 10 kDa) cannot be removed efficiently in any case since they quickly saturate the surface.

It is strongly suggested that precipitation/condensation occurs on the adsorbent surface when the DOC concentration increases significantly, which is reflected in the sudden sharp increase of the load in most cases. On the other hand, a recurrent characteristic of the adsorbents mentioned in the literature, and that which presented a higher adsorption capacity, was the pH_{zpc}, being higher (8-9) than the values measured in this study (5-5.5 for the iron compounds). The large difference in these ranges of pH_{zpc} is not yet explained and remains for future investigations. As a consequence, coulombic forces that enable a high and strong adsorption are not the main driving force due to the negative surfaces.

Calcium was added to the humic substances solution (made up with deionised water) so as to represent a water with a hardness equivalent to London water hardness. It was shown in figure 3.1 (chapter three) that calcium forms complexes with HS. Two consequences result from this interaction: *(i)* the number of sites occupied by one molecule of humic substance for adsorption can be decreased allowing more sites for others. And *(ii)* by cancelling some of the negative HS charges, intermolecular repulsion might decrease and allow HS molecules to be closer to one another near the adsorbent surface. The influence was judged to be qualitatively positive towards HS removal and to contribute to increasing the adsorption capacities calculated for the adsorbents.

As regards modelling the adsorption equilibrium, the Freundlich model fitted each adsorbent/adsorbate system. The delay in adsorption shows that in order to observe a load onto the adsorbents, residual DOC must be large. This is a constant feature of the adsorption study, due to a non-adsorbable fraction with very low MW and it cannot be well represented by any model. The Langmuir model fitted in a minority of cases and was applicable in the second region of adsorption (i.e. neither for low or high coverage). The Henry model was applicable in most cases in the low range of concentration.

CHAPTER 8

COLUMN STUDIES

8.1 Introduction

Equilibrium data from batch experiments provided valuable information regarding the adsorption of humic substances on GAC, AAFS and β–FeOOH. However, for further applications on a larger scale, such data need to be transferred onto a continuous flow process. Water treatment works and industries, apart from small units, usually operate on a continuous flow basis and the batch tanks are replaced by columns, filled with the adsorbent. Batch data can be difficult to use for columns since the adsorbent-adsorbate system is not in equilibrium (Lee et al., 2000).

Therefore, additional studies must be carried out so as to design the column for optimal operation. For this purpose, breakthrough curves are obtained from the column studies and are presented in this chapter. They show the adsorption behaviour in non-equilibrium state under the conditions described previously (see chapter four). Solutions F1 (HS<5 kDa), F12 (HS<10 kDa) and F123 (HS<50 kDa) are adsorbed on each adsorbent. Each experiment was carried out in duplicate. However, only very few results have yet been published in the literature regarding the removal of humic substances using a continuous adsorption process. This might be due to the difficulty in producing large quantities of "controlled" aquatic humic substances of low MW, suitable for column studies.

Breakthrough curves can also be modelled for the purpose of prediction of the results and to enable the design of the columns. Two analytical models of the adsorption processes are mostly used in the literature, namely *(i)* the Thomas equation and *(ii)* the Bed Depth Service Time (BDST) model (Aksu and Gönen, 2004, Chu, 2004, Al-Ghouti, 2004). Both models have been described earlier in chapter 3. However, limitations of these models must be kept in mind, particularly, in the application of the

Thomas equation which considers that chemical kinetics (pseudo-second order) limit the adsorption rate, hence limiting the optimum application to a system where diffusion transport is not limiting the process. BDST allows the prediction of adsorption when the flow or the influent concentration changes, but also neglects to consider the possible limiting rate by diffusion (Ko et al., 2000).

The first section of this chapter investigates the influence of the column depth since the smaller the column, the faster the breakthrough and the shorter the experiments. Therefore, it was of interest to reduce the size of the column down to a diameter still representative from the hydrodynamic aspect, considering that too small a diameter, compared to the column length and the size of the adsorbent grains, might lead to a short circuit in the column.

The second section examines the quality of the effluent treated through a column of GAC, AAFS or β-FeOOH. In turn, the influents are fraction F1, then solution F12 (fraction F1 plus F2) and finally solution F123 (fraction F1 plus F2 and F3). UV_{254}, DOC and SUVA of the effluent are presented and analysed.

Finally the analytical models, the Thomas equation and the Bed Depth Service Time, are applied and the results are discussed.

8.2 Effect of column diameter

Hydrodynamics in the column must be considered so as to avoid any short-circuit, which would decrease the Hydraulic Residence Time (HRT) of the humic substances solution (hence the contact time adsorbent-adsorbate) and would use the media unevenly. It is also of interest for bench experiments to reduce the size of the column so as to decrease both time and cost of experiments, especially given the difficulties involved in the separation of the various fractions of the humic substances.

Columns of 5 cm diameter were initially used for adsorption of solution F123. The design parameters (flow rate, diameter, depth) satisfied criteria to avoid any wall effect. However, supply of sufficient quantities of fractionated F123 (F1 particularly) could not be satisfied for these conditions. Therefore, it was decided to use smaller columns (called "microcolumns" vs "large column" for above) to study the adsorption of lower MW. These microcolumns have been proved to give very good results in different

contexts. For example, Al-Ghouti (2004) used columns with an internal diameter from 2.25 mm to 4.95 mm to study dye adsorption. "Minicolumns" have also been used successfully by Fettig and Sontheimer (1987a,b,c) to estimate diffusion coefficients. Li et al. (2003) also suggested that the microcolumn technique could satisfactorily simulate the bed performance for large columns.

In this study, the adsorbent used was GAC, since GAC has the largest grain size compared to AAFS and β-FeOOH. Therefore, should any channelling effect be observed, it should take place with GAC. It is assumed that if such phenomenon does not occur on GAC, then it will not occur on the iron containing adsorbents either. The new diameter and bed depth were 1 cm and 10 cm respectively. The flow rate was decreased and the velocity was 38 cm/h against 76 cm/h for the large column. The new EBCT was 16 minutes. The behaviour of both columns is shown in figure 8.1.

The higher flow rate in the bigger column should decrease the resistance to mass transfer as observed by Lee et al. (2000) and by Aksu and Gönen (2004). Consequently, adsorption would be expected to be higher and the residual UV_{254} lower. In addition, dimension criteria to avoid wall effect was not achieved in the small column. It was therefore expected to have some channelling effects at the wall, resulting in shorter contact time between the adsorbate and the adsorbent and in a higher UV absorbance of the effluent. From figure 8.1, the longer the time, the larger the difference between the microcolumn and the large column results. The large column gives slightly higher residual UV absorbance in the effluent. However, the difference between the results with the micro- and the large column is 5.6% after 60 hours. Since most results are obtained before 60 hours for fraction F1, the difference is considered as acceptable for comparing the results of fraction F1 with the results of solutions F12 and F123. Hence, up to 60 hours, channelling is unlikely and adsorption extent is not reduced in the microcolumn.

From these observations, it was concluded that the column studies could be carried out on the smaller column and would be comparable to the adsorption of F12 and F123 on the bigger columns.

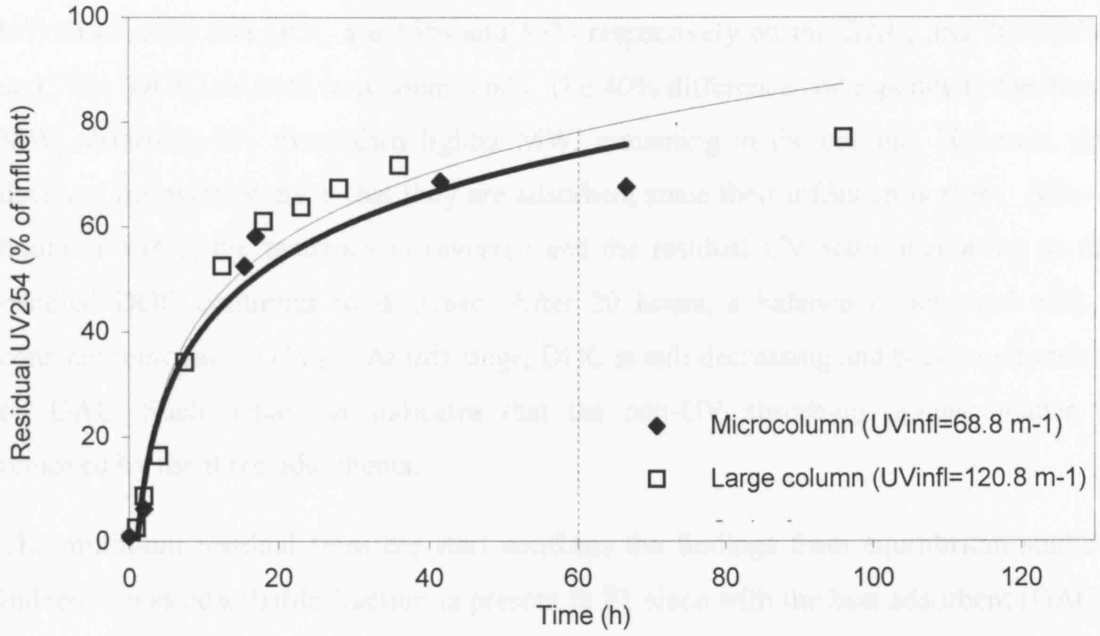

Figure 8.1 Adsorption results of F123 adsorption compared on 2 different size columns (adsorbent was GAC)

8.3 Analysis of the effluent quality: UV absorbance, DOC and SUVA value

8.3.1 Fraction F1 (0-5 kDa)

The experiments for this fraction were carried out in the microcolumns. The DOC of F1 was between 6 and 7 mg/L and SUVA was between 3 and 4. Figures 8.2 and 8.3 show the percentage removal of UV_{254} and DOC respectively.

Although only few data are available for the removal of fraction F1 on AAFS and β-FeOOH, it appears that at the start, the removal trends are different for UV and DOC. This gives important evidence of the misleading effect of using UV absorbance as a surrogate for DOC. Such an assumption is often done for reasons of simplicity (UV absorbance is quick and easy to measure compared to DOC, particularly for on-line and logged data). In 1996(a), Gu et al. confirmed this by writing "that estimates of NOM adsorption determined by UV absorbance spectrometry were about 15-100% greater than estimates determined by TOC analysis".

The breakthrough is observed on GAC after 90 hours. However over the range studied, breakthrough is not recorded for the iron compounds. During the first 5 hours, residual

UV absorbance and DOC are 15% and 55% respectively on the GAC, and 30% (UV) and 70% (DOC) on both iron compounds. The 40% difference corresponds to the heavy MW, absorbing UV more than lighter MW, remaining in the column. However, this does not necessarily mean that they are adsorbed, since their diffusion is slow. After 5 hours on GAC, the tendency is reversed and the residual UV starts increasing as the residual DOC continues to decrease. After 20 hours, a balance is achieved with a constant removal for UV_{254}. At this stage, DOC is still decreasing and becomes constant on GAC. Such behaviour indicates that the non-UV absorbing organic matter is removed by the three adsorbents.

The minimum residual from the start confirms the findings from equilibrium studies. Indeed, a non-adsorbable fraction is present in F1 since with the best adsorbent (GAC), 25-30% of DOC and 10-15% of UV_{254} are refractory to adsorption. This average was found to be approximately 20% of Natural Organic Matter (NOM), from nine different surface waters (Fettig, 1999a). It also appears clear that an accumulation of HS within the solution in the column is necessary to bring about a high enough concentration gradient to favour the adsorption. This is likely to happen when the heavier MW, slowing down under their slow diffusion, increase the concentration gradient as fresh solution enters the column.

From the very beginning, a residual DOC was also observed by Teerman and Jekel (1999) when they treated a reservoir water (usually aquatic NOM are similar to F1 in terms of MW and SUVA) on a β-FeOOH adsorbent bed. An initial residual DOC of 10% was immediately followed by a breakthrough, which showed a large difference with equilibrium results. However, the residual of 80% remained stable for several weeks, which very much agrees with the present results on GAC, when the effluent DOC remains at 55% of the influent for at least 300 hours (12.5 days). It confirms that diffusion occurring in the column is slow but still enables adsorption to happen.

An initial decrease of the effluent DOC was not observed by other authors on the same adsorbents (Othman et al., 2001, Fettig, 1999b) when using HS comparable to F1 (pretreated soil or real water with MW below 5 kDa). Three aspects of the experimental work were different:

(i) The surface charge was positive at the working pH (pH_{zpc} was above 7) whereas in this study, it is negative for both iron compounds. An alteration of the surface charge

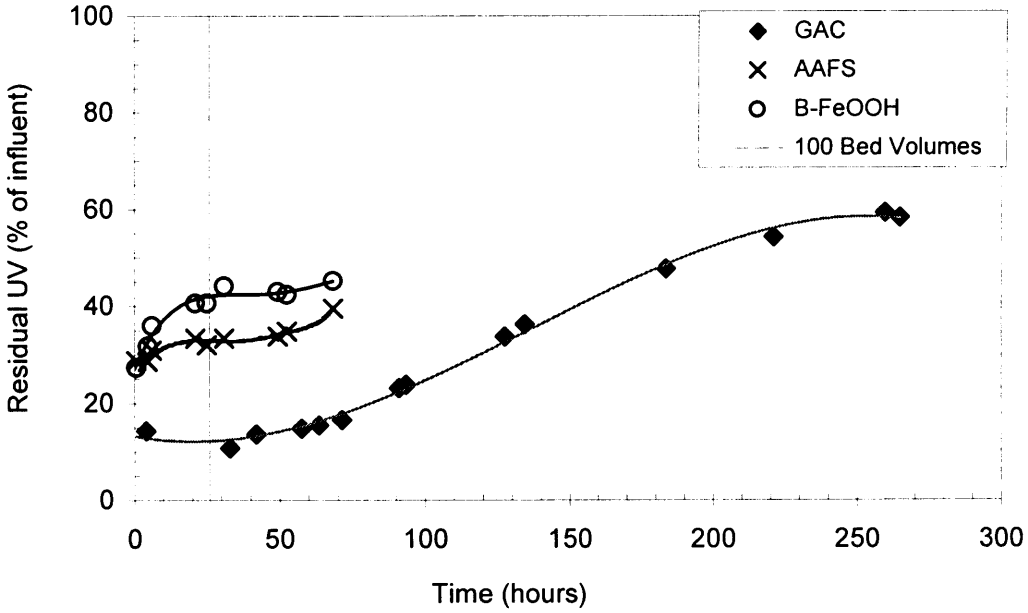

Figure 8.2 Residual UV_{254} after adsorption of F1 on GAC, AAFS and β-FeOOH.

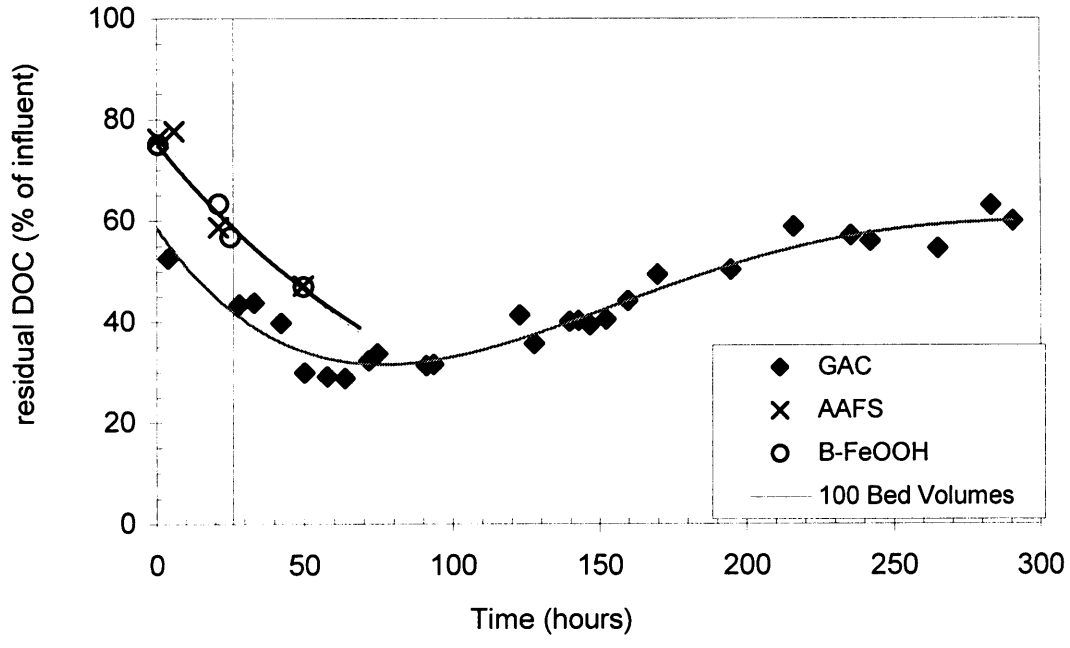

Figure 8.3 Residual DOC after adsorption of F1 on GAC, AAFS and β-FeOOH.

during the first 30-40 hours of the bed service time may have occurred leading to the enhanced adsorption of HS. However, the GAC surface was already positive at pH 7 (pH_{zpc} is 10.2). Hence the second explanation should be considered.

(ii) The HS solution contains numerous metals since it was not purified before use (Li, Na, Ca, Mg). These are likely to complex with the HS first and act as ligands. Increased adsorption of metals in presence of HS has been observed before (Lai and Chen, 2001), when studying the removal of lead and copper from water. Duan et al. (2002) suggest the following reactions:

$$-COOH + Ca^{2+} = -COOCa^{+} + H^{+} \quad (8.1)$$

$$-NH_2 + Mg^{2+} = -NHMg^{+} + H^{+} \quad (8.2)$$

Chen (1997, 1999) observed a decrease of the effluent DOC in the first 150 hours of the run. The adsorbent was an anionic resin. He also measured a decrease of the effluent pH during that phase, corresponding to the above chemical reactions. Of relevance here can be cited Duan et al.'s postulate (2002) saying "enhancement of removal of HA by the presence of Ca^{2+} and Mg^{2+} arises primarily from an alteration of the adsorption affinity".

A similar behaviour of the effluent quality (decrease of the effluent DOC initially) was obtained by Sontheimer and Hubele (1986). In the study, the adsorbent was sand and the adsorbate was ozonated humic acid (SUVA was 1.64). The effluent DOC was initially equal to the influent DOC (6.95 mg/L), i.e. 100% before dropping to 90% after a few days and down to 85% after 10 days. Deeper in the filter sand bed, it dropped further down to 80% and remained stable for more than 500 days. Sand usually has a much lower pH_{zpc} (between 2 and 3.5 for silica based inorganics according to Montgomery, (1985), 0.7 according to Chang et al.(1997)). Hence, the surface charge is responsible for the initial very low removal by AAFS and β-FeOOH.

(iii) The surface velocity (flowrate divided by the column section area) used in this work was 0.38 m/h for the small columns. Previously cited authors (Fettig, 1999, Sontheimer and Hubele (1986) used approximately 5 m/h, leading to an EBCT of about

2-4 minutes compared to 16 minutes in this work. From a longer EBCT, it would be expected that components with a slow diffusion rate would be removed more effectively. These components are the higher MW and higher SUVA components and consequently, the effluent SUVA should decrease. However SUVA hardly decreased during the first 30 hours on GAC and increased on AAFS and β-FeOOH during that time. Therefore this explanation cannot be retained.

Phenomena in the adsorbent bed can also be shown from SUVA values. Figures 8.4, 8.5 and 8.6 show the evolution of the effluent SUVA with time, respectively when using GAC, AAFS and β-FeOOH. SUVA of the effluent after being in contact with GAC is well below the SUVA of the influent. It shows that inside the column, the heavier MW of F1 are retained, and that the lightest MW are not adsorbable. Between 40 and 90 hours, the DOC remains fairly constant. During that time, UV absorbance and SUVA start to increase, which indicates that the heavier MW of F1 exit the column. But the stability of DOC implies that the lighter adsorbable MW of F1 (which do not absorb UV) are still adsorbed. Such comment also leads to the conclusion that the lighter MW are not replaced by the heavier ones at this stage. The phenomenon of displacement observed by Gu et al. (1996b) is not confirmed here. Dynamic column experiments performed by Chi and Amy (2004) used a quartz sand to remove humic substances (DOC of 9.4 mg/L and SUVA of 4). The breakthrough was immediate but also proved to be irreversible. They concluded that the mechanism for adsorption was a chemical process and ligand exchange. This would also explain the present results and would not give space for desorption.

SUVA of the effluent increases after 5 hours when using AAFS and β-FeOOH. It remains below the SUVA of the influent for AAFS, showing adsorption of the heaviest MW of F1. Fettig (1999b) found that the EBCT on γ-Al_2O_3 should be between 40 and 60 minutes for a breakthrough of 50% for removal of NOM at 200 bed volumes. If shorter than 40 minutes, the breakthrough would take place earlier. Therefore, the slow uptake on this type of adsorbent is confirmed.

However, on β-FeOOH, the influent and effluent SUVA reach the same value after 50 hours, showing this media to be a non-efficient adsorbent.

These results agree well with the equilibrium studies. F1 is well adsorbed on GAC but not on the iron compounds. However in each case, adsorption is not immediate, a non-

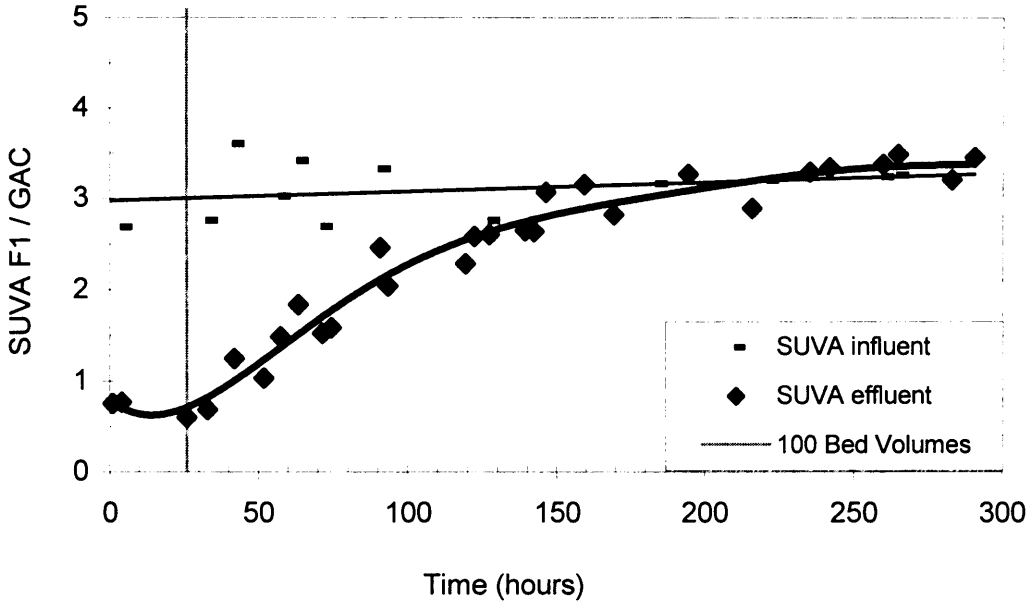

Figure 8.4 Residual SUVA after adsorption of F1on GAC.

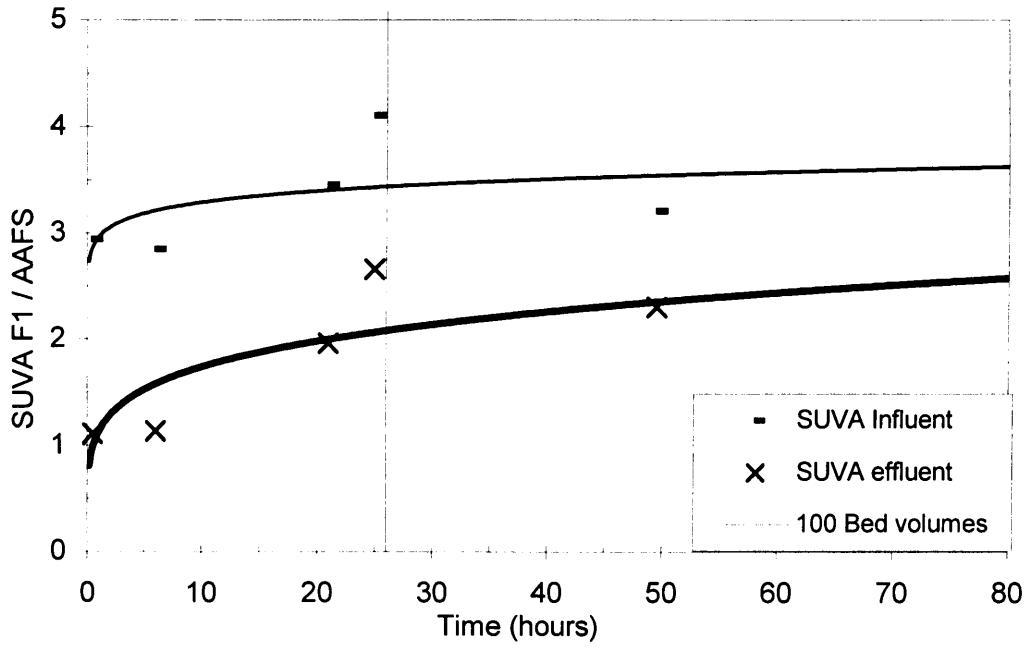

Figure 8.5 Residual SUVA after adsorption of F1 on AAFS.

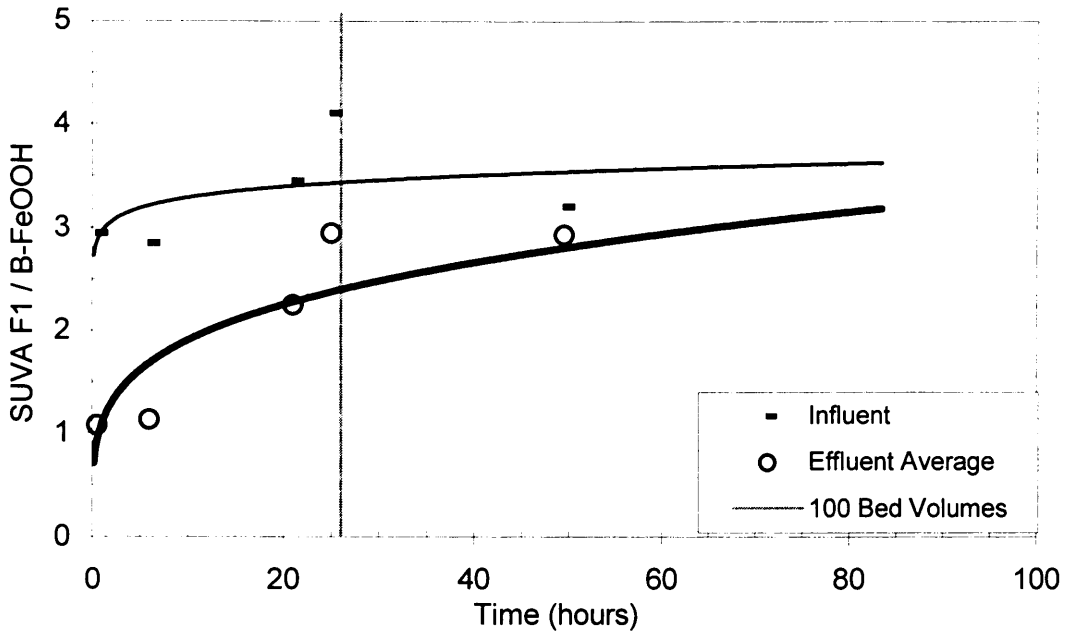

Figure 8.6 Residual SUVA after adsorption of F1 on β-FeOOH

adsorbable fraction remains due to the lowest MW. Desorption of lighter MW by heavier ones was not observed.

8.3.2 Removal of fraction F12 (0-10 kDa)

For practical reasons, solution F2 (5-10 kDa) was not used for column studies. This was due to the lack of capacity for producing a sufficient quantity of solution to supply the columns. F12 contains both F1 and F2 fractions. The influent DOC was between 8 and 9 mg/L and SUVA was approximately equal to 7. Results of adsorption in the columns are shown in Figures 8.7 and 8.8 respectively for UV_{254} and DOC. No DOC data are available for experiments done on GAC, and only limited data are available for AAFS. However, it is assumed that DOC results for adsorption on AAFS are fairly similar to β-FeOOH due to similar trends for UV absorbance.

The behaviour of F12 is very different from F1. The breakthrough appears clearly and the shape is similar to the results obtained by authors previously cited (Teerman and Jekel, 1999, Chi and Amy, 2004, Othman et al. 2001). Breakthrough takes place very early on GAC, after 5 hours (from UV absorbance data), whereas on AAFS and β-FeOOH, it is not sharp but rather slow. Li et al. (2003) clearly showed a quick breakthrough with microporous GAC compared to a GAC with mesoporosity. In their

study, the breakthrough at 50% took place at 300-400 bed volumes at pH 7, against 2000-3000 bed volumes for mesoporous GAC. This lack of mesoporosity to adsorb a wide range of MW was also shown by the low load, approximately 1 mg DOC/g GAC for all pH values between 5.5 and 10 (10 times more for mesoporous GAC). This proves the major importance of the pore size distribution for adsorption of HS on GAC. A favourable pH does not necessarily enhance adsorption in this case.

However, the effluent contains a residual DOC from the start on the three adsorbents (less obvious when looking at UV absorbance), although this is not as large as for F1. Again, the effluent DOC is high during the first 5 hours for both iron compounds. Similarly to F1, a few hours are necessary before gaining maximum DOC removal. This is attributed, as before, to the necessity of accumulating HS in the solution (within the column) so as to reach a high enough concentration gradient which will favour the diffusion to the adsorbent surface. The heaviest MW being slowed down inside the column and initially their removal corresponds to little effect on the effluent DOC. But as soon as their adsorption is favoured, the DOC decreases noticeably. Effluent DOC drops to a minimum of 25% of the influent (i.e. approximately 2 mg/L for β-FeOOH) and 15% for UV_{254}. This refractory portion of HS is attributed to fraction F1 present in F12. Maximum removal occurs between 10 and 125 hours and after that time, effluent DOC rises again, up to 60% of the influent DOC after 300 hours. This enables one to say that the breakthrough starts at 125 hours and indicates the affinity of F12 for β-FeOOH.

From figure 8.9, SUVA values show which fraction is preferentially retained in the column. As for F1, the minimum SUVA is approximately 1-1.5 in the effluent. This corresponds to the non-adsorbable HS. The constant removal of DOC (residual of 20% between 10 and 125 hours) corresponds to a steady increase of the effluent's SUVA up to 4-5. This means that the MW corresponding to F1 are adsorbed to a gradually diminishing extent. After 125 hours, the SUVA value slowly reaches the influent value, when F2 is not adsorbed more than F1.

F12 on β-FeOOH exhibits an interesting behaviour. It shows that the intermediary MW (5-10 kDa) adsorb well onto β-FeOOH. However, it also shows that the lower MW of F1 also adsorb on this media since before 100 hours, the SUVA value of the effluent remains below 3-4 (SUVA of F1). This result complements the equilibrium study,

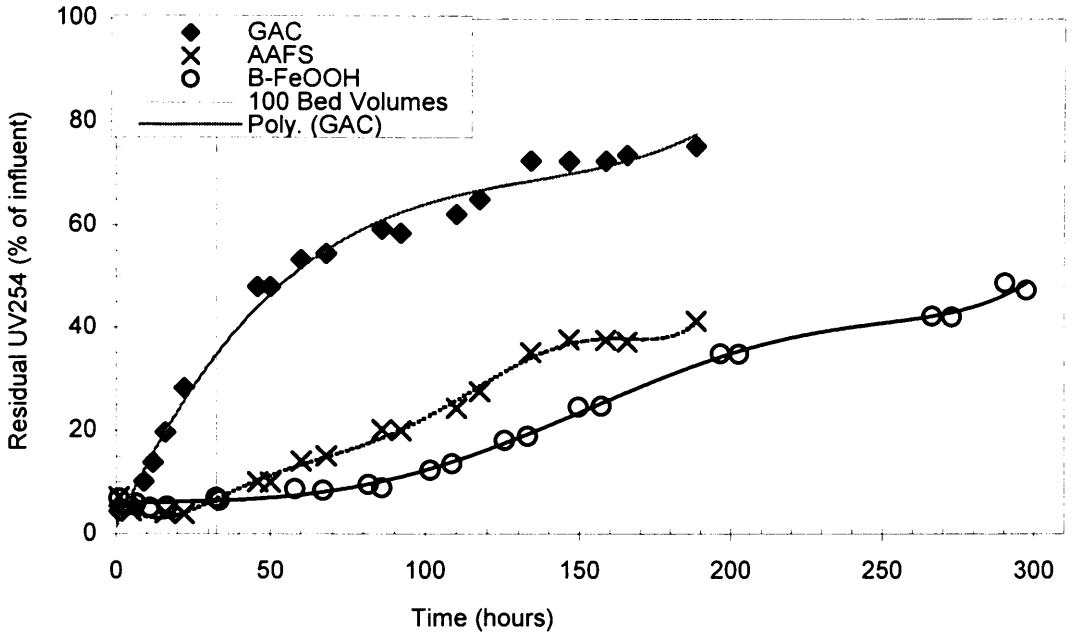

Figure 8.7 Residual UV_{254} after adsorption of F12 on GAC, AAFS and β-FeOOH.

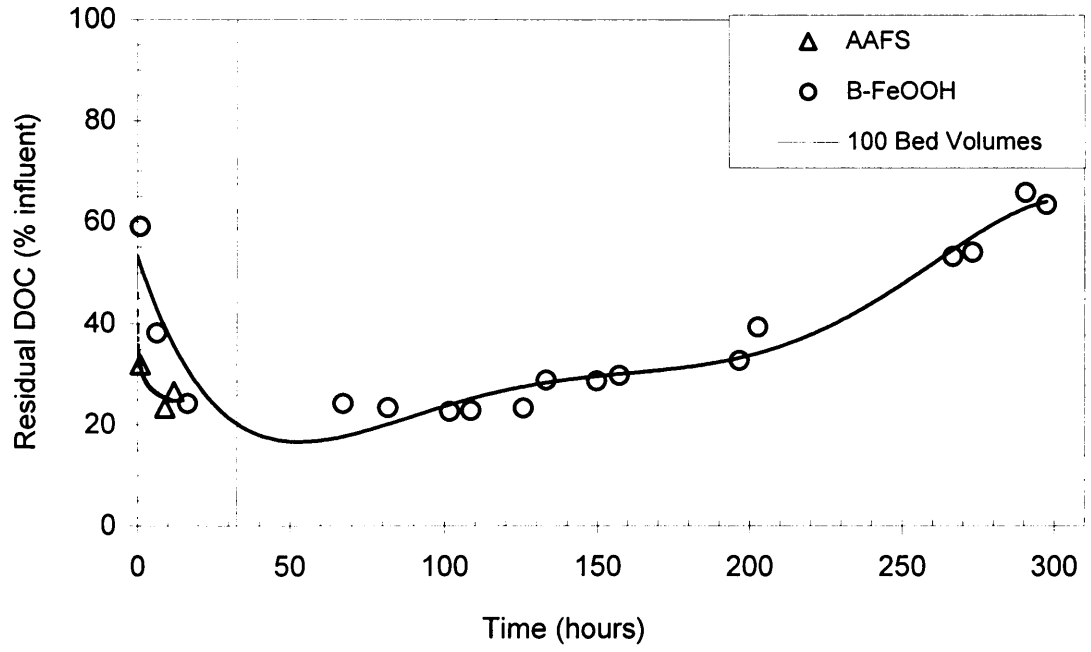

Figure 8.8 Residual DOC after adsorption of F12 on β-FeOOH (data not available for GAC).

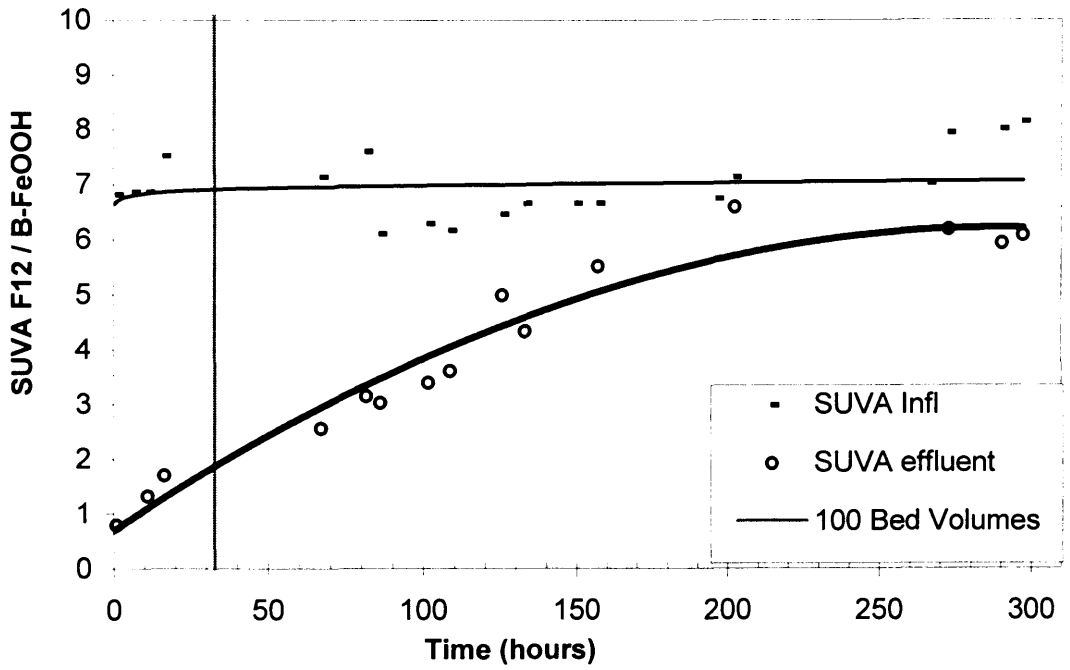

Figure 8.9 Residual SUVA after adsorption of F12 on β-FeOOH.

making this iron compound more attractive. It also provides evidence of the necessity for mesoporosity in order to adsorb the higher MW, particularly as shown for the GAC.

8.3.3 Removal of F123

Results shown below correspond to the port at 25 cm, leading to an Empty Bed Contact Time (EBCT) of 19 minutes. For comparison, the EBCT in the microcolumns was 16 minutes. Influent DOC was 12.5, 6.5 and 10 mg/L on GAC, AAFS and β-FeOOH media, indicating the difficulty experienced in reproducing exactly the same influent from the separation procedure used in this work. Results are presented in figures 8.10 and 8.11 respectively for UV absorbance and DOC of the effluent.

The breakthrough on GAC occurs very quickly; it is actually immediate for the UV absorbance and after 3-4 hours for the DOC. It confirms what was found from the equilibrium studies, i.e. that the heavier MW (mainly represented in F123) up to 50 kDa do not adsorb well on GAC due to the lack of external surface. This agrees with results obtained for the adsorption of pond water by GAC (Schreiber et al., 2005). The authors observed that the breakthrough was slightly earlier for high MW natural organic matter

and they attributed this behaviour to specific molecular interactions. As for the β-FeOOH, breakthrough occurs quickly too, immediately following the curve for GAC. It seems that adsorption is better on AAFS and this corresponds to the isotherms obtained in the previous chapter. However this is also attributed to a lower influent DOC. Overall, the iron oxihydroxide does not allow any removal of the lowest MW and AAFS is only slightly better. The intermediate MW were the best removed by adsorption on the iron compounds.

From figure 8.11, the initial decrease in DOC continues, but only on AAFS and β-FeOOH and not on GAC. Therefore, the accumulation of HS within the column is necessary, as for previous fractions, before observing a short steady DOC removal. However in this case, the decrease does not occur for UV absorbance (figure 8.10) or is not observable due to very low UV values. The unadsorbable fraction is observed too and again can be attributed to the presence of F1 in F123.

These comments are validated by figures 8.12, 8.13 and 8.14, respectively showing the SUVA of the effluent for adsorption of F123 on GAC, AAFS and β-FeOOH. On GAC, the SUVA of the effluent immediately increases steeply, rapidly becoming equal to the SUVA of the influent. This indicates that no significant distinction is made in the distribution of the MW between the influent and the effluent. However, once the SUVA curve has flattened, it remains constantly parallel and under the influent SUVA. It is concluded that high MW are adsorbed on GAC to some extent. The mechanism is likely to be precipitation or reconformation of the big molecules to penetrate micropores. On the iron compounds, the increase is sharp too, although less steep on AAFS as expected from the slowest breakthrough. The effluent's SUVA is also similar to the influent's SUVA.

Overall adsorption tendencies have reversed between F1 and F123. F123 hardly adsorbs on GAC, adsorbs well on AAFS and only a little on β-FeOOH. These results are expected since F123 contains the highest MW. However, GAC also causes the SUVA to decrease slightly during a long column run.

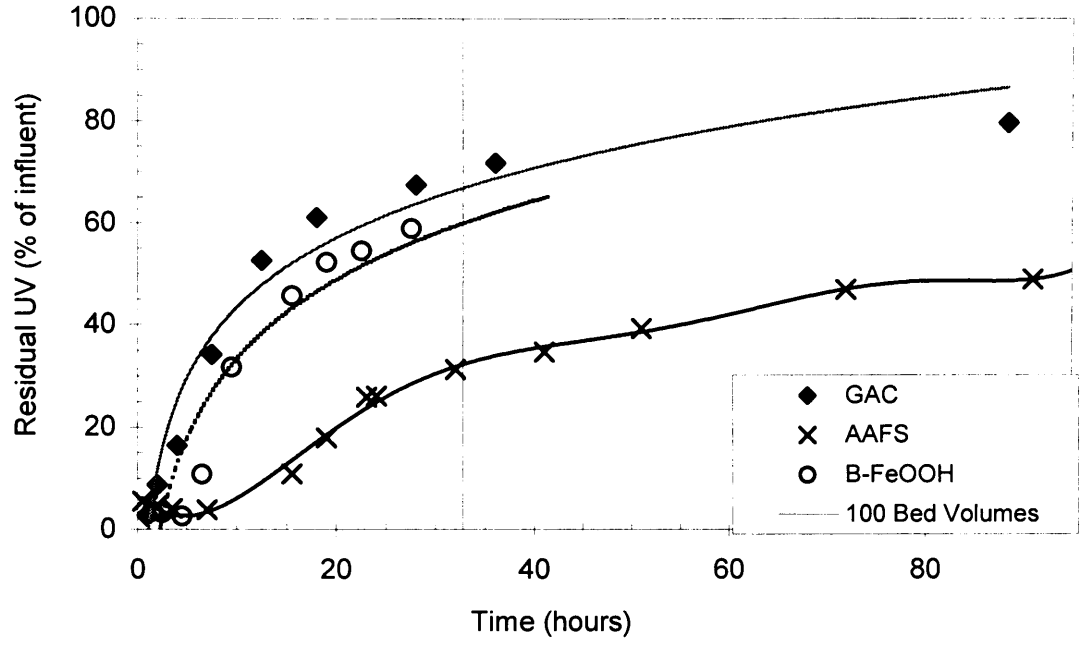

Figure 8.10 Residual UV_{254} after adsorption of F123 on GAC, AAFS and β-FeOOH

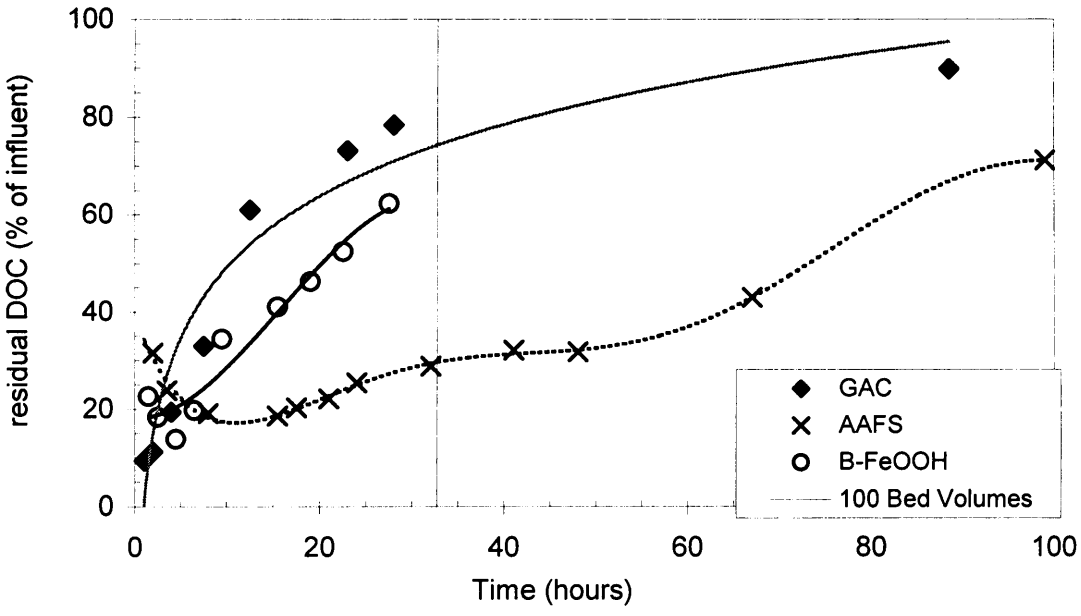

Figure 8.11 Residual DOC after adsorption of F123 on GAC, AAFS and β-FeOOH

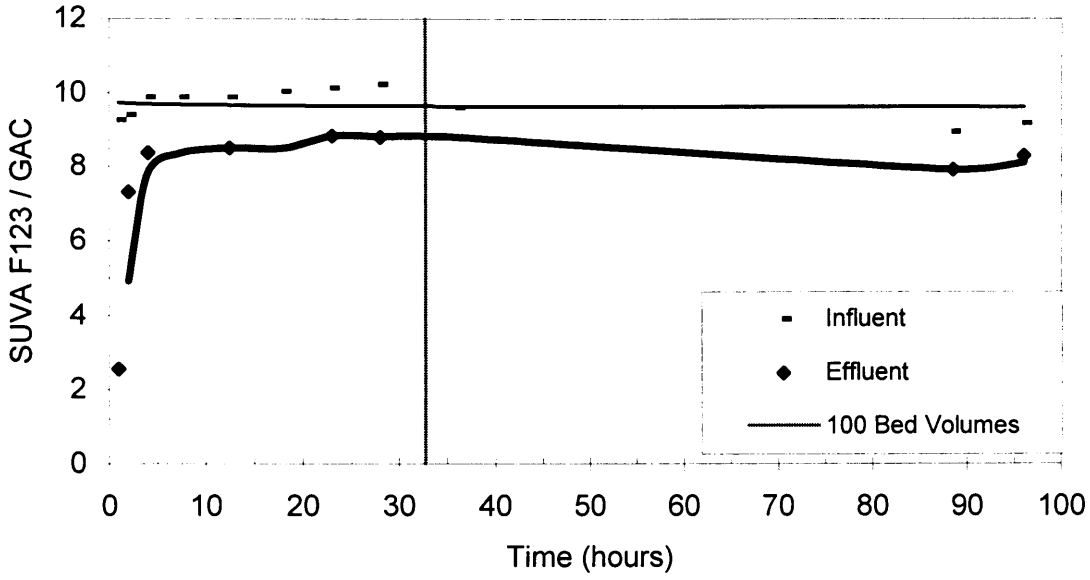

Figure 8.12 Residual SUVA after adsorption of F123 on GAC.

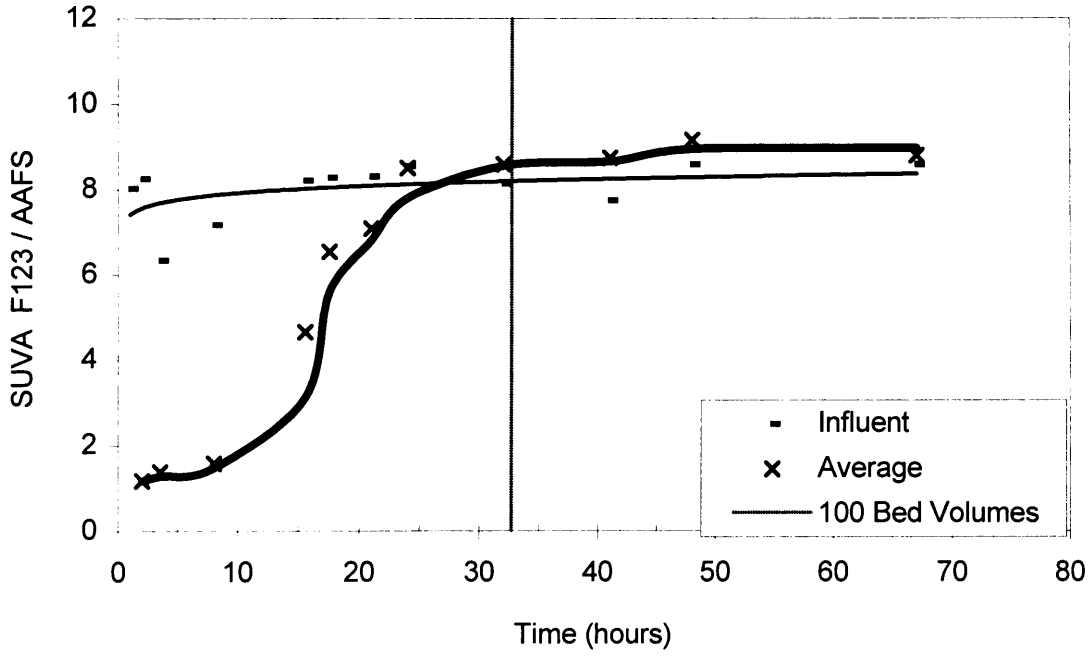

Figure 8.13 Residual SUVA after adsorption of F123 on AAFS.

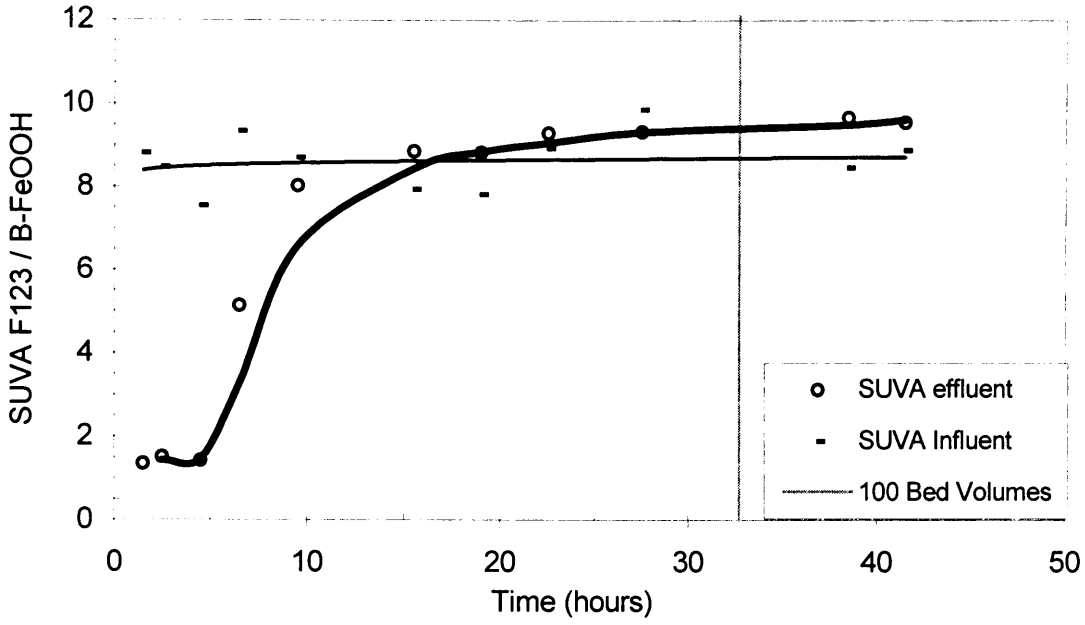

Figure 8.14 Residual SUVA after adsorption of F123 on β-FeOOH.

8.4 The Thomas model

The Thomas model is obtained from the typical breakthrough curve. It uses an equation based on the ratio C_t/C_0 (effluent concentration at time t to influent concentration at time zero) versus the volume of solution treated. The initial DOC, the flowrate and the mass of adsorbent used also influence the result as seen from equation 3.32 (detailed in chapter three). Thomas parameters are k_T (Thomas constant) and q_0 (maximum column adsorption capacity). It is usual to consider the breakthrough to occur from an effluent concentration equal to 5% of the influent concentration. However in this study, it has become clear that an initial residual DOC, due to a non-adsorbable fraction of the humic substances, is characteristic of the systems involved. Since the minimum residual DOC is between 0.5 and 1 mg/L, it corresponds to 5 to 10% of the influent DOC (C_0 is about 10 mg/L for the various experiments). Consequently, the breakthrough threshold of 5% is irrelevant in this study and it is considered to occur as soon as the effluent DOC starts to rise.

Figures 8.15, 8.16 and 8.17 show the prediction by the Thomas equation compared to the experimental points, respectively for F1, F12 and F123. For F1, only data from experiments with GAC gave results for the Thomas equation. For AAFS and β-FeOOH,

the DOC decreased during the experimental period, therefore the model was not applicable. Experimental results were obtained for GAC until 300 hours and the effluent DOC increase was recorded. For F12, no DOC data are available on GAC and AAFS. Finally for F123, the Thomas model could be fitted for the three adsorbents.

The Thomas equation is a mathematical expression for a column with a typical breakthrough (Conter and Knox, 1986). Therefore, high initial DOC or DOC decrease are not represented by this model. This is shown in figures 8.15, 8.16 (volume treated between 0 and 2 litres), and 8.17 (volume treated less than 0.125 litre for AAFS and β-FeOOH). It is attributed to the fact that the Thomas equation does not account for the fractionation inside the column. The decrease in the effluent DOC was interpreted earlier as the accumulation of heavier MW being slowed down due to the diffusion process. The model equation considers only one concentration for the adsorbate (C_t) which corresponds to the DOC. However in this work, DOC represents a lump index since the individual concentrations of each MW cannot be measured easily. The consequence is that the equation is valid only when the effluent contains a constant proportion of the MW range, i.e. exhibits a constant SUVA value. Only then will the DOC really mimic the influent concentration. The same comments are valid for F12 adsorbed on β-FeOOH (figure 8.16). In both cases when breakthrough starts, the Thomas equation gives a fair representation of the experiment.

As for F123, the Thomas equation was applied on each adsorbent, from the start of the breakthrough. The model does not fit well over the full range of data. However, considering the dispersity of the experimental results, the prediction gives the right trend for all three adsorbents.

Assumptions made in the Thomas's model are that the adsorption satisfies the pseudo-second order kinetics and the langmuirian isotherm. The first condition is satisfied from the kinetic study (see chapter six). From the equilibrium studies (chapter seven), the Langmuir model could not be applied to F1 adsorption onto GAC or β-FeOOH, nor to F2 onto β-FeOOH. However it could satisfactorily be applied to adsorption of F123 onto each adsorbent, which also corresponded to situations where adsorption took place even at low residual DOC. Consequently, the Thomas equation fits well when the Langmuir model also fitted the isotherm. It is concluded that the monolayer, as suggested by the Langmuir model, cannot be adsorbed until a high solution DOC

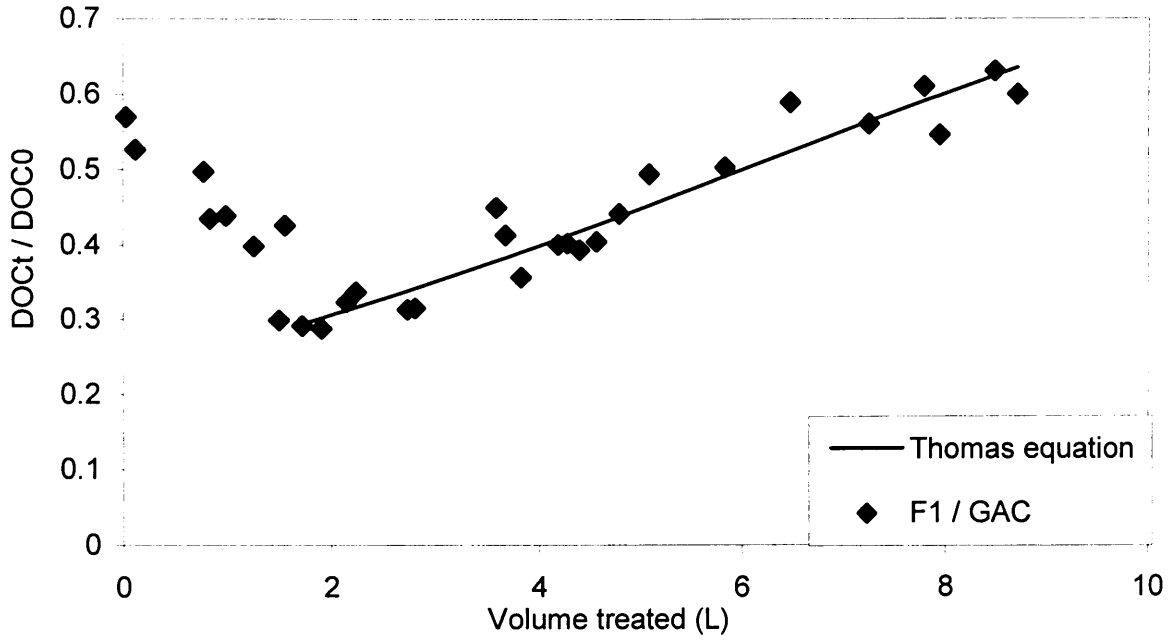

Figure 8.15 Fitting of the Thomas equation for F1 adsorption on GAC.

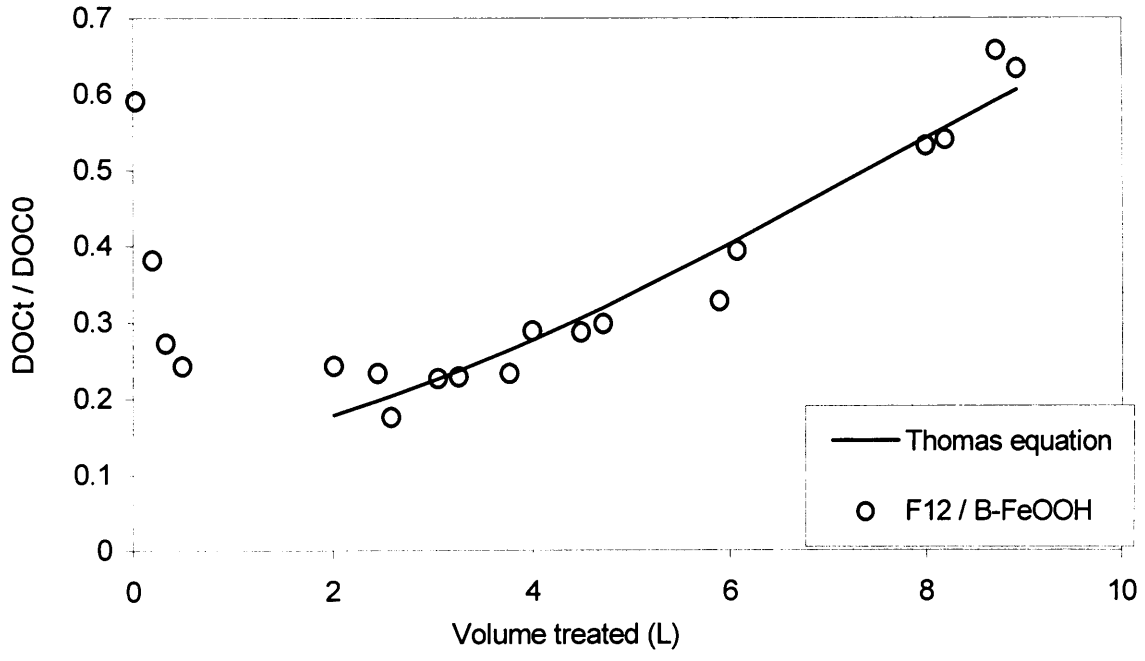

Figure 8.16 Fitting of the Thomas equation for F12 adsorption on AAFS.

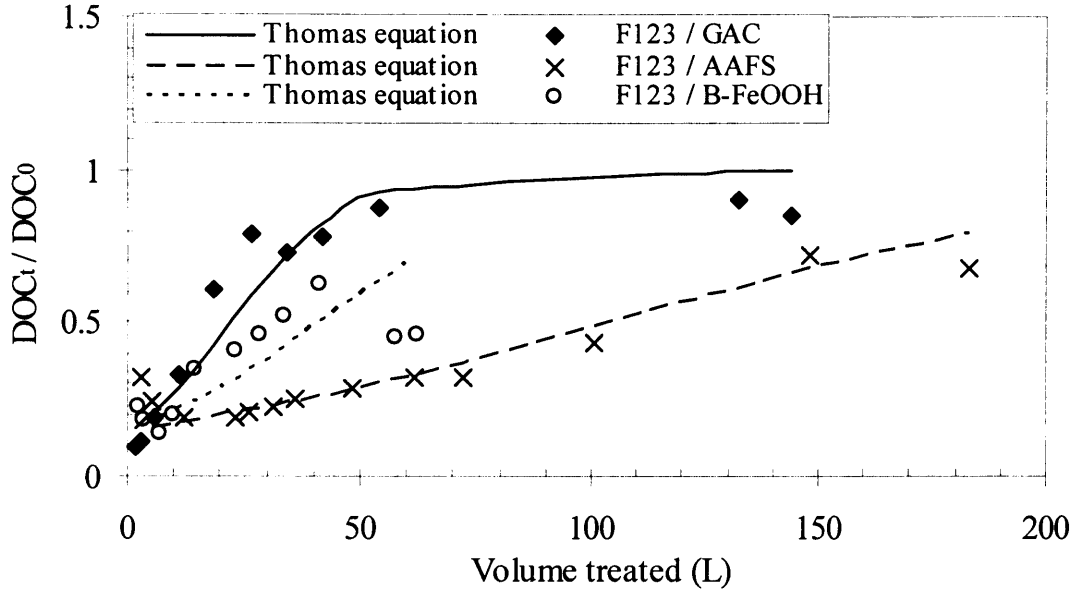

Figure 8.17 Fitting of the Thomas equation for F123 adsorption on β-FeOOH.

provides the gradient of concentration large enough to promote diffusion. As said by Lee et al. (2000), a higher concentration gradient leads to a higher mass transfer driving force, which in turn favours the adsorption. This is achieved quicker in F123 than in F1 and F12 since the bigger molecules are slower and therefore accumulate in the solution within the column, thereby increasing the gradient.

The values of Thomas parameters are shown in the following the table 8.1. The correlation regression coefficient R^2 indicates, using linear regression, how well the model fits a given set of experimental points (see equation 3.32). k_T corresponds to a rate constant (Al-Ghouti, 2004) and it is noticed that this is higher for F123 than for F1 and F12. Its increase for higher MW can be misleading since higher MW humic substances should diffuse more slowly. However, it is suggested that the slow diffusion is compensated for by the accumulation of HS of higher MW close to the surface, which increases the concentration gradient, i.e. increases the driving force, and hence results in the higher diffusion rate.

The fitting of the Thomas model gives a good correlation with experiments, from the time when effluent DOC increases. As expected, GAC has a high capacity to adsorb F1 (q_0). For F123, all results are low but AAFS is shown to be the best adsorbent for the highest MW represented in the working solution.

Table 8-1 Parameters(*) for the Thomas model and correlation coefficient

	k_T (L/h.mg)	q_0 (mg/g)	R^2
F1 / GAC	1.1×10^{-3}	9.59	0.9225
F12 / β-FeOOH	1.0×10^{-3}	5.82	0.9323
F123 / GAC	9.7×10^{-3}	1.64	0.8799
F123 / AAFS	3.7×10^{-3}	2.02	0.9757
F123 / β-FeOOH	6.5×10^{-3}	0.78	0.8910

(*) k_T is Thomas constant and q_0 is the maximum adsorption capacity, calculated from equation 3.32

8.5 Influence of bed depth and Bed Depth Service Time (BDST)

8.5.1 Influence of bed depth on F123 adsorption

So far, the interest in having a given length of column has not been analysed. However, for design purposes in water treatment works or in the industry, it must be known whether adding bed depth (meaning time and money consumption) is beneficial to the treatment in a cost-effective way. Figures 8.18 a, b c, show the residual DOC at different bed depths and different times for F123 adsorbed respectively on GAC, AAFS and β-FeOOH.

From these figures, the typical "S" shape that would indicate the zone of mass transfer (MTZ), is not observed along the column. With time, for each adsorbent, the curve becomes wider, indicative of a broader MTZ. A broadening breakthrough curve also means that the adsorbent is not used to its full capacity or the residual increase is steep and sharp (Othman, 2001). This can be attributed to a certain pore size (micropores smaller than 2.5 nm) not being accessible to the humic substances, which may be the case for heavier MW of F123 adsorbing on the GAC. Only a small external surface area (less than 168 m^2/g, see chapter 5) is left for adsorption of the heavy MW on the carbon. Such reasoning corresponds with the statement of Ersöz et al. (2004) who attribute the

broad S shape to the non-equilibrium conditions in the columns. Such conditions arise when the flow rate is faster than the diffusion rate of the adsorbate towards the adsorbent surface.

On GAC, residual DOC in the solution at 25 cm reaches 20% of the influent DOC. At 60 cm (effluent), the residual DOC has decreased to 15% of the influent DOC only. It is concluded that the main mass transfer has occurred in the first 25 cm and during the first four hours (the residual DOC increases after four hours). On AAFS, the mass transfer also takes place in the top layers (25 cm), in three and a half hours (30% residual at 25 cm and at 60 cm). This strongly suggests that the MTZ is located in the first 25 cm and that the S shape would appear, should more samples be taken between 0 and 25 cm. Similar comment is valid for the adsorption onto β-FeOOH, where the MTZ seems to be located in the first 10 cm. The curve becomes almost vertical, respectively from 7.5 hours on GAC, from 3.5 hours on AAFS and from 2.5 hours on β-FeOOH. The constant residual concentration, along the column depth, indicates that the depth does not have much influence on residual DOC. However, with time, the vertical curve continues to shift towards higher DOC in the effluent. As a consequence, it is concluded that the time factor is more important than the bed depth. This is actually in agreement with the kinetics which were shown to be slow (see kinetic chapter) and also with the fact that diffusion of heavy MW, which are the main constituents of solution F123, is very slow.

The MTZ defines the minimum column length to achieve the desired effluent concentration (Netpradit, 2004). Dries et al. (2005) actually found that HS did travel along the column depth before being removed. When assessing the impact of HS onto the adsorption of metals in fixed-bed columns, they observed the progress of a rust coloured zone, characteristic of HS. This must be considered carefully since from the breakthrough curves on β-FeOOH, the MTZ is very broad from the early stages of adsorption. The design might then lead to a very long column in which case a multiple columns system could be more suitable.

8.5.2 The Bed Depth Service Time (BDST) model

A different manner in which to approach the influence of the bed depth is to apply the Bed Depth Service Time model (BDST), which is the simplest method of predicting the column parameters according to McKay and Bino (1990). These same authors define

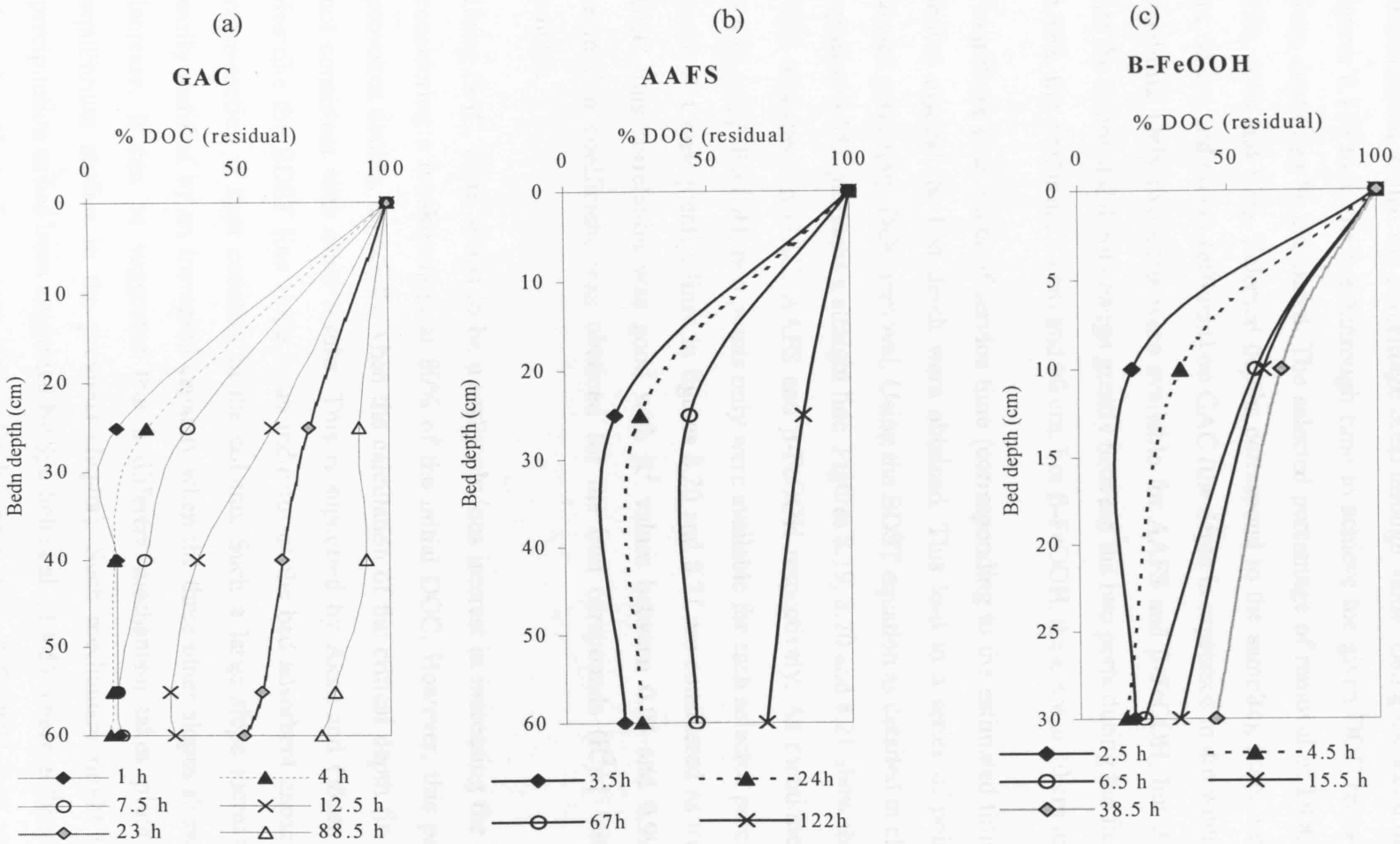

Figure 8.18 Residual DOC vs bed depth at different times of the column run, after adsorption of F123 on (a) GAC (AAFS and (c) β-FeOOH.

the breakthrough time as the time required to reach a certain reduction of the influent concentration, called the percentage breakthrough value. Using the same data as in the figures 8.18a to c, the breakthrough time to achieve the given DOC removal (%) at a given depth can be estimated. The selected percentage of removal of DOC were 20%, 40%, 60% and 80%. Selected depths correspond to the sampling ports, i.e. 25 cm, 40 cm, 55 cm and 60 cm (effluent) on GAC (the depth is expressed in dm when used in the equation). Only two ports were available for AAFS and β-FeOOH, but it is observed that the removal did not change greatly between the two ports during the first hours. On AAFS, the depths are 25 cm and 60 cm. For β-FeOOH, these are at 10 cm and 30 cm.

From these data, plots of service time (corresponding to the estimated times described above) against the bed depth were obtained. This lead to a series of points for each chosen percentage DOC removal. Using the BDST equation as detailed in chapter 3 (see equation 3.35), produces a straight line. Figures 8.19, 8.20 and 8.21 show these plots for F123 adsorbed on GAC, AAFS and β-FeOOH respectively. As mentioned above for AAFS and β-FeOOH, two points only were available for each selected percentage DOC removal. Consequently, lines in figures 8.20 and 8.21 are considered as trendlines. On GAC, this correlation was good with R^2 values between 0.94 and 0.99. No linear regression coefficient was obtained for the iron compounds (R^2=1 with only two points).

Using GAC, there seems to be a really obvious interest in increasing the bed depth if considering a breakthrough at 80% of the initial DOC. However, this particular line provokes doubts, especially when the calculation of the critical depth (in table 8.2) is not consistent with other results. This is supported by Aksu and Gönen (2004) who describe the BDST line slope as an indicator of the bed adsorbent capacity since the cross-section is kept constant in the column. Such a large slope increase cannot be easily justified by an increased capacity when the three other slopes showed a regular increase. It can be suggested that a different mechanism takes place (as for the equilibrium studies in the previous chapter). Such mechanism might be a surface precipitation as has been suggested by Sperlich et al. (2005). These authors investigated the adsorption of arsenate and salicylic acid onto β-FeOOH and attributed the adsorption to a complexation process at low coverage and to a surface precipitation process at higher surface coverage.

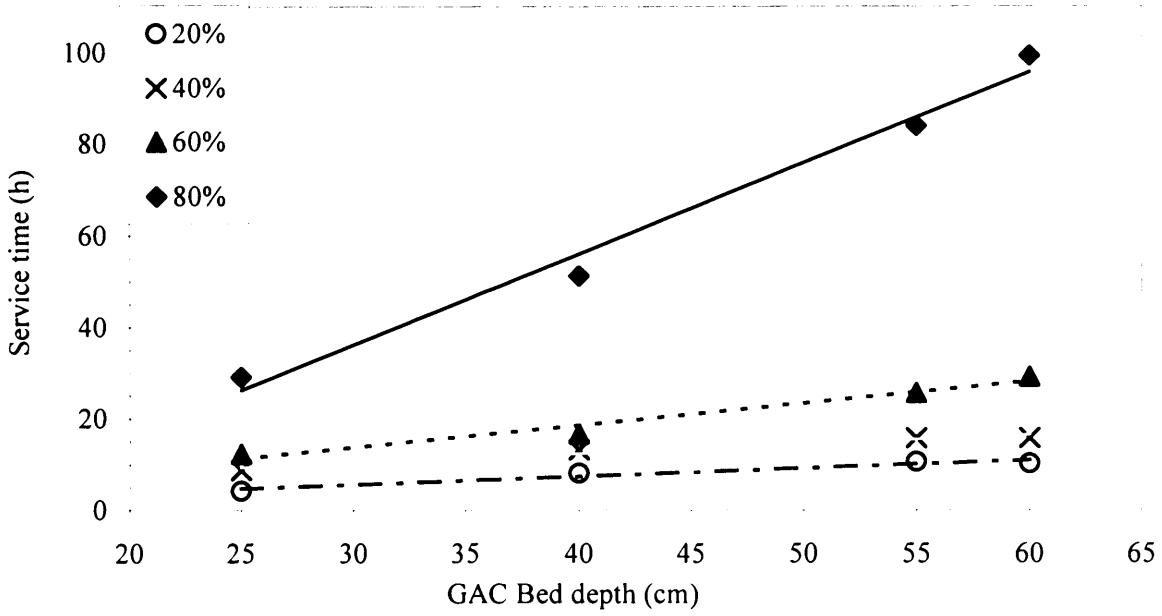

Figure 8.19 The BDST model applied for adsorption of F123 on GAC, at different percentage breakthrough points (100 C_{eff}/C_{inf}) .

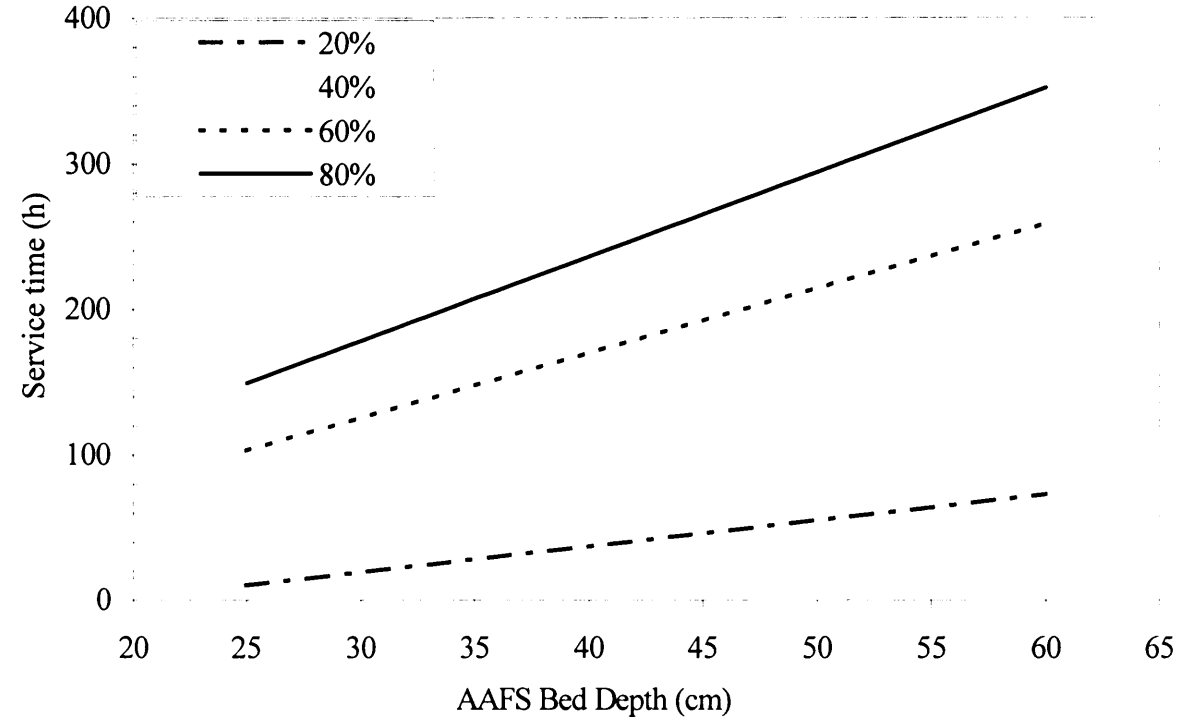

Figure 8.20 The BDST model applied for adsorption of F123 on AAFS at different percentage breakthrough points (100 C_{eff}/C_{inf}) (trendlines are presented since only two points were available on each percentage removal).

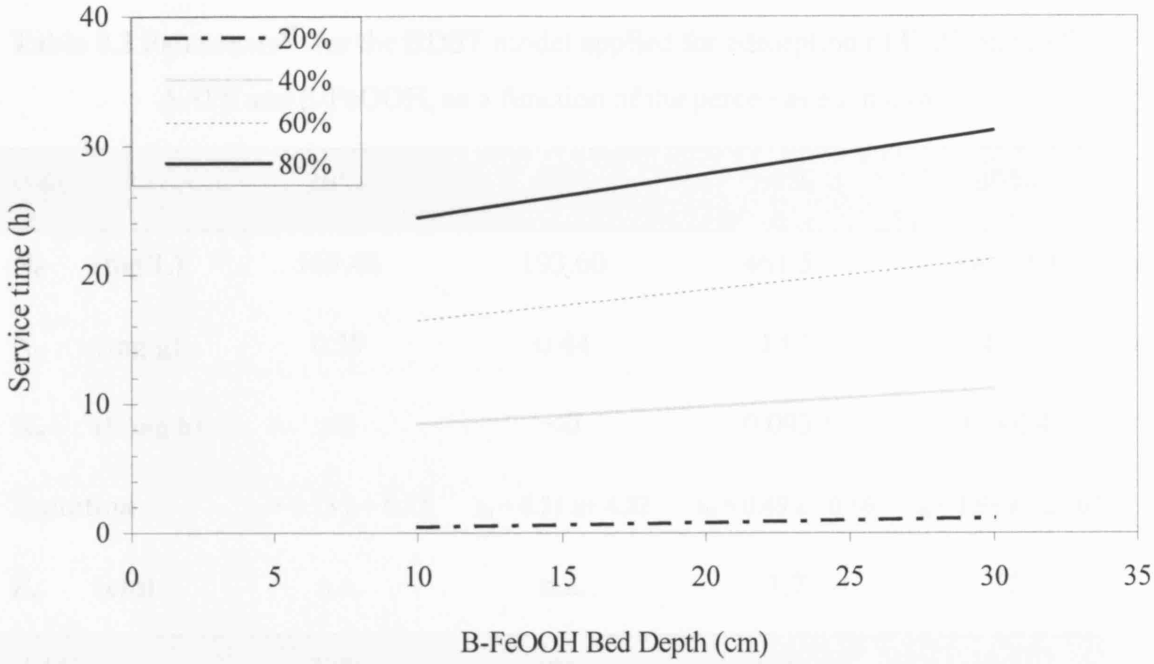

Figure 8.21 BDST model applied for adsorption of F123 on β-FeOOH at different percentage breakthrough points (100 C_{eff}/C_{inf}) (trendlines are presented since only two points were available on each percentage removal).

The depth increase brings improvement on the service time for 60% breakthrough. For more stringent results (breakthrough at 20% and 40%), increasing the length beyond 25 cm does not bring a much higher service time as can be seen from the quasi-horizontal BDST line on figure 8.19. The same phenomenon is observed for β-FeOOH (figure 8.21). The service time is significantly increased if focusing only on a higher percentage breakthrough (lines are almost parallel but spaced wide apart). On AAFS, both bed depth and percentage breakthrough influence the service time. This agrees with previous results showing that AAFS was the best adsorbent for F123. It confirms that the very heavy MW are not retained on β-FeOOH and that F123 has little affinity for GAC.

These results are shown in table 8.2. The parameters are calculated as described above and are also extensively presented by Walker and Weatherley (1997). In the equation, t_B corresponds to the breakthrough time selected (the percentage of residual DOC in the effluent) and Z is the bed depth. Z_c represents the critical bed depth, which corresponds to the Z value if t_B is equal to zero in the equation 3.35 (chapter three). Values of N_0^* (massic capacity instead of volumetric capacity, i.e. N_0 multiplied by the bulk density of

Table 8.2 Parameters(*) for the BDST model applied for adsorption of F123 on GAC, AAFS and β-FeOOH, as a function of the percentage removal.

GAC		**20%**	**40%**	**60%**	**80%**
N_0	**(mg/L)**	169.46	193.60	461.53	1891.63
N_0^*	**(mg/g)**	0.39	0.44	1.05	4.30
K_a	**(L/mg.h)**	<0	<0	0.0930	0.0034
Equation		$t_B = 0.18\ z + 0.23$	$t_B = 0.21\ z + 4.22$	$t_B = 0.49\ z - 0.86$	$t_B = 1.98\ z - 23.62$
Z_c	**(cm)**	n.a.	n.a.	1.7	12
AAFS		**20%**	**40%**	**60%**	**80%**
N_0	**(mg/L)**	930.90	1622.63	2314.57	3006.30
N_0^*	**(mg/g)**	1.05	1.82	2.60	3.38
K_a	**(L/mg.h)**	0.0043	0.0068	0.0169	<0
Equation		$t_B = 1.78\ z - 34.59$	$t_B = 3.13\ z - 21.66$	$t_B = 4.47\ z - 8.75$	$t_B = 5.80\ z + 4.18$
Z_c	**(cm)**	19	7	2	n.a.
β-FeOOH		**20%**	**40%**	**60%**	**80%**
N_0	**(mg/L)**	26.10	101.56	177.01	252.54
N_0^*	**(mg/g)**	0.02	0.08	0.13	0.19
K_a	**(L/mg.h)**	<0	<0	<0	<0
Equation		$t_B = 0.03\ z + 0.10$	$t_B = 0.14\ z + 7.08$	$t_B = 0.24\ z + 14.06$	$t_B = 0.34\ z + 21.04$
Z_c	**(cm)**	n.a.	n.a.	n.a.	n.a.

(*) parameters calculated from equation 3.35. N_0^* (mg/g) calculated by multiplying N_0 by the bulk density of the adsorbent. Z_c is not calculable (n.a.) if $K_a<0$.

the adsorbent) correspond to the BDST adsorption capacity (Walker and Weatherley, 1997) and can be compared to q_0 calculated from the Thomas equation. The order of magnitude is similar and so is the classification for better adsorption capacity of F123 at 60% removal. However, GAC is shown to be the adsorbent with the highest capacity for 80% removal; this result is not reliable as explained before. This order is surprising when considering the large proportion of heavy MW in F123 and when compared with the adsorbents capacity calculated from the Freundlich model. The latter gave the same order of magnitude for capacity on GAC and AAFS but it was also just above 3 mg/g on β-FeOOH (maximum of 0.19 mg/g here).

The explanation for this difference can be attributed to the mixing, which does not take place in the column. Since β-FeOOH does not present much internal porosity (it is mainly mesoporous), the external surface is used for adsorption. In the column and under the water pressure, the bed compaction increases, hence a decrease of this external surface. From the chapter relating the adsorbents characteristics (Chapter 5), β-FeOOH poured porosity was 0.42 and decreased to 0.34 when packed. This is below the porosity of AAFS (0.50 and 0.47 for poured and packed) and of GAC (0.51 and 0.46). Therefore, humic substances do not have a large surface to adsorb to which is equivalent to a low capacity of this compound. The other reason is the contact time, considered as the most important parameter in column design (via bed depth and flow rate). This parameter is generally limited to a few minutes in a dynamic column application (from a few minutes to 30-45 minutes). However, equilibrium in many cases (and in particular for humic substances) requires a much longer time to be achieved (AWWA, 1990), of the order of hours and of days when considering a large range of MW. Therefore, the capacity of adsorption is expected to be higher when calculated from batch experiments (Aksu and Gönen, 2004, Netpradit, 2004). This makes the batch system more attractive when the equilibrium is known to require a long time since it provides better interaction between the adsorbent and the adsorbate (Netpradit, 2004). Adsorption capacity values (N_0^*) regularly increase with the percentage breakthrough, for each adsorbent (N_0^* at 80% for GAC remains doubtful). This is explained by the fact that as breakthrough occurs later, the adsorbent is used to a greater extent, hence the higher calculated capacity.

When computable, K_a values in table 8.2 do not show any obvious trend. This has been related before (Walker and Weatherley, 1997). However, K_a can still be compared with

k_T in the Thomas equation (see table 8.1). In general, it seems that K_a is larger than k_T (breakthrough 60-80%) hence BDST predicts a slightly faster transfer rate than the Thomas equation.

Critical depth values follow opposite trends for GAC and AAFS. If the bed depth is equal to Z_c, or shorter, then the breakthrough will occur immediately (i.e. when t_B=0). However it seems that Z_c is strongly dependent upon the adsorption capacity and transfer rate, hence the difficulty in interpreting these results.

Finally, the bed depth shown in table 8.2 confirms that the main Mass Transfer Zone occurred in the first 25 cm as suggested from figure 8.18. However, the bed depth of 12 cm to achieve 20% removal of DOC (breakthrough 80%) on GAC is not consistent with the 1.7 cm necessary to remove 40% (breakthrough 60%), as discussed earlier. Critical Bed Depth to achieve 80% removal (20% breakthrough) and 60% removal (40% breakthrough) could not be computed due to a positive intercept of the BDST line. It appears that the short service time and the limited influence of the bed depth result in a positive intercept in the equation presented in table 8.2, which in turn lead to a non-calculable critical bed depth.

Results on AAFS are consistent but no critical bed depth could be computed for β-FeOOH due to a positive intercept in the equation (table 8.2). These results also show that the BDST model has its limitation. Particularly as it takes N_0^* as a constant whatever the bed depth considered. This is due to diffusion not being taken into account in the model (Ko et al., 2000).

8.6 Conclusions

From the previous results, the capacity of the column for removing humic substances of a wide range of MW using GAC, AAFS or β-FeOOH, has been estimated. GAC was proved to adsorb humic substances with MW below 5 kDa (F1) well, as expected from equilibrium studies. AAFS and β-FeOOH did not remove F1 to the same extent. For each adsorbent, a non-adsorbable fraction (low MW) was responsible for a residual DOC from the start of the run. It has also become clear that adsorption of heavier MW of each solution (F1, F12 and F123) requires a concentration gradient to build up in the

column before observing any DOC removal in the effluent. This was shown from the initial effluent DOC decrease.

Prediction of the removal is also successful using the analytical method supplied by the Thomas equation. However this method is valid only from the time when the effluent DOC started to increase. It also corresponds to the applicability of the Langmuir model for the adsorption isotherm.

As for the BDST model (adsorption of F123), the Mass Transfer Zone is broad for each adsorbent. The contact time in the columns seems to be more important than the bed depth and most of the adsorption occurs in the top layers. The adsorbents are not completely exhausted when reaching about 80% breakthrough. This gives further evidence of the slow diffusion of HS particularly for high MW.

In addition, two distinctive features appear from these results:

(i) GAC is able to remove high MW although lacking of mesoporosity (attributed to precipitation and alteration of HS conformation) and

(ii) β-FeOOH does not show such a high adsorption capacity as previously predicted, attributed to the non-equilibrium state and to the lack of surface under the media compaction.

So far, it has been shown that F123 can be fractionated into fractions of different adsorbabilities according to their affinity for GAC, AAFS or β-FeOOH. Low MW were found to be adsorbable on GAC but only very little on the iron compounds and the heavier MW were adsorbable on the iron compounds more than on GAC. Consequently, when F123 is considered as a single adsorbate, the above described analytical models have encountered difficulties in prediction of residual as DOC. Hence, the necessity of numerical models using computer programs for complex solutions might arise from these results and such a model is applied in the next chapter.

CHAPTER 9

MODELLING THE ADSORPTION OF HUMIC SUBSTANCES USING GACMAN

9.1 Introduction

The GACMan model (Granular Activated Carbon Management) has not yet been used in the field of humic substances adsorption. However, it is based on the concept of Homogeneous Surface Diffusion coupled with IAST and therefore can be considered as relevant to the present study. It has been described in section 3.7 of chapter 3.

No previous sensitivity analysis or parametric study has been carried out on this model. Therefore, in the first part of this chapter, a parametric study is explained and performed. This enables estimates to be made of the relative importance of the parameters to be input into the model so that the available resources may be directed towards accurately determining the most important parameters.

The second part of this chapter is the simulation of adsorption. GACMan was only used with the Freundlich equation in this work. This is due to the fact that the Freundlich isotherm could be fitted in each instance of the equilibrium studies whereas the Langmuir isotherm could not. However, it was mentioned by GACMan's authors that some of the equations were to be revised for both the Langmuir and the Redlich-Peterson models. The main interest in applying the model to this project is to be able to perform new simulations of using laboratory equipment with new adsorbents and new contaminants (more specific DOCs to consider different ranges of humic substances molecular weights). So far, no calibration is available for the adsorbent/adsorbate/water systems to be investigated. Performing these calibrations represent a key part of the simulations. Simulation results are compared to experimental results obtained from the column runs.

Finally, conclusions are drawn from the results as to the interest of using the GACMan simulation in this particular study.

9.2 Parametric study

9.2.1. Introduction

From Varma et al. (1999), "different parameters affect a system to different extents". If a computer model is very sensitive to a parameter, its response will vary a lot when only a small variation of this parameter is given. The analysis of sensitivity determines the accuracy required in measuring or estimating the various coefficients in the model; it is carried out by running the model several times, each time incrementing the value of the particular coefficient and examining the effect that this has upon the output. If the response's variation is acceptable (within set limits) between two increments of the parameter's value, then this increment gives sufficiently good accuracy for the coefficient under study. On the contrary, a large difference in the results following a small parameter variation indicates that one must endeavour to input a value of the parameter with as small an error as possible. In the present case, the parametric study does not assign a "sensitivity" value to a parameter (no sensitivity function is used) but shows the relative importance of the parameters and the relevant effort for their estimation can be allocated. A fluctuation of the parameter under study is given, whilst maintaining other parameters constant.

From the response of GACMan (TOC of the effluent with time as seen in figure 9.2 below), the influence of the various coefficients can be considered under two aspects: the time from which the effluent's TOC becomes non-negligible, called T_o, and the speed at which the effluent's TOC increases, called d(TOC)/dt. Arbitrarily, the non-negligible TOC value is selected as twice the detectable concentration, i.e. 1 mgL^{-1}. Although the threshold value is often selected as 5% of the influent concentration (Reynolds, 1982) this is not a suitable value here due to the presence of a non-adsorbable fraction of the TOC, as explained in the previous chapter. In addition, no specific TOC limit is established by the water quality standards.

T_o shows the beginning of the breakthrough, as the non-adsorbable fraction is set to be nul (for the parametric study). After T_o, the effluent TOC starts to increase quickly, with the speed corresponding to the slope d(TOC)/dt ("max" subscript showing the maximum speed of this increase).

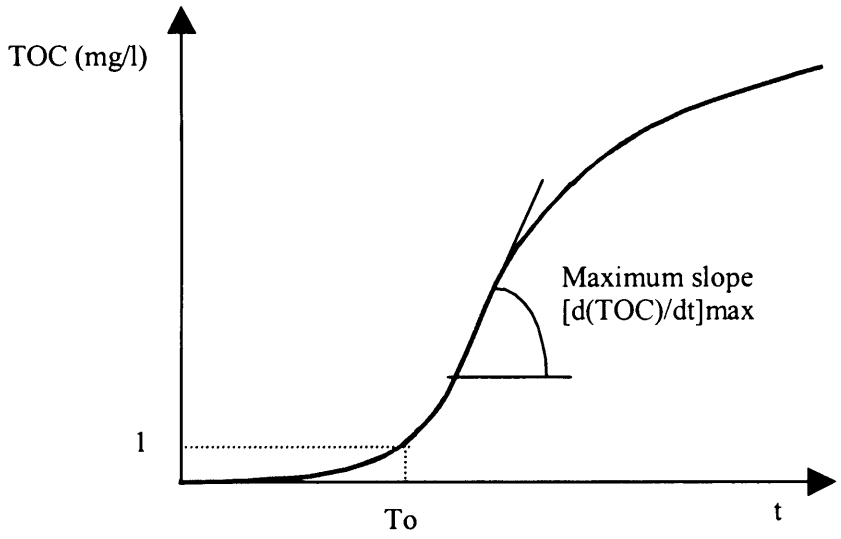

Figure 9.1 Typical GACMan response and definition of T_o and $[d(TOC)/dt]_{max}$

9.2.2. Parameters to be considered in GACMan

Three types of parameters subject to error are to be input in GACMan model:

1. Adsorbent characteristics:

Bulk density (ρ_b), porosity (ε) and median diameter (d_{50}) are parameters measured with an error due to laboratory techniques. Grain or particle density (ρ_p) is also studied since in practice, bulk and grain density are often confused. It is calculated using the following relationship:

$$\rho_p = \frac{\rho_b}{(1-\varepsilon)} \qquad (9.1)$$

2. Adsorbate characteristics:

Molecular weight (MW) and α are not measured. Ideally for each fraction, MW covers a range between two consecutive values of molecular weight cut-off (MWCO) of ultrafiltration membranes. However, MWCO is only an indicator since ultrafiltration depends on the conformation of the molecules, the bonding to the membrane, the state of the membrane and the extent of standardisation on different kinds of molecules.

Therefore, the study for this parameter will show the error due to uncertainty of the MWCO and to assuming a range of MW as a single component. This will also reinforce the aspect of multicomponent adsorption. In addition, error on MW will be reflected on the liquid diffusion coefficient D_l since above 1000 Da, molecular volume is assumed to be equal to MW and D_l is calculated as below in equation 9.2 (GACMan userguide, 1994):

$$D_l = 2.74 \times 10^{-9} \times MW^{(-1/3)} \qquad (9.2)$$

As a consequence, the error is also reflected on the surface diffusion coefficient in equation 3.53 (chapter three), in the solid phase transport. If α is imposed, the error will be the result of measurement of D_l, D_s, influent concentration and load calculation. If α is fitted, the error will be minimised only if it is within the range 0.1- 0.7.

3. Adsorption process constants:

Considering particularly the Freundlich isotherm, the parameters K and n are respectively the adsorption capacity and its intensity. Their estimation is subject to error and a typical isotherm, as observed in this study, displays a straight line over a short range. The Freundlich model is known not to be a good representation of adsorption at low concentrations (Tien, 1994). In many cases, a straight line is assumed over the whole range of results (Chen and Snoeyink, 1987, Jung et al., 2001). As an example, figure 9.2 illustrates how this may lead to errors on K and n, and the Freundlich equation appears to be valid over a poorly defined range (also true for Langmuir isotherm). From the batch experiments obtained with HS between 5 and 10 kDa adsorbed onto activated carbon, the following values for K and n were observed (based on the same set of data in figure 9.2):

- (1.29, 11.50) when all points are included to describe the plateau on the isotherm
- (1.87, 4.60) when the five points are included
- (2.41, 3.10) when the three middle points are included

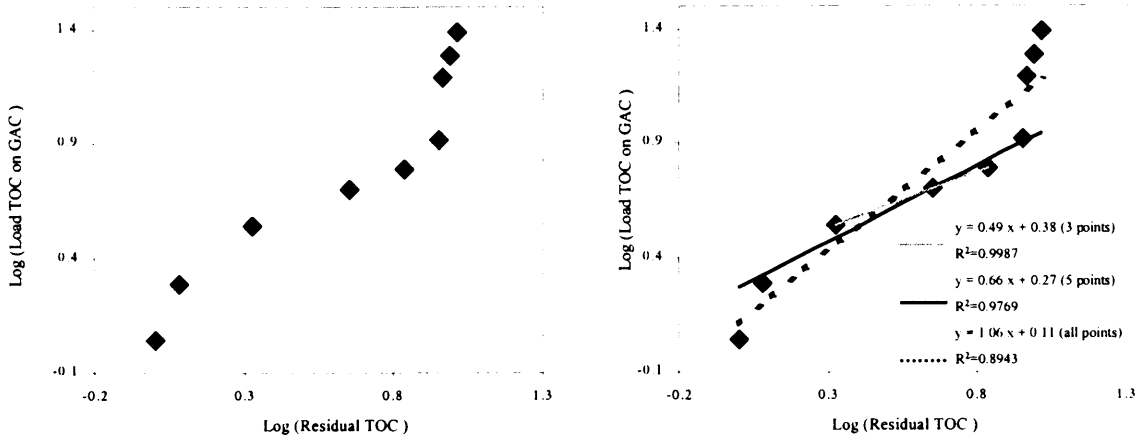

Figure 9.2 Experimental and calculated Freundlich isotherm for humic substances adsorption on GAC

These figures show a 2 and 3 fold variation for K and n respectively. It is therefore of interest to know how sensitive the model is to these parameters. From the Freundlich equation, K and n are not explicitly dependent. K expresses the capacity of the adsorbent and n the inverse of the intensity related to the distribution of energy of the adsorption sites (Tien, 1994). As the Freundlich model does not allow for a limited number of adsorption sites, a large capacity would logically lead to more low energy adsorption sites, i.e. a high K corresponds to a small n (smaller slope). Assuming that, the frequency of sites associated with a free energy of adsorption decreases exponentially with increasing free energy, shows that K and n are not independent (Montgomery, 1985). This was observed from the behaviour of humic substances adsorption after a pretreatment (Matsui et al., 1999). However, such comments remain qualitative and require both influences (K and n) on the model response to be investigated.

9.2.3. Values selected for parametric study

The size of the column and the flowrate lead to an Empty Bed Contact Time (EBCT) of 19 minutes.

Regarding the media characteristics, the parameter value and its fluctuation are selected following the mean values measured in the laboratory. The fluctuation was ± 12% for porosity, also selected for bulk and grain density (as they are linked). The largest

deviation for the median diameter was 7%. The reference is GAC 207C (see table 5.1 in chapter five for the list of GAC characteristics). From literature, a value for surface diffusion coefficient is available for MW of approximately 5000 Da (Fettig and Sontheimer, 1987c) as equal to 0.375 x 10^{-14} m^2/s (mean). Hence, the MW and fluctuation is set to 4000 ± 2000 to cover a range almost as wide as fraction F1 (0-5000 Da) and to include the 5000 Da value. From the above surface diffusion coefficient and using the concentration and equilibrium loading corresponding to the batch studies of this work, α is calculated and is equal to 0.02:

$q^*_{inf} = 0.015 \times 443 = 6.645$ kg/m^3

$C_{inf} = 15$ mg DOC/l

$\varepsilon = 0.51$

$D_l = 1.73 \times 10^{-10}$ m^2/s (from equation (9.2) at 20°C and MW=4000 Da)

$$\alpha = \frac{q^*_{inf}(t)\ D_s(t)}{c_{inf}(t)\ D_l(t)\ (1-\varepsilon)} \qquad (9.3)$$

$$\alpha = \frac{6.645 \times 0.375 \times 10^{-14}}{0.015 \times 1.73 \times 10^{-10} \times (1-0.51)} = 0.0196$$

$\alpha \approx 0.02$

This low value comes from the low maximum load for a high initial concentration. It shows that surface diffusion is probably the factor limiting adsorption rate.

To better observe the influence of α, the fluctuation range should extend further than the lowest values only. This is suggested due to the large uncertainty for α, since no precise measurement is carried out for the diffusion coefficients and its value is far out of the range suggested by GACMan (0.1-0.7). Hence the arbitrary choice of 0.15 for α.

For adsorption characteristics (K, n and α), variations of parameters are selected to cover a wide range from -50% of the mean to +100%. Other authors (Kapoor and Yang, 1991; Do and Hu, 1993) gave fluctuation ± 20% of the parameter only. However, uncertainty on the slope of the isotherm in many cases, justifies a wider range of fluctuation. Reference values are selected from the kinetic study performed with the low

Table 9.1 References values and fluctuations assigned for parametric study (column and flow do not vary)

Column	Diameter	D = 5 cm
	Length	L = 60 cm
Flow		0.026 L/min
Adsorbent	GAC 207C	ρ_b = 443 kg/m^3 ± 54
		ρ_p = 904 kg/m^3 ± 108
		d_{50} =0.918 mm ± 0.11
		ε = 0.51 ± 0.06
Adsorbate	Low MW fraction of HS (<5000 Da)	MW = 4000 Da ± 2000
		TOC = 15mg/L
Adsorption parameters	Freundlich isotherm	K = 5.6 mg/g
		n = 0.51
		α = 0.15
		and variations from 50% to 100% of these values

molecular weight fraction on GAC 207C. Table 9.1 shows the values of parameters used as reference.

9.2.4. Adsorbents characteristics

A parametric study of the adsorbents characteristics involves three parameters measured in the laboratory. These are the bulk density (B.D.), the median grain size (d_{50}) and the poured porosity (ε_p). The largest error observed was 12%, obtained for the poured porosity of β-FeOOH. An error in the porosity value also affects the bulk density. As a consequence, the variation affecting the adsorbent characteristics will be ±12%. The

selected adsorbent for the parametric study is GAC which means that as the parameter under study is submitted to variations, the other parameters remain constant with assigned values corresponding to the GAC 207C characteristics.

Figure 9.3 shows the parametric study for the bulk density. The shape of the curve is not affected by the variation of this parameter since the curves remain parallel, hence there is no effect on the speed of the breakthrough. T_0 increases with the bulk density (7.7±1 day) when the porosity is constant. From equation 3.44 in chapter 3, this behaviour is expected since an increase in the density ρ brings an increase in the adsorbate transfer.

In addition, it can be noticed that the compaction of the media with time under the weight of the water column does affect the bulk density. This is not considered in GACMan and using initially either the packed density or the poured density inevitably brings additional error. If only the porosity varies, as seen in figure 9.4, a decrease in adsorption is initially observed with the increased porosity. This is explained by the fact that less external surface is available for transfer. This is actually very particular to this model since GACMan considers the adsorbent medium as a packing of spheres. The area for adsorption is expressed in equation 3.38, showing that it decreases with a porosity increase. T_0 variation is 7.7 ± 0.6 day. In general, the results are not affected as much as with a bulk density variation. In addition, the difference of effluent concentration between the three curves decreases with time whereas it was constant for the bulk density.

Results from the variation of the median size of the adsorbent grains are illustrated in figure 9.5. T_0 is largely affected, having a value of 7 ± 1.4 days, which is the greatest variation of the three adsorbent characteristics. However with time the effluent concentration is less affected. A grain size increase corresponds to a T_0 decrease, which agrees with the above comment for the porosity. Since GACMan considers the grains as spheres, a diameter increase corresponds to less area available for adsorption (see equation 3.38).

9.2.5. Adsorbate Molecular Weight

The molecular weight (MW) is the only adsorbate characteristic input in GACMan. According to the adsorbent, it is also possible to add a non-adsorbable fraction as well as a biodegradable fraction. However these two features have a directly foreseeable consequence. The non-adsorbable fraction leads to the corresponding concentration

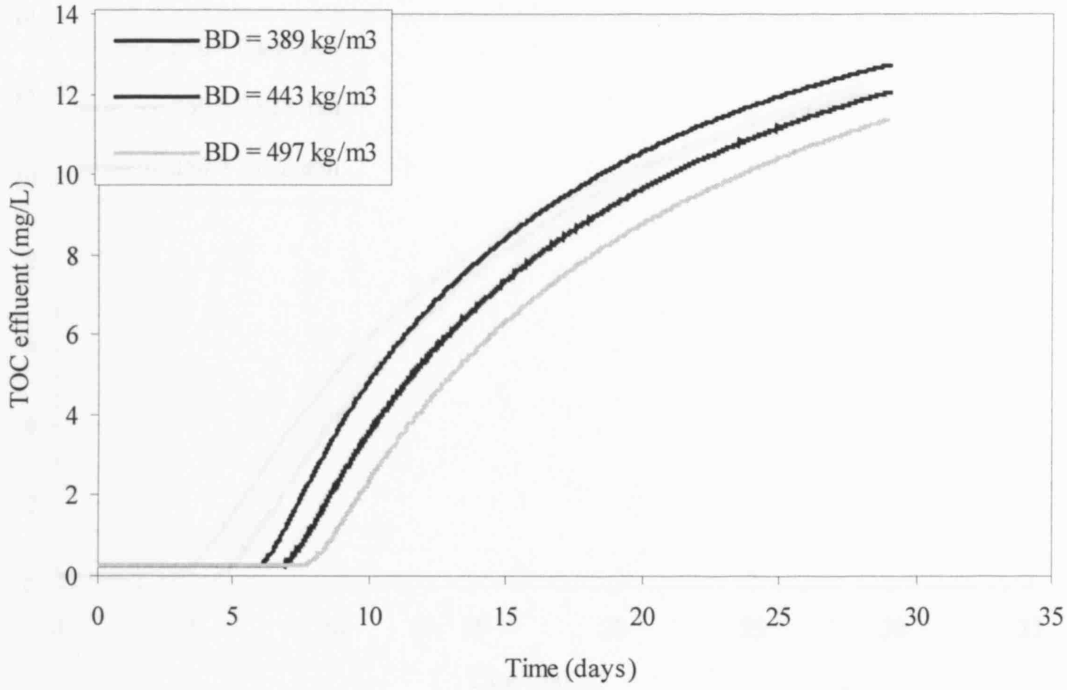

Figure 9.3 Parametric study for the bulk density (median grain size porosity are constant)

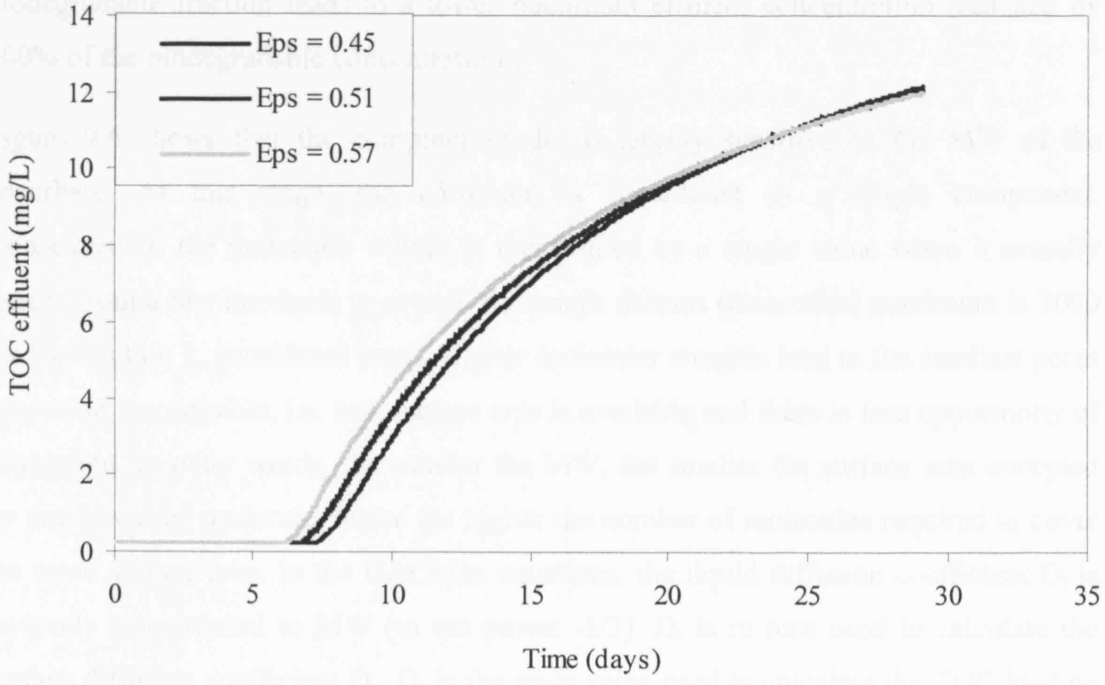

Figure 9.4 Parametric study for the porosity (median grain size and bulk density are constant)

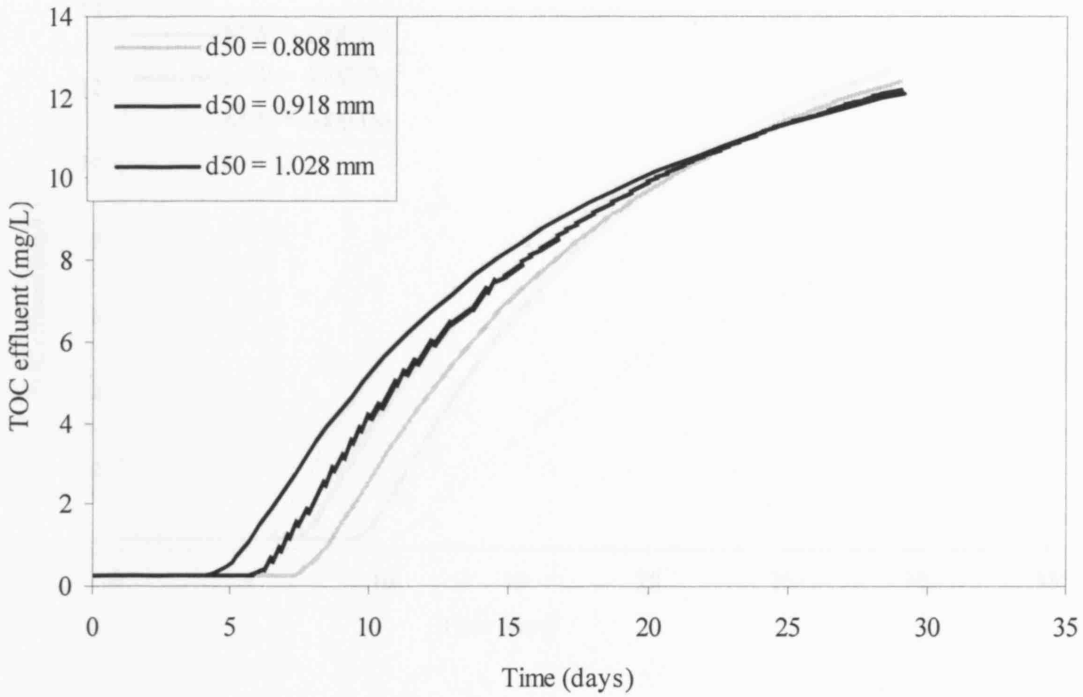

Figure 9.5 Parametric study for the median grain size (porosity and bulk density are constant)

present in the effluent (100% of the non-adsorbable concentration) and the biodegradable fraction leads to a lower maximum effluent concentration (reduced by 100% of the biodegradable concentration).

Figure 9.6 shows that the computer model is largely sensitive to the MW of the adsorbate. At this stage, the adsorbate is considered as a single component. Consequently, the molecular weight is represented by a single value when it actually ranges from a few hundreds to several thousands daltons (theoretical maximum is 5000 Da for fraction 1, considered here). Higher molecular weights lead to the smallest pores becoming inaccessible, i.e. less surface area is available and there is less opportunity of adsorption. In other words, the smaller the MW, the smaller the surface area occupied by one adsorbed molecule, hence the higher the number of molecules required to cover the same surface area. In the GACMan equations, the liquid diffusion coefficient D_l is inversely proportional to MW (to the power -1/3). D_l is in turn used to calculate the surface diffusion coefficient D_s. D_s is the main value used to calculate the TOC load on the adsorbent. As a result, the MW of 6000 brings a T_o shorter than for the MW of 2000. This proves the necessity of splitting humic substances into several ranges.

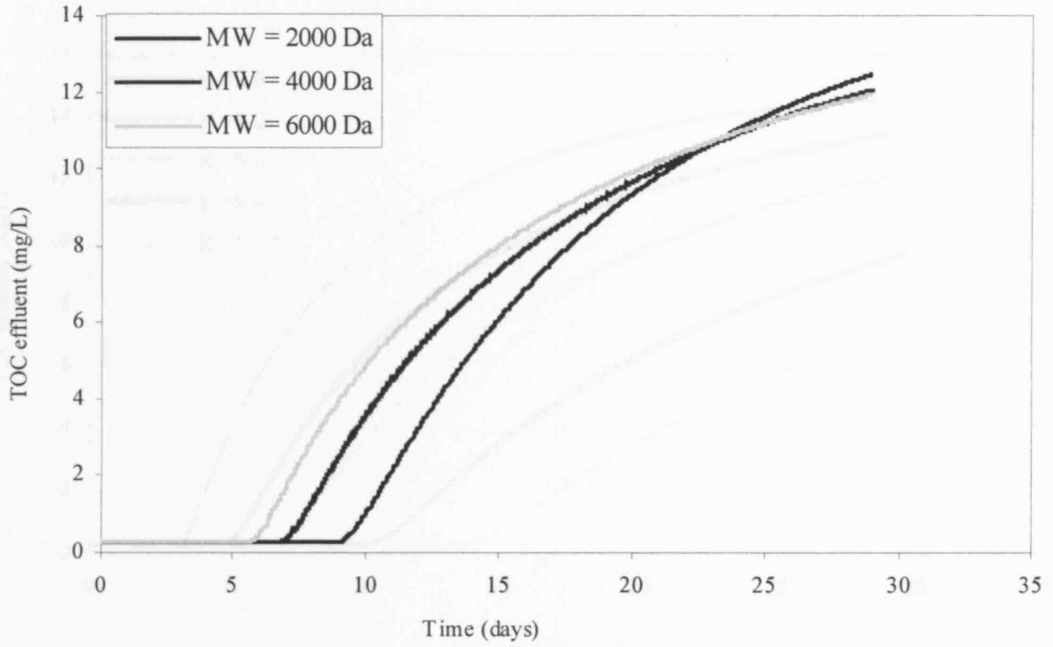

Figure 9.6 Parametric study for the Molecular Weight of humic substances

Although T_o is noticeably affected, the speed d(TOC)/dt is not significantly influenced by the imposed MW fluctuation.

The difference between 2000 and 4000 Da is more important than between 4000 and 6000 Da. T_o is equal to 6.8 days for 4000 Da and increases by 2.3 days for 2000 Da and decreases by 1.1 day for 6000 Da. Hence, as the MW increases, its effect is lessened. This shows the particular interest of splitting the small MW.

9.2.6. Adsorption parameters

The influence of adsorption parameters K, n and α is shown on figures 9.7, 9.8 and 9.9 respectively. It appears that the model is sensitive to these three parameters. Both T_o and d(TOC)/dt are influenced by K, n and α, although α brings less of a change over the set of curves. K influences particularly the time T_o (figure 9.7) whereas n and α have a more obvious influence over the slope (see figure 9.8 and 9.9). This shape of curve for α was also observed by Liu and Weber (1981) when investigating surface diffusion. The maximum slope d(TOC)/dt occurs in the early days of adsorption and the breakthrough follows very soon afterwards.

These observations are also reflected in figure 9.10 and 9.11, showing respectively the speed of the breakthrough d(TOC)/dt and the time T_o, versus the normalised parameter

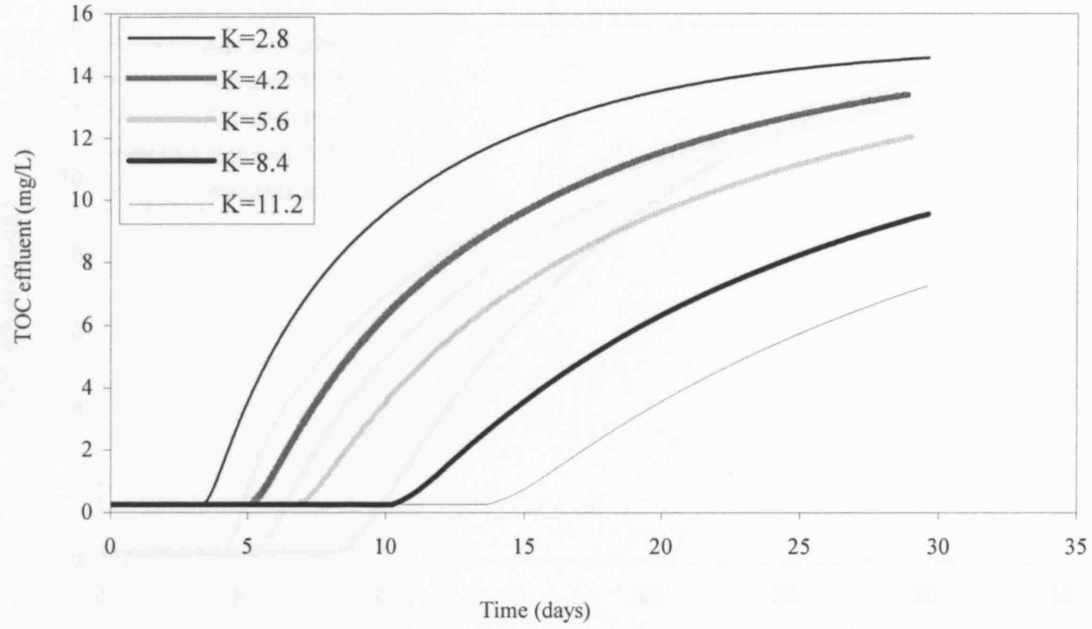

Figure 9.7 Parametric study for K (Freundlich constant) (n and **α** are constant)

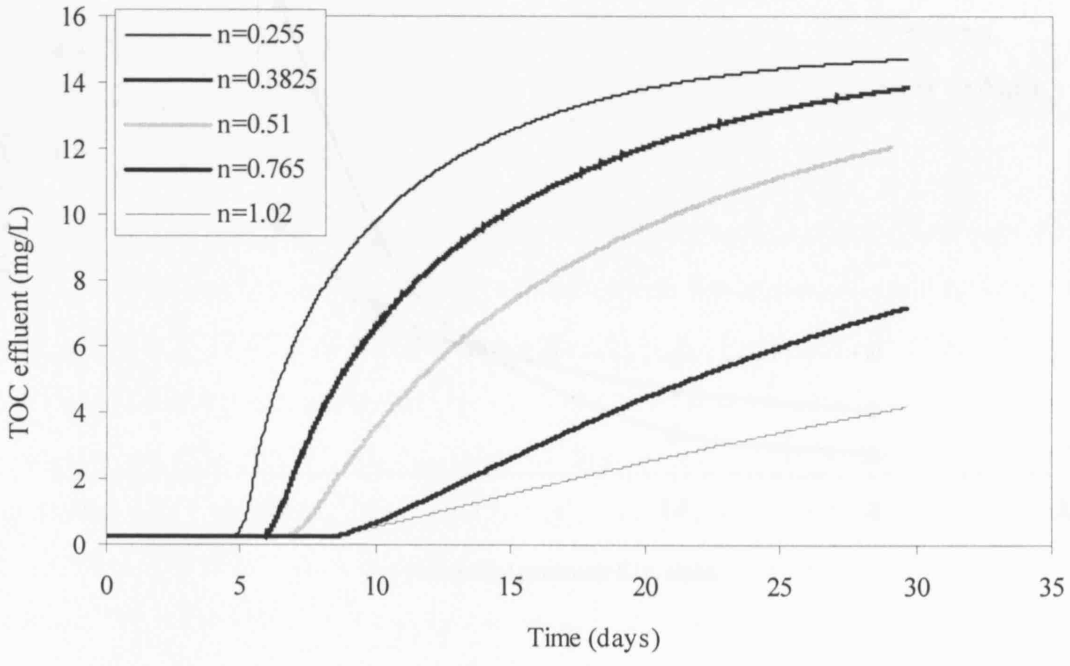

Figure 9.8 Parametric study for n (Freundlich constant) (K and **α** are constant)

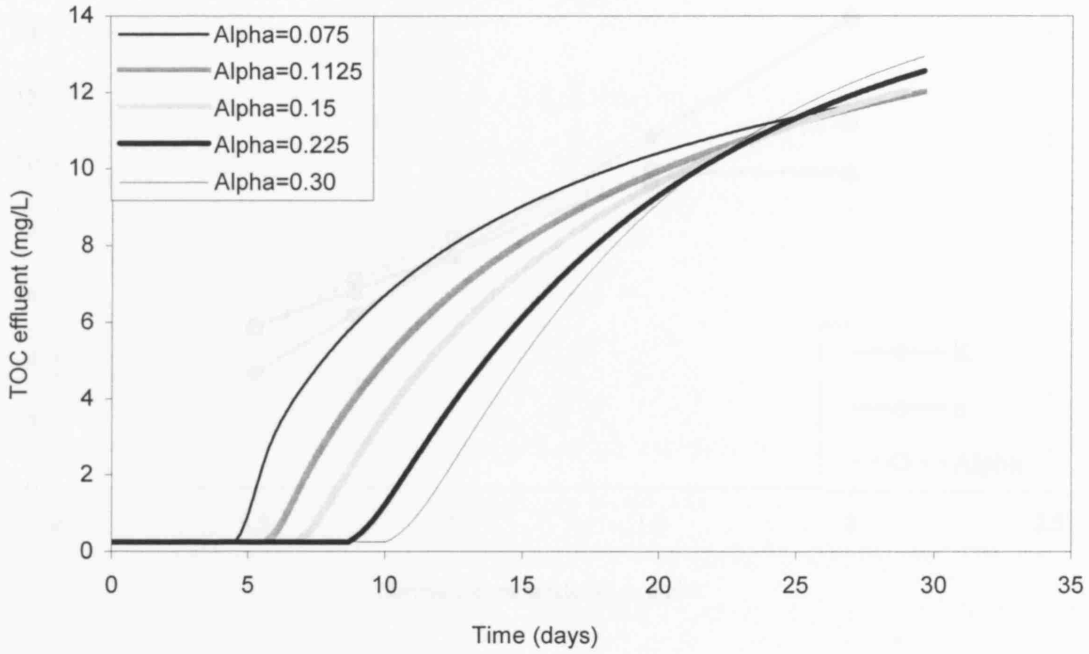

Figure 9.9 Parametric study for **α** (Freundlich constant) (K and n are constant)

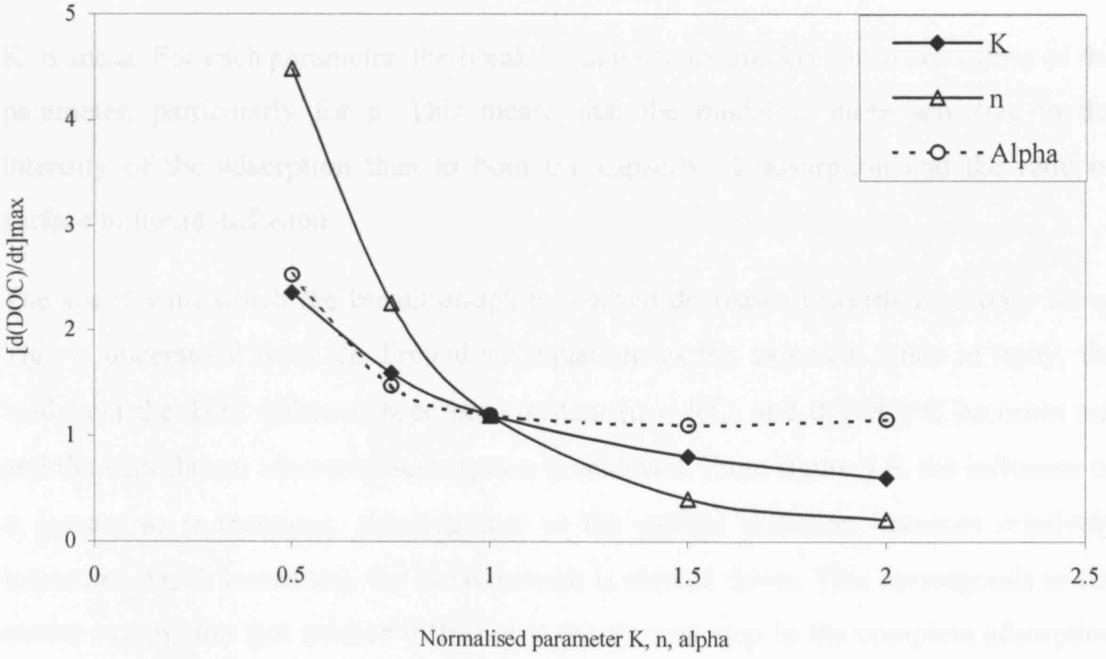

Figure 9.10 Variation of d(TOC)/dt (speed of the breakthrough) vs normalised Freundlich parameters

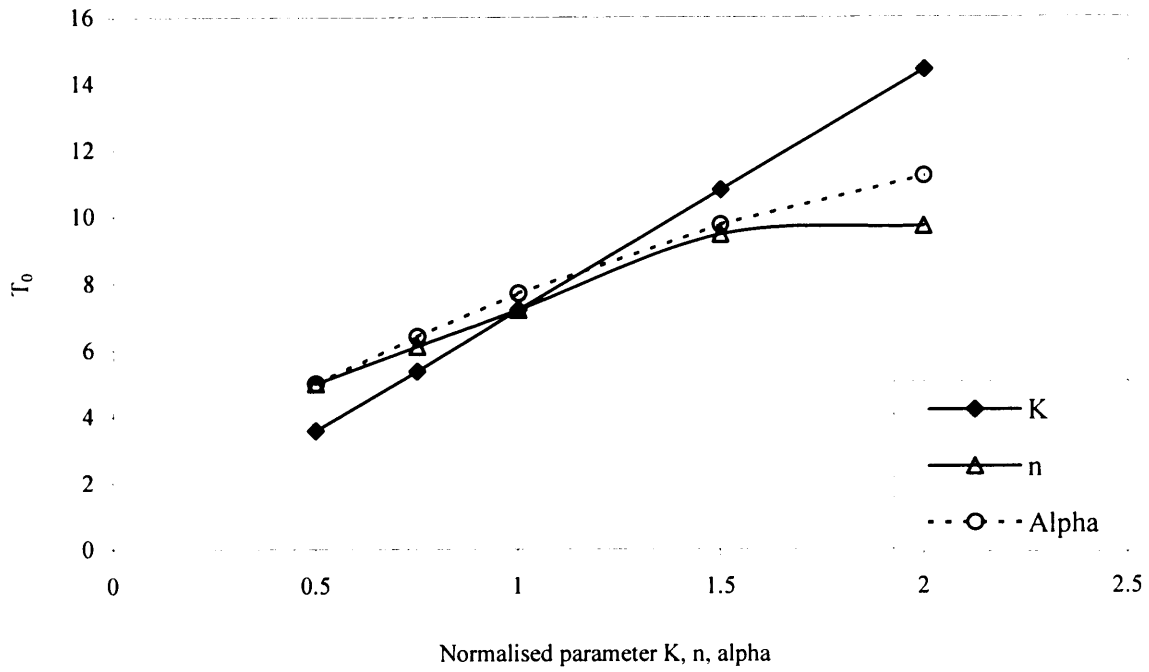

Figure 9.11 Variation of T_0 (start of the breakthrough) vs normalised Freundlich parameters

K, n and α. For each parameter, the breakthrough occurs quicker for lower values of the parameter, particularly for n. This means that the model is more sensitive to the intensity of the adsorption than to both the capacity of adsorption and the ratio of surface to liquid diffusion.

The speed with which the breakthrough is reached decreases towards zero only for n. This is understood from the Freundlich equation: as the exponent tends to unity, the load (and the TOC effluent) becomes constant ($q \approx KC$) and d(TOC)/dt becomes nul and the equilibrium adsorption-desorption is achieved. From figure 9.9, the influence of α lessens as α increases, showing that as the surface diffusion becomes relatively important (D_s/D_l increases), the breakthrough is slowed down. This corresponds to the model assumption that surface diffusion is the slowest step in the complete adsorption process. The influence of K is the least as regards the speed d(TOC)/dt.

Figure 9.11 shows a linear influence of the parameter value on T_0. The fastest increase is due to K, which is justified by the fact that K represents the adsorption capacity. On the contrary, α has an indirect influence only: it affects the surface diffusion coefficient that in turn influences the speed of TOC loading on the adsorbent (dq/dt). n does not

affect the model's answer beyond 75% of the initial value (i.e. the Freundlich exponent is equal to 0.76).

From the parametric study, it can be concluded that the most important parameters to be estimated with precision are the median size of the adsorbent grains, the molecular weight of the adsorbate and both the adsorption capacity K and intensity n.

9.3. Simulations

The model is calibrated for each system adsorbent/adsorbate/water type before running any simulation. The water type does not influence this study in any way since it did not involve any other contaminant or any particular water quality background. It was fixed as "High DOC water type". Fifteen calibrations were carried out (three adsorbents and five adsorbates F1, F2, F3, F12 and F123). Several assumptions were considered. These are:

- For F12, no K or n value is available and these are considered the same as for F2.
- The molecular weight is selected as the middle of the range covered (5000 Da for F12). For F123, the MW is set to 20000 Da since the adsorption behaviour was found to be close to F3 behaviour during the equilibrium studies.
- K and n are imposed from the values determined during the equilibrium studies.
- α is calculated using equation 9.3 as above (equation number not re-written):

$$\alpha = \frac{q^*_{\text{inf}} \times D_s}{C_{\text{inf}} \times D_l \times (1-\varepsilon)}$$

With $$q^*_{\text{inf}} = C_{\text{inf}} \times BulkDensity \qquad (9.4)$$

$$D_s = 0.374 \times 10^{-14} m^2 s^{-1}$$

$$D_l = 2.74 \times 10^{-9} \times MW^{-\frac{1}{3}} m^2 s^{-1} \qquad (9.5)$$

This value for the surface diffusion coefficient D_s is the only value found in the literature for humic substances (from Fettig, 1999).

Then α becomes

$$\alpha = \frac{BulkDensity \times D_s}{D_l \times (1-\varepsilon)} \tag{9.6}$$

$$\alpha = \frac{BulkDensity \times 1.367 \times 10^{-6}}{(1-\varepsilon) \times MW^{-\frac{1}{3}}} \tag{9.7}$$

From this last equation, the molecular weight increase also corresponds to an increase in α. This is consistent with the increase of the ratio D_s/D_l with the MW due to the fact that bigger molecules diffuse more slowly.

Data used are presented in table 9.2 below. It can be noticed how small the α values are (maximum is 0.11). The "autofit" function of α in GACMan suggests values between 0.15 and 0.7, all above the maximum calculated here. It is likely that the calculated values are underestimated due to use of a surface diffusion coefficient which is smaller than the real value.

The next step is the simulation itself. Parameters input for the simulations are:

- the characteristics of the adsorbents as measured in the laboratory
- the molecular weight MW as presented above
- the characteristics of the simulation run, including the shape diameter and depth of the filter, the flow, the length of the run and the temperature
- the adsorbates concentration and for each of them, the non-adsorbable fraction and the biodegradable fraction, the α value. K can also be modified although it was kept constant here.

From table 9.2, the values of n for adsorption of F1 on AAFS is high and cannot be used in GACMan (error message bringing the simulation to a halt). As for F12, no experimental data is available for comparison. Consequently, those simulations are not carried out in GACMan.

The simulations results are presented in figures 9.12, 9.13, 9.14, 9.15 and 9.16, respectively for the adsorption of F1 on GAC, F12 on β-FeOOH, F123 on GAC, AAFS and β-FeOOH.

Table 9.2 Parameter values used in GACMan for simulations

Adsorbate	Parameter	GAC	AAFS	B-FeOOH
F1	MW	2500	2500	2500
	K	5.5	0.01	0.01
	n	0.51	5.75	0.71
	α	0.02	0.04	0.06
F2	MW	7500	7500	7500
	K	1.44	1.08	2.5
	n	0.81	1.23	1.05
	α	0.025	0.05	0.07
F3	MW	30000	30000	30000
	K	0.54	2.55	1.60
	n	0.48	0.41	0.55
	α	0.04	0.075	0.11
F12	MW	5000	5000	5000
	K	1.44	1.08	2.5
	n	0.81	1.23	1.05
	α	0.02	0.05	0.07
F123	MW	20000	20000	20000
	K	0.30	0.60	1.04
	n	1.02	1.20	0.86
	α	0.04	0.075	0.11

All input data cited above are set as values measured from the laboratory or fixed column dimensions and the flow or Freundlich parameters determined from previous analyses. However, α is the remaining coefficient to be fitted so as to obtain the closest simulation to the experimental data. Therefore simulations results, as shown in these figures, present a set of curves corresponding to various values of α. A general comment is that none of the α values from table 9.2 gave any acceptable results and the value had to be set higher.

This confirms the previous comments as to the surface diffusion coefficient equal to 0.374×10^{-14} m^2 s^{-1} being too small.

Simulating the adsorption of F1 on GAC gives good results as shown on figure 9.12. The initial experimental data cannot be reproduced since they do not correspond to adsorption but rather are interpreted as a "preloading" required for adsorption to occur (discussed in the chapter seven). Once adsorption has really started (after 60 hours), the experimental behaviour is accurately reproduced. The best α value is approximately 0.3-0.4. However, from 200-250 hours of run, it seems that the best α value has increased beyond 0.5, which is interpreted as an evolution of the ratio of surface to liquid diffusion. The surface diffusion becomes dominant as the adsorbent is saturated. In this situation, the liquid diffusion is minimised since the gradient in the liquid film becomes insignificant when the surface is saturated. It must be emphasised that the non-adsorbable fraction was set as 0.3. Therefore the constant minimum effluent concentration is 30% of the influent concentration.

Adsorption of F12 was simulated by setting the non-adsorbable fraction equal to 0.2. From the results on figure 9.13, the beginning of adsorption is well represented until 200 hours by α in the range 0.15-0.25. Beyond that time, experimental breakthrough occurs quicker. This suggests that surface diffusion does not dominate from 200 hours which is explained by the little surface available on β-FeOOH and the MW in F12. Hence there is an accumulation of humic substances in the solution and an increase in the concentration gradient across the film close to the external surface. Such a situation would enhance the liquid film diffusion and lead to a decrease in α. It also shows the difficulty the model has in handling a wide range of MW.

The capacity of GACMan to divide the adsorbate into several components could not be exploited here. Since each component is treated independently from the others, a DOC

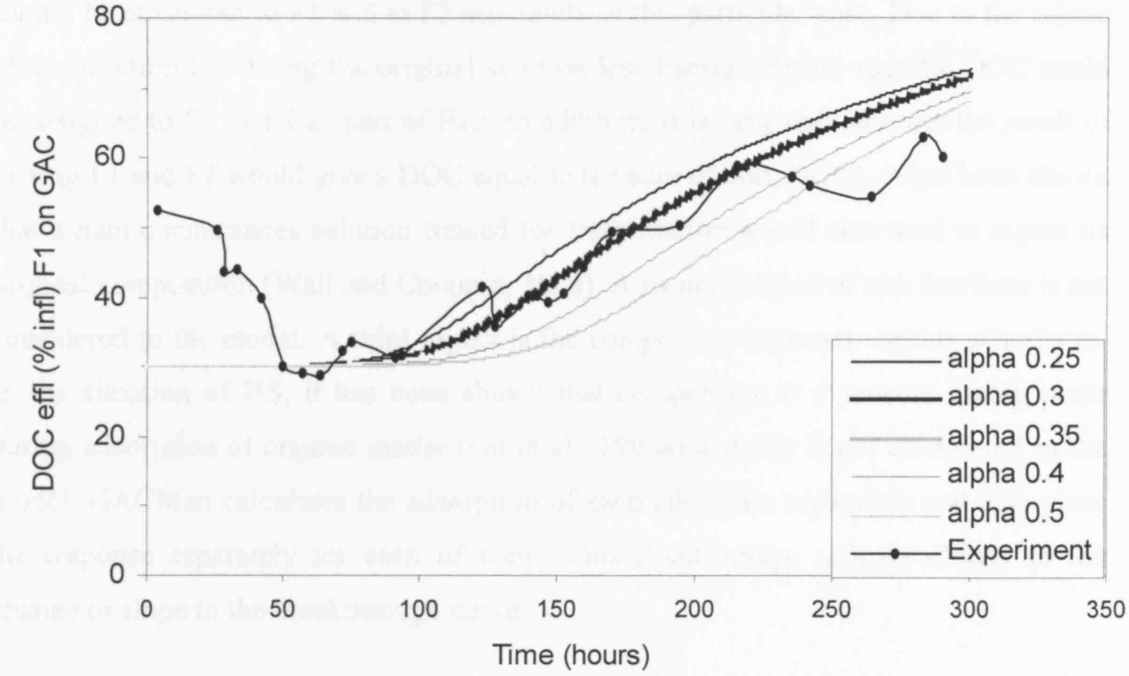

Figure 9.12 Simulation using GACMan, and experimental results for adsorption of F1 on GAC

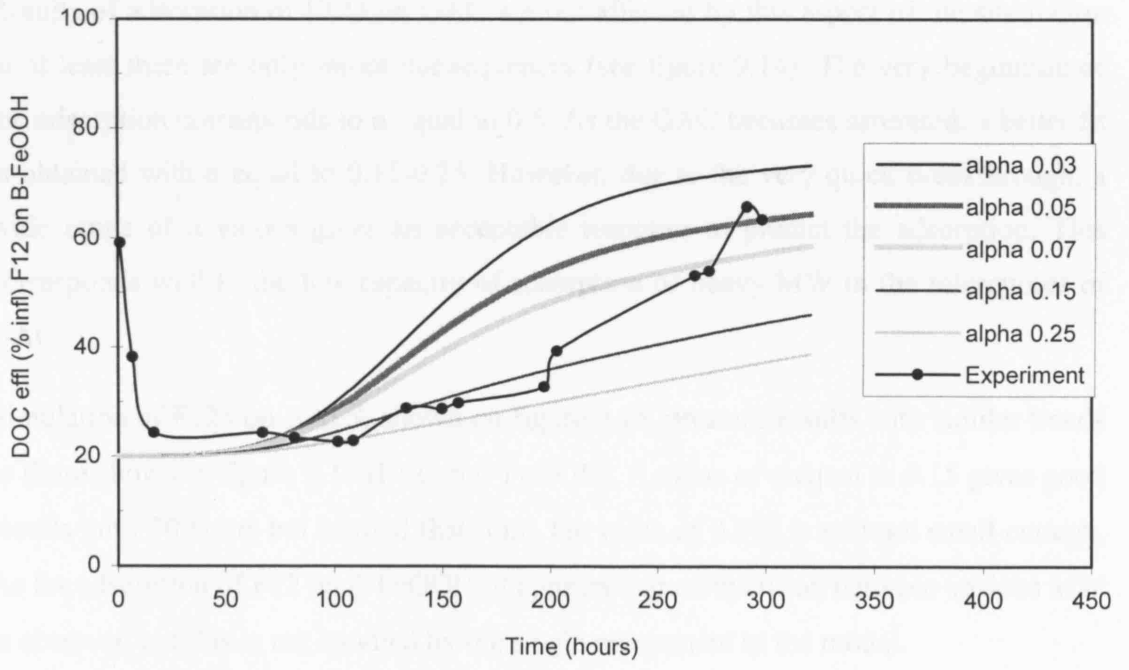

Figure 9.13 Simulation using GACMan, and experimental results for adsorption of F12 on β-FeOOH

should be attributed to F1 and to F2 separately in this particular case. Due to the nature of the solution F12 being the original solution less fraction F3, no specific DOC could be assigned to F1 or F2 as part of F12. In addition, it is very unlikely that the result of mixing F1 and F2 would give a DOC equal to the sum of both DOCs. It has been shown that a humic substances solution treated for fractionation would also tend to regain its original composition (Wall and Choppin, 2003). A recombination of two fractions is not considered in the model. A third aspect is the competition between various adsorbates. In the situation of HS, it has been shown that competition is a process taking place during adsorption of organic matter (Gu et al., 1996a) and this is not considered in the model. GACMan calculates the adsorption of each adsorbate separately and also gives the response separately for each of them. This disadvantage appears clearly in the change of slope in the breakthrough curve.

The alternative for solving this problem in GACMan is the best possible selection of the input data, such as the non-adsorbable fraction. This is also valid for simulating the adsorption of solution F123, containing the three fractions F1, F2 and F3, but in an undefined proportion.

Results of adsorption of F123 on GAC are not affected by this aspect of the simulation or at least there are only minor consequences (see figure 9.14). The very beginning of the adsorption corresponds to α equal to 0.5. As the GAC becomes saturated, a better fit is obtained with α equal to 0.15-0.25. However, due to the very quick breakthrough, a wide range of α values gives an acceptable response to predict the adsorption. This corresponds well to the low capacity of adsorption of heavy MW in the micropores of GAC.

Simulation of F123 on AAFS, shown on figure 9.15, presents results with similar trends to those shown in figure 9.13 (F12 on β-FeOOH). A value of α equal to 0.15 gives good results until 70 hours but beyond that time, the value of 0.075 is still not small enough. As for adsorption of F12 on β-FeOOH, it appears that competition between various MW is observed but this is not handled by the single component in the model.

The situation for simulating adsorption of F123 on β-FeOOH is different as seen on figure 9.16. Using the K values determined from the equilibrium studies, no values of α is able to give an acceptable simulation (see curves with K equal to 1.04). For this particular system, the adsorption parameter K must be decreased form 1.04 to 0.4 to

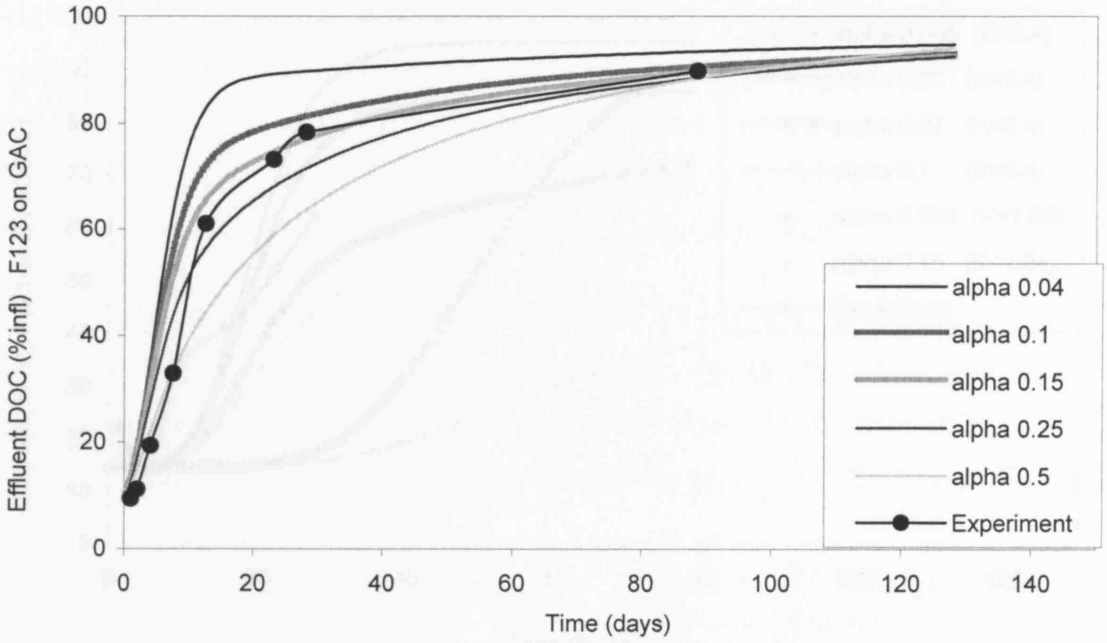

Figure 9.14 Simulation using GACMan, and experimental results for adsorption of F123 on GAC

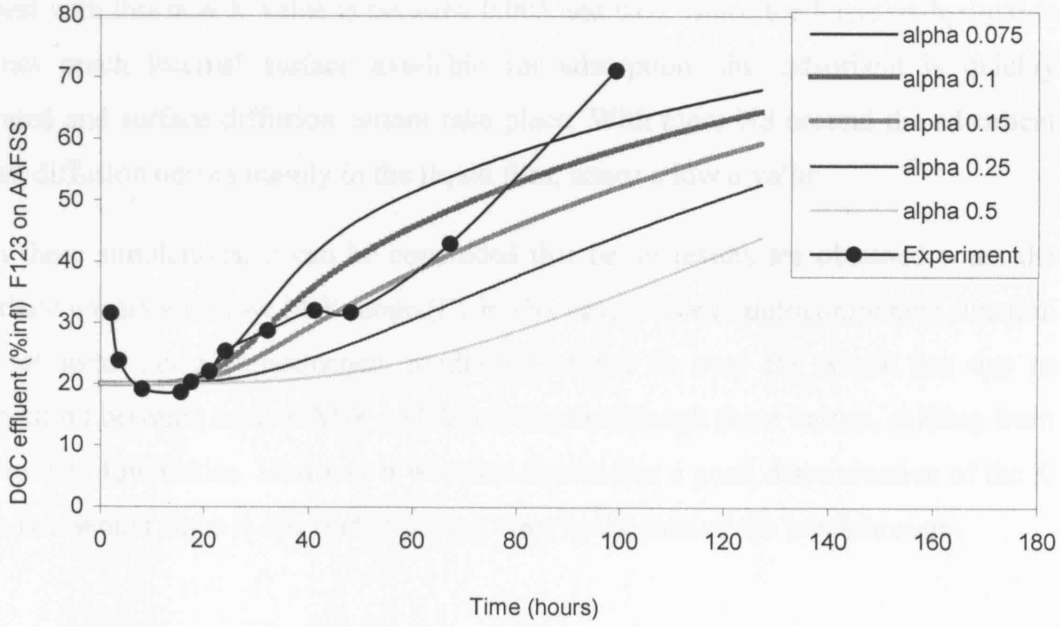

Figure 9.15 Simulation using GACMan, and experimental results for adsorption of F123 on AAFS

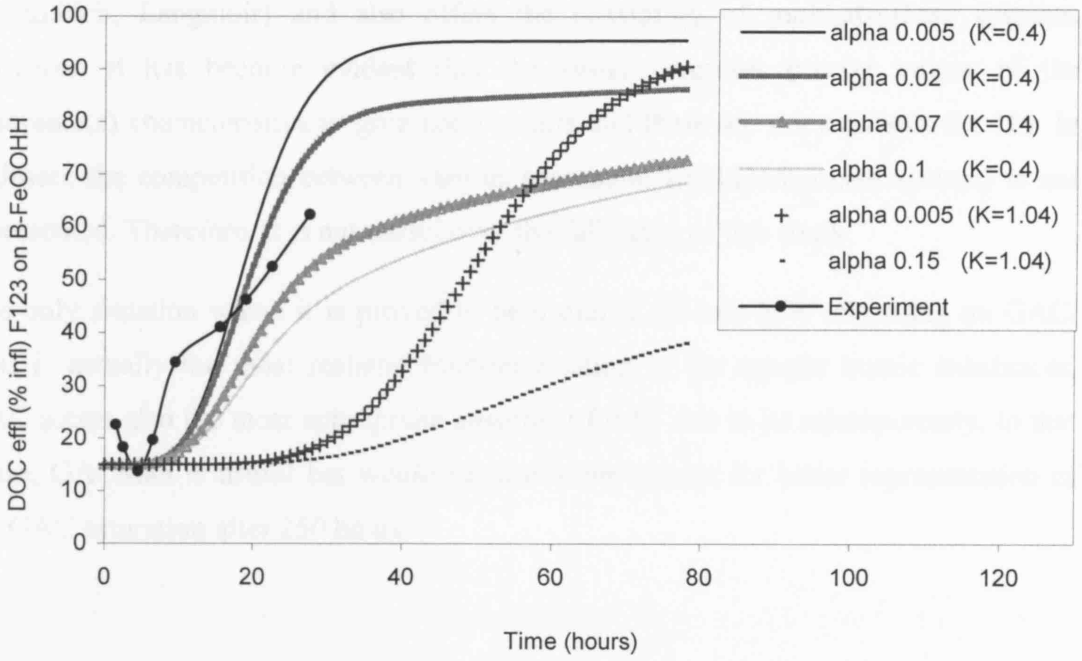

Figure 9.16 Simulation using GACMan, and experimental results for adsorption of F123 on β-FeOOH

observe the breakthrough starting from approximately 6 hours run. The α value fitting the best with this new K value is between 0.005 and 0.07. Since the ferric oxihydroxide has not much internal surface available for adsorption, this adsorbent is quickly saturated and surface diffusion cannot take place. With more HS around the adsorbent grains, diffusion occurs mainly in the liquid film, hence a low α value.

From these simulations, it can be concluded that better results are obtained when the adsorbate covers a narrow MW range (F1 in this case) since a multicomponent function was not used. As a consequence, modelling cannot fit over the whole run due to competition between several MW and this is shown through the α values, shifting from high to very low values. However it was also shown that a good determination of the K value is essential since it can lead to a large error in the start of the breakthrough.

9.4 Conclusions

The general conclusion for using this computer model is that GACMan is a powerful program that enables many adsorbent/adsorbate/water type systems to be simulated for the adsorption process. It offers several models commonly used in that field

(Freundlich, Langmuir) and also offers the possibility of multiadsorbate systems. However, it has become evident that the system requires precise values of the adsorbate(s) characteristics to give good results and these are not available for HS. In addition, the competition between various adsorbates (multicomponent system) is not represented. Therefore, it is not useful over the full range of this study.

The only situation where it is proved to be useful is for low MW adsorbing on GAC. This is actually the most realistic fraction existing in the aquatic humic substances. GAC seems also the most appropriate adsorbent for F1 due to its microporosity. In that sense, GACMan is useful but would require improvement for better representation of the GAC saturation after 250 hours.

CHAPTER 10

CONCLUSIONS AND RECOMMENDATIONS FOR FURTHER WORK

10.1 Conclusions

The investigation related in the previous nine chapters enables numerous conclusions to be drawn regarding the use of three media (granular activated carbon GAC, coated activated alumina AAFS and ferric oxihydroxide β-FeOOH) to adsorb humic substances with molecular weights up to 50 kDa. These conclusions are presented here, following the same logical order as the chapters.

- **Adsorbent and adsorbate characteristics**

Tools used to analyse and describe the adsorbents were the FTIR, the pH_{zpc}, the scanning electronic microscopy (SEM), laboratory sieving techniques and the adsorption of the nitrogen gas. These techniques have brought complementary insight into the characteristics and properties of each adsorbent.

FTIR showed the importance of the hydroxyl group OH on each adsorbent and also of hydroxo complexes (H bonds to surface oxygen atoms). FTIR strongly supported the suggestion that the coating on AAFS is a ferric or ferrous sulphate. However, the structure of akaganeite could not be confirmed. The point of zero charge, pH_{zpc}, has indicated that the iron compounds are acidic and GAC is basic (5.0 for AAFS, 5.4 for β-FeOOH and 10.6 for GAC). GAC is slightly positive at neutral (working) pH whereas the iron compounds are negative, which is not in favour of HS adsorption. Yet, the large difference with the low pH_{zpc} for β-FeOOH compared to values stated in the literature, is not understood. This same analysis has also indicated that calcium is not a neutral ion and tends to decrease the surface charge.

SEM information gives an excellent idea of the surface roughness and structure. GAC clearly shows a layered graphite like structure with numerous cavities. AA, AAFS and β-FeOOH show no obvious cavities and a smooth surface (AAFS has a surface that seems smoothened by the coating).

β-FeOOH is less porous than GAC and aluminas, which is attributed to the absence of high temperature treatment during the activation step of the media. The adsorbent grain size distribution was particularly narrow for the aluminas, with the lowest median diameter equal to 0.4 mm. GAC and β-FeOOH have a wide grain size distribution. However, the latter was more subject to attrition and was also the denser of the three media, which had a particular effect on the compaction of the adsorbent, with possible consequences in the adsorption column (β-FeOOH can loose almost 20% of its porosity).

Adsorption of nitrogen on the adsorbent surface gives extremely valuable information regarding the adsorption, including indications of the surface area, the pore size and pore size distribution of the media. However, data must be interpreted cautiously according to the method used. GAC shows almost no hysteresis on the isotherm, indicating that mainly micropores are present, probably slit-shaped. Alumina is mainly mesoporous, with parallel plates interconnected to form the porosity network (crystal layer structure). β-FeOOH also stands principally in the mesoporous range with interconnected ink-bottle shaped pores. Surface area is large for GAC (980 m^2/g) and much smaller for AAFS and β-FeOOH, around 286 and 360 m^2/g respectively.

The examination of the GAC indicates that it has a large microporous area and little meso- and macroporous area (BET and t-plots analyses). This agreed well with the BJH method whereby GAC pore size distribution displayed only a small peak centered on 3.5 nm and with the HK method which indicated a major accumulation of porosity below 2 nm (microporosity). The iron compounds were examined in the same way and did not present any microporous area; the peak at 3.5 nm was strong for AAFS and very strong and narrow for β-FeOOH. However, results obtained by the HK method did not corroborate the total absence of microporosity on these two adsorbents. A high microporous volume was unexpectedly attributed to AAFS and still more so for β-FeOOH. Such a strong contradiction with the t-plots results has been attributed to the fact that the t-plots cannot handle well the presence of a small proportion of

microporous area. Final interpretation is that microporosity is also present on the iron compounds, but to a minor extent.

The examination of the humic substances has been essential in setting up the experimental work for adsorption studies and in understanding/interpreting the results. This task was compulsory since the present adsorbate is not a simple and well defined molecule. On one hand, calculation of errors on the measured parameters have validated the results of UV absorbance, DOC and SUVA. On the other hand, freezing the acidified samples for four weeks, before performing the DOC analysis, has shown unaltered DOC results. This method is validated and completely new to this work. SUVAs were around 2, 5.8 and 8.3 respectively for F1, F2 and F3 and F123 was similar to F3. It is kept in mind that assessment of the MW is very different according to the authors and to the preparation method. In this study, aggregation might have occured during centrifugation, together with possible retention by PES membrane, therefore altering the original MW distribution. HS characterisation requires two parameters out of the three (UV, DOC, SUVA) since a high DOC or a high UV absorbance only does not give any idea of the type of humic present (MW), and SUVA only does not give any idea of the concentration.

The main conclusion on the expected conformation of HS (neutral pH and low ionic strength), is that the molecules are probably elongated. The gyration radius for each fraction was also estimated.

An aspect often neglected is the ageing of the solution. It did occur in several cases, leading to a decrease in UV absorbance, a larger decrease in DOC and consequently an increase of SUVA.

- **Kinetic studies**

The mixing speed affects the external diffusion rate and this was clearly shown on the studies using AAFS and β-FeOOH, which have a high mesoporosity. On GAC, the influence was not important which is attributed to the porosity being mainly in the microporous range, hence there is little effect on the external transport resistance. The mixing speed is also of utmost importance when it leads to attrition of the media. However, this is not usually taken into account in most studies, although the bulk

characteristics of the media are modified. Consequently, in this work, data beyond 399 minutes were discarded when the speed was 300 rpm.

From the various models applied, it is generally concluded that a model rarely fits over the whole period of study but rather several models fit over different periods of time within the process, which means that the mechanisms controlling adsorption rate vary. Three stages are often observed *(i)* an instantaneous adsorption lasting a few minutes *(ii)* a regular adsorption lasting between one and a half to three hours and *(iii)* the last stage when the adsorbent becomes saturated and adsorption slows down (equilibrium).

The pseudo-first order model cannot represent the whole range of data and fits in the three consecutive sections. The pseudo-second order model fits better over the whole range, although the instantaneous adsorption during the first minutes is not well represented either. However loads are well predicted for β-FeOOH.

The Elovich equation represents fairly well the experimental data for GAC and AAFS. Its applicability is shown thanks to low time constants and good correlation coefficients.

The intraparticle diffusion model applies well for stage (ii) adsorption only. Reliable diffusion coefficients were estimated for GAC and β-FeOOH. A different phenomenon occurred on AAFS, as adsorption seemed to follow a second stage (i) instead of stage (iii), which was attributed to the flaking of the coating, thus generating more bare surface. As a result, the dominant mechanism on AAFS varies, starting with the adsorption being limited by internal diffusion, then diffusion accompanied by a chemical reaction and later by external diffusion. The external diffusion model applies well in different stages of adsorption, most likely due to attrition generating new grains hence exposing a new external surface. Hence, it is not applicable as such over the whole range of data, which is to be expected since the mixing is not likely to limit external adsorption.

It is important to comment that having a multi molecular weight adsorbate is likely to result in a multiplicity of mechanisms. The models used here do not account for such additional mechanisms (competition, displacement, pore plugging due to large molecules). Splitting the adsorbate into several components before applying the models would bring more insight into understanding the kinetics. However in reality, the mixture of the MW is expected to bring about discrepancies in the results due to micropore blockage and inhibited intraparticle diffusion. New models incorporating these factors would represent an ideal way forward.

- **Batch systems**

The isotherms were obtained for the adsorption of each fraction and of the complete solution (F123) onto each adsorbent. It is shown that GAC offers a large capacity for the removal of low MW (F1). The isotherm is concave (favourable) thanks to the GAC positive surface that gives space for coulombic forces and electrostatic attraction that binds the lower MW to the carbon surface. On the contrary for the iron adsorbents AAFS and β-FeOOH, the isotherm representing adsorption of F1, is convex (unfavourable) and corresponds to negative surface charges. On these two media, only the intermediate MW between 5 and 10 kDa (F2) can be efficiently removed, with both short and long range forces involved. The tendency for F2 on GAC is reversed and these intermediate MW do not adsorb well on the activated carbon. Very heavy MW (above 10 kDa) cannot be removed efficiently in any case since they quickly saturate the surface. F3 adsorbs better on the iron compounds than on GAC (convex) although adsorption has decreased when compared to F2. As for the complete solution F123, it behaves like F3 and is not efficiently adsorbed by any media.

It is strongly suggested that precipitation/condensation occurs on the adsorbent surface when the DOC concentration increases significantly, reflected in the sudden sharp increase of the load in most cases. As a consequence of negative surfaces, coulombic forces that enable a high and strong adsorption cannot be the main driving force.

Calcium was added to the humic substances solution (made up with deionised water) so as to represent a water with a hardness equivalent to London water hardness. Since calcium form complexes with HS, two consequences have resulted from this interaction: *(i)* the number of sites occupied by one molecule of humic substance for adsorption might have decreased, leaving more sites available for other HS. And *(ii)* by cancelling some of the negative HS charges, intermolecular repulsion might have been reduced and allowed HS molecules to be closer to one another near the adsorbent surface. The influence was judged to be qualitatively positive towards HS removal and to contribute to an increase in the adsorption capacities calculated for the adsorbents (not new to this work).

As regards modelling the adsorption equilibrium, the Freundlich model fitted for each configuration adsorbent/adsorbate. The delay in adsorption is a constant feature of the adsorption study, due to a non-adsorbable fraction with very low MW and it was not

well represented by any model. The Langmuir model fitted in a minority of cases (not for F1); it was applicable in the second region of adsorption but neither at low or high coverage. The Henry model was applicable in most cases, but only in the low range of concentration.

For heavy MW, it seems that the surface becomes more homogeneous. In reality, this means that, as the MW increases, the energy of adsorption becomes less important as a decisive criteria for adsorption.

- **Column studies**

It was initially shown that small columns could be used instead of large column, providing for a more practical experimental process together with reliable results.

The capacity of the adsorbents GAC, AAFS or β-FeOOH for removing a wide MW range of humic, has been estimated. GAC was proven to adsorb well humic substances with MW below 5 kDa (F1), in agreement with adsorption in batch systems. Accordingly, AAFS and β-FeOOH did not remove F1 to the same extent. This tendency was reversed for F123 which was not adsorbed on GAC but adsorbed well onto AAFS.

With each adsorbent, a non-adsorbable fraction (low MW) was responsible for a residual DOC from the start of the run (15% UV and 30% DOC for F1, 5% UV and 25% DOC for F12 and 3-5% UV and 20% DOC for F123).

A phenomenon that has not been mentioned in the consulted literature is the initial DOC decrease in the column effluent, over several hours, before a steady concentration or the start of breakthrough is observed. The only case where this was not observed was for adsorption of F123 onto GAC. It is concluded that adsorption of heavier MW of each solution (F1, F12 and F123) requires a concentration gradient to build up in the column before observing any DOC removal in the effluent.

Prediction of the removal is also successful using the analytical method supplied by the Thomas equation, but only from the time when the effluent DOC started to increase. It also corresponds to the applicability of the Langmuir model for the adsorption isotherm.

As for the BDST model (adsorption of F123), the Mass Transfer Zone is broad for each adsorbent. The contact time in the columns seems to be more important than the bed depth and most of the adsorption occurs in the top first layers. The adsorbents are not

completely exhausted when reaching about 80% breakthrough. This gives another evidence of the slow diffusion of HS particularly for high MW. A critical bed depth cannot be computed where the BDST equation gives a positive intercept, which seemed to correspond to situations where the bed depth did not greatly influence.

In addition, two distinctive features appear from these results:

(i) GAC is able to remove high MW although lacking of mesoporosity (attributed to precipitation and alteration of HS conformation) and

(ii) β-FeOOH does not show such a high adsorption capacity as previously predicted, attributed to the non-equilibrium state and to the lack of surface under the media compaction.

Low MW were found to be adsorbable on GAC but only to a very limited extent on the iron compounds and the heavier MW were more adsorbable on the iron compounds than on GAC. Consequently, when F123 is considered as a single adsorbate, the above cited analytical models have encountered difficulties in predicting the residual DOC.

- **Modelling with GACMan**

The parametric study has indicated that the most important parameters, to be estimated with precision, were *(i)* the median grain size for the bulk adsorbent characteristics, *(ii)* the MW for the adsorbate characteristic (the only one input in GACMan), and *(iii)* both the Freundlich constant K and adsorption intensity n (slope of the isotherm). In general, fluctuations on the parameters did not change the general shape of the breakthrough curve but shifted the curve or stretched/shrank it slightly. The humic substances MW's influence increased as the MW decreased. As for Freundlich parameters' influence, K_F influences most the time when breakthrough starts. The intensity of adsorption (via the exponent n) has most influence on the speed of the breakthrough.

The best results were obtained when the adsorbate coverered a narrow MW range (F1) since a multicomponent function was not used. This coincides with MW being one of the most important parameters to be input with precision. As a consequence, modelling cannot fit over the whole run due to competition between several MW and this is shown through the α values, shifting from high to very low values.

GACMan is a powerful program that enables the simulation of adsorption process for many adsorbent/adsorbate/water type systems. It offers several models commonly used in that field (e.g. Freundlich, Langmuir) and also offers the possibility of multiadsorbates systems. However, full exploitation of the model requires knowledge of the precise characteristics of the adsorbate and this is not the case for HS. An example is the impossibility of using the multicomponent function if the distribution of the MW is not input accurately. In any case, competition between various adsorbates (multicomponent system) would not be represented.

However, the model proved to be useful in simulating the adsorption of low MW on GAC. F1 is actually the most realistic fraction existing in aquatic humic substances. GAC was the only microporous medium studied in this work and as such, proved to be the most appropriate adsorbent for F1. In this situation, it is concluded that the GACMan model can be useful but would require improvement to better represent the GAC saturation after 250 hours.

10.2 Recommendations for further work

Complementary work should be carried out to fullfill the aims and objectives initially set for this research. The following points could be addressed:

- To investigate the kinetics for fractions F1, F2 and F3 separately.
- To perform experiments on the columns using fractions F2 and F3.
- To use the multicomponent function in GACMan with the column results for F2 and F3 adsorption, in addition to F1, F2 and F123 adsorption results.

Besides, additional areas of interest are identified which will assist in understanding and approaching new aspects of this vast topic that is the humic substances removal using inorganic adsorbents. These are:

- After analysing the FTIR spectra and SEM photographs for the blank adsorbents, it would be relevant to analyse the used adsorbents in the same ways.
- The unadsorbable fraction represents mainly the low MW. It is recommended to investigate the influence of this fraction onto the more adsorbable one, in terms of competition or interaction.

- Attrition takes place, particularly for β-FeOOH. This depends upon the mixing speed and the hydrodynamic regime and could generate more microscopic eddies around the new smaller grains. It is recommended that the influence of attrition on adsorption should be examined. It is also of interest to determine whether or not the phenomenon takes place in the column and to what extent.
- With a larger concern for the environment and effluent quality standards, the leaching of iron and aluminium should be examined.
- The value of the pH_{zpc} of β-FeOOH (5.4) has been confirmed by using two different electrolytes. Since a higher value (closer to 7-8) is generally mentioned in the literature, it is advised to investigate further this characteristic of the iron adsorbent.
- By decreasing the pH of the working solution slightly towards the pH_{zpc}, would adsorption be slightly or largely improved?
- It was suggested that, after fractionation, the humic substances somehow regain their original MW distribution. This suggestion of a "memory effect" needs further investigation for confirmation.
- GAC 207C is mainly microporous and slightly mesoporous GACs have been mentioned to better adsorb higher MW. Therefore, it is recommended to investigate the activation stage during the activated carbon preparation in order to modify the pore size distribution and tailor it towards an optimum adsorption of HS.

CHAPTER 11

REFERENCES

A

Agbenin J.O. and van Raig B. (1999) Rate processes of calcium, magnesium and potassium desorption from variable-charge soils by mixed ion-exchange resins. *Geoderma* **93**, 141-157.

Ahmedna M., Marshall W.E. and Rao R.M. (2000) Surface properties of granular activated carbons from agricultural by-products and their effects on raw sugar decolorization. *Bioresource Technology* **71**, 103-112.

Aksu Z. and Dönmez G. (2003) A comparative study on the biosorption characteristics of some yeast for Remazol Blue reactive dye. *Chemosphere* **50**, 1075-1083.

Aksu Z. and Gönen F. (2004) Biosorption of phenol by immobilized activated sludge in a continuous packed bed: prediction of breakthrough curves. *Process biochemistry* **39**, 599-613.

Aharoni C. and Sparks D.L. (1991) Kinetics of soil chemical reactions – a theoretical treatment. In: Sparks D.L. and Suarez D.L. (Eds), Rates of soil chemical processes. *SSSA Special publication*, **27**, 1-18.

Al-Ghouti M. Khraisheh M.A.M., Ahmad M.N.M. and Allen S. (2005) Thermodynamic behaviour and the effect of temperature on the remoal of dyes from aqueous solution using modified diatomite: a kinetic study. *J. Colloid Interface Sci.* **287** (1) 6-13.

Al-Ghouti M.A.S. (2004) Mechanisms and chemistry of dye adsorption on diatomite and modified diatomite. PhD dissertation. The Queen's University of Belfast, Ireland.

Allpike B.P., Heitz A., Joll C.A., Kagi R.I., Abbt-Braun G., Frimmel F.H., Brinkmann T., Her N. and Amy G. (2005). Size exclusion chromatography to characterize DOC removal in drinking water treatment. *Environ. Sci. Technol.* **39**, 2334-2342.

Amy G. and Cho, J. (1999) Interactions between natural organic matter (NOM) and membranes: rejection and fouling. *Wat. Sci. & Technol.* **40** (9) 131-140.

André C. (2003) PhD Transfer report (internal Report). University College London.

Aracheandio I., Güell C., Medina F., Lamuela-Raventós R. and López F. (2002) Note. Vinegar decolourization by re-activated carbon. *Food Sci. Tech. Int.* **8** (4) 239-242.

Atkinson, R.J., Posner, A.M., Quirk, J.P. (1967) Adsorption of potential-determining ions at the ferric oxide-aqueous electrolyte interface. *The journal of physical chemistry* **71** (3) 550-558.

Au K.-K., Penisson A.C. Yang and S. O'Melia C.R. (1999) Natural organic matter at oxide/water interfaces: complexation and conformation. *Geochimica and Cosmochimica Acta.* **63** (19) 2903-2917.

Avena M.J. and Koopal L.K. (1998) Desorption of humic acids from an iron oxide surface. *Environ. Sci. Technol.* **32**, 2572-2577.

Avena M.J. and Koopal L.K. (1999) Kinetics of humic acid adsorption at solid-water interfaces. *Environ. Sci. Technol.* **33**, 2739-2744.

AWWA (1990) Water quality and treatment (4th ed.) Mc Graw Hill.

B

Badruzzaman M, Westerhoff P. and Knappe D.R.U. (2004) Intraparticle diffusion and adsorption of arsenate onto granular ferric hydroxide (GFH). *Water Res.* **38**, 4002-4012.

Bailey J.K., Brinker C.J. and Mecartney M.L. (1993) Growth mechanisms of iron oxide particles of differing morphologies from the forced hydrolysis of ferric chloride solutions. *J. Colloid Interface Sci.* **157**, 1-13.

Bakoyannakis D.N., Deliyanni E.A., Zouboulis A.I., Matis K.A., Nalbandian L. and Kehagias Th. (2003) Akaganeite and goethite-type nanocrystals: synthesis and characterization. *Microporous and mesoporous materials*, **59**, 35-42.

Balnois E., Wilkinson K.J., Lead J.R and Buffle J. (1999) Atomic force microscopy of humic substances: effects of pH and ionic strength. *Environ. Sci. Technol.* **33** (21) 3911-3917.

Bansal R.C. Donnet J.B. and Stoeckli F. (1988) Active Carbon. Marcel Dekker, New York.

Becker W. C., Au K. K., Chevallier M. W., O'Melia C. R. and Young J. S. (2001) The effects of oxidation on the performance of granular filter media filters: the role of

natural organic matter. *Proceeding of "Advances in rapid granular filtration in water treatment"* 4-6 April 2001, London, UK, 47-57.

Beckett R., Ju Z. and Giddins J.C. (1987) Determination of molecular weights distributions of fulvic and humic acids using flow-field fractionation. *Environ. Sci.* Technol. **21**, 289-295.

Bhummasobhana A., Scamehorn J.F., Osuwan S., Harwell J.H. and Baramee S. (1996) Surfactant-enhanced carbon regeneration in liquid phase application. *Sep. Sci. Technol.* **31**, 5, 629-641.

Bian B., Watanabe Y., Tambo N., and Ozawa G. (1999) Removal of humic substances by UF and NF membrane systems. *Wat. Sci. & Technol.* **40** (9) 121-130.

Bob M. and Walker H.W. (2001) Enhanced adsorption of natural organic matter on calcium carbonate particles through surface charge modification. *Colloid and Surfaces. A: Physicochemical and engineering aspects* **191**, 17-25.

Bolto B., Abbt-Braun G., Dixon D., Eldrige R., Frimmel F., Hesse S., King S, and Toifl M. (1999) Experimental evaluation of cationic polyelectrolytes for removing natural organic matter from water. *Wat. Sci. & Technol.* **40** (9) 71-80.

Bolto B., Dixon D., Eldridge R. and King S. (2002) Removal of THM precursors by coagulation or ion exchange. *Wat. Res.* **36**, 5066-5073.

Brunauer, S, Deming L.S., Deming W.S. and Teller E. (1940). A theory of the van der Waals adsorption of gases. *J. Amer. Chem. Soc.* **62**, 1723-1732.

C

Cameron R.S., Thornton, B.K., Swift, R.S. and Posner, A.M. (1972) Molecular weight and shape of humic acid from sedimentation and diffusion measurements on fractionated extracts. *J. Soil Sci.* **23**. 394-408.

Chang M.-Y. and Juang R.-S. (2004) Adsorption of tannic acid, humic acid, and dyes from water using the composite of chitosan and activated clay. *J. Colloid Interface Sci.* **278**, 18-25.

Chang Y., Li C.-W., and Benjamin M.M. (1997) Iron oxide-coated media for NOM adsorption and particulate filtration. *JAWWA.* **89** (5) 100-113.

Chen P.H. (1999) Removing aquatic organic substances by anion-exchange resin and activated carbon. *Environ. Int.* **25** (5) 655-662.

Chen P.H. (1997) Adsorption of organic compounds in water using a synthetic adsorbent. *Environ. Int.* **23** (1) 63-73.

Chen A.S.C. and Snoeyink V.L. (1987) Activated alumina adsorption of dissolved organic compounds before and after ozonation. *Enviro. Sci. technol.* **21**, 83-90.

Chen B., Hui C.W. and McKay G. (2001) Film-pore diffusion modeling for the sorption of metal ions from aqueous effluents onto peat. *Wat. Res.* **35** (14) 3345-3356.

Cheng W., Dastgheib S.A. and Karanfil T. (2005) Adsorption of dissolved natural organic matter by modified activated carbons. *Wat. Res.* **39**, 2281-2290.

Cheung C.W., Porter J.F. and McKay G. (2000) Elovich equation and modified second-order equation for sorption of cadmium ions onto bone char. *J. Chem. Technol. Biotechnol.* **75**, 963-970.

Cheung C.W., Porter J.F. and McKay G. (2001) Sorption kinetic analysis for the removal of cadmium ions from effluents using bone char. *Wat. Res.* **35** (3) 605-612.

Chi F.-H. and Amy G.L. (2004) Kinetic study on the sorption of dissolved natural organic matter onto different aquifer materials: the effects of hydrophobicity and functional groups. *J. Colloid Interface Science* 274 (2) 380-391.

Chin Y.-P., Aiken G. and O'Loughlin E. (1994) Molecular weight, polydispersity and spectroscopic properties of humic substances. *Environ. Sci. Technol.* 28, 1853-1858.

Chorover J. and Amistadi, M.K. (2001) Reaction of forest floor organic matter at goethite, birnessite and smectite surfaces. *Geochim. Cosmochim. Acta,* **65** (1) 95-109.

Chow C.W.K., van Leeuven J.A., Drikas M., Fabris R., Spark K.M. and Page D.W. (1999) The impact of the character of natural organic matter in conventional treatment with alum. *Wat. Sci. & Technol.* **40** (9) 97-104.

Choy K.K.H., Porter J.F. and McKay G. (2004) Intraparticle diffusion in single and multicomponent acid dye adsorption from wastewater onto carbon. *Chem. Eng. J.* **103**, 133-145.

Chu K.H. (2004) Improved fixed bed models for metal biosorption. *Chemical Engineering Journal*, **97**, 233-239.

Clark M.M., Wang, Y. and Combe, C. (2000) Measuring the diffusivity of humic acid. *Symposia papers, Am. Chem. Soc.* **40** (2) 297-298.

Conter L. and Knox R. (1986) Groundwater Pollution Control. Lewis, USA. 96-101.

Cook R.L. and Langford C.H. (1998) Structural characterization of a fulvic acid and a humic acid using solid-state ramp-CP-MAS ^{13}C Nuclear Magnetic Resonance. *Environ. Sci. Technol.* **32**, 719-725.

Crittenden J.C., Luft P., Hand D.W., Oravitz J.L., Loper S.W. and Ari M. (1985) Prediction of multicomponent adsorption equilibria using Ideal Adsorbed Solution Theory. *Environ. Sci. Technol.* **19** (11) 1037-1043.

D

De Laat A.W.M., van den Heuvel G.L.T. (1995) Molecular fractionation in the adsorption of polyacrylic acid salts onto $BaTiO_3$. *Colloids Surf. A*, 98, 53-59.

De Wit J.C.M., Van Riemsdijk W.H. and Koopal L.K. (1993a). Proton binding to humic substances: 1. Electrostatic effects. *Environ. Sci. Technol.* **27**, 2005-2014.

De Wit J.C.M., Van Riemsdijk W.H. and Koopal L.K. (1993b), Proton binding to humic substances: 2. Chemical heterogeneity and adsorption models. *Environ. Sci. Technol.* **27**, 2015-2022.

Degrémont (1989) Mémento technique de l'eau. *Degrémont*, 9th ed.

Deliyanni E.A., Bakoyannakis D.N., Zouboulis A.I., Matis K.A. and Nalbandian L. (2001) Akaganéite-type β-FeO(OH) nanocrystals: preparation and characterization. *Microporous and mesoporous materials* **42,** 49-57.

Diallo M.S., Goddard Ill W.A. and Johnson J,H. Jr (2000) Small angle neutron scattering investigations of Suwanee River fulvic acid aggregates in aqueous solutions. *Symposia papers, Am. Chem. Soc.* **40** (2) 541-545.

Ding J.Y. and Wu S.C. (1997) Transport of organochlorine pesticides in soil columns enhanced by dissolved organic carbon. *Wat. Sci. Technol.* **35**, 139-145.

Ding L., Mariñas B.J., Schideman L.C. and Snoeyink V.L. (2006) Competitive effects of natural organic matter: parametrization and verification of the three-component adsorption model COMPSORB. *Environ. Sci. Technol.* **40**, 350-356.

Do D.D. and Hu X. (1993) An energy-distributed model for adsorption kinetics in large heterogeneous microporous particles. *Chemical Engineering*, **48** (11) 2119-2127.

Doan P.T. (2001) Characterization of Cu-Co-Cr-K catalysis. MSc thesis, Faculty of Mississipi State University, USA.

Drever J.I. (1994) The geochemistry of natural waters.*3rd ed.*London, Prentice Hall.

Dries J., Bastiaens L., Springael D., Kuypers S., Agathos S.N. and Diels L. (2005) Effects on humic acids on heavy metal removal by zero-valent iron in batch and

continuous flow column systems. *Wat. Res.* **39** (15) 3531-3540.

Duan J., Wilson F., Graham N. and Tay J.H. (2002) Adsorption of humic acid by powdered activated carbon in saline water conditions. *Desalination*, **151**, 53-66.

E

Ebie K., Li F., Azuma Y., Yuasa A. and Agishita T. (2001) *Wat. Res.* **35**, (1) 167-179.

Edzwald J.K.and Tobiason J.E . (1999) Enhanced coagulation: US requirements and a broader view. *Wat. Sci. & Technol.* **40** (9) 63-70.

Egeberg P.K., Christy A.A. and Eikenes M. (2002) The molecular size of natural organic matter (NOM) determined by diffusimetry and seven other methods. *Wat. Res.* **36**, 925-932.

Eikebrokk B. (1999) Coagulation-direct filtration of soft, low alkalinity humic waters. *Wat. Sci.&* Technol. **40** (9) 55-62.

Ersöz A., Sa R. and Denizli A. (2004) Ni(II) ion-imprinted solid-phase extraction and preconcentration in aqueous solutions by packed-bed columns. *Analytica Chimica Acta*, **502**, 91-97.

Evanko C.R. and Dzombak, D.A. (1998) Influence of structural features on sorption of NOM-Analogue organic acids to goethite. *Environ. Sci. Technol.* **32,** 2846-2855.

Everett D.H. (1958) Industrial carbon and graphite, p.272, Society of Chemical Industry, London.

Everett D.H. (1988) Basic principles of colloids science. The Royal Society of Chemistry.

F

Fair G., Geyer J.C. and Okun D.A. (1968) Water and wastewater treatment engineering. Vol. 2: water purification and wastewater treatment and disposal.

Fettig J. (1999a) Characterisation of NOM by adsorption parameters an effective diffusivities. *Environ Int.* 25 (3) 335-346.

Fettig J. (1999b) Removal of humic substances by adsorption / ion exchange. *Wat. Sci. & Tech.* **40** (9) 173-182.

Fettig J. (2005) Modelling the uptake of natural organic matter (NOM) by different granular sorbent media. *Journal of Water Supply: Research and Technology-AQUA* **54.2**, 83-93.

Fettig J. and Sontheimer, H. (1987a) Kinetics of adsorption on activated carbon: I.

Single-solute systems. *Journal of Environmental Engineering.* **113** (4) 764-779.

Fettig J. and Sontheimer, H. (1987b) Kinetics of adsorption on activated carbon: II. Multisolute systems. *Journal of Environmental Engineering.* **113** (4) 780-794.

Fettig J. Sontheimer, H. (1987c) Kinetics of adsorption on activated carbon: III. Natural organic material. *Journal of Environmental* Engineering. **113** (4) 795-810.

Fettig J. (1985) Zur kinetic der adsorption organischer Substanz Gemische Waessriegen Loesungen an Aktivkhole, PhD Karlsruhe University, Karlsruhe, Germany.

Filip Z. and Kubát J. (2001) Microbial utilization and transformation of humic substances extracted from soils of long-term field experiments. *Eur. J. Soil Biol.* **37**, 167-174.

Filius J.D., Lumsdon, D.G., Meeussen J.C.L., Hiemstra T. and Van Riemsdijk, W.H. (2000) Adsorption of fulvic acid on goethite. *Geochimica et Cosmochimica Acta* **64** (1) 51-60.

Filius J.D., Hiemstra T. and Van Riemsdjijk W.H. (1997) Adsorption of small weak organics acids on goethite: Modeling of mechanisms. *J. Colloid Interface Sci.* **195**, 368-380.

Frederick, H.T. and Cannon, F.S. (2001) Calcium-NOM loading onto GAC. *J. Amer. Wat. Works Assoc.* **Dec**. 77-89.

Frost R.L., Weier M.L., Martens W., Kloprogge T. and Ding Z. (2003) Dehydration of synthetic and natural vivianite. *Thermochimica Acta,* **401** (2) 121-130.

G

GACMan userguide (1994). Water Research Centre, Swindon, UK.

Giles C.H., MacEwan T.H., Nakhua S.N. and Smith D. (1960) *J. Chem. Soc.* 3973.

Goyne K.W., Chorover J., Zimmerman A.R., Komarneni S and Brantley S.L. (2004) *J. Colloid Interface Sci.* **272**, 10-20.

Graham N.J.D. (1999) Removal of humic substances by oxidation/biofiltration processes - a review. *Wat. Sci. & Tech.* **40** (9) 141-148

Gregg S.J. and Sing S.W. (1982) Adsorption, surface area and porosity. Academic Press, London.

Gu B., Schmitt J., Chen Z., Liang L. and McCarthy J.F. (1994) Adsorption and desorption of natural organic matter on iron oxide: mechanisms and models. *Environ. Sci. Technol.* **28**, 38-46.

Gu B., Schmidt J., Chen Z., Liang L. and McCarthy J.F. (1995) Adsorption and desorption of different organic matter fractions on iron oxides. *Geochim. Cosmochim. Acta*, **59**, 219-229.

Gu, B., Mehlorn, T. L. Liang, L. and McCarthy, J. F. (1996a) Competitive adsorption, displacement, and transport of organic matter on iron oxide: I. Competitive adsorption. *Geochim. Cosmochim. Acta.* **60**, 1943-1950.

Gu B., Mehlorn, T. L. Liang, L. and McCarthy, J. F. (1996b) Competitive adsorption, displacement, and transport of organic matter on iron oxide: II. Displacement and transport. *Geochim. Cosmochim. Acta.* **60,** 2977-2992.

Guo M. and Chorover J. (2001) Relationships among characteristics of dissolved organic matter. *Symposia papers, Am. Chem. Soc.* **41** (2) 311-315.

H

Hayes M.H.B., MacCarthy P., Malcolm R.L. and Swift R.S. (1989) Humic Substances: in search of a structure II. *John Wiley and Sons.*

Heijman S.G.J., Van Paassen A.M., Van der Meer W.G.J.and Hopman R. (1999) Adsorptive removal of natural organic matter during drinking water treatment. *Wat. Sci. & Technol.* **40** (9) 183-190.

Hesse S., Kleiser G. and Frimmel F.H. (1999) Characterization of refractory organic substances (ROS) in water treatment. *Wat. Sci. & Technol.* **40** (9) 1-7.

Hiemenz P.C. (1986) Principles of colloid and surface chemistry. 2nd Ed. Marcel Dekker.

Ho Y.S. and McKay G. (1999) Comparative sorption kinetic studies of dyes and aromatic compounds onto fly ash. *J. Environ. Sci. Health*, **A34**, 1179-1204.

Hozalski R. M., Bouwer E. J. and Goel S. (1999) Removal of natural organic matter (NOM) from drinking water supplies by ozone-filtration. *Wat. Sci.& Technol.* **40,** 157-163.

Huck P.M. (1999) Development of a framework for quantifying the removal of humic substances filtration. *Wat. Sci. Technol.* **40** (9) 149-156.

I

Illés E. and Tombácz E. (2004) The role of variable surface charge magnetite. *Colloids and Surfaces. A: Physicochem. Engin. Aspects.* **230**, 99-109.

Imai A., Fukushima T., Matsushige K. and Kim Y.H. (2001) Fractionationation and characterization of dissolved organic matter in a shallow eutrophic lake, its inflowing rivers, and other organic matter sources. *Wat. Res.* **35** (17) 4019-4028.

J

Jarionec M., Choma J. and Kruk M. (2003) Assessment of reliability of the Horwath-Kawazoe pore size analysis method using argon adsorption isotherms on ordered mesoporous silicas. *Colloids and Surfaces A: Physicochem. Eng. Aspects* **214**, 263-269.

Jolivet J.P. (2000) Metal oxide chemistry and synthesis: from solution to solid state. John Wiley & Sons.

Jung M.-W., Ahn K.H-H., Lee Y., Kim K.-P., Rhee J.-S., Park J.T. and Paeng K.-J. (2001) Adsorption characteristics of phenol and chlorophenols on granular activated carbon (GAC). *Microchemical Journal* **70**, 123-131.

K

Kam S.-K. and Gregory, J. (2001) The interaction of humic substances with cationic polyelectrolytes. *Wat. Res.* **35** (15) 3557-3566.

Kanungo S.B. (1994) Adsorption of cations on hydrous oxides of iron. 1. Interfacial behaviour of amorphous FeOOH and β-FeOOH (akaganeite) in different electrolyte solutions. *J. Colloid Interface Sci.* **162**, 86-92.

Kapoor A. and Yang R.T. (1991) Contribution of concentration dependent surface diffusion to rate of adsorption. *Chemical Engineering Science* **46** (8) 1995-2002.

Kim H.-C. and Yu M.-J. (2005) Characterization of natural organic matter in conventional water treatment proceses for selection of treatment processes focused on DBPs control. *Wat. Res.* **39**, 4779-4789.

Kitis M., Karanfil T., Wigton A. and Kilduff J.E. (2002) Probing reactivity of dissolved organic for disinfection by-product formation using XAD-8 resin adsorption and ultrafiltration fractionation. *Wat. Res.* **36** (15) 3834-3848.

Ko D.C.K., Cheung C.W., Choy K.K.H., Porter J.F. and McKay G. (2004) Sorption equilibria of metal ions on bone char. *Chemosphere* **54**, 273-281.

Ko D.C.K., Porter J.F. and McKay G. (2000) Optimised correlation for the fixed bed sorption of metal ions on bone char. *Chem. Eng. Sci.* **55**, 5819-5829.

Krasmer S.W. and Amy G. (1995) Jar-tests evaluations of enhanced coagulation. *Journal of AWWA* **87**, *93-107.*

Kronberg L. (1999) Water treatment practice and the formation of genotoxic chlorohydroxyfuranones. *Wat. Sci.& Technol.* **40** (9) 31-36.

Krishnan K.A.and Anirudhan T.S. (2002) Removal of mercury (II) from aqueous solutions and chlor-alkali industrial effluent by steam activated and sulphurised activated carbons prepared from bagass pith: kinetics and equilibrium studies. *Journal of harzadous materials* **B92**, 161-183.

Kulovaara M., Corin N., Backlund P. and Tervo J. (1996) Impact of UV_{254}-radiation on aquatic humic substances. *Chemosphere* **33** (5) 783-790.

Kummert R. and Stumm W. (1980) *J. Colloid Interface Sci.* **75**, 373.

L

Lai C.H. and Chen V.Y. (2001) Removal of metal ions and humic acid from water by iron-coated filter media. *Chemosphere* **44**, 1177-1184.

Lambert S.D. and Graham N.J.D. (1995a) Removal of non-specific dissolved organic matter from upland potable water supplies -I. Adsorption. *Wat. Res.* **29**, 2421-2426.

Lambert S.D. and Graham, N.J.D. (1995b) Removal of non-specific dissolved organic matter from upland potable water supplies -II. Ozonation and adsorption. *Wat. Res.* **29** (10) 2427-2433.

Lambert S.D., (1992). Removal of colour-causing natural organic matter from potable water by pre-ozonation and adsorption. PhD Imperial College of Science, Technology and Medicine, University of London.

Lastoskie C., Gubbins K.E. and Quirke N. (1994) Pore size distribution analysis and networking: studies of microporous sorbents. *Studies in Surface Science and Catalysis* **87**, 51-60.

Lazaridis N.K., Karapantsios T.D. and Georgantas D. (2003) Kinetic analysis for the removal of a reactive dye from aqueous solution onto hydrotalcite by adsorption. *Wat. Res.* **37**, 3023-3033.

Lead J.R., Wilkinson, K.J. Starchev, K. Canonica, S. and Buffle, J. (2000) Determination of diffusion coefficients of humic substances by fluorescence correlation spectroscopy: role of solution conditions. *Environ. Sci. Technol.* **34**, 1365-1369.

Lee V.K.C., Porter J.F. and McKay G. (2000) Development of fixed-bed absorber correlation models. *Ind. Eng. Chem. Res.* **39**, 2427-2433.

Lee S.A., Fane A.G. and Waite T.D. (2005) Impact of natural organic matter on floc size and structure effects in membrane filtration. *Environ. Sci. Technol.* **39**, 6477-6486.

Leenheer J.A. (1994) Chemistry of dissolved organic matter in rivers, lakes and reservoirs. In Environmental Chemistry of Lakes and Reservoirs. Baker L.A. Ed. *Advances in chemistry series,* **237**. American Chemical Society, Washington D.C. 195-222.

Li F., Yuasa A., Ebie K. and Azuma Y. (2003) Microcolumn test and model analysis of activated carbon adsorption of dissolved organic matter after precoagulation: effects of pH and pore size distribution. *J. Colloid Interface Sci.*, **262** (2) 331-341.

Li F., Yuasa A., Ebie K., Azuma Y., Hagishita T. and Matsui Y. (2002) Factors affecting the adsorption capacity of dissolved organic matter onto activated carbon: modified isotherm analysis. *Wat. Res.* **36**, 4592-4604.

Li Q., Snoeyink V.L., Mariñas B.J. and Campos C. (2003) Elucidating competitive adsorption mechanisms of atrazine and NOM using model compounds. *Wat. Res.* **37**, 773-784.

Liu K.-T. and Weber W.J. Jr (1981) Characterization of mass transfer parameters for adsorber modeling and design. *Journal WPCF.* **53** (10) 1541-1550.

Lorenc-Grabowska E. and Gryglewicz G. (2005) Adsorption of lignite-derived humic acids on coal-based mesoporous activated carbons. *J. Colloid Interface Sci.* **284**, 416-423.

M

Marczewski A.W. (2002) A practical guide to adsorption on heterogeneous surfaces. An overview on http://adsorption.org/awm/ads

Maartens A., Swart, P. and Jacobs, E.P. (1999) Removal of natural organic matter by ultrafiltration: characterisation, fouling and cleaning. *Wat. Sci. & Technol.* **40** (9) 113-120.

Matsui Y.M., Yuasa A. and Li F.S. (1998) Overall adsorption isotherm of natural organic matter. *J. Envir. Engrg.,* November, 1099-1107.

Matsui Y.M, Yuasa A. and Li F.S.(1999) Pretreatment effects on activated carbon adsorption of humic substances: distributed fictive component analysis. *Wat. Sci. &*

Technol. **40** (9) 223-230.

McKnight (2000) Use of fluorescence for characterizing source and speciation of aquatic humic substances. *Symposia papers, Am. Chem. Soc.,* **40** (2) 659-660.

McKay G. (2001) Solution to the homogeneous surface diffusion model for batch adsorption systems using orthogonal collocation. *Chem. Eng. J.* **81**, 213-221.

McKay G. and Bino M.J. (1990) Fixed bed adsorption for the removal of pollutants from water. *Environmental Pollution* **66**, 33-53.

McKay G., Bino M.J. and Altememi A. (1986) External mass transfer during the adsorption of various pollutants onto activated carbon. *Wat. Res.* **20** (4) 435-442.

Melin E.S. and Odegaard, H. (1999) Biofiltration of ozonated humic water in expanded clay aggregate filters. *Wat. Sci. & Technol.* **40** (9) 165-172.

Metcalf and Eddy (1991) Wastewater engineering, treatment, disposal and reuse. *Mc Graw-Hill International Editions* (3rd ed).

Molina-Sabio M., Munecas-Vidal, Rodriguez-Reinoso F. (1991) Modification in porous texture and oxygen surface groups of activated carbons by surface groups. In *Rodriguez-Reinoso F. (Ed.),* Characterization of Porous Solids II, Elsevier, Amsterdam.

Montgomery J.M. (1985) Water treatment principles and design. Montgomery Consulting Engineers, Inc. *John Wiley & Sons, Inc.*

Moriguchi T. Yano K., Tahara M. and Yaguchi K. (2005). Metal-modified silica adsorbents for removal of humic substances in water. *J. Colloid Interface Sci.* **283**, 300-310.

Morris G. and Newcombe G. (1993) Granular activated carbon: the variation of surface properties with the adsorption of humic substances. *J. Colloid Interface Sci.* **159**, 239.

Mustin M. (1987) Le compost, gestion de la matière organique (1987) *Eds François Dubusc, Paris.*

Myers A.L and Prausnitz J.M. (1965) Thermodynamics of mixed-gas adsorption. *Journal of AIChE.* **11** (1) 121.

Myneni S.C.B., Brown J.T., Martinez G.A. and Meyer I. (1999) Imaging of humic substance macromolecular structures. *Science* **286**, 1335-1337.

Myneni S.C.B. Soft X-ray spectroscopy and spectromicroscopy studies of organic molecules in the environment. *Rev. Mineral. Geochem.* Application of synchrotron

radiation in Low-Temperature Geochemistry and Environmental Science, **49**, 485-579.

N

Namjesnik-Dejanovic K., Maurice P.A., Aiken G.R., Cabaniss S., Chin Y.-P. and Pullin M.J. (2000) Adsorption and fractionation of a muck fulvic acid on kaolinite and goethite at pH 3.7, 6 and 8. *Soil Sci.* **165** (7) 545-559.

Netpradit S. Thiravetyan P. and Towprayoon S. (2004) Evaluation of metal hydroxide sludge for reactive dye adsorption in a fixed-bed column system. *Wat. Res.* **38**, 71-78.

Newcombe G. (1999) Charge vs porosity - Some influences on the adsorption of natural organic matter (NOM) by activated carbon. *Wat. Sci. & Technol.* **40** (9) 191-198.

Nissinen T.K., Miettinen I.T., Martikainen P.J. and Vartiainen T. (2001). Molecular size distribution of natural organic matter in raw and drinking waters. *Chemosphere*, **45**, 865-873.

O

O'Melia C.R., Becker, W.C.and Au, K.K. (1999) Removal of humic substances by coagulation. *Wat. Sci. & Technol.* **40** (9) 47-54.

Ødeegard H., Eikebrokk B. and Storhaug R. (1999) Processes for the removal of the humic substances from water - an overview based on norwegian experiences. *Wat. Sci. & Technol.* **40** (9) 37-46.

Othman M.Z., Roddick F.A. and Hobday M.D. (2000) Evaluation of victorian low rank coal-based adsorbents for the removal of organic compounds from aqueous systems. *Wat. Res.* **34**, 18, 4351-4358.

Othman M.Z., Roddick F.A. and Snow R. (2001) Removal of dissolved organic compounds in fixed-bed columns: evaluation of low-rank coal adsorbents. *Wat. Res.* **35,** 12, 2943-2949.

P

Parfitt R.L., Fraser A.R. and Farmer V.C. (1977) Adsorption on hydrous oxides. III Fulvic acid and humic acid on goethite, gibbsite and immogolite. *J. Soil Sc.* **28**, 289-296.

Peng X., Luan Z., Chen F., Tian B. and Jia Z. (2005) Adsorption of humic acid onto pillared bentonite. *Desalination*, **174**, 135-143.

Piccolo A. (2001) The supramolecular structure of humic substances. *Soil Sc.* **166** (11) 810-832.

Pradhan J.K., Bhattacharya, Das S.C., Panda R.K. (2000*) Materials Science and Engineering* **B77**, 185-192.

Q

Quinlivan P.A., Li L. and Knappe D.R.U. (2005) Effects of activated carbon characteristics on the simultaneous adsorption of aqueous organic micropollutants and natural organic matter. *Wat. Res.* **39**, 1663-1673.

R

Radke C.J.and Prausnitz J.M. (1972) Thermodynamics of multisolute adsorption from dilute liquid solutions. *Journal of AIChE* **18** (4) 761-768.

Ram S. (2001) Infrared spectral study of molecular vibrations in amorphous, nanocrystallyne and AlO(OH). α H_2O bulk crystals. *Infrared Physics and Technology* **42**, 547-560

Randall S.R., Sherman D.M., Ragnarsdottir K.V. and Collins C.R. (1999*) Geochim. Cosmochim. Acta* **63** (19/20) 2971-2987.

Ratnaweera H., Gjessing, E. and Oug, E. (1999) Influence of physical-chemical characteristics of natural organic matter (NOM) on coagulation properties: an analysis of eight Norwegian water sources. *Wat. Sci. & Technol.* **40** (9) 89-96.

Ravikovitch P.I., Haller G.L. and Neimark A.V. (1998) Density functional theory model for calculating pore size distributions: pore structure of nanoporous catalysts. *Advances in colloids and interface science* **77**, 203-226.

Reynolds T.D. (1982) Unit operations and processes in environmental engineering. PWS Publishing Company.

Rouquerol F., Rouquerol J. and Sing K.S.W. (1999) Adsorption by Powders and Porous Solids: Principles, Methodology and Applications. *Academic Press* London.

S

Sander S., Mosley L.M. and Hunter K.A. (2004). Investigation of interparticle forces in natural waters: effects of adsorbed humic acids on iron oxide and alumina surface properties. *Environ. Sci. Technol.* **38**, 4791-4796.

Sawyer C.N., McCarty P.L. and Parkin G.F. (1994) Chemistry for environmental engineering.McGraw-Hill, 4th ed.

Schreiber B., Brinkmann T., Schmalz V. and Worch E. (2005) Adsorption of dissolved organic matter onto activated carbon – the influence of temperature, absorption wavelength, and molecular size. *Wat. Res.* **39**, 3449-3456.

Schroth B.K. and Sposito G. (1997) Surface charge properties of kaolinite. *Clays and Clay Miner.* **45**, 85-91.

Seida Y. and Nakano, Y. (2000) Removal of Humic Substances by layered double hydroxyde containing iron. *Wat. Res.* **34** (5) 1487-1494.

Sing K. (2001) The use of nitrogen adsorption for the characterisation of porous materials. Review. *Colloids and Surfaces. A: Physicochemical and engineering aspects,* **187-188**, 3-9.

Snoeyink V.L. and Jenkins D. (1980) Water chemistry. John Wiley & Sons.

Socrates G. (2000) Infrared and Raman characteristic group frequencies: tables and charts. *3rd Ed. Chichester.*

Sontheimer H. and Hubele, C. (1986) The use of ozone and granular activated carbon in drinking water treatment. *Treatment of Drinking Water for Organic Contaminants Proceedings of the Second National Conference on Drinking Water*, Edmonton, Canada, April 7th and 8th, 1986.

Sontheimer H., Crittenden J.C. and Summers R. S. (1988) Activated carbon for water treatment, 2nd ed. DVGW-Forschungsstelle, Karlsrue.

Specht C.H., Kumke M.U. and Frimmel F.H. (2000) Characterization of NOM adsorption to clay minerals by size exclusion chromatography. *Wat. Res.* **34** (16) 4063-4069.

Sperlich A., Werner A., Genz A., Amy G., Worch E. and Jekel M. (2005) Breakthrough behaviour of granular ferric hydroxide (GFH) fixed-bed adsorption filters: modeling and experimental approaches. *Wat. Res.* **39**, 1190-1198.

Sposito G. (1995) The Environmental Chemistry of Aluminium. 2nd Ed. CRC Press.

Standard Methods for the Examination of Water and Wastewater (1998) 20th ed.

Streat M., Patrick, J.W. and Camporro Perez M.J. (1995) Sorption of phenol and para-chlorophenol from water using conventional and novel activated carbons. *Wat. Res.* **29** (2) 467-472.

Stumm W. and Morgan J.J. (1995) Aquatic chemistry. Wiley New York (3rd ed).

Sutton R. and Sposito G. (2005) Molecular structure in soil humic substances: the new view. *Environ. Sci. Technol.* **39** (23) 9009-9015 (Critical review).

T

Teermann I.P. and Jekel M.R (1999) Adsorption of humic substances onto β-FeOOH and its chemical regeneration. *Wat. Sci. & Technol.* **40**,199-206.

Thorsen T. (1999) Membrane filtration of humic substances - state of the art. *Wat. Sci. & Technol.* **40** (9) 105-112.

Thurman E.M. (1985) Organic chemistry of natural waters. Dordrecht, Netherlands: Martinus Nijhoff / Dr. W. Junk.

Tien C. (1994) Adsorption calculations and modelling. *Butterworth Heinemann* USA.

Tipping E. (2002) Cation binding by humic substances. Cambridge University Press.

Thomas W.J. and Crittenden B. (1998) Adsorption Technology and Design. Butterworth-Heinemann.

Tombácz E., Libor Z., Illés E., Majzik A. Klumpp E. (2004) The role of reactive surface sites and complexation by humic acids in the interaction of clay mineral and iron oxide particles. *Organic Geochemistry* **35**, 257-267.

U

USEPA (1998a) National primary drinking regulations: disinfectants and disinfection byproducts; Final rule. 40 CFR parts 9, 141 and 142, Federal Register, **63** (241) 69390-69476 (December 16, 1998).

V

Van Benschoten J.E. and Edzwald, J.K. (1990) Chemical aspects of coagulation using aluminium salts - II. Coagulation of fulvic acid using alum and polyaluminium chloride. *Wat. Res.* **24**, 1527-1535.

Van der Weerd H., Van Riemsdijk W.H. and Leijnse A. (1999) Modeling the dynamic adsorption/desorption of a NOM mixture: effect of physical and chemical heterogeneity. *Environ. Sci. Technol.* **33**, 1675-1681.

Varma A., Morbidelli M. and Wu H. (1999) Parametric sensitivity in chemical systems. *Cambridge University Press*, UK.

Vermeer A.W.P., Van Riemsdijk, W.H. and Koopal, L.K. (1998a) Adsorption of humic acid to mineral particles. 1. Specific and electrostatic interactions. *Langmuir* **14**, 2810-2819.

Vermeer A.W.P. and Koopal, L.K. (1998b) Adsorption of humic acid to mineral particles. 2. Polydispersity effects with polyelectrolyte adsorption. *Langmuir* **14**, 4210-4216.

W

Walker G.M. and Weatherley L.R. (1997) Adsorption of acid dyes on granular activated carbon in fixed beds. *Wat. Res.* **31** (8) 2093-2101.

Wall N.A. and Chopin G.R. (2003) Humic acids coagulation: influence of divalent cations. *Applied geochemistry* **18**, 1573-1582.

Weber W.J. Jr, McGinley P.M. and Katz L.E. (1991) Sorption phenomena in subsurface systems: concepts, models and effects on contaminant fate and transport. *Wat. Res.* **25** (5) 499-528.

Weber W. J. Jr, Pirbazari M., Long J.B. and D.A. Barton (1980) Potential mechanisms for removal of humic acids from water by activated carbon. in Activated Carbon Adsorption of Organics from the Aqueous Phase, **1**, 317-336. *I.H. Suffet and M.J. Mc Guire, Ed. Ann Arbor and Science Publishers* MI, USA.

Weber W.J. Jr (1972) Physicochemical processes for water quality control. Wiley, New York.

Weishaar J. and Aiken, G. (2001) Evaluation of specific Ultra-Violet absorbance as an indicator of the chemical content of Dissolved Organic Carbon. *Symposia Paper, Am. Chem. Soc.* **41** (2) 843-845.

Wilkinson K.J., Balnois E., Leppard G.G. and Buffle J. (1999) Characteristic features of the major components of freshwater colloidal organic matter revealed by transmission electron and atomic force microscopy. *Colloids and Surfaces A: Physicochemical and engineering aspects* **155**, 287-310.

Workman J. and Springsteen A.W. (1997) Applied spectroscopy: a compact reference for practitioners. *San Diego: Academic Press.*

Wu F.-C., Tseng R.-L. and Juang R.-S. (2002) Adsorption of dyes and humic acid from water using chitosan-encapsulated activated carbon. *J. Chem. Technol. Biotechnol.* **77**, 1269-1279.

Y

Yuasa A., Li F., Matsui Y. and Ebie K. (1997) Characteristics of competitive adsorption of aquatic humic substances onto activated carbon. *Wat. Sci.& Technol.* **36** (12) 231-238.

Z

Zhang X. and Bai R. (2003) Mechanisms and kinetics of humic acid adsorption onto chitosan-coated granules. *J. Colloids Interface Sci.* **264**, 30-38.

Zhou Q. (1996) Surface characteristics and dissolution kinetics of two standard kaolinites. *Masters thesis*, Kent University, Kent OH, USA.

Zhou H. and Smith D.W. (2001) Advanced technologies in water and wastewater treatment. *Canadian journal of civil engineering* (Suppl.1) **28**, 49-66.

Zhou Q., Maurice P.A. and Cabaniss S.E. (2001) Size fractionation upon adsorption of fulvic acid on goethite: Equilibrium and kinetic studies. *Geochim. Cosmochim. Acta* **65** (5) 803-812.

APPENDIX

SEM photographs of used adsorbents

GAC 207C after adsorption of humic substance 0-5 kDa (F1) and 0-10 kDa (F12)

observation of microbial growth (bacteria and yeast)

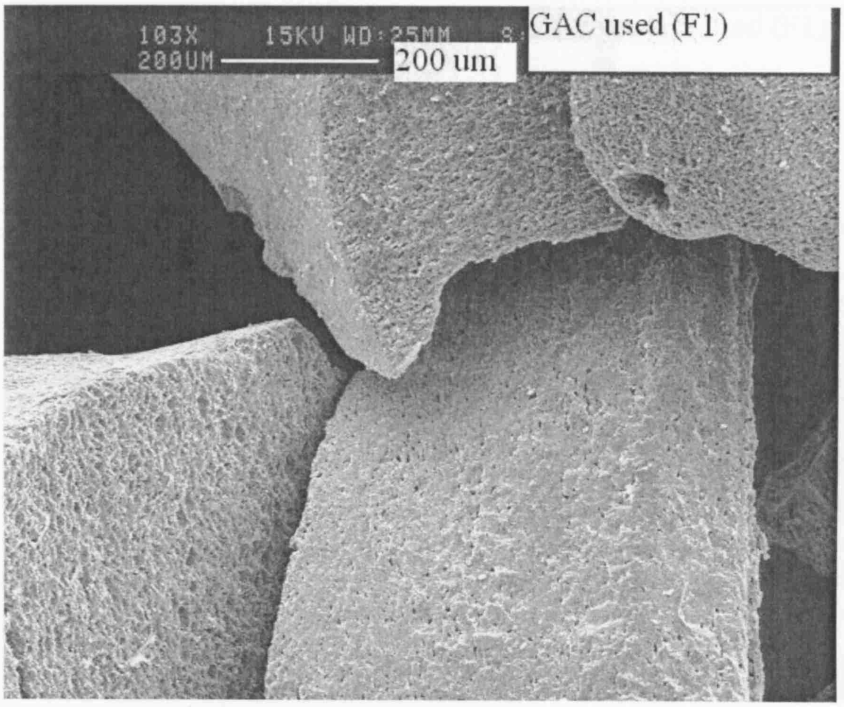

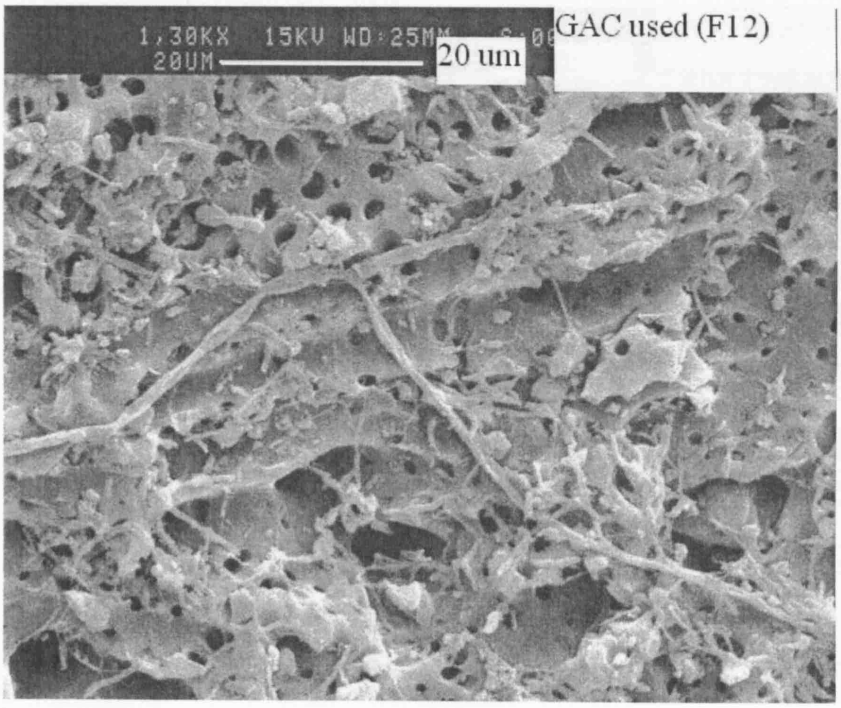

AAFS after adsorption of humic substance 0-5 kDa (F1)

the iron coating has detached from the activated alumina surface

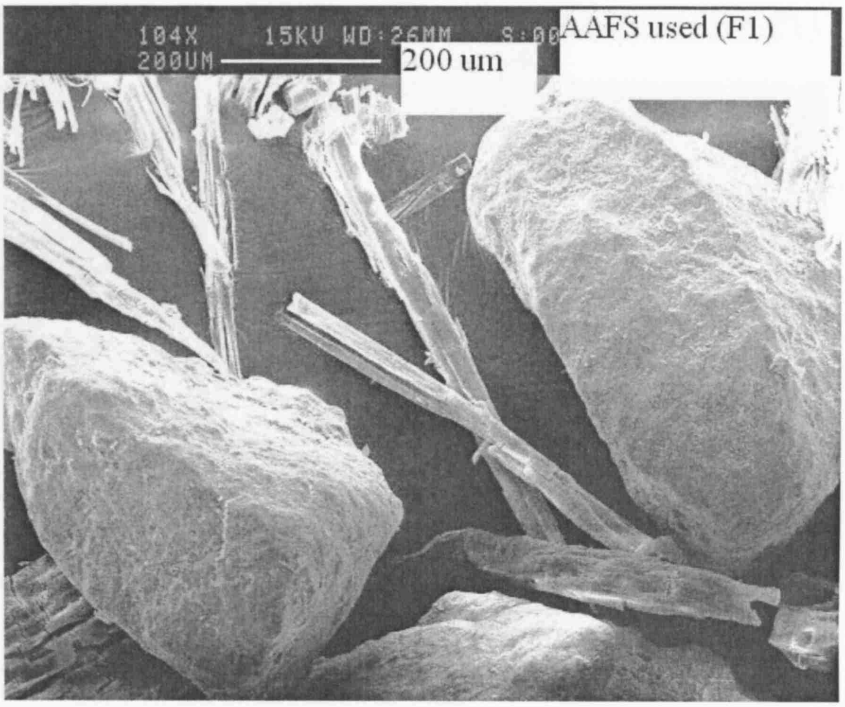

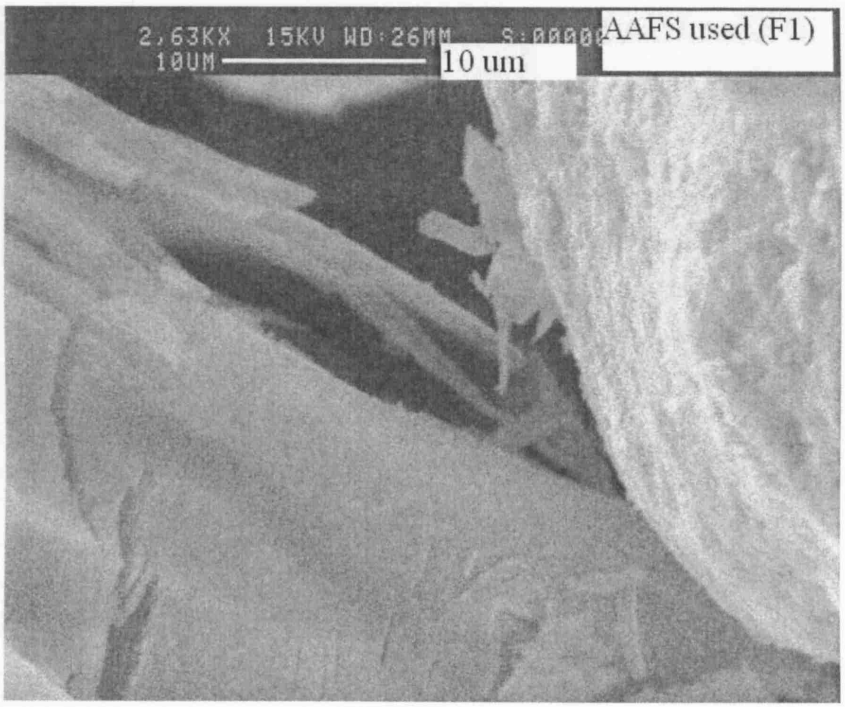

β-FeOOH after adsorption of humic substance 0-5 kDa (F1)

observation of microbial growth (bacteria)